UNIVERSITY OF SOUTHAMPTON
FACULTY OF ENGINEERING AND APPLIED SCIENCE
INSTITUTE OF SOUND AND VIBRATION RESEARCH

THE INFLUENCE OF STRUCTURAL-ACOUSTIC COUPLING ON THE DYNAMIC BEHAVIOUR OF A ONE-DIMENSIONAL VIBRO-ACOUSTIC SYSTEM

by

Gihwan Kim

A thesis submitted for the degree of

Doctor of Philosophy

January 2009

UNIVERSITY OF SOUTHAMPTON

ABSTRACT

Faculty of Engineering and Applied Science

Institute of Sound and Vibration Research

Doctor of Philosophy

THE INFLUENCE OF STRUCTURAL-ACOUSTIC COUPLING ON THE DYNAMIC BEHAVIOUR OF A ONE-DIMENSIONAL VIBRO-ACOUSTIC SYSTEM

by Gihwan Kim

The aim of this thesis is to investigate the structural-acoustic coupling effects on the dynamic behaviour of a vibro-acoustic system under passive/active control. The simplest model of a vibro-acoustic system one can consider is a one-dimensional acoustic cavity driven by a single-degree-of-freedom (SDOF) structure. This simple model is used to demonstrate the physical characteristics of the coupling phenomenon. This simple analytical model can provide various degrees of structural-acoustic coupling, which are dependent upon (i) the structural-acoustic stiffness ratio, (ii) structural-acoustic natural frequency ratio, (iii) structural damping, and (iv) acoustic damping. In this case, although the geometric coupling factor is not included because the SDOF structure has a single mode, 80 percent of the factors that determine the degree of coupling can be accounted for by the simple analytical model. The coupling mechanism, in the simple vibro-acoustic system, is investigated using the mobility-impedance approach. In order to provide the threshold of the degree of coupling, a coupling factor is calculated in terms of non-dimensional structural-acoustic parameters. Vibro-acoustic responses are represented by the acoustic potential energy in the cavity and the kinetic energy of the structure coupled to the acoustic cavity.

The vibro-acoustic responses are investigated for various coupled cases. The principles are demonstrated by controlling the acoustic potential energy in the one-dimensional finite acoustic tube driven by the SDOF structure. Three control strategies are applied; passive control, active feedforward control and decentralised velocity feedback control. Passive control is investigated to achieve physical insight into the relative benefits of passive control

treatments. In the more *strongly coupled* case, acoustical modifications were preferable for the reduction of the acoustic potential energy. On the other hand, in the more *weakly coupled* case, structural modifications were more effective. For harmonic disturbance, an active feedforward control strategy is considered for the control of the acoustic potential energy in the cavity driven by the structure under external harmonic excitation. For the active feedforward control systems, this study uses the concept of optimal impedance, which is defined as the ratio of the control force to the velocity of a secondary source when the acoustic potential energy is minimised. In the more *strongly coupled* case, all the acoustic modes were effectively suppressed at the resonance frequencies. On the other hand, in the more *weakly coupled* case, all the acoustic modes were controllable as in the more *strongly coupled* case. However, the structural mode was generally uncontrollable. For broadband disturbance, decentralised velocity feedback control is formulated to investigate the relative control effectiveness of structural and acoustic actuators for the control of the acoustic potential energy. In the more *strongly coupled* case, the control configuration of using the acoustic actuator was preferable. On the other hand, in the more *weakly coupled* case, the decentralised velocity feedback control strategy using both the actuators was desirable.

CONTENTS

Chapter 3. Passive Control of Acoustic Potential Energy in a Vibro-acoustic System 50

Chapter 4. Active Feedforward Control of Acoustic Potential Energy in a Vibro-acoustic System 92

Chapter 5. Decentralised Velocity Feedback Control of Acoustic Potential Energy in a Vibro-acoustic System 138

Chapter 6. Conclusions 187

Appendices   **192**

References   **211**

LIST OF FIGURES

LIST OF TABLES

GLOSSARY OF TERMS

A, B	Complex wave amplitudes
B_a	Bulk modulus
c	Complex sound speed
c_0	Sound speed in the lossless medium
c_b	Complex sound speed in the absorptive medium
$E_K(\omega)$	Structural kinetic energy
$\hat{E}_k(\hat{L})$	Normalised structural kinetic energy
$E_P(\omega)$	Acoustic potential energy
$\hat{E}_P(\hat{L})$	Acoustic potential energy normalised by that at the static state
$E_{pFRF}(\omega)$	Measured approximate acoustic potential energy
$F(x,\omega)$	External excitation force
F_{CA}, F_{CS}	Velocity feedback control force
F_0	Force
F_a	Acoustic reaction force
F_P	Primary force
F_S	Secondary control force
$F_{S\,opt}$	Optimal secondary control force
F_s	Structural force
$f(t)$	External time harmonic fore
$f_P(t)$	Primary time force
$f_S(t)$	Secondary time force
f_1, f_2	Frequencies at half-power points
f_s	Natural frequency
f_{s1}	Natural frequency of the standard or the modified loudspeaker
f_{s2}	Natural frequency of the loudspeaker with the known dummy mass
$G(j\omega)$	Feedforward controller
G_{opt}	Optimal feedforward controller
H_A, H_S	Velocity feedback gain
$\mathbf{h}_S$	Transfer function vector
j	$\sqrt{-1}$
J_P	Approximate acoustic potential energy
$\hat{J}_{P\min}(\hat{L})$	Normalised minimum level of the acoustic potential energy
k	Complex acoustic wavenumber
k_b	Complex acoustic wavenumber in the absorptive medium
K_a	Acoustic bulk stiffness
K_s	Structural stiffness

$\hat{K}$	Structural-acoustic stiffness ratio
L	Tube length
$\hat{L}$	L/λ
L_0	Acoustic medium length
L_b	Absorptive medium length
M_s	Structural mass
m_s	Known dummy mass
m	Number of measuring points
n	Integer
$P(x,\omega)$	Acoustic pressure in the acoustic tube
$\hat{P}(\hat{x},\hat{L})$	Normalised acoustic pressure
$P_P(x,\omega)$	Acoustic pressure due to primary force
$\hat{P}_P(\hat{x},\hat{L})$	Normalised acoustic pressure due to primary force
$P_S(x,\omega)$	Acoustic pressure due to secondary control force
$\hat{P}_S(\hat{x},\hat{L})$	Normalised acoustic pressure due to secondary control force
$P_{FRF}(x_i,\omega)$	Transfer frequency response function of the sound pressure with respect to the input voltage
P_1	Acoustic pressure at $x=0$
P_2	Resulting acoustic pressure at $x=L$
P_S	Acoustic pressure on the structure
P_L	Acoustic pressure on the arbitrary impedance
P_s	Non-dimensionalising factor for the acoustic pressure
$\mathbf{p}$	m-length vector of the normalised total sound pressure
$\mathbf{p}_P$	m-length vector of normalised sound pressure due to the primary source
$\mathbf{p}_S$	m-length vector of normalised sound pressure due to the secondary source
$\mathbf{p}_{FRF}$	Measured frequency response function vector
$\mathbf{p}_{FRF}{}^H$	*Hermitian* transpose of the vector $\mathbf{p}_{FRF}$
S	Cross-sectional area
$U(x,\omega)$	Particle velocity in the acoustic tube
$\hat{U}(\hat{x},\hat{L})$	Normalised particle velocity
$U_P(x,\omega)$	Particle velocity due to primary force
$\hat{U}_P(\hat{x},\hat{L})$	Normalised particle velocity due to primary force
$U_S(x,\omega)$	Particle velocity due to secondary control force
$\hat{U}_S(\hat{x},\hat{L})$	Normalised particle velocity due to secondary control force
U	Non-dimensionalising factor for the particle velocity
U_1	Particle velocity at $x=0$
U_2	Resulting particle velocity at $x=L$
U_L	Particle velocity on the arbitrary impedance
$U_{L\,opt}$	Velocity due to both the primary force and secondary control force at $x=L$

U_{LP}	Velocity due to the primary source at $x = L$
U_{LSopt}	Velocity due to optimal secondary control force at $x = L$
U_S	Particle velocity on the structure
U_s	Structural velocity
x	Co-ordinate for the acoustic field in the cavity
$\hat{x}$	Any normalised position along the tube
x_i	i^{th} measuring point
Y_S	Uncoupled structural mobility
Y_{CS}	Coupled structural mobility
Z_{A0}	Acoustic input impedance at $x = 0$
$\hat{Z}_{A0}$	Normalised acoustic input impedance at $x = 0$
Z_{AL}	Acoustic input impedance at $x = L$
$\hat{Z}_{AL}$	Normalised acoustic input impedance at $x = L$
Z_L	Arbitrary impedance
$\hat{Z}_L$	Normalised arbitrary impedance
Z_{opt}	Optimal impedance
Z_S	Uncoupled structural impedance
$\hat{Z}_S$	Normalised structural impedance
Z_{VA}, Z_{VS}	Controlled impedance via velocity feedback controller
$\hat{Z}_{VA}$, $\hat{Z}_{VS}$	Normalised controlled impedance via velocity feedback controller
Z_{11}, Z_{22}	Point impedance
Z_{12}, Z_{21}	Transfer impedance
η_a	Acoustic loss factor
η_s	Structural loss factor
ρ_0	Ambient density
ρ_b	Ambient density in the absorptive medium
λ	Acoustic wavelength
ω	Excitation frequency
ω_a	Fundamental natural frequency of a closed-closed tube when $L/\lambda = 1/2$
ω_s	Uncoupled structural natural frequency
$\hat{\omega}$	Structural-acoustic natural frequency ratio ($= \omega_a / \omega_s$)

CHAPTER 1

INTRODUCTION

1.1 Background

Within the context of vibro-acoustics, there are two main analytical systems involving wave fields, which are purely structural and purely acoustical systems. When these two uncoupled subsystems combine, more intriguing physical characteristics appear. The interaction between structural vibration and acoustic wave propagation has been the subject of much research. The mutual structural-acoustic interaction is dependent upon the properties of both uncoupled structural and acoustical systems [Kinsler *et al* (1982) and Fahy (2001)]. Elastic structures in a free-field tend to vibrate in a direction normal to the surface at resonance frequencies [Cremer and Heckl (1973)]. The structural vibration causes sound radiation to an acoustic field displacing and compressing a surrounding fluid in contact with the structural surface [Fahy (1985)].

When the acoustic field is limited to an acoustic cavity enclosed by an arbitrary structure under structural excitation, it is more challenging to investigate the physical behaviour of the vibro-acoustic system. For an enclosed air cavity interacting with a plane structure, a modal-interaction model has been derived by Fahy (1985), which describes the behaviour of the

1

enclosed fluid and structure in terms of the uncoupled natural modes. Analytical approaches based on a modal representation have been used in the analysis of structural-acoustic interaction in rectangular cavities with five acoustically rigid walls and one flexible wall. The effect of an underlying acoustic cavity on the flexible plate vibration was studied by Dowell and Voss (1963). They showed that only the fundamental plate mode was strongly affected by the cavity. Pretlove (1965, 1966) presented the concept of cavity- and plate-controlled modes in the rectangular cavity under flexible structural excitation, which depends on the relative energy contribution of each subsystem. The structural-acoustic interaction was discussed in terms of the relative plate and acoustic cavity stiffness in which the coupled modes were obtained from uncoupled *in vacuo* plate and cavity modes. Dowell *et al* (1977) generalised the concept based on plate and cavity modes by discussing the coupling between the structural plate and acoustic cavity in the vibro-acoustic system. In the case when a structural natural frequency is unchanged by the acoustic pressure in the cavity such that it behaves like an *in vacuo* structural plate, the acoustic pressure loading on the plate can be neglected. In another case when there is a significant change in a structural resonance frequency due to the acoustic pressure in the cavity, the effect of the cavity modifies the effective stiffness. The former is called a *weakly coupled* case and the latter is called a *strongly coupled* case in this thesis. The time-averaged acoustic potential energy is considered as a measure of the global acoustic environment in an enclosure [Bullmore *et al* (1987)]. It is useful to assess the effectiveness of passive or active control by investigating the control effects on the acoustic potential energy in the enclosure of interest.

Sound and vibration problems can be solved by passive or active control methods. Passive control involves modification of the stiffness, mass or damping of the vibrating system so that it is less responsive to its excitation source [Mead (1999)]. The modification may take the form of basic structural changes [Wang *et al* (1982) and Olhoff (1976)] or adding passive elements such as masses [McMillan and Keane (1996, 1997)], vibration isolators [Crede (1965) and Nashif *et al* (1985)] and various dampers [Lazan (1959), Mead (1960) and Hendy (1986)]. On the other hand, active control systems require actuators driven by control inputs fed through controllers using signals from sensors on the vibrating system. The active control of sound and vibration has been investigated in single-input single-output (SISO) systems and in multiple-input multiple-output (MIMO) systems under feedforward control or feedback control [Nelson and Elliott (1992) and Fuller *et al* (1996)].

Active noise control (ANC) and active noise and vibration control (ANVC) systems have given successful results for the control of tonal and stationary random disturbances. Nelson and Elliott (1992) have implemented control systems for the control of tonal disturbances in propeller aircrafts or engine noise in cars. ANC or ANVC systems have also been applied to the control of stationary random noise in aircrafts [Mathur *et al* (1997) and Guigou and Fuller (1999)] and in cars [Sutton *et al* (1994) and Park *et al* (2002)]. These control systems require MIMO adaptive feedforward or feedback controllers with a large numbers of sensors and actuators, which are relatively bulky, heavy and costly systems. The practical problems encountered in the control systems using large-area distributed transducers motivated the desire to find decentralised controllers. A decentralised control system is composed of multiple independent small localised control units that have single-input single-output (SISO) feedback controllers. SISO feedback control can provide active damping, which is effective in reducing the response at resonance frequencies by implementing direct velocity feedback. Petitjean *et al* (2002) investigated low-frequency wide-band sound radiation control of a panel incorporated with large number of control units providing damping to low-frequency resonance modes. They found similar vibration reduction on the panel whether it was under decentralised velocity feedback control or under MIMO optimal feedback control. Elliott *et al* (2002) proposed a new control configuration based on decentralised velocity feedback control units on a panel using a piezoceramic patch actuator with a small accelerometer on the centre. They noticed that the active damping effect on the total kinetic energy and total sound radiation grows as the control gain is gradually increased. However, this control behaviour is valid up to an optimal feedback gain, above which the control effect diminishes and the kinetic energy and the sound radiation increases again. The control mechanism is that the velocity feedback control units work as sky-hook dampers which absorb the structural energy. The physical behaviour of the velocity feedback control with large control gain is to pin the panel at the sensor positions.

The subject of this thesis is to investigate the influence of structural-acoustic coupling on the dynamic behaviour of a one-dimensional vibro-acoustic system under passive/active control under various structural-acoustic coupling conditions: with *strong, weak and intermediate coupling*. Previous literatures in this area are first reviewed before the detail objectives are outlined.

1.2 Literature review

1.2.1 Modelling of a vibro-acoustic system

The control of sound and vibration in vibro-acoustic systems stretches across a wide range of applications such as airplane fuselages [Elliott *et al* (1990), Bullmore *et al* (1990) and Guigou and Fuller (1999)], car compartments [Sutton *et al* (1994) and Nefske et al (1982)], etc. Elliott *et al* (1990) presented a series of in-flight experiments on the active control of propeller-induced passenger cabin noise in an aircraft. They implemented a local control system (two-loudspeaker and two-microphone) and a global control system (16-loudspeaker and 32-microphone) inside the cabin. Bullmore *et al* (1990) carried out theoretical studies and compared the results to the previous experimental work [Elliott *et al* (1990)]. They modelled the structural response of the aircraft fuselage as a finite, isotropic thin cylindrical shell, and the cabin acoustic response as a cylindrical room. The theoretical results showed good agreement with the previous experimental results provided that the theoretical external acoustic pressure forcing of the shell is representative of the measured propeller pressure field on the aircraft fuselage. Guigou and Fuller (1999) investigated the control of aircraft interior noise by applying a foam-PVDF smart skin mounted in the cockpit. They implemented a feedforward control system to reduce sound field interior noise in the fuselage disturbed by the crown panel of an aircraft, which was excited by a loudspeaker located outside of the cockpit and driven by band-limited random excitation. Sutton *et al* (1994) developed an active control system for the control of interior noise in automobiles by counteracting the low-frequency rumble noise with loudspeakers installed inside the compartment. Nefske *et al* (1982) reviewed the formulation of the finite element method for structural-acoustic analysis of an enclosed cavity using an acoustic model of a passenger compartment under structural excitation.

Practical vibro-acoustic systems can be depicted as simple models, which include key factors such as acoustic fluid in an enclosure, a structural system under external excitation being coupled with the acoustic fluid and structural-acoustic coupling [Dowell *et al* (1977)]. The structural-acoustic coupling was described by a compact matrix formulation for the steady-state analysis of structural-acoustic systems by Kim and Brennan (1998). They investigated a structural-acoustic coupling theory in modal coordinates using the impedance-mobility

approach in the combined flexible structure – 3D (three-dimensional) arbitrary enclosure system. Also, they showed that the degree of coupling is dependent upon five factors: (i) the ratio of the acoustic bulk stiffness to structure stiffness; (ii) the coincidence of the acoustic and structural uncoupled natural frequencies; (iii) geometric coupling between the acoustic and structural modes; (iv) structural damping in the flexible structure; and (v) acoustic damping in the cavity.

Figure 1.1 depicts a combined flexible structure – 3D arbitrary enclosure system where the flexible structure, under an external force, excites the interior sound field in the arbitrary enclosure. This simplified structural-acoustic model can be used to investigate the interior sound field in various automobiles and flight vehicles excited by vibrating walls. The structural-acoustic interaction in the coupled system results in coupled structural modes in the flexible structure and coupled acoustic modes in the sound fields of the enclosure. The uncoupled structural and acoustic modes are structural normal modes *in-vacuo* and acoustic normal modes of the cavity surrounded by rigid walls respectively.
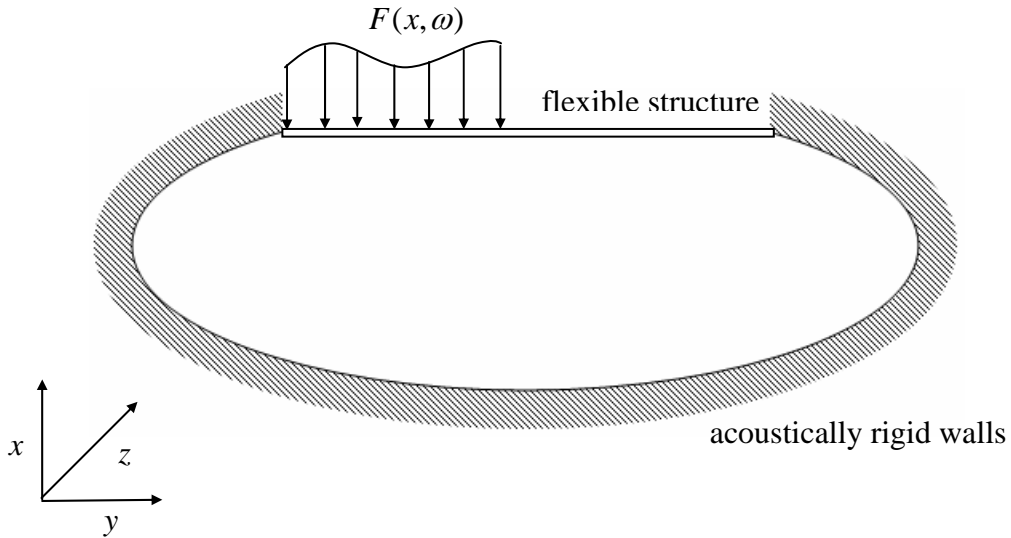
Figure1.1 Combined flexible structure – 3D arbitrary enclosure system where the flexible structure is under an external excitation force $F(x,\omega)$, which is acting in the negative x direction at driving frequency ω

1.2.2 Passive control

Passive control of vibration can be implemented by modifying the stiffness, mass or damping of the vibrating systems. The modification can be achieved by basic structural changes or the addition of passive elements such as masses, springs, fluid dampers or damped rubbers [Mead (1999)]. Lyon (1963) computed the sound pressure in the rectangular parallelepiped enclosure with one flexible wall under incident sound excitation in various frequency ranges. He showed the possibility of estimating the sound pressure inside the enclosure combined with various panels. The coupled frequencies and modes in a rectangular cavity backed by a simply supported plate have been presented as a function of the thickness of the plate by Scarpa (2000).

Various structural and acoustical passive control treatments have been applied to a vibrating plate coupled with an acoustic cavity in an enclosure. Narayanan *et al* (1981) investigated the reduction of transmitted sound through a viscoelastic sandwich panel into a rectangular enclosure. The results were that significant noise reduction could be obtained by the constrained damping layer treatment at the fundamental structural resonance of the sandwich panel. Masahiro *et al* (2007) investigated the attenuation effects on the radiated acoustic power of the vibrating panel which incorporated honeycomb structures, which allow Helmholtz resonator effects. They presented the possibility of using this passive control model in various fields including floor impact insulation to achieve the attenuation at arbitrary frequencies. Liu *et al* (2006) discussed passive and active vibro-acoustic noise control methods for attenuating interior noise in box structures, which can be cabins of vehicles and aircrafts. They adopted the structural intensity method to predict the possible locations of passive dampers on the structure and concluded that the dampers should be put at the locations which are nearby the energy source positions. Ross and Burdisso (1999) proposed the concept of a weak sound radiating cell and applied the cell on the vibrating piston coupled with a cavity under base structural excitation. The cell mounted on the vibrating structure acts nearly out-of-phase and nearly of the same strength over a wide frequency range providing the control of low-frequency structurally radiated noise. Esteve and Johnson (2005) presented an adaptive-passive solution to control the broadband sound transmission into a simply supported cylinder excited by an external plane wave. They applied passive distributed vibration absorbers for structural modes and adaptive Helmholtz

resonators for acoustic modes in the cavity. Their numerical simulations demonstrated that optimum noise reduction required the adaptive Helmholtz resonators for acoustic modes and the distributed vibration absorbers for the structural resonances that manifest themselves in the acoustic spectrum. Moreland (1984) added layers of damping material to the enclosure walls and put absorptive linings on the interior walls for noise reduction in the enclosure in various frequency ranges. He concluded that extensional damping layers or porous absorbent lining on the interior walls provided little noise reduction at low frequencies. Oh *et al* (1999) identified the interior sound field characteristics of a cavity with aluminium foam lining on the walls of a rectangular enclosure. They determined the suitable thickness of the sound absorber which maximises the sound absorption effects in the enclosure.

More recently, vibro-acoustic problems have been dealt with in a one-dimensional cavity driven by a single-degree-of-freedom (SDOF) structural driver to investigate the influence of physical parameters of acoustical and structural systems on the sound field in the cavity. Hong and Kim (1996) have developed the analysis method of general vibro-acoustic problems in a one-dimensional model incorporating structural damping and absorbing material on the structural driver. Cura *et al* (1995) investigated structural-acoustic interaction in a uni-dimensional acoustic cavity coupled to a SDOF system. They concluded that the resonance frequencies of the coupled model were modified by the effect of the interaction between fluid and structure. The resonance frequencies of the coupled model had significant changes only when an acoustical resonance frequency matched a structural resonance frequency. The resonance response of the acoustic cavity to the structural excitation had significant variation when there was a relatively low variation of the viscous damping of the structural or acoustic systems.

Previous passive control strategies in vibro-acoustic systems have been implemented either structurally or acoustically by many researchers. They have investigated sound reduction in enclosures coupled with structural systems incorporating structural or acoustical treatments. However, there is a gap in the knowledge on the relative benefits of passive control treatments to minimise the sound pressure of the cavity in various structural-acoustic coupling cases since the acoustic response in the cavity has quite different characteristics depending on the degree of coupling [Dowell *et al* (1977)].

1.2.3 Active control

Since the first active control concept was patented by Lueg (1936), various analytical studies of active control have been carried out with the aim of determining the physical guidelines for effective control design. The fundamental theory of the active control of the sound field in enclosures has been developed by Nelson *et al* (1987) and Elliott *et al* (1987). Nelson *et al* (1987) presented an analysis of active methods to produce global sound reduction in a harmonically excited rectangular enclosure. They demonstrated that substantial reductions in the total acoustic potential energy in the enclosure were possible using secondary sound sources located at a distance from the primary source which is less than half wavelength at the frequency of interest. Elliott *et al* (1987) carried out a comparative investigation on the measured results of active minimisation experiments and those predicted from theory [Nelson *et al* (1987)] in the lightly damped rectangular enclosure, which was two dimensional over the frequency range of interest. The conditions under which significant reductions in the total acoustic potential energy in the enclosure could be achieved were experimentally investigated using a primary and three secondary loudspeakers.

The active control of harmonic sound transmission into various acoustic cavities has been of interest in recent years. Fuller and Jones (1987) investigated the feasibility of using active vibration control of aircraft fuselages to reduce the interior noise level in a finite aluminium cylinder model. The cylinder model was excited by one monopole source, representative of a single propeller, and controlled by a mini-shaker attached to the exterior of the cylinder. They found that the active vibration control system provided reasonably good reduction on the interior noise levels at resonance and off-resonance frequencies of the cylinder model. Elliott *et al* (1990) presented a series of in-flight experiments on the active control of propeller-induced passenger cabin noise in an aircraft using two loudspeakers. They investigated at the first three harmonics of the blade passage frequency and simultaneously controlled three harmonics with effective noise reduction at some seat locations.

Snyder and Tanaka (1993) investigated the minimisation of radiated acoustic power and acoustic potential energy in a rigid walled rectangular cavity coupled with a flexible panel. The adaptive feedforward control systems were implemented using vibration-based error sensors such as shaped piezoelectric polymer film sensors which were an alternative to the

use of acoustic error sensors such as microphones. They concluded that the use of vibration error signals in an adaptive feedforward active control system was a practical alternative to attenuate acoustic radiation of the panel via vibration control inputs. Balachandran *et al* (1996) developed analytical and experimental studies for controlling the interior noise in a rectangular enclosure with a flexible wall excited by an external speaker. The active control was implemented by using lead zirconate titanate piezoelectric (PZT) actuators bonded to the flexible wall. They demonstrated that significant noise reductions can be realised by using active control schemes. Mohammad and Elliott (2005) investigated the active control of sound transmission into a rectangular enclosure coupled with a flexible structural panel driven by a unit point force using a secondary acoustic source. Their interest was the effect of full structural-acoustic coupling between the vibrating panel and the interior acoustic field in the cavity. They demonstrated that a better reduction in the interior acoustic field is obtained when the secondary source is close to the panel rather than when it is remote.

The majority of previous research has been carried out in coupled structural-acoustic systems with one type of structural-acoustic coupling, which is the enclosure coupled with a particular panel. They demonstrated considerable sound reduction in the enclosures under feedforward control. However there exists a need to investigate the control of the sound field in the coupled system with various structural-acoustic coupling, and the physical behaviour of the feedforward controller in each coupling case.

The active control of the sound field in a structural-acoustic coupled system subject to random disturbances can also be implemented using feedback controllers. The active feedback control strategy has been investigated in the minimisation of sound transmission and radiation from flexible plates. Fuller (1990) investigated the active control of sound transmission from a clamped elastic circular thin plate, under a plane acoustic wave incident, using point forces. The optimal control gain to minimise a cost function proportional to the radiated acoustic power was calculated based on quadratic optimization. His results demonstrated that global attenuation of broadband radiated sound levels can be achieved with one or two control forces at resonance and off-resonance frequencies with control efficiency determined by the nature of the coupling between the plate modes of response and the transmitted field. Meirovitch and Thangjitham (1990) studied the problem of suppressing the acoustic radiation pressure generated by the vibration of a simply-supported rectangular elastic plate. The influence on the control effectiveness of various design factors, such as controlled modes and actuators,

was investigated. They concluded that satisfactory control can be achieved by a sufficient number of actuators and by the choice of a relatively large number of modes.

The active control of sound transmission through a panel can be implemented by using piezoelectric control actuators. Wang *et al* (1991) demonstrated the relative benefits of piezoelectric control actuators and point force actuators to reduce sound transmission through a thin rectangular plate mounted in an infinite baffle under an incident harmonic plane wave. The results showed that point force actuators provided more effective control of the sound transmission than piezoelectric actuators. Johnson and Elliott (1995) investigated the active control of sound power radiation from a rectangular panel mounted in a baffle excited by a single incident harmonic plane wave using a secondary piezoelectric actuator to determine the effect of cancelling the net volume velocity of the panel. They showed that the first radiation mode was the dominant radiator of sound power at low frequencies and the cancellation of the volume velocity was a good strategy for the reduction of sound power transmission at low frequencies. Also, they suggested that a volume velocity sensor, such as polyvinylidene fluoride (PVDF) film, and a uniform-force actuator can be used as matched actuator/sensor pair in a feedback control system to achieve the same attenuation possible as with a feedforward control system.

When flexible plates under external excitation combine with an acoustic cavity, noise is transmitted into the enclosure. The active control of sound transmission into enclosures has been investigated by many researchers. Pan *et al* (1989) developed the active control of sound transmission into a rectangular cavity coupled with a test panel, which has resonance frequencies well separated from the cavity resonance frequencies, using point force actuators. They demonstrated two different control mechanisms for minimising the sound transmission through a panel into a cavity. The system response dominated by a panel-controlled mode or by cavity controlled modes can be minimised by suppressing the panel-vibration or by adjusting the panel-velocity distribution respectively. Griffin *et al* (1999) developed an approach whereby the feedback control of structural and acoustic problems in a cylinder can be described as a flexible structure response. The cylinder, representative of a space launch vehicle, was assumed in which a measure of the disturbance and a direct measurement of the sound pressure were not available. They concluded that it is possible to actively suppress radiated sound in an acoustic cavity subject to a broadband disturbance through flexible structure using structural sensing and feedback control. Al-Bassyiouni and Balachandran

(2005) investigated the active control of sound transmission through a flexible panel into an enclosure subject to an incident spherical wave using piezoelectric actuators bonded on the panel. They highlighted the general model description using a spherical wave incidence instead of a plane wave incidence.

Recent developments in sensor and actuator technologies opened new research direction to decentralised control. Centralised control systems operate with large number of error sensors and actuators via a multi-input multi-output (MIMO) controller, which is a centralised controller connecting all the sensors and actuators for specific modes. Decentralised control overcomes the shortcoming of centralised control which is that they are complex, costly and heavy. Decentralised control systems can be implemented by multiple single-input single-output (SISO) localised independent control units that may significantly mitigate computation load. Control of the structure may involve the modification of mass, stiffness and damping effects on the vibration of the structure. However for the specific case of the control of the structure the most suitable strategy is active damping, which can be obtained by feeding back from velocity sensors on the vibrating structure to control actuators [Preumont (2002)]. Elliott *et al* (2002) investigated reductions in both the kinetic energy and radiated sound power from a panel excited by a plane acoustic wave, which incorporated an array of collocated 4×4 force actuators and velocity sensors in decentralised velocity feedback control scheme. They have shown that both the kinetic energy of the panel and its transmitted sound power can be significantly reduced for an optimal value of feedback gain under the decentralised control scheme which is conditionally stable. Also, they implemented decentralised control using 16 piezoelectric actuators and 16 velocity sensors for practical purpose and compared the results with a force actuator and velocity sensor array. The resulting reduction in the kinetic energy and sound power were not as great as with the force actuators but were still worthwhile. Huang *et al* (2003) investigated an active vibration isolation system which involves electromagnetic actuators installed in parallel with each of four passive mounts between a flexible equipment structure and a base structure. Decentralised velocity feedback control was experimentally implemented and showed good control performance in the reduction of vibration of the equipment structure over a wide frequency range.

Decentralised control schemes have been also used to reduce sound transmission through a panel coupled with an acoustic cavity. Gardonio *et al* (2004) theoretically and experimentally investigated sound radiation/transmission through a smart panel, incorporating 16 closely

spaced accelerometer sensors and piezoceramic actuator transducer pairs connected by single-channel velocity feedback controllers, well coupled with a rectangular enclosure. The panel was excited by a monopole source in the cavity or by a transverse point force. The theoretical and experimental results demonstrated that for both the acoustic and force sources, good reductions of the kinetic energy of the panel and its total sound power radiation can be achieved at low frequencies for optimal control gain. Kim and Brennan (1999) investigated the feedforward control of harmonic and random sound transmission into a rectangular cavity excited by a plane acoustic wave analytically and experimentally. They configured the active control in three ways with (i) use of a single point-force actuator, (ii) use of a single acoustic piston source and (iii) simultaneous use of both a point-force actuator and an acoustic piston source. Both the acoustic and structural actuators were driven via independent controllers with the same reference signal. Also, they showed that the configuration of both acoustic and structural actuators was desirable for the active control of harmonic and random sound transmission into a coupled structural-acoustic system whose response was governed by plate and cavity-controlled modes.

The literature review has been presented in the area of the active control of sound radiation and transmission through a flexible structure into an acoustic cavity. Previous research has shown that it is possible to achieve good reduction in the structural kinetic energy of the vibrating structure and its sound radiation/transmission. However, the influence on the control effectiveness was not tackled versus a key factor characterising vibro-acoustic systems such as the degree of structural-acoustic coupling. Vibro-acoustic problems, where the structural-acoustic coupling is a key parameter, may require a robust control strategy using structural and acoustic actuators. The characteristics of the sound-pressure response in the cavity depend on the coupling mechanism and can be adjusted by varying the structural modal properties [Pan (1992)] which can be changed by cavity modes in a *strongly coupled* case and unchanged in a *weakly coupled* case [Dowell *et al* (1977)]. The previous successful control performance of decentralised control motivates the investigation on the active control of the interior sound field in a vibro-acoustic system. The vibro-acoustic system may be effectively controlled in various coupled cases by using structural and acoustic actuators driven by decentralised velocity feedback controllers.

1.3 Aim and objectives

The simplest model of a vibro-acoustic system is a one-dimensional acoustic cavity, closed at one end by a hard wall and at the other by a single-degree-of-freedom (SDOF) structure. This simple model has been used to demonstrate the physical characteristics of the coupling phenomenon. The equation of motion of a mass-spring system coupled with a one-dimensional acoustic cavity can be found in many textbooks [Richards and Mead (1968) and Fahy (2001)]. The advantages of using the geometrically simple model to develop the analysis of vibro-acoustic problems are: (i) to verify the analysis procedure in the cavity where plane waves propagate compared to the available exact solutions and (ii) to give better physical insight into the nature of vibro-acoustic problems, which can be straightforwardly extended to three-dimensional systems [Hong and Kim (1995)].

The simple model was used to evaluate the sound transmission through small cavity-backed panels at the fundamental resonance frequency [Guy and Pretlove (1973)]. Craggs and Ayorinde (1990) used the simple model to calculate the resonance frequencies of a structural-acoustic coupled system introducing the concept of *isochronism* between uncoupled structural and acoustic natural frequencies. Hong and Kim (1996) have developed the analysis method of general vibro-acoustic problems using the simple model incorporating structural damping and absorbing material on the structural driver. They demonstrated that the effects of acoustic absorbing material applied on all or part of the structure as well as structural damping elements can be handled using the simple model. Cura *et al* (1995) investigated structural-acoustic interaction in the simple model. They discussed the influence on the structural-acoustic interaction for the different parameters: the geometrical characteristics of the cavity (area of the cross-section and length), the physical quantities characterising the fluid (density and viscous damping) and the structural driver (mass, viscous damping and stiffness). Also, they concluded that the resonance frequencies of the coupled model were modified by the effect of the interaction between fluid and structure, with respect to those of the uncoupled systems. Lacour *et al* (2000) conducted experiments on the active control of enclosed sound fields in the simple model via wall impedance change. The simple model involved a primary source, vibrating harmonically with fixed velocity amplitude, at the left end and controlled impedance at the right end. The controlled acoustic impedance was implemented two ways: the first is a direct feedforward control and the second is a hybrid passive/active feedback

control with absorbing material. They concluded that the one-dimensional sound field can be successfully controlled for broadband excitation by using a hybrid feedback control method when feedforward control cannot be applied.

This thesis is mainly concerned with the passive/active control of the acoustic potential energy in a structural-acoustic coupled system under various coupled conditions: with *strong, intermediate and weak coupling*. The principles are demonstrated by controlling the acoustic potential energy in a one-dimensional finite acoustic tube driven by a single-degree-of-freedom (SDOF) structure in the three coupled cases and when the structural natural frequency is below and above the fundamental acoustic mode of a closed-closed tube respectively. Figure 1.2 shows a combined SDOF structural driver – 1D (one-dimensional) finite closed tube system where the structural driver, under an external force, excites the interior sound field in the finite closed tube surrounded by rigid walls. Compared to a general 3D (three-dimensional) model shown in figure 1.1, the SDOF structure represents the flexible structure being composed of a rigid mass M_s and a complex spring $K_s(1+j\eta_s)$ incorporated with structural damping where K_s is structural stiffness and η_s is a constant structural loss factor. In addition, the 1D finite closed tube replaces the 3D arbitrary enclosure.
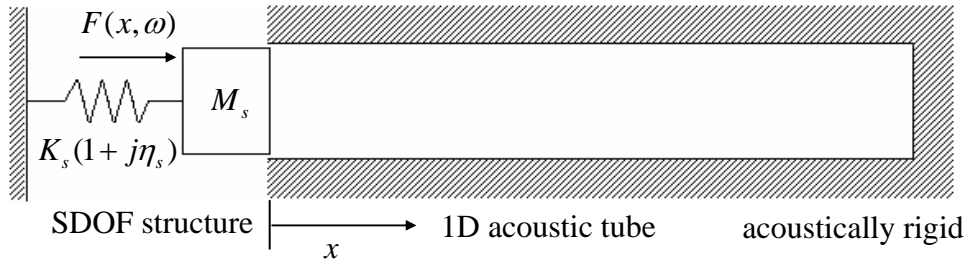
Figure 1.2 Combined single-degree-of-freedom (SDOF) structural driver – 1D (one-dimensional) finite closed tube system where the SDOF structure is under an external excitation force $F(x,\omega)$ in the x direction at frequency ω and the 1D finite closed tube is surrounded by rigid walls

This simple analytical model can provide various degrees of structural-acoustic coupling, which are dependent upon (i) the structural-acoustic stiffness ratio; (ii) structural-acoustic

natural frequency ratio; (iii) structural damping; and (iv) acoustic damping. In this case, although the geometric coupling factor is not included because the SDOF structure has a single mode, 80 percent of the factors to determine the degree of coupling can be accounted for by the simple analytical model.

The effects of the structural-acoustic coupling on the following three control strategies are investigated.

- passive control strategy - to achieve the physical insight into the relative benefits of passive control treatments such as stiffness, mass, structural damping, acoustic damping and absorptive medium
- active feedforward control - to investigate the physical behaviour of the feedforward controller minimising the acoustic potential energy in the vibro-acoustic system under harmonic excitation of the structure
- decentralised velocity feedback control - to investigate the relative control effectiveness of structural and acoustic actuators on the reduction of the acoustic potential energy in the vibro-acoustic system under broadband excitation of the structure

1.4 Contributions

The original contributions of the work reported in this thesis are

1. Provision of a non-dimensional coupling factor to determine the threshold of the degree of coupling for the dynamic behaviour of vibro-acoustic systems (Chapter 2)
2. Determination of the relative benefits of passive control treatments in various structural acoustic coupled cases through a parametric study of structural-acoustic non-dimensional parameters (Chapter 3)
3. Physical interpretation on the effectiveness of a feedforward control system discussing the control mechanism for minimising the acoustic potential energy in the vibro-acoustic system under harmonic excitation of the structure in various structural-acoustic coupled cases (Chapter 4)

4. Provision of a novel control strategy using structural and acoustic actuators in a decentralised velocity feedback control scheme for the control of the acoustic potential energy in the vibro-acoustic system under random excitation of the structure in various structural-acoustic coupled cases (Chapter 5)

1.5 Thesis structure

This thesis investigates three control strategies for the control of the acoustic potential energy in a combined single-degree-of-freedom (SDOF) structure – 1D (one-dimensional) tube system under various structural-acoustic coupled conditions: passive control (Chapter 3), feedforward control (Chapter 4) and decentralised velocity feedback control (Chapter 5). For passive control, the relative control effects of passive treatments on the acoustic potential energy are investigated based on non-dimensional structural-acoustic parameters in chapter 3. The effectiveness of a feedforward control system and a decentralised velocity feedback control system is investigated under harmonic excitation in chapter 4 and under random excitation in chapter 5 respectively for the active control of the acoustic potential energy.

In Chapter 2, the dynamic behaviour of the 1D vibro-acoustic system and structural-acoustic coupling mechanism are investigated based on the mobility-impedance approach. The dynamic behaviour is discussed for various vibro-acoustic systems such as: a semi-infinite tube, a finite-open tube and a finite-closed tube driven by a SDOF structure at one end. An arbitrary-impedance terminated tube is investigated by deriving acoustic input impedance using an impedance approach. Also, the acoustic pressure and particle velocity in the analytical model are presented in terms of non-dimensional structural-acoustic parameters. The coupling mechanism is investigated based on the mobility-impedance approach. In order to provide the threshold of the degree of coupling, a coupling factor is calculated in a combined SDOF structure – finite closed tube system. The vibro-acoustic response, in the closed tube system, is represented by the acoustic potential energy in the cavity and the kinetic energy of the structure coupled to the acoustic cavity. The vibro-acoustic responses are discussed in various coupled cases determined by the threshold of the degree of coupling.

In Chapter 3, the effects of passive treatments on the reduction of the acoustic potential energy in a simple vibro-acoustic system are investigated in various coupling cases: *strong, intermediate and weak coupling.* The simple vibro-acoustic model is configured by a one-dimensional finite-closed tube driven by a single-degree-of-freedom (SDOF) structure. The passive control of the acoustic potential energy is investigated involving structural and acoustical modifications based on structural-acoustic non-dimensional parameters: structural-acoustic stiffness ratio (stiffness), structural-acoustic natural frequency ratio (mass), structural loss factor (structural damping) and acoustic loss factor (acoustic damping). Also, the effect of absorptive medium on the reduction of the acoustic potential energy is investigated by placing it at the rigid end surface of the cavity. Experimental investigation on the acoustic potential energy in a vibro-acoustic system is carried out based on the non-dimensional structural-acoustic properties in the *more strongly coupled* case and in the *more weakly coupled* case.

In Chapter 4, the main concern is to investigate the performance of feedforward control of the acoustic potential energy in a combined SDOF structure – one dimensional acoustic tube system under the three coupled conditions discussed in chapter 3. An analytical model of the vibro-acoustic system, driven by a SDOF structure and controlled by an acoustic piston in a feedforward control scheme, is described. The control performance on the acoustic potential energy is studied by investigating the optimal feedforward controller. In order to investigate the physical mechanism of the feedforward control on the acoustic potential energy, the physical characteristics of the optimal impedance, presented by the secondary source, are discussed. When the acoustic potential energy is minimised, the feedforward control effects on the dynamic behaviour of the primary structure are discussed in terms of the kinetic energy of the structure. The quantitative feedforward control effect on the acoustic potential energy is investigated by presenting a cumulative sum of the acoustic potential energy over the frequency range of interest. Experimental validation on the control performance of the feedforward controller is carried out to validate the theoretical results.

In Chapter 5, the active velocity feedback control of the acoustic potential energy, in the simple vibro-acoustic model of interest in this thesis, is investigated under broadband disturbance in the three coupled cases discussed in chapters 3 and 4. The active velocity feedback control system is configured in three ways: using (i) an acoustic actuator, (ii) a structural actuator and (iii) both the actuators. Relative control effectiveness of the acoustic

actuator and the structural actuator, driven by velocity feedback controllers, is investigated. When the active velocity feedback control is implemented using the acoustic actuator, the optimal gain of the velocity feedback controller is determined in each coupled case when the summed acoustic potential energy, over the frequency range of interest, is minimised. When the active velocity feedback control is implemented using the structural actuator, the critical damping of the SDOF structure is used as the gain of the velocity feedback controller driving the secondary structural actuator, since the velocity feedback unit works as a *skyhook damper* and obviously stops the structure at the optimal condition. The dynamic coupling between the structural actuator and the acoustic cavity is considered to investigate the control effectiveness of the acoustic potential energy. When the decentralised velocity feedback control is implemented using both the actuators, the active damping of the acoustic actuator is optimised under the velocity feedback control implemented by the structural actuator. The velocity feedback control effect on the dynamic behaviour of the primary structure is discussed in terms of the kinetic energy of the SDOF structure coupled to the acoustic cavity. The relative control performance of the velocity feedback controllers is demonstrated in terms of the cumulative sum of the acoustic potential energy over the frequency range of interest. The best control configuration is suggested for the control of the acoustic potential energy in the various coupled cases.

CHAPTER 2

ANALYTICAL MODEL OF A ONE-DIMENSIONAL VIBRO-ACOUSTIC SYSTEM

2.1 Introduction

In this chapter a simple vibro-acoustic model, which is used extensively in this thesis, is described. The simple vibro-acoustic system consists of a finite one-dimensional acoustic tube excited by a single-degree-of-freedom (SDOF) structure at one end with arbitrary impedance at the other end. The chapter mainly concerns an investigation into the structural-acoustic coupling effects on the dynamic behaviour of the simple vibro-acoustic system based on the mobility-impedance approach. A non-dimensional coupling factor is provided to determine the threshold of the degree of structural-acoustic coupling.

Structural vibration induces acoustic wave propagation in the cavity to which the structure is connected. The analysis of the vibro-acoustic system starts from the investigation of purely structural and acoustic systems. Acoustic wave propagation in the cavity has been studied

extensively and the related wave equations have been presented in many text books for example [Kinsler e*t al* (1982) and Fahy (2001)]. They discuss the mutual structural-acoustic interaction in vibro-acoustic systems and present the physical characteristics of the systems which are dependent upon the properties of both the purely structural and acoustic systems. The analysis of vibro-acoustic systems can be simplified by using the mobility-impedance approach [Hixson (1977) and Kim and Brennan (1999)]. The concepts of mobility and impedance are exploited for the analysis of the structural-acoustic coupling in vibro-acoustic systems. The degree of coupling in vibro-acoustic systems is one of key factors to characterise the vibro-acoustic response [Dowell *et al* (1977)]. In the case when a structural natural frequency is unchanged by the acoustic pressure in the cavity such that it behaves like an *in-vacuo* structure, the acoustic pressure loading on the structure can be neglected. In another case when there is a significant change in a structural resonance frequency due to the acoustic pressure in the cavity, the dynamic behaviour of the structure is subject to the acoustic pressure loading. The former is called a *weakly coupled* case and the latter is called a *strongly coupled* case in this thesis. The physical characteristics of the coupling phenomenon can be achieved by using a simple vibro-acoustic model. The simple model makes it possible to verify the analysis procedure, in the cavity where plane waves propagate, compared to the available exact solutions. Also, the simple geometry may give better physical insight into the nature of vibro-acoustic problems, which can be straightforwardly extended to three-dimensional systems.

In this chapter, the dynamic behaviour of the simple vibro-acoustic system is investigated in the various coupled cases and when the structural natural frequency is below and above the fundamental acoustic mode of a closed-closed tube respectively. In section 2.2, the acoustic input impedance in a simple vibro-acoustic model, under SDOF structural excitation at one end and terminated by arbitrary impedance at the other end, is derived using an impedance approach. Also, the acoustic pressure and particle velocity in the analytical model are presented in terms of non-dimensional structural-acoustic parameters. In section 2.3, the coupling mechanism is investigated based on the mobility-impedance approach. In order to provide the threshold of the degree of coupling, a coupling factor is calculated in a combined SDOF structure – finite closed tube system. In section 2.4, the vibro-acoustic responses, in the closed tube system, are represented by the acoustic potential energy in the cavity and the kinetic energy of the structure coupled to the acoustic cavity. The vibro-acoustic responses are discussed in the various coupled cases determined by the threshold of the degree of

coupling with corresponding ODS (operational deflection shapes). This chapter is closed in section 2.5 with some conclusions.

2.2 Arbitrary impedance terminated system

The mutual structural-acoustic interaction in vibro-acoustic systems is determined by respective uncoupled structural and acoustic impedances. In the case when a one-dimensional tube, under structural excitation at one end, is terminated by an arbitrary impedance at the other end, the uncoupled acoustic impedance can be simply derived by using the impedance approach. The acoustic input impedance of the one-dimensional acoustic tube, terminated by an arbitrary impedance at the other end, is derived at both the ends of the tube using the impedance approach. For the comparative analysis of the vibro-acoustic system, non-dimensionalised structural-acoustic parameters are introduced. Also, the acoustic pressure and the particle velocity in the vibro-acoustic system are derived in terms of the non-dimensional parameters.

2.2.1 Acoustic input impedance using the impedance approach

Figure 2.1 depicts an acoustic pressure and particle velocity representation of a combined single-degree-of-freedom (SDOF) structure – acoustic tube system, which is subjected to an external time harmonic force on the structure $f(t) = F_0 e^{j\omega t}$ at $x = 0$ and is terminated by an arbitrary impedance Z_L at $x = L$. The acoustic pressure and the particle velocity at $x = 0$ in the tube are denoted by P_1 and U_1 respectively, and the resulting acoustic pressure and particle velocity at $x = L$ are denoted by P_2 and U_2 respectively. Also, the acoustic pressure and the particle velocity on the structure are denoted by P_S and U_S respectively, and on the arbitrary impedance are denoted by P_L and U_L respectively.
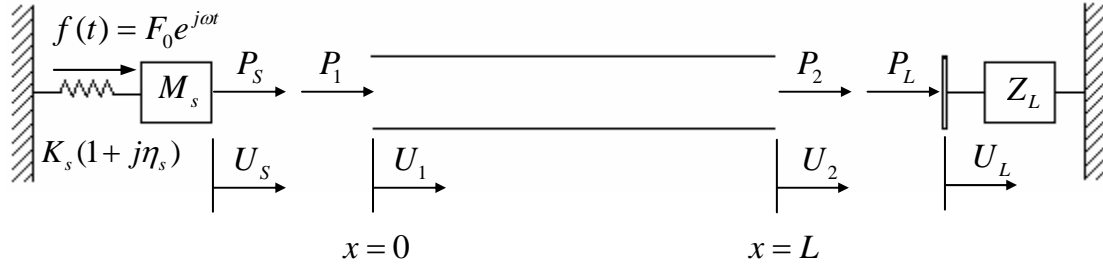
Figure 2.1 Acoustic pressure and particle velocity representation of a combined structure – acoustic tube system which is under the external time harmonic force on the structure, $f(t) = F_0 e^{j\omega t}$ at $x = 0$ and is terminated by arbitrary impedance Z_L at $x = L$. M_s and K_s are structural mass and stiffness of a spring with a constant structural loss factor η_s respectively. Also, $j = \sqrt{-1}$ and ω is a driving frequency

The SDOF structure is composed of a mass and a spring with a constant structural loss factor. The structural damping model is adopted rather than viscous damping for convenience being consistent an acoustic model. The uncoupled structural impedance can be calculated by adding up the mechanical impedances of the mass and the stiffness connected in parallel [Hixson (1977)], which is given by

$$Z_S = j\omega M_s + \frac{K_s(1 + j\eta_s)}{j\omega} \tag{2.1}$$

where Z_S is the uncoupled structural impedance of the SDOF structure, M_s is structural mass and K_s is stiffness of a spring with a constant structural loss factor η_s respectively. When considering the characteristics of the structural impedance with frequency, spring and mass effects are dominant at low frequency and at high frequency respectively. The structural system has resonance at the frequency which the reactive parts of the uncoupled structural impedance sum to zero.

The acoustic input impedance is defined by the ratio of the acoustic force to the acoustic particle velocity at the input position ($x = 0$), which is

$$Z_{A0} = \frac{SP_1}{U_1}$$
(2.2)

where Z_{A0} is the acoustic input impedance, and P_1 and U_1 are acoustic pressure and particle velocity at the input position ($x = 0$) in the tube with cross-sectional area S respectively. The acoustic input impedance defined in equation (2.2) is the uncoupled acoustic impedance of the acoustic tube depicted in figure 2.1.

The acoustic pressure at the end points of the tube can be described in terms of impedances and particle velocities, and is given by

$$SP_S = Z_S U_S$$
(2.3)

$$\begin{bmatrix} SP_1 \\ SP_2 \end{bmatrix} = \begin{bmatrix} Z_{11} & Z_{12} \\ Z_{21} & Z_{22} \end{bmatrix} \begin{bmatrix} U_1 \\ U_2 \end{bmatrix}$$
(2.4)

$$SP_L = Z_L U_L$$
(2.5)

where Z_{11}, Z_{22}, Z_{12} and Z_{21} represent point and transfer impedances of the acoustic tube with cross-sectional area S.

When the acoustic tube, depicted in figure 2.1, is terminated by the arbitrary impedance Z_L at $x = L$, $P_L = -P_2$ by equilibrium of forces, and $U_L = U_2$ by continuity of motion. The particle velocity U_2 can be calculated by combining equations (2.4) and (2.5), and is given by

$$U_2 = -\frac{Z_{21}}{Z_L + Z_{22}} U_1$$
(2.6)

The acoustic input impedance Z_{A0} at $x = 0$ can be calculated from the acoustic pressure and the particle velocity relations, given in equations (2.4) and (2.6), using the definition of the acoustic input impedance given in equation (2.2) to give

$$Z_{A0} = Z_{11} - \frac{Z_{12} Z_{21}}{Z_L + Z_{22}}$$
(2.7)

The acoustic pressure and the particle velocity in the open tube, shown in figure 2.1, take the form of two travelling waves in opposite directions, which are given by

$$P(x,\omega) = Ae^{-jkx} + Be^{jkx} \tag{2.8}$$

$$U(x,\omega) = \frac{1}{\rho_0 c}(Ae^{-jkx} - Be^{jkx}) \tag{2.9}$$

where A and B are complex wave amplitudes. Also the parameter ρ_0 is ambient density and the parameter c is a complex sound speed in the lossy acoustic medium with a constant acoustic loss factor η_a. The loss in the absorptive medium can be represented by a complex acoustic wavenumber which is defined by [Brennan and To (2001)]

$$k = \omega\left(\frac{\rho_0}{B_a(1 + j\eta_a)}\right)^{\frac{1}{2}} \tag{2.10}$$

where k is a complex acoustic wavenumber and B_a is the bulk modulus, which is pressure increase needed to cause given relative decrease in volume under uniform compression. For small acoustic loss factors, the complex acoustic wavenumber given in equation (2.10) can be rewritten as

$$k = \frac{\omega}{c} \approx \frac{\omega}{c_0}(1 - j\frac{1}{2}\eta_a) \tag{2.11}$$

where c is the complex sound speed in the lossy acoustic medium, which is approximately

$$c \approx c_0 / \left(1 - j\frac{1}{2}\eta_a\right) \tag{2.12}$$

where $c_0 = \sqrt{B_a/\rho_0}$. The real part of the complex wave number relates to the wave propagation and the imaginary part governs the wave attenuation in the acoustic medium.

The acoustic pressure and the particle velocity at $x = 0$ can be obtained by setting x to zero in equations (2.8)~(2.9) to give

$$P_1 = A + B \tag{2.13}$$

$$U_1 = \frac{1}{\rho_0 c}(A - B) \tag{2.14}$$

and the resulting acoustic pressure and particle velocity at $x = L$ are given in the same manner by

$$P_2 = (A + B)\cos kL - j(A - B)\sin kL \tag{2.15}$$

$$U_2 = \frac{1}{\rho_0 c}[(A - B)\cos kL - j(A + B)\sin kL] \tag{2.16}$$

Combining equations (2.13)~(2.16) gives the transfer matrix of the acoustic tube, which is given by [Munjal (1987)]

$$\begin{bmatrix} P_2 \\ U_2 \end{bmatrix} = \begin{bmatrix} \cos kL & -j\rho_0 c \sin kL \\ -j\sin kL / \rho_0 c & \cos kL \end{bmatrix} \begin{bmatrix} P_1 \\ U_1 \end{bmatrix} \tag{2.17}$$

Rearranging equation (2.17) gives the impedance matrix of the acoustic tube, which is

$$\begin{bmatrix} P_1 \\ P_2 \end{bmatrix} = \begin{bmatrix} \rho_0 c \dfrac{\cos kL}{j\sin kL} & -\rho_0 c \dfrac{1}{j\sin kL} \\ -\rho_0 c \dfrac{1}{j\sin kL} & \rho_0 c \dfrac{\cos kL}{j\sin kL} \end{bmatrix} \begin{bmatrix} U_1 \\ U_2 \end{bmatrix} \tag{2.18}$$

Equation (2.4) can thus be written as

$$
\begin{bmatrix} SP_1 \\ SP_2 \end{bmatrix} = \begin{bmatrix} \rho_0 cS \dfrac{\cos kL}{j \sin kL} & -\rho_0 cS \dfrac{1}{j \sin kL} \\ -\rho_0 cS \dfrac{1}{j \sin kL} & \rho_0 cS \dfrac{\cos kL}{j \sin kL} \end{bmatrix} \begin{bmatrix} U_1 \\ U_2 \end{bmatrix} \tag{2.19}
$$

Substituting the corresponding impedances in equation (2.19) into equation (2.7) gives the acoustic input impedance Z_{A0} at $x = 0$, which is given by

$$
Z_{A0} = \rho_0 cS \frac{\dfrac{Z_L}{\rho_0 cS} \cos kL + j \sin kL}{\cos kL + j \dfrac{Z_L}{\rho_0 cS} \sin kL} \tag{2.20}
$$

The general acoustic input impedance given in equation (2.20) has specific forms according to the impedance ratio $Z_L / \rho_0 cS$. When the impedance ratio $Z_L / \rho_0 cS = 1$, the acoustic input impedance Z_{A0} is that of a semi-infinite tube [Kinsler *et al* (1982)], which is

$$
Z_{A0} = \rho_0 cS \qquad \textit{semi-infinite tube} \tag{2.21}
$$

When the impedance ratio $Z_L / \rho_0 cS = 0$, the acoustic tube has an open condition at $x = L$ and the acoustic input impedance is

$$
Z_{A0} = j \rho_0 cS \frac{\sin kL}{\cos kL} \qquad \textit{open tube} \tag{2.22}
$$

Also, when the impedance ratio $Z_L / \rho_0 c_0 S$ is infinitely large, the acoustic input impedance Z_{A0} is that of a rigidly closed tube, which is

$$
Z_{A0} = -j \rho_0 cS \frac{\cos kL}{\sin kL} \qquad \textit{closed tube} \tag{2.23}
$$

The acoustic input impedance at $x = L$, Z_{AL} can be obtained simply by replacing the arbitrary impedance Z_L with the uncoupled structural impedance Z_S, and is given by

$$Z_{AL} = \rho_0 cS \frac{\dfrac{Z_S}{\rho_0 cS} \cos kL + j \sin kL}{\cos kL + j \dfrac{Z_S}{\rho_0 cS} \sin kL} \tag{2.24}$$

It can be seen that the behaviour of the impedance Z_{AL} is affected by the impedance ratio $Z_S / \rho_0 cS$. The impedance Z_{AL} is that of an open tube given in equation (2.22) in the case when the impedance ratio $Z_S / \rho_0 cS$ is extremely small, and is that of a closed tube given in equation (2.23) in the case when the impedance ratio $Z_S / \rho_0 c_0 S$ is infinitely large.

2.2.2 Non-dimensional structural-acoustic parameters

For frequency dependent structural and acoustic characteristics in the combined system depicted in figure 2.1, the parameter L/λ is defined as

$$\frac{L}{\lambda} = \frac{\omega}{c_0} \frac{L}{2\pi} \tag{2.25}$$

where L is the tube length, λ is acoustic wavelength, ω is the driving frequency and c_0 is sound speed in the lossless acoustic medium.

One of the non-dimensional parameters used to characterise the vibro-acoustic system is the structural-acoustic stiffness ratio given by

$$\frac{K_a}{K_s} = \frac{B_a S / L}{K_s} \tag{2.26}$$

where K_a is acoustic bulk stiffness, which is the acoustic stiffness of the closed tube when the structural motion is static. In addition, ρ_0 is the ambient density of the acoustic medium in the tube with cross-sectional area S.

Another important parameter is the proximity of the uncoupled structural natural frequency and the uncoupled fundamental acoustic natural frequency. The structural-acoustic natural frequency ratio is defined by

$$\frac{\omega_a}{\omega_s} = \frac{\pi c_0}{L} \sqrt{\frac{M_s}{K_s}} \tag{2.27}$$

where $\omega_a (= \pi c_0 / L)$ is the uncoupled fundamental acoustic natural frequency of a closed-closed tube when $L/\lambda = 1/2$ in equation (2.25). Also, $\omega_s (= \sqrt{K_s / M_s})$ is the uncoupled structural natural frequency.

2.2.3 Acoustic pressure and particle velocity

Acoustic pressure and particle velocity in the acoustic tube are the combination of a positive going wave and a negative going wave, which are given in equations (2.8)~(2.9). The complex wave amplitudes can be calculated by applying corresponding boundary conditions.

Since the structure and the acoustic tube share the same velocity at the input position ($x = 0$), the acoustic particle velocity at the point can be represented by the ratio of the force F_0 to the sum of the uncoupled structural impedance Z_S given in equation (2.1), and the uncoupled acoustic input impedance Z_{A0} given in equation (2.20). The particle velocity at $x = 0$, $U(0, \omega)$ is given by

$$U(0, \omega) = \frac{F_0}{Z_S + Z_{A0}} \tag{2.28}$$

On the other hand, the acoustic tube is terminated by the arbitrary impedance Z_L at $x = L$. So, the particle velocity at $x = L$, $U(L, \omega)$ is given by

$$U(L, \omega) = \frac{SP(L, \omega)}{Z_L} \tag{2.29}$$

where $P(L,\omega)$ is the acoustic pressure at $x = L$ due to the force F_0.

Substituting boundary conditions given in equations (2.28)~(2.29) into equations (2.8)~(2.9) gives complex wave amplitudes A and B, which are

$$A = \frac{\rho_0 c}{2} \frac{F_0}{Z_S + Z_{A0}} \left[1 + \frac{\dfrac{Z_L}{\rho_0 cS} \cos kL + j \sin kL}{\cos kL + j \dfrac{Z_L}{\rho_0 cS} \sin kL} \right] \tag{2.30}$$

$$B = \frac{\rho_0 c}{2} \frac{F_0}{Z_S + Z_{A0}} \left[-1 + \frac{\dfrac{Z_L}{\rho_0 cS} \cos kL + j \sin kL}{\cos kL + j \dfrac{Z_L}{\rho_0 cS} \sin kL} \right] \tag{2.31}$$

Substituting the complex wave amplitudes given in equations (2.30)~(2.31) into equations (2.8)~(2.9) gives the acoustic pressure and the particle velocity in the vibro-acoustic system depicted in figure 2.1, which are

$$P(x,\omega) = \rho_0 c \frac{F_0}{Z_S + Z_{A0}} \frac{\dfrac{Z_L}{\rho_0 cS} \cos k(L-x) + j \sin k(L-x)}{\cos kL + j \dfrac{Z_L}{\rho_0 cS} \sin kL} \tag{2.32}$$

$$U(x,\omega) = \frac{F_0}{Z_S + Z_{A0}} \frac{\cos k(L-x) + j \dfrac{Z_L}{\rho_0 cS} \sin k(L-x)}{\cos kL + j \dfrac{Z_L}{\rho_0 cS} \sin kL} \tag{2.33}$$

For general comparative analysis between structural properties and corresponding acoustic properties, it is convenient to non-dimensionalise the primary acoustic pressure and the particle velocity as follows:

$$\hat{P}(\hat{x},\hat{L}) = \frac{1}{\hat{Z}_S + \hat{Z}_{A0}} \frac{2}{2-j\eta_a} \frac{\hat{Z}_L \cos\left(\pi(2-j\eta_a)(1-\hat{x})\hat{L}\right) + j\frac{2}{2-j\eta_a}\sin\left(\pi(2-j\eta_a)(1-\hat{x})\hat{L}\right)}{\frac{2}{2-j\eta_a}\cos\left(\pi(2-j\eta_a)\hat{L}\right) + j\hat{Z}_L \sin\left(\pi(2-j\eta_a)\hat{L}\right)} \quad (2.34)$$

$$\hat{U}(\hat{x},\hat{L}) = \frac{1}{\hat{Z}_S + \hat{Z}_{A0}} \frac{\frac{2}{2-j\eta_a}\cos\left(\pi(2-j\eta_a)(1-\hat{x})\hat{L}\right) + j\hat{Z}_L \sin\left(\pi(2-j\eta_a)(1-\hat{x})\hat{L}\right)}{\frac{2}{2-j\eta_a}\cos\left(\pi(2-j\eta_a)\hat{L}\right) + j\hat{Z}_L \sin\left(\pi(2-j\eta_a)\hat{L}\right)} \quad (2.35)$$

where $\hat{P}(\hat{x},\hat{L}) = P(\hat{x},\hat{L})/P_s$, $\hat{U}(\hat{x},\hat{L}) = U(\hat{x},\hat{L})/U$, $\hat{Z}_S = Z_S/\rho_0 c_0 S$, $\hat{Z}_{A0} = Z_{A0}/\rho_0 c_0 S$, $\hat{Z}_L = Z_L/\rho_0 c_0 S$ and $\hat{L} = L/\lambda$. $\hat{x}(=x/L)$ is any normalised position along the tube. Also, P_s and U are non-dimensionalising factors for the acoustic pressure and the particle velocity, which are defined by F_0/S and $F_0/\rho_0 c_0 S$ respectively.

The normalised structural impedance $\hat{Z}_S(=Z_S/\rho_0 c_0 S)$ and the normalised acoustic impedance $\hat{Z}_{A0}(=Z_{A0}/\rho_0 c_0 S)$ in equations (2.34)~(2.35) can be written in a non-dimensional form using non-dimensional parameters given in equations (2.25)~(2.27) as

$$\hat{Z}_S = -j\frac{1-(2\hat{\omega}\hat{L})^2 + j\eta_s}{2\pi\hat{K}\hat{L}} \quad (2.36)$$

$$\hat{Z}_{A0} = \frac{2}{2-j\eta_a} \frac{\hat{Z}_L \cos\left(\pi(2-j\eta_a)\hat{L}\right) + j\frac{2}{2-j\eta_a}\sin\left(\pi(2-j\eta_a)\hat{L}\right)}{\frac{2}{2-j\eta_a}\cos\left(\pi(2-j\eta_a)\hat{L}\right) + j\hat{Z}_L \sin\left(\pi(2-j\eta_a)\hat{L}\right)} \quad (2.37)$$

where $\hat{K}(=K_a/K_s)$ is the structural-acoustic stiffness ratio and $\hat{\omega}(=\omega_a/\omega_s)$ is the structural-acoustic natural frequency ratio respectively.

2.3 Structural-acoustic coupling in a vibro-acoustic system

The vibro-acoustic response can be generally characterised by the degree of the structural-acoustic coupling. A coupling mechanism is investigated based on a conceptual representation of a vibro-acoustic system using the mobility-impedance approach. Also, a coupling factor is used to investigate the effect of the structural-acoustic parameters on the degree of coupling in a vibro-acoustic system.

2.3.1 Conceptual representation of a vibro-acoustic system

The velocity of the structure, in the combined system depicted in figure 2.1, at the input position ($x = 0$), U_S is equal to the particle velocity at the point given in equation (2.28) by continuity of motion, which can be rewritten as

$$U_S = \frac{F_0}{Z_S + Z_{A0}} \tag{2.38}$$

where Z_S is the uncoupled structural impedance and Z_{A0} is the uncoupled acoustic impedance of the tube respectively.

Figures 2.2(a) and (b) describe conceptual structural-acoustic coupled representation of the combined system, depicted in figure 2.1, at the input position ($x = 0$) in terms of uncoupled structural and acoustic impedances. The uncoupled structural impedance Z_S and uncoupled acoustic impedance Z_{A0} are connected in parallel as shown in figure 2.2(a) sharing the same velocity. The driving force F_0 is distributed between the structure and the acoustic cavity according to their impedances. The uncoupled structural impedance Z_S is the ratio of the effective force applied to the structure F_s to the velocity U_S. The uncoupled acoustic impedance Z_{A0} represents the ratio of the effective force applied to the cavity F_a to the velocity U_S as shown in figure 2.2(b).
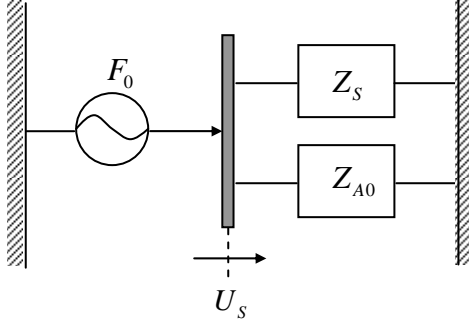
Figure 2.2(a) coupled system represented by uncoupled structural impedance Z_S and uncoupled acoustic impedance Z_{A0}
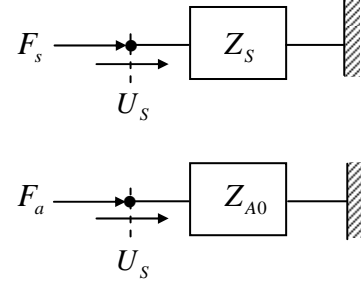
Figure 2.2(b) structural force F_s and acoustic force F_a, where the driving force $F_0 = F_s + F_a$

The structural velocity at the input position ($x = 0$), U_S given in equation (2.38) can be rewritten in terms of the uncoupled structural mobility Y_S and the uncoupled acoustic impedance Z_{A0}, which is

$$U_S = \frac{Y_S}{1 + Y_S Z_{A0}} F_0 \tag{2.39}$$

Equation (2.39) can be represented by a block diagram which has a single input force F_0 applied to the structure and a single output velocity U_S at the input position ($x = 0$) with a closed loop transfer function $Y_S / (1 + Y_S Z_{A0})$ as shown in figure 2.3. The structural velocity U_S is affected by both the uncoupled structural mobility Y_S and the uncoupled acoustic impedance Z_{A0}.
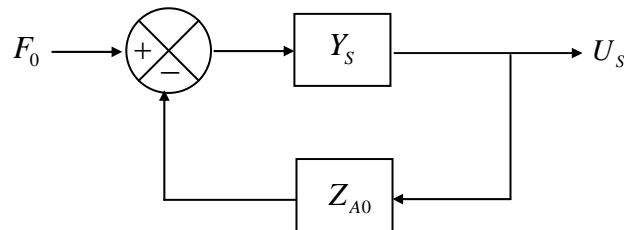
Figure 2.3 A block diagram representation of equation (2.39) where F_0 is the input force applied to the structure, U_S is output velocity at the input position ($x = 0$), Y_S is the uncoupled structural mobility and Z_{A0} is the uncoupled acoustic impedance

Equation (2.39) can be rewritten by dividing by the force F_0 to give

$$Y_{CS} = \frac{Y_S}{1 + Y_S Z_{A0}}$$
(2.40)

where Y_{CS} is the ratio of the structural velocity U_S to the force F_0 and is defined as a coupled structural mobility. The degree of the structural-acoustic coupling in the combined system is determined by the magnitude of $Y_S Z_{A0}$ defined as the *coupling factor*.

The coupled structural mobility Y_{CS} tends to the uncoupled structural mobility Y_S in the case when the modulus of the coupling factor $\left| Y_S Z_{A0} \right| << 1$. This case implies that the uncoupled acoustic impedance Z_{A0} is much smaller than the uncoupled structural impedance Z_S. The effect of the acoustic impedance on the structure is negligible and the structural response is determined only by the structural characteristics as though it is *in-vacuo*. In this case, this structural-acoustic coupled system is said to be *weakly coupled*. The coupled system, under weakly coupled condition, means physically an acoustic tube driven by a heavy and stiff structure.

In the other case when the modulus of the coupling factor $\left| Y_S Z_{A0} \right| >> 1$, the coupled structural mobility Y_{CS} is the inverse of the uncoupled acoustic impedance Z_{A0}. The response of the structure is subject to the acoustic characteristics of the tube. The structural response has peaks and troughs at the frequencies with low and high acoustic impedances respectively. This structural-acoustic coupled system is said to be *strongly coupled*. In this case, the physical system, under a strongly coupled condition, is an acoustic tube driven by a light and flexible structure.

2.3.2 Coupling factor

The degree of structural-acoustic coupling in a vibro-acoustic system can be determined by the modulus of a coupling factor as discussed in section 2.3.1. The coupling factor of a vibro-

33

acoustic system is defined by the product of the uncoupled structural mobility Y_S and uncoupled acoustic impedance Z_{A0}.

The coupling factor of the combined SDOF structure – finite closed tube system can be obtained from the uncoupled structural and acoustic impedances given in equations (2.1) and (2.23), which is

$$Y_S Z_{A0} = \rho_0 c S \frac{\omega}{K_s(1+j\eta_s) - \omega^2 M_s} \frac{\cos kL}{\sin kL} \tag{2.41}$$

Alternatively, it can be written in terms of the non-dimensional parameters given in equations (2.25)~(2.27) as

$$Y_S Z_{A0} = \hat{K}\left(\frac{2\pi\hat{L}}{1-(2\hat{\omega}\hat{L})^2 + j\eta_s}\right)\left(\frac{2}{2-j\eta_a}\frac{\cos\left(\pi(2-j\eta_a)\hat{L}\right)}{\sin\left(\pi(2-j\eta_a)\hat{L}\right)}\right) \tag{2.42}$$

The coupling factor, given in equation (2.42), is the product of three terms representing: (i) the structural-acoustic stiffness ratio, (ii) the uncoupled structural mode and (iii) the uncoupled acoustic modes in the vibro-acoustic system.

The coupling factor $Y_S Z_{A0}$ is proportional to the structural-acoustic stiffness ratio. Physically, a large stiffness ratio represents a closed tube driven by a flexible structure. In this case the structural response in the vibro-acoustic system is subject to acoustic characteristics of the closed tube under a more *strongly coupled* condition. On the other hand, a small stiffness ratio represents a closed tube driven by a stiff structure. In this case the structural response in the vibro-acoustic system is determined only by the structural characteristics under a more *weakly coupled* condition.

The modulus of the uncoupled structural mode related term given in equation (2.42) can be written as

$$\left| \frac{2\pi\hat{L}}{1-(2\hat{\omega}\hat{L})^2 + j\eta_s} \right| = \frac{2\pi\hat{L}}{\sqrt{\left(1-(2\hat{\omega}\hat{L})^2\right)^2 + \eta_s^2}} \tag{2.43}$$

The term $2\hat{\omega}\hat{L}$ in the denominator is equal to ω/ω_s, so this term depends on how close the frequency is to the structural natural frequency. The modulus in equation (2.43) has a maximum value at the structural natural frequency and thus the vibro-acoustic system becomes *more strongly coupled*. At the structural natural frequency, the modulus decreases with the structural loss factor η_s. When the structural loss factor η_s is smaller, the vibro-acoustic system is under a *more strongly coupled* condition. Otherwise, the vibro-acoustic system is under a *more weakly coupled* condition.

The cotangent term representing the uncoupled acoustic modes given in equation (2.42) can be expanded using trigonometric identities as

$$\frac{\cos\left(\pi(2-j\eta_a)\hat{L}\right)}{\sin\left(\pi(2-j\eta_a)\hat{L}\right)} = \frac{\cos(2\pi\hat{L})\cosh(\pi\eta_a\hat{L}) + j\sin(2\pi\hat{L})\sinh(\pi\eta_a\hat{L})}{\sin(2\pi\hat{L})\cosh(\pi\eta_a\hat{L}) - j\cos(2\pi\hat{L})\sinh(\pi\eta_a\hat{L})} \tag{2.44}$$

The maximum modulus of the uncoupled acoustic mode related term given in equation (2.42) can be approximately determined at $L/\lambda = n/2$ for a small acoustic loss factor η_a, which is

$$\left| \frac{2}{2-j\eta_a} \frac{\cos\left(\pi(2-j\eta_a)\hat{L}\right)}{\sin\left(\pi(2-j\eta_a)\hat{L}\right)} \right|_{max} \approx \frac{2}{\pi\eta_a n} \tag{2.45}$$

where $\sin(2\pi\hat{L}) = 0$, $\cos(2\pi\hat{L}) = \pm 1$, $\sinh(\pi\eta_a\hat{L}) \approx \pi\eta_a\hat{L}$ and $\cosh(\pi\eta_a\hat{L}) \approx 1$. It can be seen that the maximum modulus decreases with the acoustic loss factor η_a and at higher frequencies. The vibro-acoustic system is more *strongly coupled* for a smaller acoustic loss factor η_a and at lower frequencies. Otherwise, the structural-acoustic interaction in the vibro-acoustic system becomes more *weakly coupled*.

Figures 2.4(a) and (b) show the modulus of the coupling factor $Y_S Z_{A0}$, given in equation (2.42), for various values of structural-acoustic stiffness ratio K_a / K_s and natural frequency ratio ω_a / ω_s. The structural natural frequency is at $L / \lambda = 0.1$ in figure 2.4(a) and at $L / \lambda = 0.8$ in figure 2.4(b). Also, the uncoupled acoustic modes are at $L / \lambda = n / 2$ in figures 2.4(a) and (b) where n is an integer.

In one extreme case when the stiffness ratio $K_a / K_s = 10^3$, the modulus of the coupling factor is much larger than the threshold of 1 as shown in figures 2.4(a) and (b) (solid line). In this case, the vibro-acoustic system behaves like a *strongly coupled* system. When the structural natural frequency is below the fundamental acoustic mode, the degree of coupling, in figure 2.4(a), is less with frequency due to the mobility of the structural mass reducing as $1 / \omega$. Also, when the structural natural frequency is above the fundamental acoustic mode, the degree of coupling, in figure 2.4(b), is more strongly coupled with frequency up to the structural natural frequency due to the mobility of the structural stiffness increasing as ω. The degree of coupling is reduced at frequencies higher than the structural natural frequency.

In another extreme case when the stiffness ratio $K_a / K_s = 10^{-3}$, the modulus of the normalised coupling factor is much smaller than the threshold of 1 as shown in figure 2.4(a) and (b) (dashed line). In this case, the vibro-acoustic system behaves like a *weakly coupled* system. The degree of coupling shows similar behaviour with frequency for the change of the structural natural frequency.

In the intermediate case when the stiffness ratio $K_a / K_s = 1$, the vibro-acoustic system shows compounded behaviour of previous two extreme cases as shown in figure 2.4(a) and (b) (dotted line). When the structural natural frequency is below the fundamental acoustic mode, the vibro-acoustic system has a more *strongly coupled* condition at the first three peaks, which are the uncoupled structural mode at $L / \lambda = 0.1$ and the uncoupled acoustic modes at $L / \lambda = 0.5$ and at $L / \lambda = 1$ as shown in figure 2.4(a). The degree of coupling is more *weakly coupled* with frequency due to the mobility of the structural mass. Also, when the structural natural frequency is above the fundamental acoustic mode, the vibro-acoustic system is more *strongly coupled* at all the four peaks as shown in figure 2.4(b).

In summary, the degree of coupling in a vibro-acoustic system is mainly determined by the structural-acoustic stiffness ratio K_a / K_s in the two extreme cases. However, in the intermediate case, the degree of coupling is dependent on coincidence of uncoupled structural and acoustic resonances. When the structural natural frequency ω_s is close to a multiple of the acoustic fundamental natural frequency ω_a, the vibro-acoustic system becomes more *strongly coupled*. Otherwise, the vibro-acoustic system becomes more *weakly coupled*.
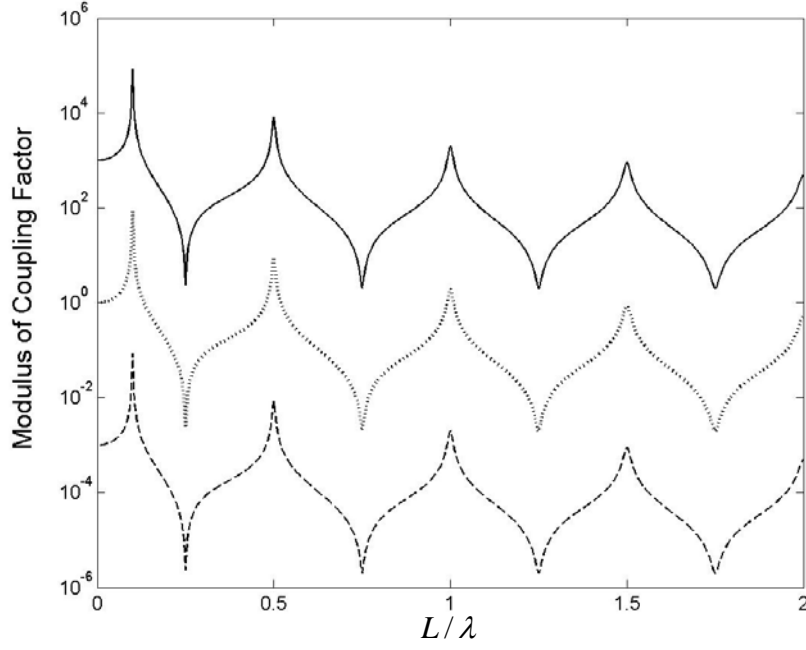
(a) *Structural natural frequency is at* $L/\lambda = 0.1$ ($\omega_a/\omega_s = 5$)
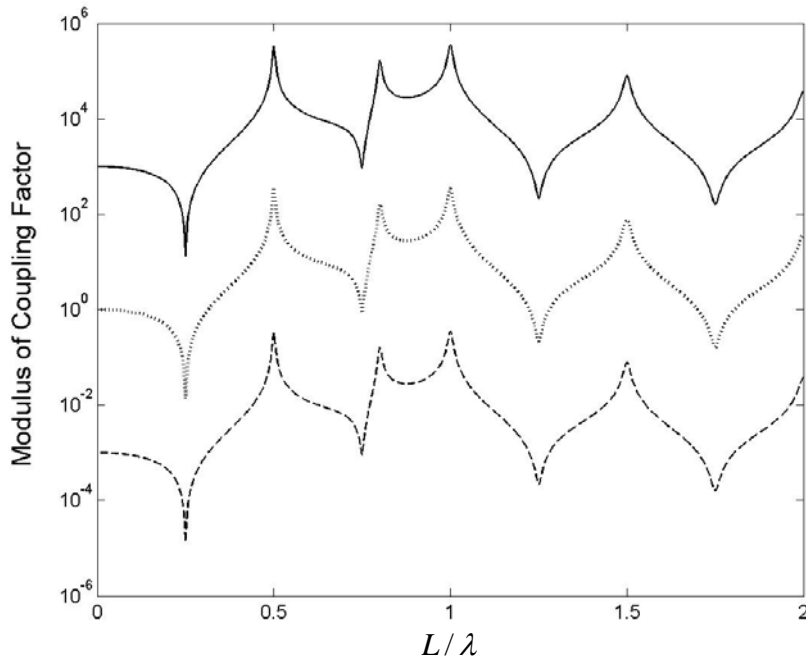
(b) *Structural natural frequency is at* $L/\lambda = 0.8$ ($\omega_a/\omega_s = 0.6$)

Figure 2.4 Modulus of a coupling factor for various structural-acoustic stiffness ratios K_a/K_s where a structural loss factor $\eta_s = 10^{-2}$ and an acoustic loss factor $\eta_a = 10^{-2}$ (solid line: $K_a/K_s = 10^3$, dashed line: $K_a/K_s = 10^{-3}$ and dotted line: $K_a/K_s = 1$)

2.4 Vibro-acoustic response in various coupled cases

In this section, the dynamic behaviour of the coupled system, depicted in figure 2.1, is discussed under various coupling conditions demonstrated in section 2.3 for the specific case of an infinitely large impedance at $x = L$. The vibro-acoustic response is represented by the acoustic potential energy in the cavity under structural excitation and the kinetic energy of the structure coupled to the cavity.

2.4.1 Acoustic potential energy in an acoustic cavity

The total time-averaged acoustic potential energy in a one-dimensional acoustic cavity is given by integrating the relevant energy density over the entire volume considered [Nelson and Elliott (1992)], which is given for the complex sound speed c by

$$E_P(\omega) = \frac{S}{4\rho_0 |c|^2} \int_0^L |P(x,\omega)|^2 dx \qquad (2.46)$$

where $E_P(\omega)$ is the acoustic potential energy and $P(x,\omega)$ is the acoustic pressure at any position in the cavity.

For the specific case of a closed tube, the acoustic pressure $P(x,\omega)$ can be written by setting the impedance ratio $Z_L / \rho_0 cS$ to infinity in equation (2.32) to give

$$P(x,\omega) = -j\rho_0 c \frac{F_0}{Z_S + Z_{A0}} \frac{\cos k(L-x)}{\sin kL} \qquad (2.47)$$

where the uncoupled acoustic impedance Z_{A0} is that of the closed tube given in equation (2.23). The acoustic pressure given in equation (2.47) can also be rewritten in terms of non-dimensional parameters. Setting $\hat{Z}_L$ to infinity in equation (2.34) gives the non-dimensional acoustic pressure in the cavity to be

$$\hat{P}(\hat{x}, \hat{L}) = -j \frac{1}{\hat{Z}_S + \hat{Z}_{A0}} \frac{2}{2 - j\eta_a} \frac{\cos\left(\pi(2 - j\eta_a)(1 - \hat{x})\hat{L}\right)}{\sin\left(\pi(2 - j\eta_a)\hat{L}\right)} \tag{2.48}$$

The normalised structural impedance $\hat{Z}_S$ is defined in equation (2.36) and the normalised acoustic input impedance $\hat{Z}_{A0}$ can be obtained by setting $\hat{Z}_L$ to infinity in equation (2.37) to give

$$\hat{Z}_{A0} = -j \frac{2}{2 - j\eta_a} \frac{\cos\left(\pi(2 - j\eta_a)\hat{L}\right)}{\sin\left(\pi(2 - j\eta_a)\hat{L}\right)} \tag{2.49}$$

Hence, the acoustic potential energy normalised by that at the static state ($\hat{L} = 0$) can be written in terms of non-dimensional parameters as

$$\hat{E}_p(\hat{L}) = \frac{\int_0^1 |\hat{P}(\hat{x}, \hat{L})|^2 d\hat{x}}{\int_0^1 |\hat{P}(\hat{x}, 0)|^2 d\hat{x}} \tag{2.50}$$

where $\hat{E}_P(\hat{L}) = E_P(\hat{L}) / E_P(0)$. The acoustic potential energies $E_P(\hat{L})$ and the acoustic potential energy at the static state ($\hat{L} = 0$), $E_P(0)$ are defined respectively by

$$E_P(\hat{L}) = \frac{S |P_s|^2}{4\rho_0 |c|^2} \int_0^1 |\hat{P}(\hat{x}, \hat{L})|^2 d\hat{x} \tag{2.51}$$

$$E_P(0) = \frac{S |P_s|^2}{4\rho_0 |c|^2} \int_0^1 |\hat{P}(\hat{x}, 0)|^2 d\hat{x} \tag{2.52}$$

The acoustic potential energy at the static state, given in equation (2.52), can be approximately calculated by setting $\hat{L} \approx 0$ into the acoustic pressure given in equation (2.48). The acoustic potential energy at the static state for small structural and acoustic loss factors is

$$E_P(0) \approx \frac{S |P_s|^2}{4\rho_0 |c|^2} \left(\frac{\hat{K}}{1 + \hat{K}}\right)^2 \tag{2.53}$$

The acoustic potential energy at the static state is determined by a structural-acoustic stiffness ratio K_a / K_s in the cavity with specific cross-sectional area S, ambient density ρ_0, complex sound speed c and the non-dimensionalising factor $P_s (= F_0 / S)$.

2.4.2 Kinetic energy of a structure coupled with an acoustic cavity

The structural velocity at the input position ($x = 0$) can be affected by the acoustic pressure in a vibro-acoustic system depending on the degree of structural-acoustic coupling. The structural kinetic energy is defined by [Meirovitch (1986)], which is

$$E_K(\omega) = \frac{1}{2} M_s \mid U_s \mid^2 \tag{2.54}$$

where $E_K(\omega)$ is the structural kinetic energy, M_s is the structural mass and U_s is the structural velocity. The structural kinetic energy can be rewritten by substituting the structural velocity given in equation (2.38) into equation (2.54) as

$$E_K(\omega) = \frac{1}{2} M_s \mid F_0 \mid^2 \left| \frac{1}{Z_S + Z_{A0}} \right|^2 \tag{2.55}$$

where F_0 is the excitation force, Z_S is the uncoupled structural impedance, and Z_{A0} is the acoustic input impedance of a closed tube given in equation (2.23). The structural kinetic energy, given in equation (2.55), can be written in a non-dimensional form as

$$\hat{E}_K(\hat{L}) = \left| \frac{1}{\hat{Z}_S + \hat{Z}_{A0}} \right|^2 \tag{2.56}$$

where $\hat{E}_K(\hat{L}) = E_K(\hat{L}) / \left(\frac{1}{2} M_s \mid F_0 / \rho_0 c_0 S \mid^2 \right)$ and $\hat{Z}_{A0} (= Z_{A0} / \rho_0 c_0 S)$ is the normalised acoustic input impedance of a closed tube given in equation (2.49).

2.4.3 Simulation results of the vibro-acoustic response

In this section, some simulation results on the acoustic potential energy, given in equation (2.50), and on the structural kinetic energy, given in equation (2.56), are presented in various coupled cases with physical interpretation. Also, the structural and acoustic ODS (Operational Deflection Shapes) are demonstrated in order to investigate their contribution to the acoustic potential energy and spatial distribution in the cavity.

Figures 2.5(a), (b) and 2.7(a), (b) show the acoustic potential energy and the structural kinetic energy in a combined structure – finite closed tube in various structural-acoustic coupled cases when the structural natural frequency is at $L/\lambda = 0.1$ and at $L/\lambda = 0.8$ respectively. The acoustic potential energy is normalised by that at the static state ($L/\lambda = 0$) in each coupled case and the structural kinetic energy is arbitrarily normalised by that at $L/\lambda = 2$. Also, figures 2.6(a), (b), (c) and 2.8(a), (b), (c) demonstrate the ODS, normalised by maximum modulus, with respect to the normalised arbitrary position x/L in various coupled cases when the structural natural frequency is at $L/\lambda = 0.1$ and at $L/\lambda = 0.8$ respectively. The structural and acoustic ODS are calculated by using the real part of the acoustic pressure in the cavity.

In the *strongly coupled* case with a structural-acoustic stiffness ratio $K_a/K_s = 10^3$, the natural frequency ratio ω_a/ω_s has a negligible effect on the vibro-acoustic responses due to insignificant structural impedance. The acoustic potential energy in the cavity has acoustic modes of an open-closed tube at $L/\lambda = (2n-1)/4$ as shown in figures 2.5(a) and 2.7(a) (solid line) where n is an integer. The minimum of the acoustic potential energy is roughly constant with frequency due to the velocity of the structural mass being controlled by the acoustic pressure in the cavity. In this case, the structure has a negligible effect on the acoustic potential energy providing an open-tube condition at $x = 0$. The kinetic energy of the structure has resonances at $L/\lambda = (2n-1)/4$ and is subject to the acoustic pressure in the cavity as shown in figures 2.5(b) and 2.7(b) (solid line). Also, the structural kinetic energy has anti-resonances at $L/\lambda = n/2$ due to the dominant acoustic input impedance in equation (2.55), which has resonances at $L/\lambda = n/2$. The acoustic potential energy, shown in figures 2.5(a) and 2.7(a) (solid line), is contributed by each acoustic mode. The acoustic potential energy is dominated by the fundamental acoustic ODS as shown in figures 2.6(a) and 2.8(a).

Also, the acoustic ODS in the acoustic potential energy have low amplitudes at the input position ($x = 0$) and high amplitudes at the end of the closed tube.

In the *weakly coupled* case with a structural-acoustic stiffness ratio $K_a / K_s = 10^{-3}$, the vibro-acoustic responses are sensitive to the natural frequency ratio ω_a / ω_s. If the structural natural frequency is at $L/\lambda = 0.1$ below the fundamental acoustic mode, the acoustic potential energy has a dominant structural mode at $L/\lambda = 0.1$ and acoustic modes of a closed-closed tube at $L/\lambda = n/2$ as shown in figure 2.5(a) (dashed line) where n is an integer. The minimum of the acoustic potential energy in the cavity reduces with frequency due to the velocity of the structural mass reducing as $1/\omega$. The kinetic energy of the structure is not affected by the acoustic pressure in the cavity as *in-vacuo* and has a resonance at $L/\lambda = 0.1$ as shown in figure 2.5(b) (dashed line). In this case, the structural ODS dominates over the acoustic potential energy but the acoustic ODS is insignificant as shown in figure 2.6(b). Also, the acoustic ODS has generally the same amplitudes at both the ends of the cavity but the structural ODS has a lower amplitude at the input position ($x = 0$) due to the rigid boundary condition at the other end.

In the *weakly coupled* case, when the structural natural frequency is at $L/\lambda = 0.8$ above the fundamental acoustic mode, the acoustic potential energy in the cavity has a structural mode at $L/\lambda = 0.8$ and acoustic modes of a closed-closed tube at $L/\lambda = n/2$ as shown in figure 2.7(a) (dashed line) where n is an integer. Also, the minimum of the acoustic potential energy increases due to the structural stiffness effect and reduces due to the structural mass effect at frequencies below and above the structural natural frequency respectively. The kinetic energy of the structure is generally determined by only the structural characteristics. However, the structural kinetic energy is affected by the acoustic pressure at $L/\lambda = 0.5$ and at $L/\lambda = 1$ as shown in figure 2.7(b) (dashed line) due to the more strongly coupled structure into the cavity caused by the less structural mass with the same stiffness compared to the case of the structural natural frequency is at $L/\lambda = 0.1$. In this case, the structural and acoustic ODS have more or less equivalent contribution to the acoustic potential energy as shown in figure 2.8(b). The spatial distribution of the ODS at both the ends of the cavity has similar trends to the case of the structural natural frequency at $L/\lambda = 0.1$.

In the *intermediate* case with a structural-acoustic stiffness ratio $K_a / K_s = 1$, the vibro-acoustic responses show different behaviour according to the natural frequency ratio ω_a / ω_s as in the *weakly coupled* case. When the structural natural frequency is at $L/\lambda = 0.1$, the acoustic potential energy has a dominant structural mode at $L/\lambda = 0.13$ and acoustic modes of a closed-closed tube mostly at $L/\lambda = n/2$ as shown in figure 2.5(a) (dotted line) where n is an integer. The structural mode is at the higher frequency than that in the *weakly coupled* case, which is due to the acoustic bulk stiffness added into the structural stiffness. The minimum of the acoustic potential energy reduces with frequency for the same reason as in the *weakly coupled* case. The structural kinetic energy has resonances at $L/\lambda = 0.13$ and at $L/\lambda = n/2$ being subject to the acoustic pressure in the cavity as shown in figure 2.5(b) (dotted line). Also, the structural kinetic energy has anti-resonances at $L/\lambda = n/2$ for the same reason as in the *strongly coupled* case. In this case, the structural and acoustic ODS in the acoustic potential energy have similar spatial distribution to those in the *weakly coupled* case as shown in figure 2.6(c).

In the *intermediate* case, when the structural natural frequency is at $L/\lambda = 0.8$, the acoustic potential energy has only acoustic modes as shown in figure 2.7(a) (dotted line) due to more strongly coupled structure. Compared to the case of the structural natural frequency at $L/\lambda = 0.1$, the structural mode has an insignificant contribution to the acoustic potential energy. The minimum of the acoustic potential energy is roughly constant for the same reason as in the *strongly coupled* case. The kinetic energy of the structure has resonances at the resonance frequencies of the acoustic pressure in the cavity as shown in figure 2.7(b). Also, the anti-resonances occur at $L/\lambda = n/2$ for the same reason as in the *strongly coupled* case. In this case, the acoustic ODS has more or less equivalent contribution to the acoustic potential energy as shown in figure 2.8(c). The acoustic ODS has low amplitudes at the input position ($x = 0$) and high amplitudes at the other end as in the *strongly coupled* case.
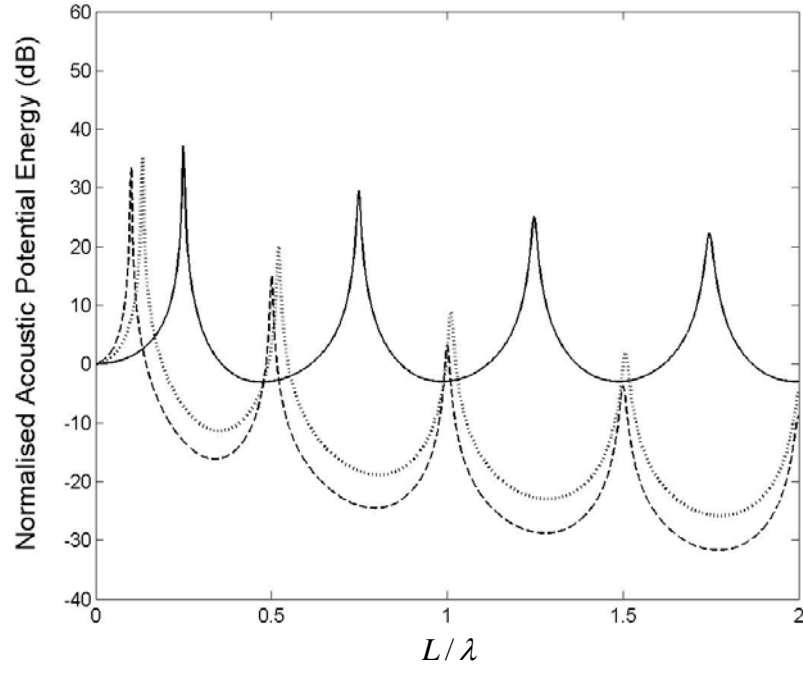
(a) Normalised acoustic potential energy
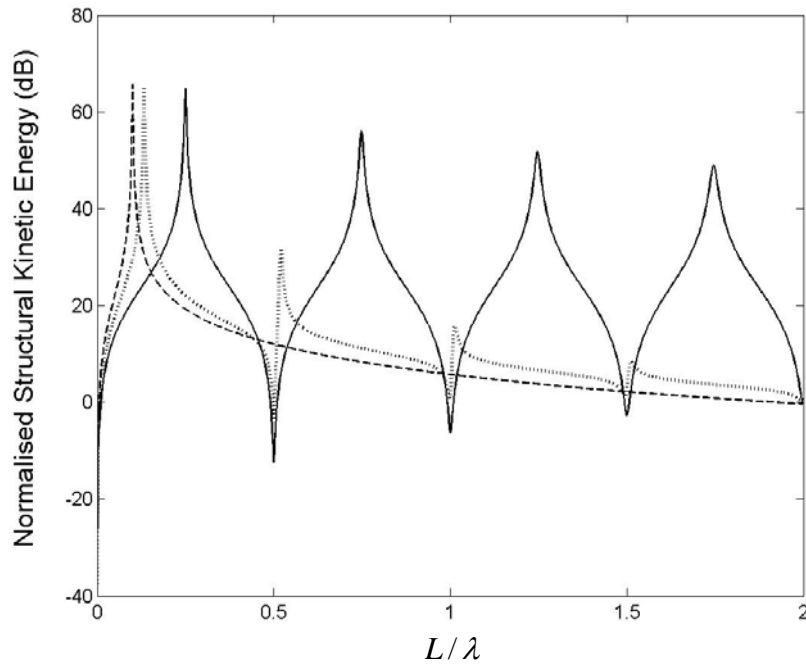
(b) Normalised structural kinetic energy

Figure 2.5 (a) acoustic potential energy normalised by that at the static state ($L/\lambda = 0$) in each coupled case (b) structural kinetic energy arbitrarily normalised by that at $L/\lambda = 2$ where the structural natural frequency is at $L/\lambda = 0.1$ ($\omega_a / \omega_s = 5$), the constant structural and acoustic loss factors $\eta_s = 10^{-2}$ and $\eta_a = 10^{-2}$ respectively (solid line: strongly coupled case with $K_a / K_s = 10^{3}$, dashed line weakly coupled case with $K_a / K_s = 10^{-3}$ and dotted line: intermediate case with $K_a / K_s = 1$)

45
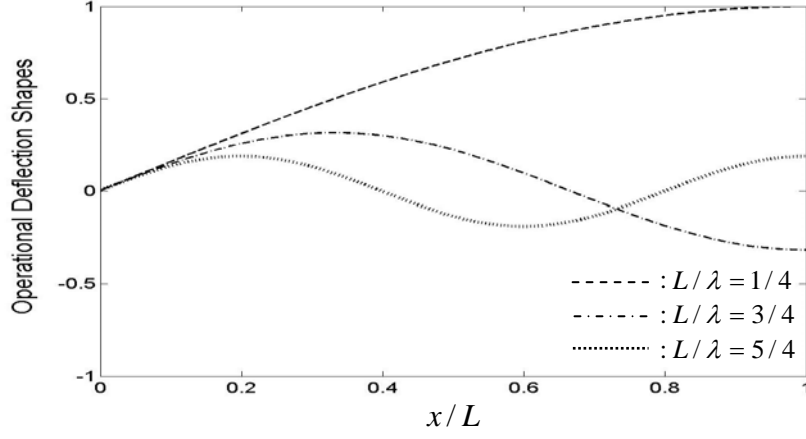
(a) Strongly coupled case
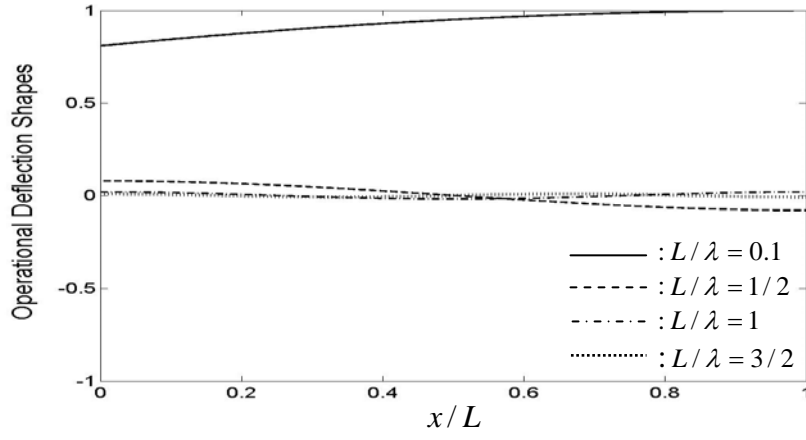
(b) Weakly coupled case
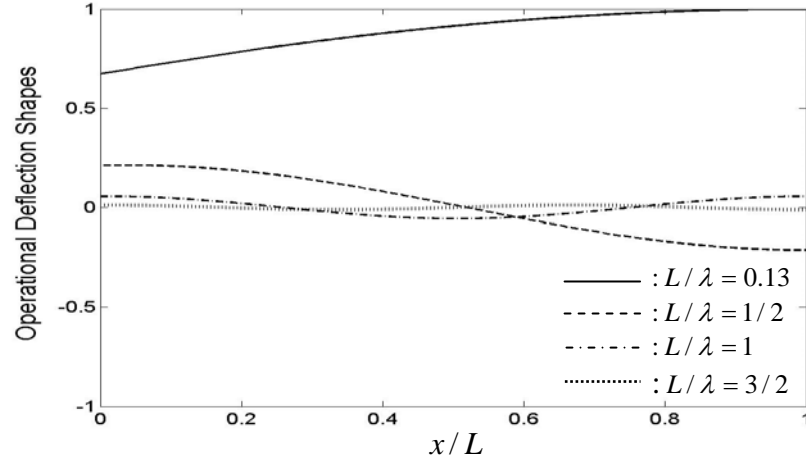
(c) Intermediate case

Figure 2.6 Operational deflection shapes of the acoustic pressure in the cavity normalised by maximum modulus: (a) strongly coupled case with $K_a / K_s = 10^3$, (b) weakly coupled case with $K_a / K_s = 10^{-3}$ and (c) intermediate case with $K_a / K_s = 1$ where the structural natural frequency is at $L / \lambda = 0.1$ ($\omega_a / \omega_s = 5$), the constant structural and acoustic loss factors $\eta_s = 10^{-2}$ and $\eta_a = 10^{-2}$ respectively
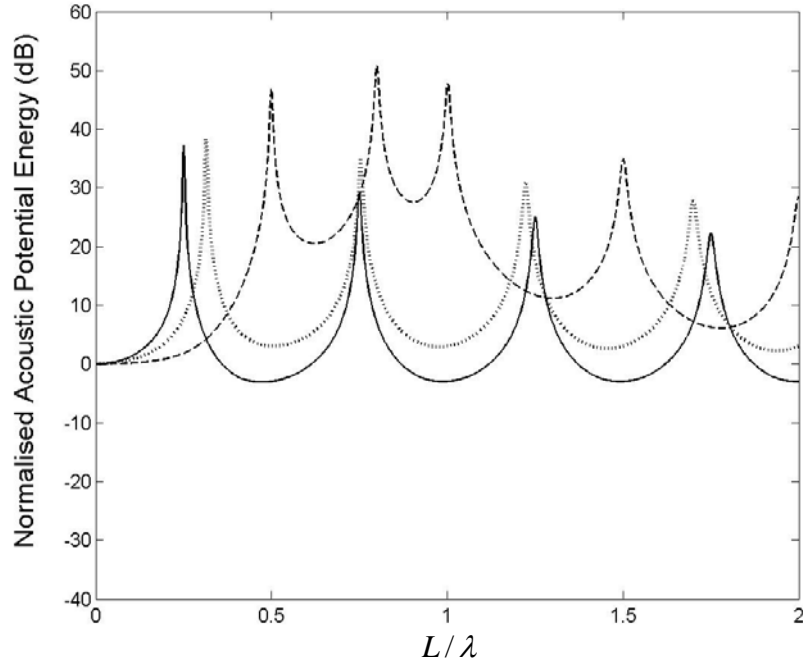
(a) Normalised acoustic potential energy
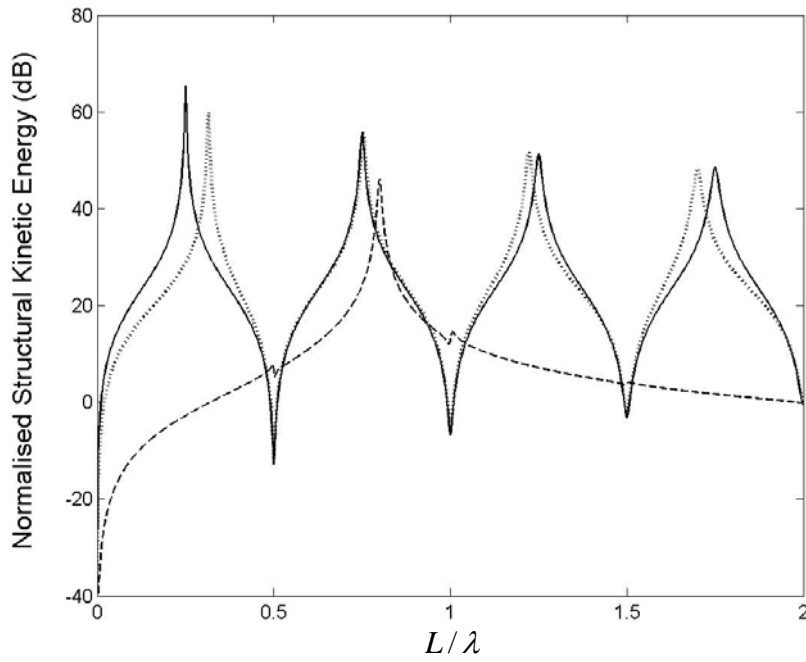
(b) Normalised structural kinetic energy

Figure 2.7 (a) acoustic potential energy normalised by that at the static state ($L/\lambda = 0$) in each coupled case (b) structural kinetic energy arbitrarily normalised by that at $L/\lambda = 2$ where the structural natural frequency is at $L/\lambda = 0.8$ ($\omega_a / \omega_s = 0.6$), the constant structural and acoustic loss factors $\eta_s = 10^{-2}$ and $\eta_a = 10^{-2}$ respectively (solid line: strongly coupled case with $K_a / K_s = 10^3$, dashed line weakly coupled case with $K_a / K_s = 10^{-3}$ and dotted line: intermediate case with $K_a / K_s = 1$)
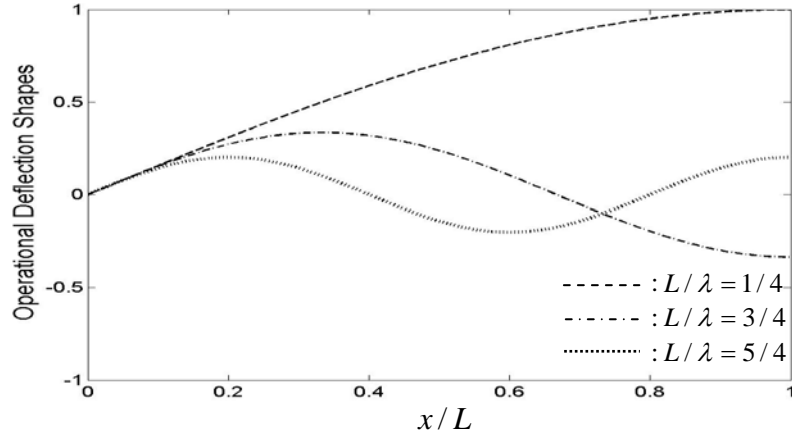
(a) Strongly coupled case
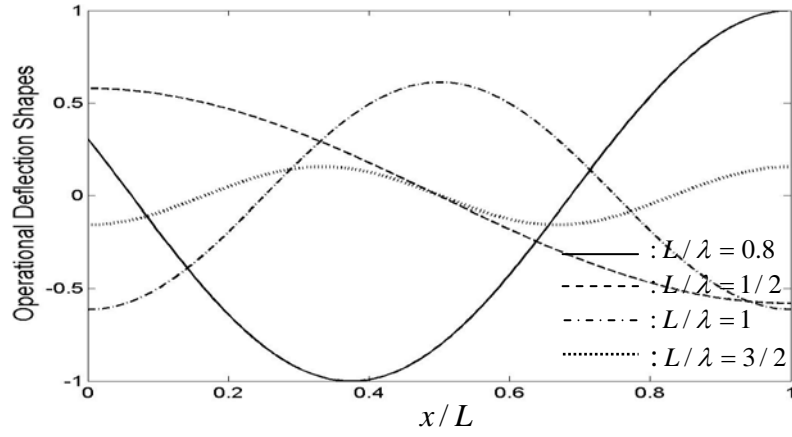
(b) Weakly coupled case
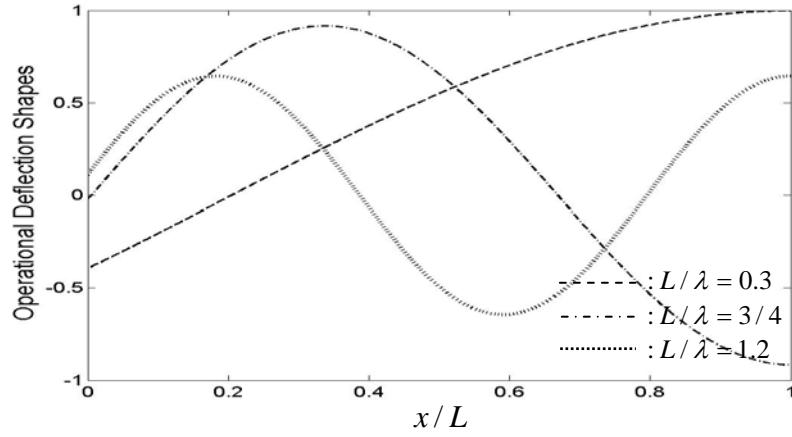
(c) Intermediate case

Figure 2.8 Operational deflection shapes of the acoustic pressure in the cavity normalised by maximum modulus: (a) strongly coupled case with $K_a / K_s = 10^3$, (b) weakly coupled case with $K_a / K_s = 10^{-3}$ and (c) intermediate case with $K_a / K_s = 1$ where the structural natural frequency is at $L/\lambda = 0.8$ ($\omega_a / \omega_s = 0.6$), the constant structural and acoustic loss factors $\eta_s = 10^{-2}$ and $\eta_a = 10^{-2}$ respectively

2.5 Conclusions

The dynamic behaviour of a simple vibro-acoustic system has been investigated in various coupled cases. The simple vibro-acoustic system consists of a finite one-dimensional acoustic tube excited by a single-degree-of-freedom (SDOF) structure at one end and terminated by an arbitrary impedance at the other end. In order to investigate the mutual structural-acoustic interaction in the vibro-acoustic system, a coupling factor has been derived for this system using the mobility-impedance approach. The dynamic behaviour of the vibro-acoustic system has been discussed by investigating the acoustic potential energy and the structural kinetic energy.

The vibro-acoustic responses can be characterised by the degree of the structural-acoustic coupling in the simple vibro-acoustic system. In the *strongly coupled* case, the acoustic potential energy has a major contribution from the acoustic modes and the structural kinetic energy is subject to the acoustic loading in the cavity. On the other hand, in the *weakly coupled* case, the acoustic potential energy is dominated by the structural mode and the structural kinetic energy is generally determined by only the structural characteristics as though it is *in-vacuo*. In this case, the structural natural frequency below the fundamental acoustic mode makes the vibro-acoustic system more *weakly coupled*. Also, in the *intermediate* case, the vibro-acoustic responses are frequency dependent and show compound behaviour of the previous two extreme cases depending on the natural frequency ratio.

The degree of structural-acoustic coupling in the simple vibro-acoustic system will be exploited for the analysis of vibro-acoustic responses in passive and active control schemes in the following chapters.

CHAPTER 3

PASSIVE CONTROL OF ACOUSTIC POTENTIAL ENERGY IN A VIBRO-ACOUSTIC SYSTEM

3.1 Introduction

This chapter considers the effects of passive control treatments on the reduction of the acoustic potential energy in a combined SDOF (single-degree-of-freedom) structure - 1D (one-dimensional) finite closed tube system. The three coupled cases, discussed in chapter 2, are studied when the structural natural frequency is below and above the fundamental acoustic mode of a closed-closed tube respectively. The passive control treatments involve structural and acoustical modifications. The structural modifications are implemented by changing structural stiffness, structural mass and structural damping. Also, the acoustical modifications are implemented by changing acoustic damping and placing absorptive medium in the cavity. When applying different media in a vibro-acoustic system, the transfer matrix relation can be used to relate the sound pressure and the particle velocity at one end of an acoustic element to those at the other end [Munjal (1987) and Song *et al* (1999)].

In section 3.2 is an investigation into the passive control of the acoustic potential energy involving structural and acoustical modifications based on structural-acoustic non-dimensional parameters: structural-acoustic stiffness ratio (stiffness), structural-acoustic natural frequency ratio (mass), structural loss factor (structural damping) and acoustic loss

factor (acoustic damping). In section 3.3, the effect of an absorptive medium on the reduction of the acoustic potential energy is investigated by placing it at the rigid end surface of the cavity. In section 3.4, an experimental investigation on the acoustic potential energy is carried out based on the non-dimensional structural-acoustic properties in the *more strongly coupled* case and in the *more weakly coupled* case. This chapter is closed in section 3.5 with some general conclusions about the effects of the passive control treatments on the reduction of the acoustic potential energy in various coupled cases.

3.2 Passive control of acoustic potential energy

Passive control treatments can be implemented by modifying stiffness, mass and damping. In this section, passive control of the acoustic potential energy, in a combined SDOF structure – finite closed tube system depicted in figure 3.1, is investigated by way of a parametric study: the effect of changing the structural-acoustic stiffness ratio K_a / K_s (stiffness), structural-acoustic natural frequency ratio ω_a / ω_s (mass), structural loss factor η_s (structural damping) and acoustic loss factor η_a (acoustic damping). The closed tube system is as depicted in figure 2.1 but with an infinitely large impedance Z_L. The effects of the structural-acoustic parameters on the acoustic potential energy are investigated for two natural frequency ratio cases, namely that the structural natural frequency is below or above the fundamental acoustic mode of a closed-closed tube. The passive control performance is evaluated by examining the summed acoustic potential energy over the frequency range ($0 \leq L / \lambda \leq 2$) for the broadband control.
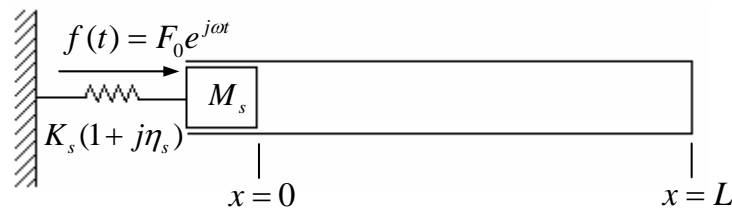
Figure 3.1 Combined SDOF structure – finite closed tube system under the external time harmonic force on the structure, $f(t) = F_0 e^{j\omega t}$ at $x = 0$. The tube has an infinitely large impedance Z_L in the analytical model depicted in figure 2.1. M_s and K_s are structural mass and stiffness of a spring with a constant structural loss factor η_s respectively.

3.2.1 Effect of changing a structural-acoustic stiffness ratio K_a / K_s
- modifying structural stiffness

The modification of the structural-acoustic stiffness ratio K_a / K_s is carried out by increasing the structural stiffness in the combined SDOF structure – finite closed tube system depicted in figure 3.1. The acoustic potential energy in the cavity, defined in equation (2.46), is calculated for a given stiffness ratio and in the case when the structural stiffness is increased by a factor of 5. Figures 3.2(a), (b), (c) and figures 3.3(a), (b), (c) show the acoustic potential energy, in the simple vibro-acoustic system, for a given stiffness ratio when the structural natural frequency is at $L / \lambda = 0.1$ and at $L / \lambda = 0.8$ respectively. The acoustic potential energy is normalised by that at the static state ($L / \lambda = 0$) for a given stiffness ratio before increasing the structural stiffness.

In the *strongly coupled* case with a structural-acoustic stiffness ratio $K_a / K_s = 10^3$, the effect of changing the structural stiffness by a factor of 5 on the acoustic potential energy is negligible for the two natural frequency ratios ω_a / ω_s as shown in figures 3.2(a) and 3.3(a). In this case, the acoustic potential energies for the two values of the structural stiffness overlap due to insignificant structural impedance.

In the *weakly coupled* case with a structural-acoustic stiffness ratio $K_a / K_s = 10^{-3}$ and the structural natural frequency at $L / \lambda = 0.1$, the structural mode at $L / \lambda = 0.1$ is effectively shifted to $L / \lambda = 0.22$ by the stiffness change and the amplitude is reduced as shown in figure 3.2(b). Also, the amplitude of the fundamental acoustic mode at $L / \lambda = 0.5$ is increased due to the proximity of the structural mode. In this case, the summed acoustic potential energy over the frequency range of interest deceases by about 7dB due to the shifted structural mode with smaller amplitude.

In the *weakly coupled* case, when the structural natural frequency is at $L / \lambda = 0.8$, the structural mode at $L / \lambda = 0.8$ is shifted to $L / \lambda = 1.8$ with smaller amplitude by the stiffness change as shown in figure 3.3(b). The fundamental and second acoustic modes are decreased due to the increased structural stiffness effect. However, the peaks at the third and fourth acoustic modes are increased due to the proximity of the structural mode. In this case, the

summed acoustic potential energy over the frequency range decreases by about 4dB. The relatively small reduction in the summed acoustic potential energy is due to the more dominating structural mode in the case when the structural natural frequency is at $L/\lambda = 0.1$ as described in the ODS (operational deflection shapes) of the acoustic pressure shown in figures 2.6(b) and 2.8(b).

In the *intermediate* case with a structural-acoustic stiffness ratio $K_a/K_s = 1$ and the structural natural frequency at $L/\lambda = 0.1$, the structural mode at $L/\lambda = 0.13$ is shifted to $L/\lambda = 0.22$ with smaller amplitude by the stiffness change as shown in figure 3.2(c). The shifted structural mode increases the fundamental acoustic mode at $L/\lambda = 0.5$ for the same reason as in the *weakly coupled* case. In this case, the summed acoustic potential energy over the frequency range decreases by about 5dB.

In the *intermediate* case, when the structural natural frequency is at $L/\lambda = 0.8$, the acoustic modes in the acoustic potential energy are shifted to higher frequencies due to the increased structural stiffness as shown in figure 3.3(c). In this case, the summed acoustic potential energy over the frequency range decreases by about 3dB. Compared to the case of the structural natural frequency at $L/\lambda = 0.1$, the relatively small reduction on the summed acoustic potential energy is due to the more strongly coupled structure, which causes only acoustic modes to feature significantly in the acoustic potential energy.

To summarise the various cases considered, the change of the structural-acoustic stiffness K_a/K_s is more effective on reducing the acoustic potential energy in the more *weakly coupled* case and when the structural natural frequency is below the fundamental acoustic mode.
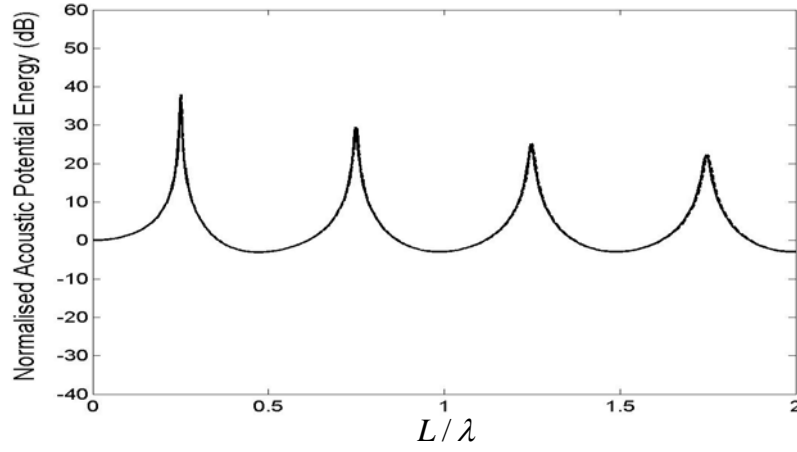
(a) Strongly coupled case ($K_a/K_s = 10^3$)
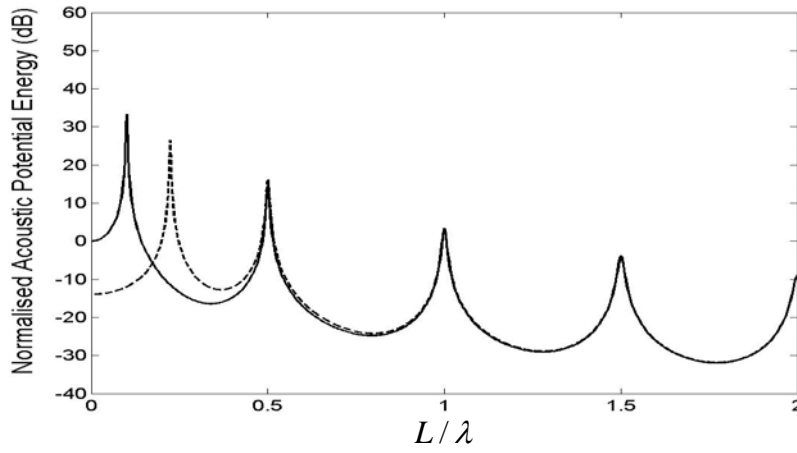
(b) Weakly coupled case ($K_a/K_s = 10^{-3}$)

(c) Intermediate case ($K_a/K_s = 1$)

Figure 3.2 Acoustic potential energy normalised by that at the static state ($L/\lambda = 0$) for a given stiffness ratio in the case when the structural stiffness is increased by a factor of 5 where the structural and acoustic loss factors $\eta_s = \eta_a = 10^{-2}$ (solid line: before increasing the structural stiffness where the structural natural frequency is at $L/\lambda = 0.1$ ($\omega_a/\omega_s = 5$), and dashed line: after increasing the structural stiffness where the structural natural frequency is at $L/\lambda = 0.22$ ($\omega_a/\omega_s = 1.1$))

(a) Strongly coupled case ($K_a / K_s = 10^3$)

(b) Weakly coupled case ($K_a / K_s = 10^{-3}$)

(c) Intermediate case ($K_a / K_s = 1$)

Figure 3.3 Acoustic potential energy normalised by that at the static state ($L/\lambda = 0$) for a given stiffness ratio in the case when the structural stiffness is increased by a factor of 5 where the structural and acoustic loss factors $\eta_s = \eta_a = 10^{-2}$ (solid line: before increasing the structural stiffness where the structural natural frequency is at $L/\lambda = 0.8$ ($\omega_a / \omega_s = 0.6$), and dashed line: after increasing the structural stiffness where the structural natural frequency is at $L/\lambda = 1.8$ ($\omega_a / \omega_s = 0.3$))

3.2.2 Effect of changing a structural-acoustic natural frequency ratio ω_a / ω_s - modifying structural mass

The modification of the structural-acoustic natural frequency ratio ω_a / ω_s is carried out by increasing the structural mass in the combined SDOF structure – finite closed tube system depicted in figure 3.1. The acoustic potential energy in the cavity is calculated for a given stiffness ratio and in the case when the structural mass is increased by a factor of 5. Figures 3.4(a), (b), (c) and figures 3.5(a), (b), (c) show the acoustic potential energy for a given stiffness ratio when the structural natural frequency is at $L/\lambda = 0.1$ and at $L/\lambda = 0.8$ respectively. The acoustic potential energy is normalised by that at the static state ($L/\lambda = 0$) for a given stiffness ratio before increasing the structural mass.

In the *strongly coupled* case with a structural-acoustic stiffness ratio $K_a / K_s = 10^3$, the effect of changing the structural mass by a factor of 5 on the acoustic potential energy is generally negligible for the two natural frequency ratios ω_a / ω_s as shown in figures 3.4(a) and 3.5(a). When the structural natural frequency is at $L/\lambda = 0.1$, the acoustic modes in the acoustic potential energy have minor shifts to lower frequencies due to the increased structural mass. The increased structural mass provides an increased structural impedance at the input position ($x = 0$). Hence, the acoustic modes of an open-closed tube at $L/\lambda = (2n-1)/4$ shift toward those of a closed-closed tube at $L/\lambda = n/2$ where n is an integer. On the other hand, when the structural natural frequency is at $L/\lambda = 0.8$, the acoustic potential energies for the two values of the structural mass overlap due to more strongly coupled structure. Under the more *strongly coupled* condition, the mass change of the structural impedance has less effect on the acoustic potential energy.

In the *weakly coupled* case with a structural-acoustic stiffness ratio $K_a / K_s = 10^{-3}$ and the structural natural frequency at $L/\lambda = 0.1$, the structural mode at $L/\lambda = 0.1$ is shifted to $L/\lambda = 0.05$ with smaller amplitude by the mass change as shown in figure 3.4(b). Also, the amplitudes of the acoustic modes at $L/\lambda = n/2$ are reduced due to the impedance of the structural mass increasing as ω where n is an integer. In this case, the summed acoustic potential energy over the frequency range of interest deceases by about 7dB due to the reduced structural and acoustic modes.

In the *weakly coupled* case, when the structural natural frequency is at $L/\lambda = 0.8$, the structural mode at $L/\lambda = 0.8$ is effectively shifted to $L/\lambda = 0.36$ with smaller amplitude by the mass change as shown in figure 3.5(b). The fundamental acoustic mode at $L/\lambda = 0.5$ has more or less the same amplitude due to the proximity of the structural mode. Also, the amplitudes of the rest of the acoustic modes are decreased for the same reason as in the case when the structural natural frequency is at $L/\lambda = 0.1$. In this case, the summed acoustic potential energy over the frequency range of interest decreases by about 9dB. The relatively large reduction in the summed acoustic potential energy is due to the more effective shift of the structural mode.

In the *intermediate* case with a structural-acoustic stiffness ratio $K_a / K_s = 1$ and the structural natural frequency at $L/\lambda = 0.1$, the structural mode at $L/\lambda = 0.13$ is shifted to $L/\lambda = 0.06$ with smaller amplitude by the mass change as shown in figure 3.4(c). The acoustic modes are shifted to those of a closed-closed tube at $L/\lambda = n/2$ due to the increased structural impedance where n is an integer. Also, the amplitudes of the acoustic modes are reduced for the same reason as in the *weakly coupled* case. In this case, the summed acoustic potential energy over the frequency range of interest decreases by about 6dB.

In the *intermediate* case, when the structural natural frequency is at $L/\lambda = 0.8$, the acoustic modes in the acoustic potential energy are shifted to lower frequencies due to the increased structural mass as shown in figure 3.5(c). The increased structural mass causes the acoustic modes to shift toward those of a closed-closed tube at $L/\lambda = n/2$ where n is an integer. Also, the further shift of higher acoustic modes is due to the impedance of the structural mass increasing as ω. In this case, the summed acoustic potential energy over the frequency range of interest decreases by about 1dB. Compared to the case of the structural natural frequency at $L/\lambda = 0.1$, the relatively small reduction in the summed acoustic potential energy is due to the more strongly coupled structure, which causes only acoustic modes to feature in the acoustic potential energy.

To summarise the various cases considered, the change of the structural-acoustic natural frequency ratio ω_a / ω_s is more effective on reducing the acoustic potential energy in the more *weakly coupled* case and when the structural natural frequency is above the fundamental acoustic mode.
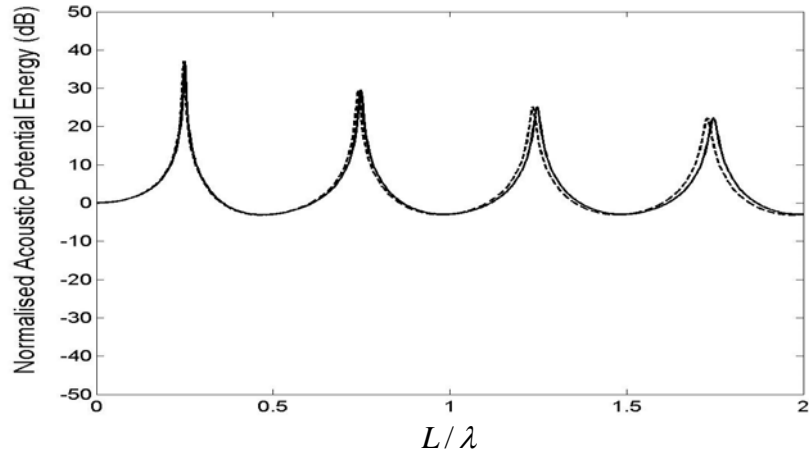
(a) Strongly coupled case ($K_a / K_s = 10^3$)
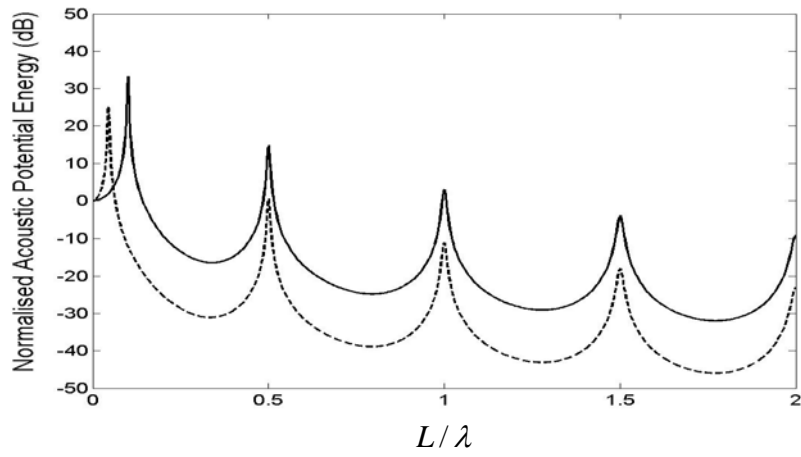
(b) Weakly coupled case ($K_a / K_s = 10^{-3}$)
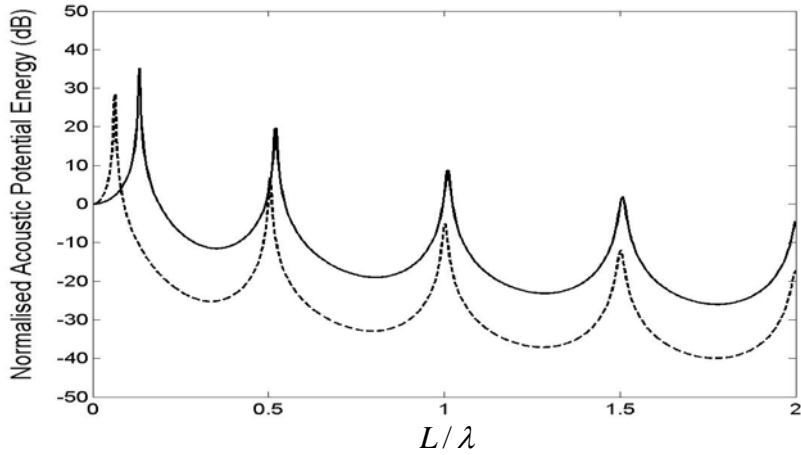
(c) Intermediate case ($K_a / K_s = 1$)

Figure 3.4 Acoustic potential energy normalised by that at the static state ($L/\lambda = 0$) for a given stiffness ratio in the case when the structural mass is increased by a factor of 5 where the structural and acoustic loss factors $\eta_s = \eta_a = 10^{-2}$ (solid line: before increasing the structural mass where the structural natural frequency is at $L/\lambda = 0.1$ ($\omega_a / \omega_s = 5$), and dashed line: after increasing the structural mass where the structural natural frequency is at $L/\lambda = 0.05$ ($\omega_a / \omega_s = 11.2$))
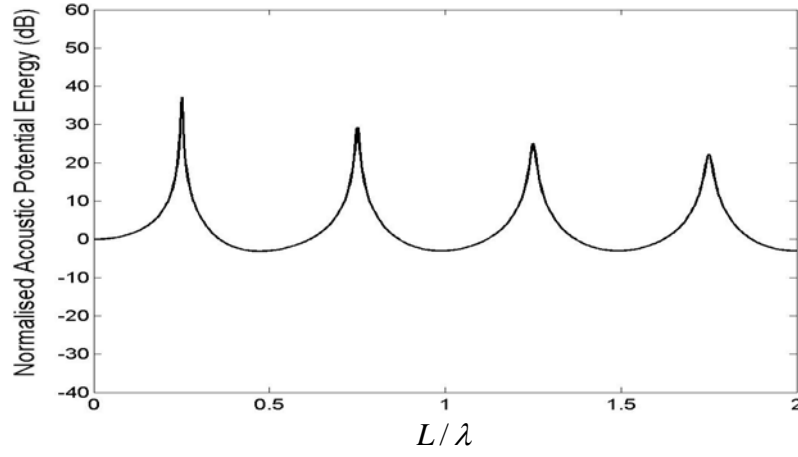
(a) Strongly coupled case ($K_a / K_s = 10^3$)
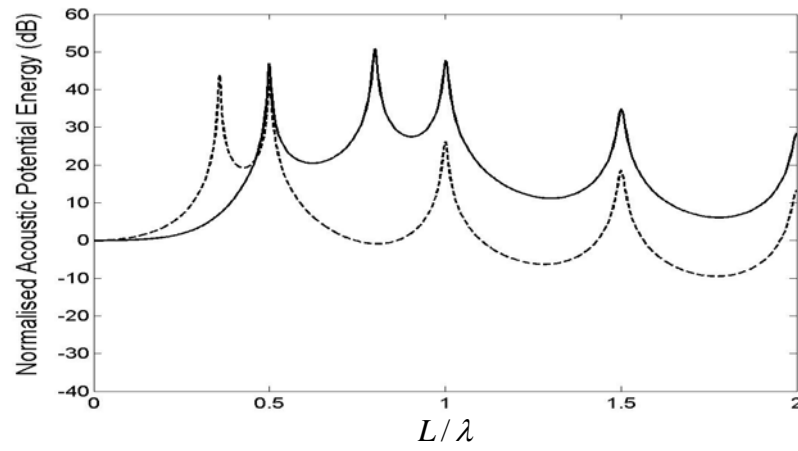
(b) Weakly coupled case ($K_a / K_s = 10^{-3}$)
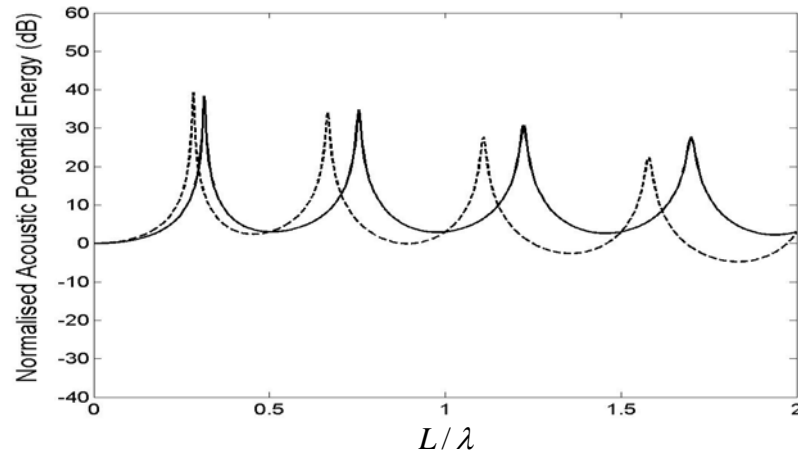
(c) Intermediate case ($K_a / K_s = 1$)

Figure 3.5 Acoustic potential energy normalised by that at the static state ($L/\lambda = 0$) for a given stiffness ratio in the case when the structural mass is increased by a factor of 5 where the structural and acoustic loss factors $\eta_s = \eta_a = 10^{-2}$ (solid line: before increasing the structural mass where the structural natural frequency is at $L/\lambda = 0.8$ ($\omega_a / \omega_s = 0.6$), and dashed line: after increasing the structural mass where the structural natural frequency is at $L/\lambda = 0.36$ ($\omega_a / \omega_s = 1.4$))

3.2.3 Effect of changing a structural loss factor η_s

- modifying structural damping

The passive treatment of structural damping is implemented by increasing the structural loss factor η_s in the combined SDOF structure – finite closed tube system depicted in figure 3.1. The acoustic potential energy in the cavity is calculated for a given stiffness ratio and in the case when the structural loss factor is increased by a factor of 5. Figures 3.6(a), (b), (c) and figures 3.7(a), (b), (c) show the acoustic potential energy for a given stiffness ratio when the structural natural frequency is at $L/\lambda = 0.1$ and at $L/\lambda = 0.8$ respectively. The acoustic potential energy is normalised by that at the static state ($L/\lambda = 0$) for a given stiffness ratio before increasing the structural loss factor.

In the *strongly coupled* case with a structural-acoustic stiffness ratio $K_a/K_s = 10^3$, the effect of increasing the structural loss factor by a factor of 5 on the acoustic potential energy is negligible for the two natural frequency ratios ω_a/ω_s as shown in figures 3.6(a) and 3.7(a). In this case, the acoustic potential energies for the two values of the structural loss factor overlap since the effect of the structural impedance is negligible.

In the *weakly coupled* case with a structural-acoustic stiffness ratio $K_a/K_s = 10^{-3}$ and the structural natural frequency at $L/\lambda = 0.1$, the structural loss factor change is effective in reducing the amplitude of the structural mode at $L/\lambda = 0.1$ as shown in figure 3.6(b). However, the acoustic modes at $L/\lambda = n/2$ are not affected by the structural loss factor change where n is an integer. In this case, the summed acoustic potential energy over the frequency range of interest deceases by about 9dB. The vibro-acoustic response, at low frequencies below the first acoustic resonance, can be explained by way of the low-frequency approximated model described in Appendix. A. The low-frequency acoustic potential energy in the cavity can be described by the stored strain energy in the acoustic spring depicted in figure A.1, which is the low-frequency approximation of the one-dimensional acoustic tube. In the case when the structural-acoustic stiffness ratio K_a/K_s is much smaller than 1, the amplitude of the strain energy is mainly subject to the structural loss factor at the resonance frequency.

In the *weakly coupled* case, when the structural natural frequency is at $L/\lambda = 0.8$, the structural mode at $L/\lambda = 0.8$ is effectively reduced as shown in figure 3.7(b). However, the structural loss factor change has insignificant effects on the acoustic modes at $L/\lambda = n/2$ where n is an integer. In this case, the summed acoustic potential energy over the frequency range of interest deceases by about 4dB. Compared to the case of the structural natural frequency at $L/\lambda = 0.1$, the structural mode is more effectively reduced due to decreased critical damping of the structure. The critical damping is proportional to square root of the product of the structural stiffness and the structural mass. In this case, the structure has less structural mass with a given structural-acoustic stiffness ratio for the higher structural natural frequency. Also, the relatively small reduction in the summed acoustic potential energy is due to the less dominant structural mode over the acoustic potential energy as described in the ODS of the acoustic pressure shown in figures 2.6(b) and 2.8(b).

In the *intermediate* case with a structural-acoustic stiffness ratio $K_a / K_s = 1$ and the structural natural frequency at $L/\lambda = 0.1$, the structural loss factor change is effective on reducing the amplitude of the structural mode at $L/\lambda = 0.13$ as shown in figure 3.6(c). However, the acoustic modes at $L/\lambda = n/2$ are not affected by the structural loss factor change for the same reason as in the *weakly coupled* case where n is an integer. In this case, the summed acoustic potential energy over the frequency range of interest decreases by about 7dB.

In the *intermediate* case, when the structural natural frequency is at $L/\lambda = 0.8$, the amplitudes of the acoustic modes in the acoustic potential energy are reduced at resonance frequencies due to the structural loss factor change as shown in figure 3.7(c). The smaller reduction of the amplitudes at higher resonance frequencies is due to the structural damping decreasing as ω. Compared to the case of the structural natural frequency at $L/\lambda = 0.1$, the acoustic pressure in the cavity is more effectively subject to the structural damping due to the more strongly coupled structure. In this case, the summed acoustic potential energy over the frequency range of interest decreases by about 4dB. The relatively small reduction in the summed acoustic potential energy is due to the more strongly coupled structure, which causes only acoustic modes in the acoustic potential energy.

To summarise the various cases considered, the change of the structural loss factor η_s is generally effective at the structural mode, but is ineffective at the acoustic modes on reduction

of the acoustic potential energy in the cavity. The summed acoustic potential energy, over the frequency range of interest, decreases more effectively in the more *weakly coupled* case and in the case when the structural natural frequency is below the fundamental acoustic mode.
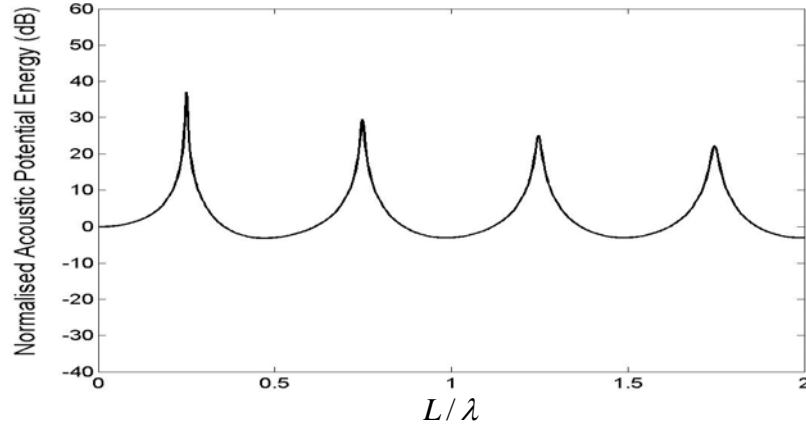
(a) Strongly coupled case ($K_a / K_s = 10^3$)
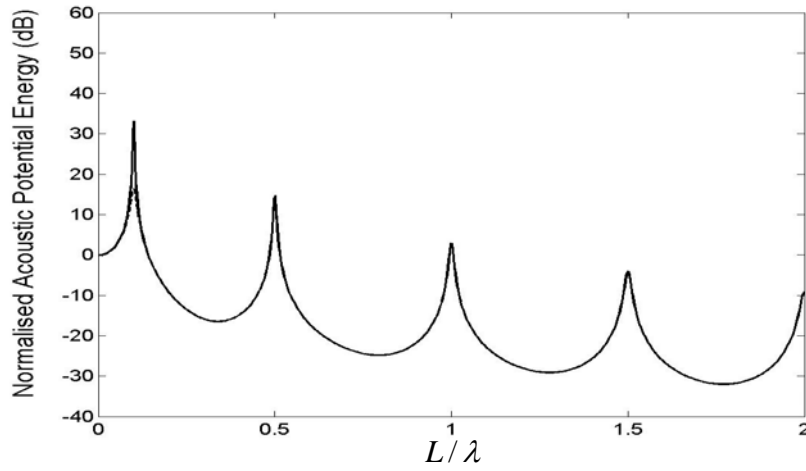
(b) Weakly coupled case ($K_a / K_s = 10^{-3}$)
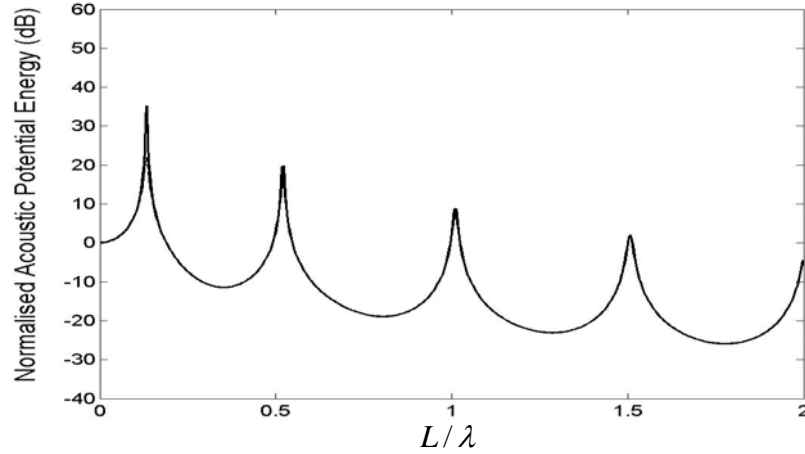
(c) Intermediate case ($K_a / K_s = 1$)

Figure 3.6 Acoustic potential energy normalised by that at the static state ($L/\lambda = 0$) for a given stiffness ratio in the case when the structural loss factor is increased by a factor of 5 where the structural natural frequency is at $L/\lambda = 0.1$ ($\omega_a / \omega_s = 5$) (solid line: before increasing the structural loss factor where the structural and acoustic loss factors $\eta_s = \eta_a = 10^{-2}$, and dashed line: after increasing the structural loss factor where the structural loss factor $\eta_s = 5 \times 10^{-2}$ and the acoustic loss factor $\eta_a = 10^{-2}$)

(a) Strongly coupled case ($K_a / K_s = 10^3$)
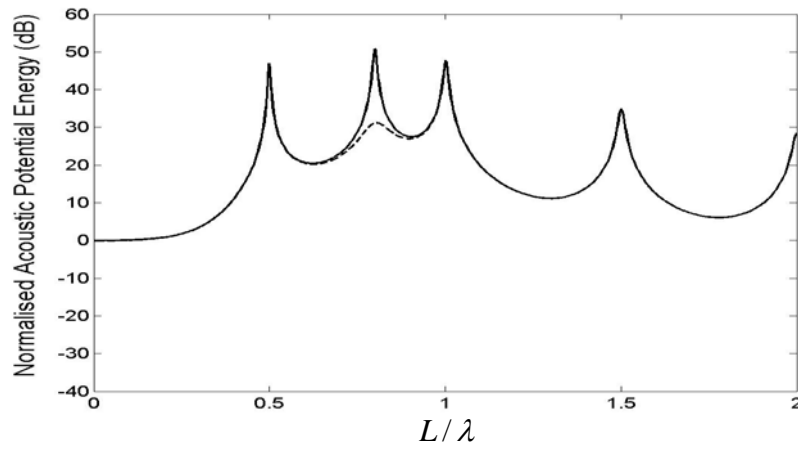
(b) Weakly coupled case ($K_a / K_s = 10^{-3}$)
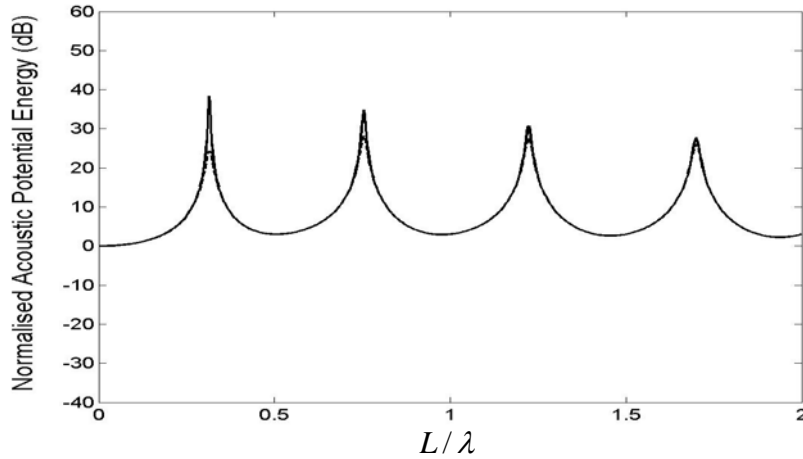
(c) Intermediate case ($K_a / K_s = 1$)

Figure 3.7 Acoustic potential energy normalised by that at the static state ($L/\lambda = 0$) for a given stiffness ratio in the case when the structural loss factor is increased by a factor of 5 where the structural natural frequency is at $L/\lambda = 0.8$ ($\omega_a / \omega_s = 0.6$) (solid line: before increasing the structural loss factor where the structural and acoustic loss factors $\eta_s = \eta_a = 10^{-2}$, and dashed line: after increasing the structural loss factor where the structural loss factor $\eta_s = 5 \times 10^{-2}$ and the acoustic loss factor $\eta_a = 10^{-2}$)

3.2.4 Effect of changing an acoustic loss factor η_a

- modifying acoustic damping

The passive treatment of acoustic damping is implemented by increasing the loss factor η_a of the acoustic medium in the combined SDOF structure – finite closed tube system depicted in figure 3.1. The acoustic potential energy in the cavity is calculated for a given stiffness ratio and in the case when the acoustic loss factor is increased by a factor of 5. Figures 3.8(a), (b), (c) and figures 3.9(a), (b), (c) show the acoustic potential energy for a given stiffness ratio when the structural natural frequency is at $L/\lambda = 0.1$ and at $L/\lambda = 0.8$ respectively. The acoustic potential energy is normalised by that at the static state ($L/\lambda = 0$) for a given stiffness ratio before increasing the acoustic loss factor.

In the *strongly coupled* case with a structural-acoustic stiffness ratio $K_a / K_s = 10^3$, the effect of changing the acoustic loss factor on the acoustic potential energy is significant for the two natural frequency ratios ω_a / ω_s as shown in figures 3.8(a) and 3.9(a). All the acoustic modes in the acoustic potential energy are effectively reduced at the resonance frequencies. The summed acoustic potential energy over the frequency range of interest decreases by about 12dB for both the natural frequency ratios.

In the *weakly coupled* case with a structural-acoustic stiffness ratio $K_a / K_s = 10^{-3}$, the acoustic loss factor change is effective only at the acoustic modes at $L/\lambda = n/2$, where n is an integer, on the reduction of the acoustic potential energy for the two natural frequency ratios ω_a / ω_s as shown in figures 3.8(b) and 3.9(b). In the case when the structural natural frequency is at $L/\lambda = 0.1$, the insignificant effect at the structural mode is due to the amplitude of the strain energy mainly subject to the structural loss factor at the resonance frequency as described in Appendix. A. The summed acoustic potential energy, over the frequency range of interest, decreases by about 0.2dB due to the insignificant effect at the dominating structural mode. Also, in the case when the structural natural frequency is at $L/\lambda = 0.8$, the summed acoustic potential energy decreases by about 4dB. The relatively large reduction in the acoustic potential energy is due to the more strongly coupled structure, which causes more dominant acoustic modes over the acoustic potential energy.

In the *intermediate* case with a structural-acoustic stiffness ratio $K_a/K_s = 1$ and the structural natural frequency at $L/\lambda = 0.1$, the acoustic potential energy is reduced effectively at the acoustic modes, i.e. at $L/\lambda = n/2$ where n is an integer as shown in figure 3.8(c). Also, the amplitude of the structural mode at $L/\lambda = 0.13$ can be reduced to some degree by the acoustic loss factor change. As discussed in the low-frequency approximated model described in Appendix. A, the amplitude of the strain energy is affected by both the structural and acoustic loss factors at the resonance frequency when the structural-acoustic stiffness ratio K_a/K_s is equal to 1. In this case, the summed acoustic potential energy over the frequency range of interest decreases by about 8dB. Also, in the case when the structural natural frequency is at $L/\lambda = 0.8$, the amplitudes of the all the acoustic modes are effectively reduced as shown in figure 3.9(c). In this case, the summed acoustic potential energy decreases by about 11dB. Compared to the case of the structural natural frequency at $L/\lambda = 0.1$, the summed acoustic potential energy is more effectively reduced for the same reason as in the *weakly coupled* case.

To summarise the various cases considered, the change of the acoustic loss factor η_a is generally effective at the acoustic modes, but is ineffective at the structural mode on reduction of the acoustic potential energy. The summed acoustic potential energy, over the frequency range of interest, decreases more effectively in the more *strongly coupled* case and in the case when the structural natural frequency is above the fundamental acoustic mode.
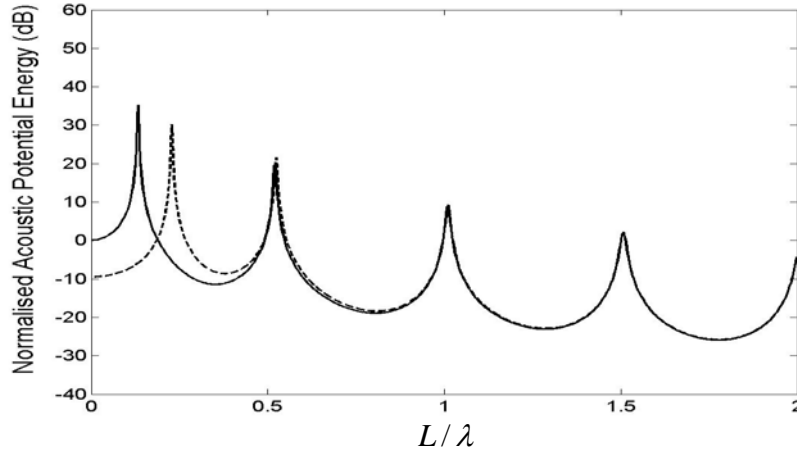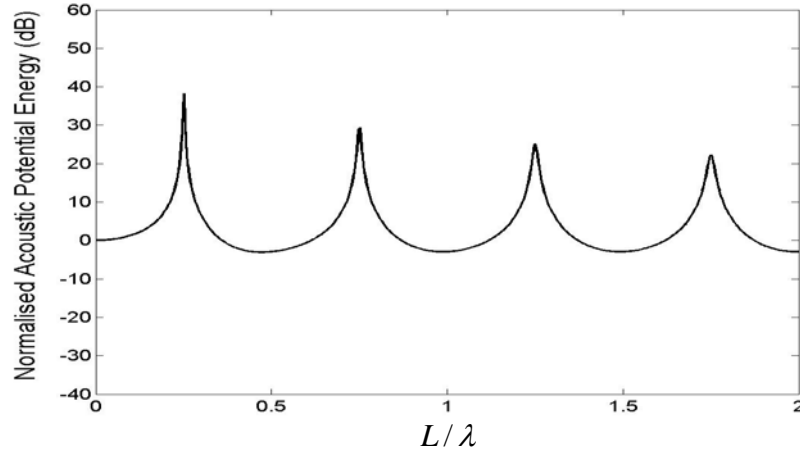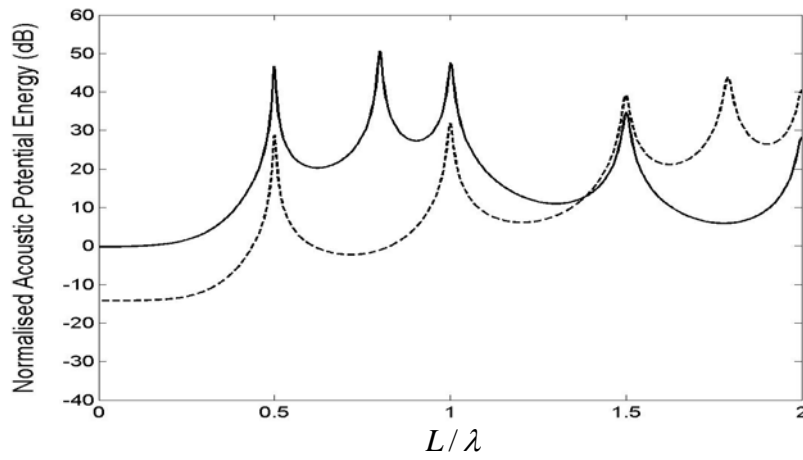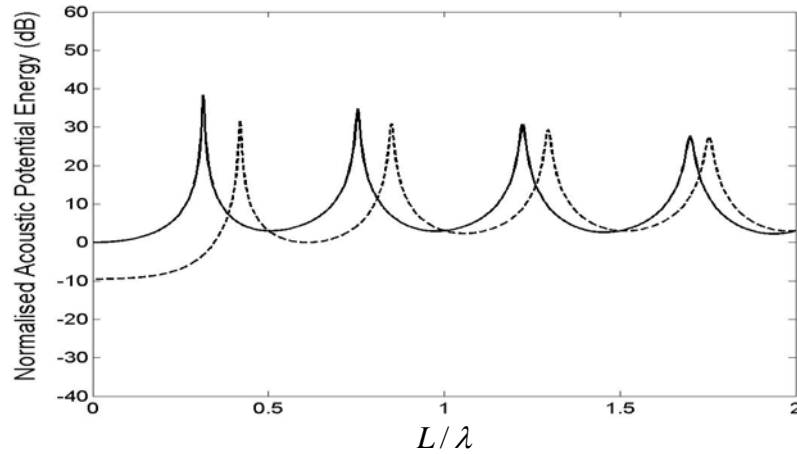
.

(a) Strongly coupled case ($K_a / K_s = 10^3$)

(b) Weakly coupled case ($K_a / K_s = 10^{-3}$)

(c) Intermediate case ($K_a / K_s = 1$)

Figure 3.8 Acoustic potential energy normalised by that at the static state ($L/\lambda = 0$) for a given stiffness ratio in the case when the acoustic loss factor is increased by a factor of 5 where the structural natural frequency is at $L/\lambda = 0.1$ ($\omega_a / \omega_s = 5$) (solid line: before increasing the acoustic loss factor where the structural and acoustic loss factors $\eta_s = \eta_a = 10^{-2}$, and dashed line: after increasing the acoustic loss factor where the acoustic loss factor $\eta_a = 5 \times 10^{-2}$ and the structural loss factor $\eta_s = 10^{-2}$)

(a) Strongly coupled case ($K_a / K_s = 10^3$)

(b) Weakly coupled case ($K_a / K_s = 10^{-3}$)

(c) Intermediate case ($K_a / K_s = 1$)

Figure 3.9 Acoustic potential energy normalised by that at the static state ($L/\lambda = 0$) for a given stiffness ratio in the case when the acoustic loss factor is increased by a factor of 5 where the structural natural frequency is at $L/\lambda = 0.8$ ($\omega_a / \omega_s = 0.6$) (solid line: before increasing the acoustic loss factor where the structural and acoustic loss factors $\eta_s = \eta_a = 10^{-2}$, and dashed line: after increasing the acoustic loss factor where the acoustic loss factor $\eta_a = 5 \times 10^{-2}$ and the structural loss factor $\eta_s = 10^{-2}$)

3.2.5 Summary of passive treatments on acoustic potential energy

In this section, the passive control of the acoustic potential energy, in the simple vibro-acoustic system depicted in figure 3.1, is summarised according to the passive treatments considered. For two values of the structural natural frequency, the comparison of the summed acoustic potential energy over the frequency range ($0 \leq L/\lambda \leq 2$), normalised by that before increasing the corresponding parameter by a factor of 5, is shown in table 3.1. The structural natural frequency is at $L/\lambda = 0.1$ ($\omega_a/\omega_s = 5$), which is below the first acoustic resonance, or is at $L/\lambda = 0.8$ ($\omega_a/\omega_s = 0.6$), which is above the first acoustic resonance for a given stiffness ratio.

In the *strongly coupled* case, the acoustical modification, involving the change of the acoustic loss factor η_a, is preferable for the reduction of the acoustic potential energy in both the cases of two values of the structural natural frequency.

In the *weakly coupled* case, the structural modification, involving the change of the stiffness ratio K_a/K_s, the natural frequency ratio ω_a/ω_s or the structural loss factor η_s, is preferable for the reduction of the acoustic potential energy. In the case when the structural natural frequency is at $L/\lambda = 0.1$, the structural loss factor η_s is more effective in reducing the acoustic potential energy. On the other hand, in the case when the structural natural frequency is at $L/\lambda = 0.8$, the change of the natural frequency ratio ω_a/ω_s is more effective in reducing the acoustic potential energy.

In the *intermediate* case, the acoustical modification, involving the change of the acoustic loss factor η_a, is preferable for the reduction of the acoustic potential energy. Also, in the case when the structural natural frequency is at $L/\lambda = 0.8$, the acoustic loss factor change has more significant effect on the reduction.

Table 3.1 Comparison of normalised summed acoustic potential energy over the frequency range ($0 \le L/\lambda \le 2$) according to the passive treatments in the case when the structural natural frequency is at $L/\lambda = 0.1$($\omega_a/\omega_s = 5$) and at $L/\lambda = 0.8$($\omega_a/\omega_s = 0.6$)

| | Natural frequency ratio | | | |
| | $\omega_a/\omega_s = 5$ / $\omega_a/\omega_s = 0.6$ | | | |
degree of coupling	stiffness ratio K_a/K_s	natural frequency ratio ω_a/ω_s	structural loss factor η_s	acoustic loss factor η_a
Strong	0 / 0	0 / 0	0 / 0	-12dB / -12dB
Weak	-7dB / -4dB	-7dB / -9dB	-9dB / -4dB	-0.2dB / -4dB
Intermediate	-5dB / -3dB	-6dB / -1dB	-7dB / -4dB	-8dB / -11dB

3.3 Passive control of acoustic potential energy using an absorptive medium

In this section, an absorptive medium is used as one of passive control treatments for the reduction of the acoustic potential energy in the simple vibro-acoustic system depicted in figure 3.1. The passive control effect is investigated for a given stiffness ratio when the structural natural frequency is at $L/\lambda = 0.1$ and at $L/\lambda = 0.8$ respectively. The absorptive medium is placed at the rigid end surface of the closed tube as shown in figure 3.10. The closed tube is composed of the acoustic medium in the region of $0 \le x \le L_0$, which has ambient density ρ_0 and complex sound speed c, and the absorptive medium in the region of $L_0 \le x \le L$, which has ambient density ρ_b and complex sound speed c_b.
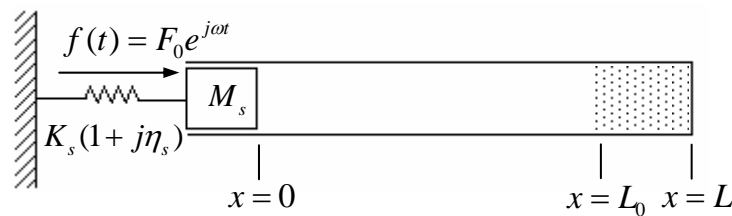
Figure 3.10 Combined SDOF structure – finite closed tube system, which has the absorptive medium at the rigid end surface of the closed tube in the region of $L_0 \le x \le L$

Sound propagation in a rigid-frame porous material is governed by the effective density and the effective bulk modulus of the fluid in the pore space. Theses quantities are frequency-dependent, complex and non-linear. Due to the complexity of these quantities, it is difficult to obtain physical insight into the acoustic behaviour. Brennan and To (2001) derived very simple expressions of the characteristic impedance and wavenumber for sound propagation in the rigid-frame porous material. The loss in the absorptive medium can be represented by a complex acoustic wavenumber as that given in equation (2.11)

$$k_b = \frac{\omega}{c_b} \approx \frac{\omega}{c_0}(1 - j\frac{1}{2}\eta_b) \qquad (3.1)$$

where k_b is the complex wavenumber in the absorptive medium. The complex sound speed in the absorptive medium c_b can be defined for small loss factors by

$$c_b \approx c_0 / \left(1 - j\frac{1}{2}\eta_b\right) \qquad (3.2)$$

where c_0 is the sound speed in lossless medium and η_b is the constant loss factor in the absorptive medium. The constant loss factor η_b in the absorptive medium is frequency-dependent in a rigid-porous frame material but is considered as a constant value in the very simple model adopted here for convenience.

The acoustic potential energy, in the simple vibro-acoustic system with two different media depicted in figure 3.10, can be calculated by summing up the acoustic potential energy in each medium, which is defined in equation (2.46), to give

$$E_p(\omega) = \frac{S}{4\rho_0 |c|^2}\int_0^{L_0} |P(x,\omega)|^2 \ dx + \frac{S}{4\rho_b |c_b|^2}\int_{L_0}^{L} |P(x,\omega)|^2 \ dx \qquad (3.3)$$

When applying different media in a vibro-acoustic system, the transfer matrix relationship can be used to relate the sound pressure and the particle velocity at one end of an acoustic element to those at the other end. The transfer matrix relationship of the simple vibro-acoustic system

with absorptive medium as shown in figure 3.10 can be written using equation (B.18) in Appendix. B as

$$\begin{bmatrix} P_1 \\ U_1 \end{bmatrix} = \begin{bmatrix} \cos kL_0 & j\rho_0 c \sin kL_0 \\ j\sin kL_0 / \rho_0 c & \cos kL_0 \end{bmatrix} \begin{bmatrix} \cos k_b L_b & j\rho_b c_b \sin k_b L_b \\ j\sin k_b L_b / \rho_b c_b & \cos k_b L_b \end{bmatrix} \begin{bmatrix} P_3 \\ U_3 \end{bmatrix} \qquad (3.4)$$

where P_1 and U_1 are the sound pressure and the particle velocity at $x = 0$ respectively, and P_3 and U_3 are the sound pressure and the particle velocity at $x = L$ respectively. Also, $k(= \omega / c)$ and $k_b(= \omega / c_b)$ are complex wave numbers in the acoustic medium with length L_0 and in the absorptive medium with length $L_b(= L - L_0)$ respectively.

The particle velocity U_3 is zero because the closed tube is rigidly terminated at $x = L$. In this case the uncoupled acoustic impedance at the input position ($x = 0$) is given by

$$Z_{A0} = S \frac{P_1}{U_1} \bigg|_{U_3 = 0} \qquad (3.5)$$

The uncoupled acoustic impedance can be rewritten by combining equation (3.4) with equation (3.5) to give

$$Z_{A0} = -j\rho_0 cS \frac{\rho_b c_b \cos kL_0 \cos k_b L_b - \rho_0 c \sin kL_0 \sin k_b L_b}{\rho_b c_b \sin kL_0 \cos k_b L_b + \rho_0 c \cos kL_0 \sin k_b L_b} \qquad (3.6)$$

If L_0 and L_b are set to L and zero respectively, then the uncoupled acoustic impedance becomes that of the closed tube without the absorptive medium given in equation (2.23).

The normalised uncoupled acoustic impedance is given in terms of non-dimensional parameters respectively by

$$\hat{Z}_{A0} = -j \frac{2}{2 - j\eta_a} \frac{\rho_b (2 - j\eta_a) \cos kL_0 \cos k_b L_b - \rho_0 (2 - j\eta_b) \sin kL_0 \sin k_b L_b}{\rho_b (2 - j\eta_a) \sin kL_0 \cos k_b L_b + \rho_0 (2 - j\eta_b) \cos kL_0 \sin k_b L_b} \qquad (3.7)$$

where $kL_0 = \pi(2 - j\eta_a)\hat{L}\hat{L}_0$, $k_b L_b = \pi(2 - j\eta_b)\hat{L}\hat{L}_b$, $\hat{L}_0 = L_0 / L$ and $\hat{L}_b = L_b / L$. Also, η_a and η_b are the constant acoustic loss factors in the acoustic medium ($0 \le x \le L_0$) and in the absorptive medium ($L_0 \le x \le L$) respectively.

The transfer matrix relationship for the sound pressure P and the particle velocity U at an arbitrary position in the acoustic medium ($0 \le x \le L_0$) in figure 3.10 is given using equation (B.20) in Appendix. B to give

$$\begin{bmatrix} P \\ U \end{bmatrix} = \begin{bmatrix} \cos kx & -j\rho_0 c \sin kx \\ -j\sin kx / \rho_0 c & \cos kx \end{bmatrix} \begin{bmatrix} P_1 \\ U_1 \end{bmatrix} \tag{3.8}$$

The sound pressure at an arbitrary position in the region of $0 \le x \le L_0$ can be written by expanding the transfer matrix in equation (3.8) to give

$$P(x, \omega) = \left(\cos kx\right) P_1 - (j\rho_0 c \sin kx) U_1 \tag{3.9}$$

The particle velocity at $x = 0$, U_1 can be written in terms of the uncoupled structural and acoustic impedances which is given in equation (2.28) and repeated here for convenience

$$U_1 = \frac{F_0}{Z_S + Z_{A0}} \tag{3.10}$$

Similarly, the sound pressure at $x = 0$, P_1 can be written using equations (3.5) and (3.10) as

$$P_1 = \frac{Z_{A0}}{Z_S + Z_{A0}} \frac{F_0}{S} \tag{3.11}$$

Substituting the particle velocity U_1 and sound pressure P_1 given in equations (3.10)~(3.11) into equation (3.9) gives the sound pressure at an arbitrary position in the acoustic medium ($0 \le x \le L_0$), which is

$$P(x,\omega) = \frac{F_0}{S} \frac{1}{Z_S + Z_{A0}} \left(Z_{A0} \cos kx - j\rho_0 cS \sin kx \right) \qquad (0 \le x \le L_0) \qquad (3.12)$$

The sound pressure given in equation (3.12) can be written in non-dimensional form as

$$\hat{P}(\hat{x},\hat{L}) = \frac{1}{\hat{Z}_{CS}} \left(\hat{Z}_{A0} \cos kx - j\frac{2}{2-j\eta_a} \sin kx \right) \qquad (3.13)$$

where $\hat{P}(\hat{x},\hat{L}) = P(\hat{x},\hat{L})/P_s$, $kx = \pi(2-j\eta_a)\hat{L}\hat{x}$, $\hat{L} = L/\lambda$ and $\hat{x}(=x/L)$ is any normalised position along the tube. The static pressure P_s is defined as the ratio of the static force F_0 to the cross-sectional area S of the closed tube.

The transfer matrix relationship for the sound pressure and the particle velocity at an arbitrary position in the absorptive medium ($L_0 \le x \le L$) in figure 3.10 is given using equation (B.22) in Appendix. B to give

$$\begin{bmatrix} P \\ U \end{bmatrix} = \begin{bmatrix} \cos k_b x & -j\rho_b c_b \sin k_b x \\ -j\sin k_b x/\rho_b c_b & \cos k_b x \end{bmatrix} \begin{bmatrix} \cos kL_0 & -j\rho_0 c \sin kL_0 \\ -j\sin kL_0/\rho_0 c & \cos kL_0 \end{bmatrix} \begin{bmatrix} P_1 \\ U_1 \end{bmatrix} \qquad (3.14)$$

The sound pressure at an arbitrary position in the region of $L_0 \le x \le L$ can be written by expanding the transfer matrix in equation (3.14) to give

$$P(x,\omega) = \left(\cos k_b x \cos kL_0 - (\rho_b c_b/\rho_0 c)\sin k_b x \sin kL_0 \right) P_1$$

$$-j\left(\rho_0 c \cos k_b x \sin kL_0 + \rho_b c_b \sin k_b x \cos kL_0 \right) U_1 \qquad (3.15)$$

Substituting the particle velocity and the sound pressure at $x = 0$ given in equations (3.10)~(3.11) into equation (3.15) gives the sound pressure at an arbitrary position in the absorptive medium ($L_0 \le x \le L$), which is

$$P(x,\omega) = \frac{F_0}{S} \frac{1}{Z_S + Z_{A0}} \left[Z_{A0} \left\{ \cos k_b x \cos kL_0 - (\rho_b c_b/\rho_0 c)\sin k_b x \sin kL_0 \right\} \right.$$

$$-j\left\{\rho_0 cS \cos k_b x \sin kL_0 + \rho_b c_b S \sin k_b x \cos kL_0\right\}\Big] \qquad (L_0 \le x \le L) \qquad (3.16)$$

The sound pressure given in equation (3.16) can be rewritten in non-dimensional form as

$$\hat{P}(\hat{x}, \hat{L}) = \frac{1}{\hat{Z}_{CS}}\left[\hat{Z}_{A0}\left\{\cos k_b x \cos kL_0 - \frac{\rho_b}{\rho_0}\frac{2-j\eta_a}{2-j\eta_b}\sin k_b x \sin kL_0\right\}\right.$$

$$\left. -j\left\{\frac{2}{2-j\eta_a}\cos k_b x \sin kL_0 + \frac{\rho_b}{\rho_0}\frac{2}{2-j\eta_b}\sin k_b x \cos kL_0\right\}\right] \qquad (3.17)$$

where, $k_b x = \pi(2-j\eta_b)\hat{L}\hat{x}$.

The acoustic potential energy given in equation (3.3) can be written in non-dimensional form as

$$\hat{E}_P(\hat{L}) = \frac{\displaystyle\int_0^{\hat{L}_0} |\hat{P}(\hat{x},\hat{L})|^2 \ d\hat{x} + \frac{\rho_0}{\rho_b}\frac{4+\eta_b^2}{4+\eta_a^2}\int_{\hat{L}_0}^1 |\hat{P}(\hat{x},\hat{L})|^2 \ d\hat{x}}{\displaystyle\int_0^1 |\hat{P}(\hat{x},0)|^2 \ d\hat{x}} \qquad (3.18)$$

where $\hat{E}_P(\hat{L}) = E_P(\hat{L})/E_P(0)$. $E_P(0)$ is the acoustic potential energy in the absence of control defined in equation (2.52) and the acoustic potential energy $E_P(\hat{L})$ is defined by

$$E_P(\hat{L}) = \frac{S|P_s|^2}{4\rho_0 |c|^2}\int_0^{\hat{L}_0} |\hat{P}(\hat{x},\hat{L})|^2 \ d\hat{x} + \frac{S|P_s|^2}{4\rho_b |c_b|^2}\int_{\hat{L}_0}^1 |\hat{P}(\hat{x},\hat{L})|^2 \ d\hat{x} \qquad (3.19)$$

Figures 3.11(a), (b), (c) and figures 3.12(a), (b), (c) show the acoustic potential energy for a given stiffness ratio when the structural natural frequency is at $L/\lambda = 0.1$ and at $L/\lambda = 0.8$ respectively. The acoustic potential energy is normalised by that at the static state ($L/\lambda = 0$) for a given stiffness ratio without the absorptive medium.

In the *strongly coupled* case with a structural-acoustic stiffness ratio $K_a/K_s = 10^3$, the effect of the absorptive medium on the acoustic potential energy is significant for the two natural frequency ratios ω_a/ω_s as shown in figures 3.11(a) and 3.12(a). All the acoustic modes are effectively reduced at the resonance frequencies. The summed acoustic potential energy over the frequency range of interest decreases by about 9dB in the case of both the natural frequency ratios.

In the *weakly coupled* case with a structural-acoustic stiffness ratio $K_a/K_s = 10^{-3}$, the absorptive medium is effective only at the acoustic modes at $L/\lambda = n/2$, where n is an integer, for both the natural frequency ratios ω_a/ω_s as shown in figures 3.11(b) and 3.12(b). In the case when the structural natural frequency is at $L/\lambda = 0.1$, the structural mode at $L/\lambda = 0.1$ is not affected by the absorptive medium in the cavity. The summed acoustic potential energy, over the frequency range of interest, decreases by about 0.1dB due to the insignificant effect at the dominating structural mode. Also, in the case when the structural natural frequency is at $L/\lambda = 0.8$, the summed acoustic potential energy decreases by about 3dB. The relatively large reduction on the summed acoustic potential energy is due to the more dominating structural mode in the case when the structural natural frequency is at $L/\lambda = 0.1$ as discussed in section 3.2.

In the *intermediate* case with a structural-acoustic stiffness ratio $K_a/K_s = 1$ and the structural natural frequency at $L/\lambda = 0.1$, the acoustic potential energy is reduced effectively at the acoustic modes at $L/\lambda = n/2$ where n is an integer as shown in figure 3.11(c). Also, the amplitude of the structural mode at $L/\lambda = 0.13$ can be reduced to some degree by the absorptive medium in the cavity. In this case, the summed acoustic potential energy, over the frequency range of interest, decreases by about 5dB. Also, in the case when the structural natural frequency is at $L/\lambda = 0.8$, the amplitudes of the all the acoustic modes are effectively reduced by the absorptive medium as shown in figure 3.12(c). In this case, the summed acoustic potential energy decreases by about 8dB. The relatively large reduction on the summed acoustic potential energy is due to the more strongly coupled structure as discussed in section 3.2.

To summarise the various cases considered, the effect of the absorptive medium, placed at the rigid end surface of the closed tube, on reduction of the acoustic potential energy is similar to that of changing the acoustic loss factor discussed in section 3.2.4. The absorptive medium in the cavity is generally effective at the frequencies where the acoustic modes dominate the acoustic response, but is ineffective at the structural mode for the reduction of the acoustic potential energy. The summed acoustic potential energy, over the frequency range of interest, decreases more in the more *strongly coupled* case and in the case when the structural natural frequency is above the fundamental acoustic mode.
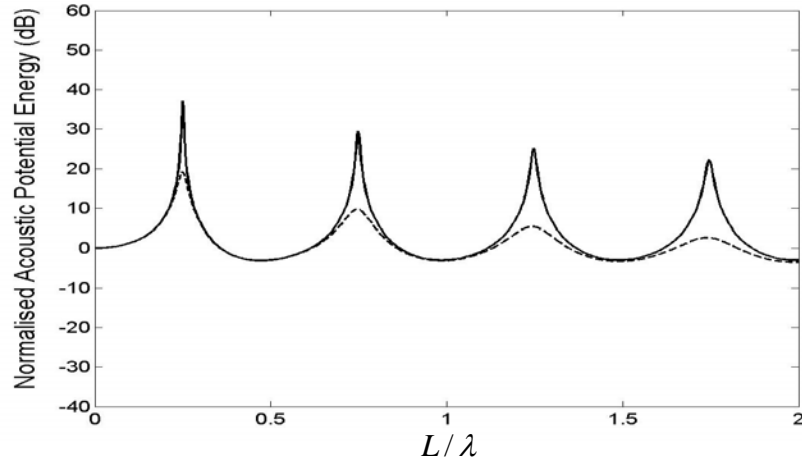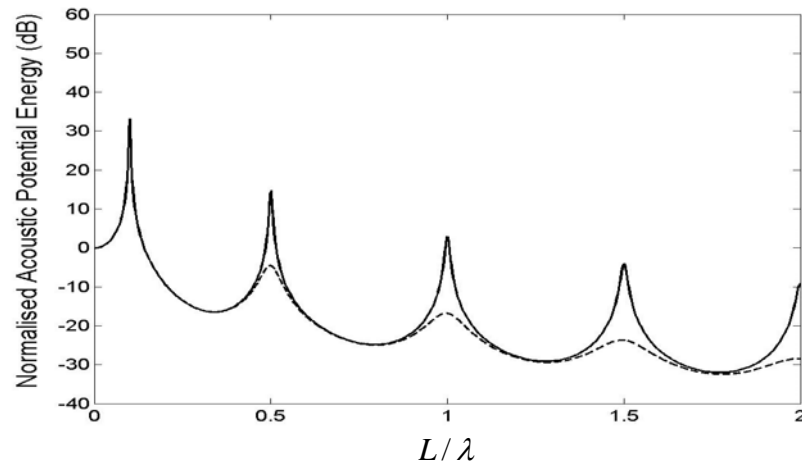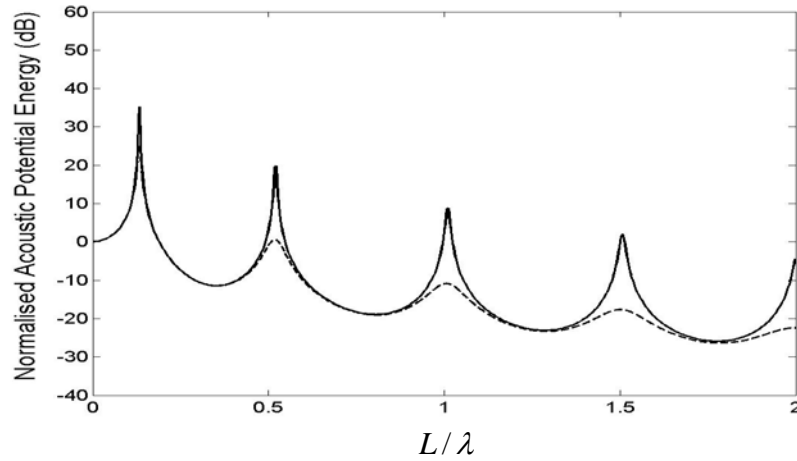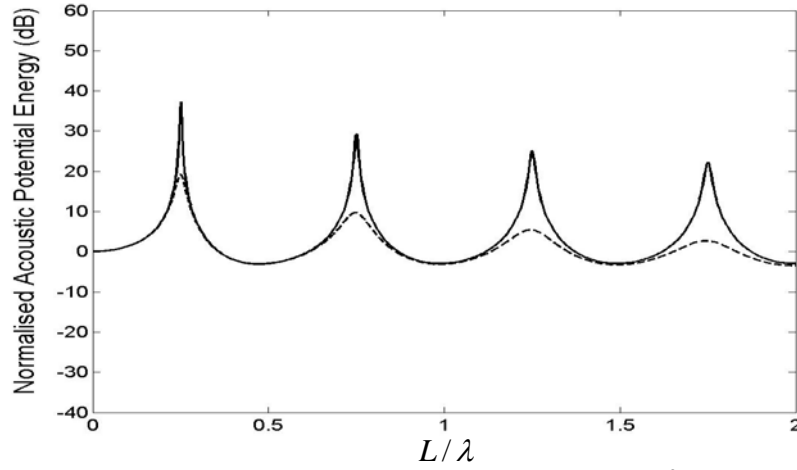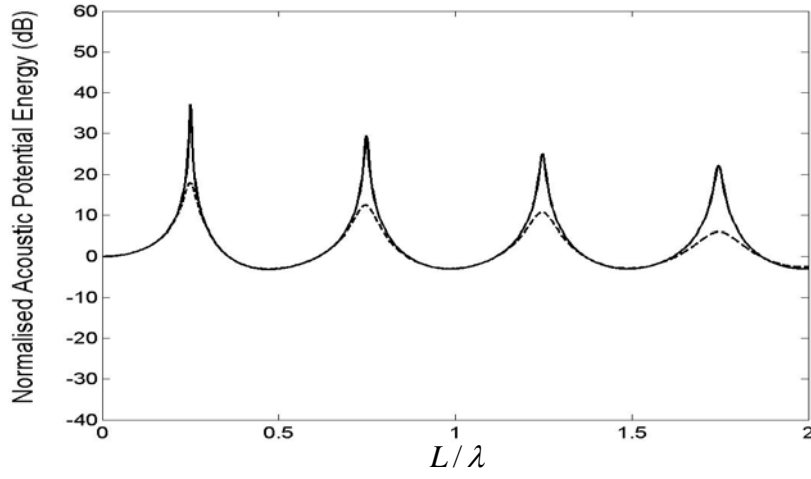
(a) Strongly coupled case ($K_a / K_s = 10^3$)
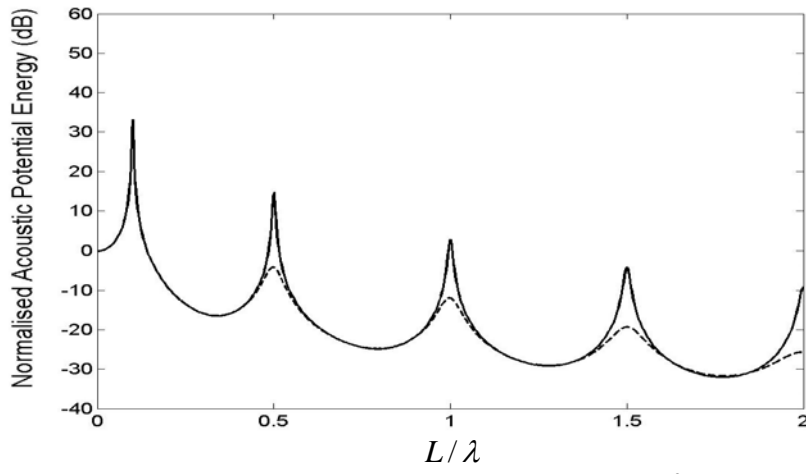
(b) Weakly coupled case ($K_a / K_s = 10^{-3}$)
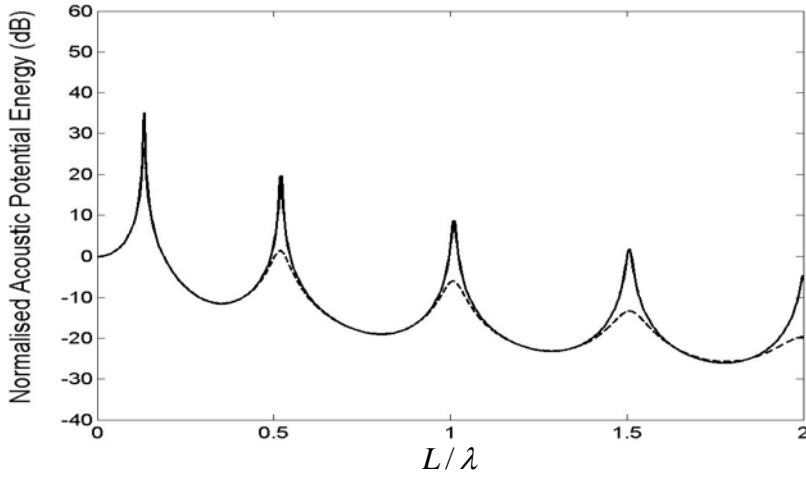
(c) Intermediate case ($K_a / K_s = 1$)

Figure 3.11 Acoustic potential energy normalised by that at the static state ($L/\lambda = 0$) without the absorptive medium for a given stiffness ratio in the case when the absorptive medium is applied in the region $L_0 \le x \le L$ where the structural natural frequency is at $L/\lambda = 0.1$ ($\omega_a / \omega_s = 5$) and the structural and acoustic loss factors $\eta_s = \eta_a = 10^{-2}$ (solid line: without the absorptive medium, and dashed line: with the absorptive medium $L_0 / L = 0.7$, $L_b / L = 0.3$ and the loss factor $\eta_b = 0.2$)
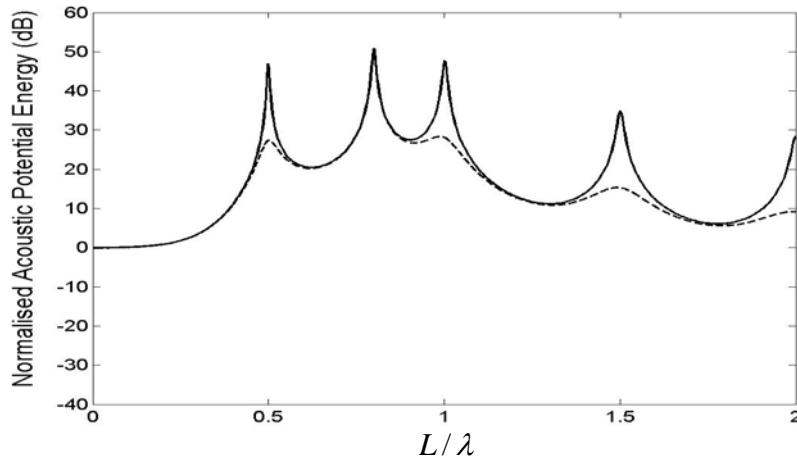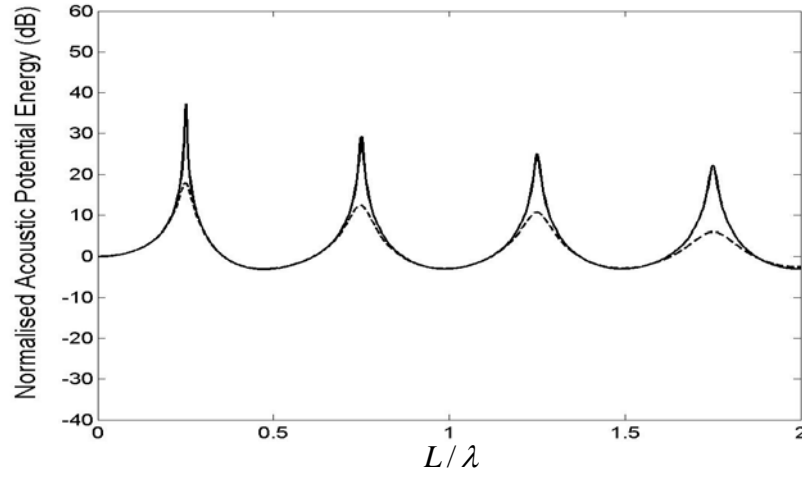
(a) Strongly coupled case ($K_a / K_s = 10^3$)
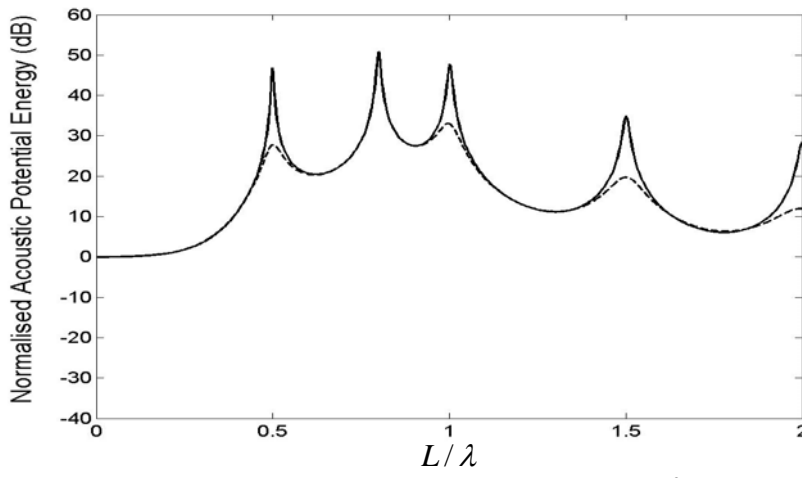
(b) Weakly coupled case ($K_a / K_s = 10^{-3}$)
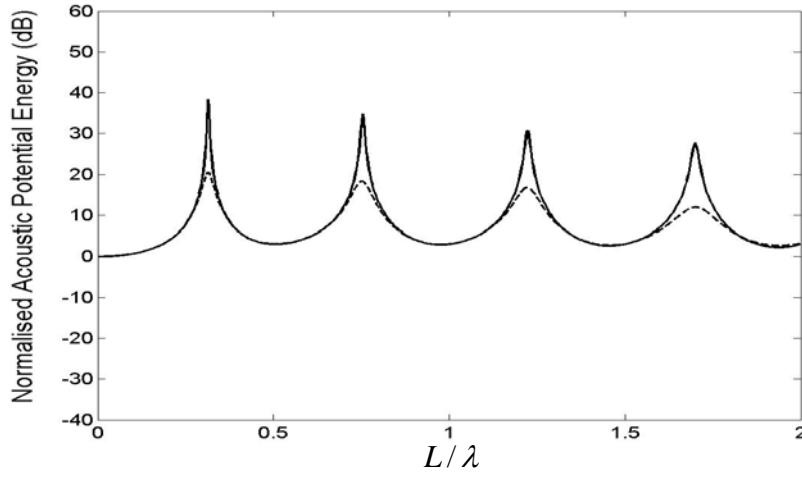
(c) Intermediate case ($K_a / K_s = 1$)

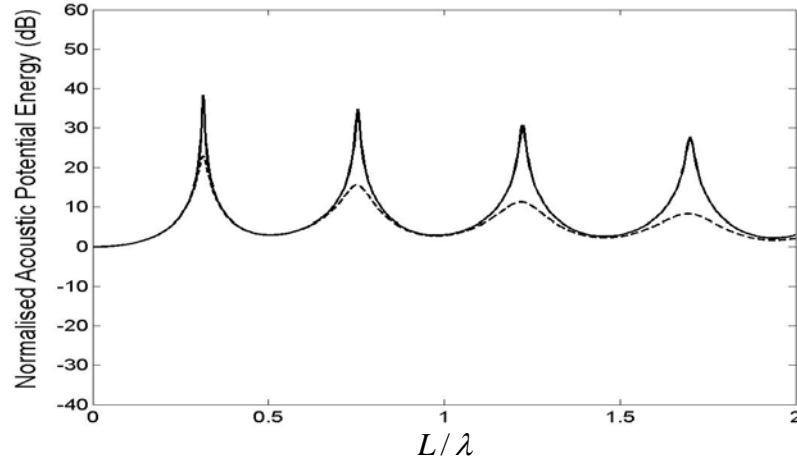*Figure 3.12 Acoustic potential energy normalised by that at the static state ($L / \lambda = 0$) without the absorptive medium for a given stiffness ratio in the case when the absorptive medium is applied in the region $L_0 \leq x \leq L$ where the structural natural frequency is at $L / \lambda = 0.8$ ($\omega_a / \omega_s = 0.6$) and the structural and acoustic loss factors $\eta_s = \eta_a = 10^{-2}$ (solid line: without the absorptive medium, and dashed line: with the absorptive medium $L_0 / L = 0.7$, $L_b / L = 0.3$ and the loss factor $\eta_b = 0.2$)*

3.4 Experimental investigation on a vibro-acoustic system

Some experimental work was carried out in order to validate the analytical model shown in figure 3.1 and to support the simulation results. The experimental rig was configured with a loudspeaker, a finite water pipe, microphones and accelerometers for the SDOF structure, a finite acoustic tube, acoustic and structural sensors respectively. The loudspeaker was modified for different structural characteristics under different structural-acoustic coupling conditions. The structural modification of the loudspeaker was based on non-dimensional structural-acoustic parameters, defined in chapter 2, dominating over the degree of structural-acoustic coupling. The finite acoustic tube driven by the standard or modified speaker was investigated by measuring the frequency response functions of the sound pressure in the vibro-acoustic system with respect to the input voltage to the loudspeaker. The acoustic potential energy in the vibro-acoustic system was approximately calculated by summing up the squared magnitudes of the measured frequency response functions at every measurement point along the acoustic tube.

3.4.1 Experimental setup

A test-rig was designed to behave in the similar way to the analytical model, depicted in figure 3.1, as shown in figure 3.13. The loudspeaker had a diaphragm of radius $46mm$ and was excited by the dynamic signal analyser (Data Physics) through the A1 acoustic amplifier (Cambridge Audio A1 V2.0). The other end ($x = L$) of the tube was terminated by a thick wooden plate ($10mm$) to give a closed tube. Also, the acoustic tube had dimensions of length $L = 1m$, diameter $\phi = 0.1m$ and wall thickness $t = 4mm$. The frequency response functions of the sound pressure in the tube were measured with respect to the input voltage to the loudspeaker by using seven omni-directional sub-miniature microphones (type EM-60B). The microphones were placed equidistantly along the centre line of the tube with spaces of $d = 0.16m$, and were sealed by silicone.

The measured sound pressure at every measurement point was passed to the dynamic signal analyser through an ISVR 8-channel acoustic amplifier. The frequency response function of the sound pressure at each measurement point with respect to the input voltage to the

loudspeaker was calculated. The first microphone was placed at $x = 0.02m$ on the side of the loudspeaker diaphragm and the seventh one was at $x = 0.98m$. The distance between the microphones was determined so that the distance between them was less than a quarter of a wave length at the maximum frequency ($500\,\text{Hz}$). The acoustic field inside the tube had plane wave propagation within the frequency range of interest ($0 \sim 500\,\text{Hz}$): the first resonance frequency in the radial direction was 1.7 kHz. The frequency range was sufficient to investigate one structural mode and three acoustic modes.
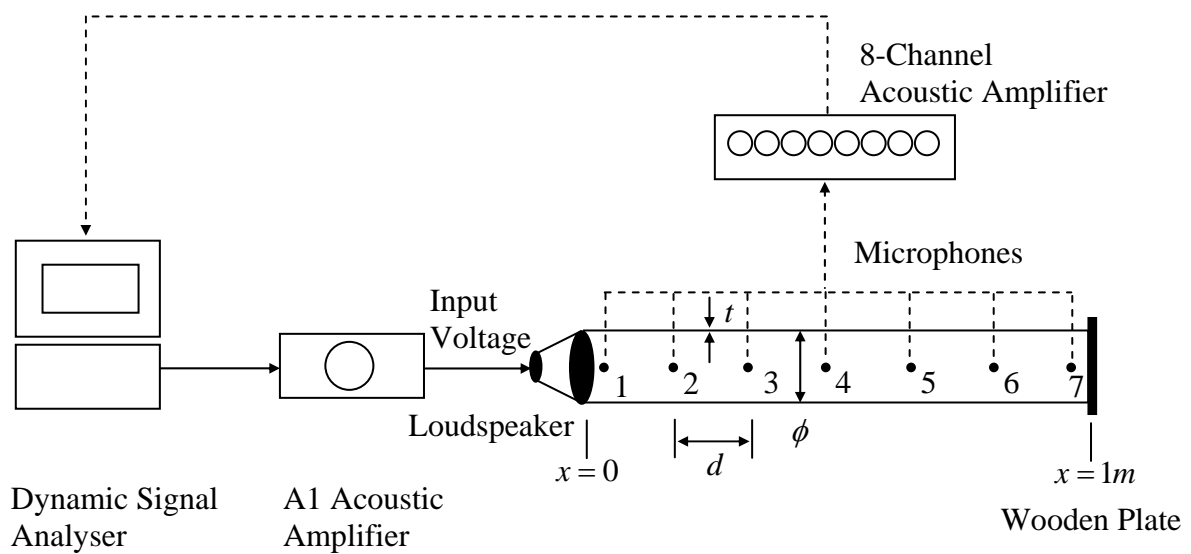
(a) Schematic diagram
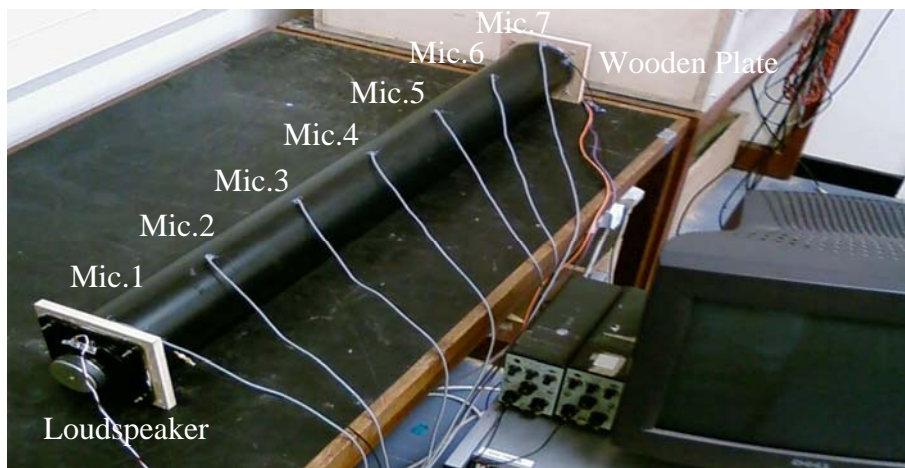
(b) Experimental setup

Figure 3.13 Experimental setup of a one-dimensional acoustic tube driven by a loudspeaker: (a) schematic diagram (b) experimental setup

3.4.2 Structural modification of a loudspeaker

The main concern of this experiment was to investigate the acoustic potential energy in a vibro-acoustic system in different coupled cases: *more strongly and more weakly coupled*. For the more weakly coupled case, it was required to modify the structural characteristics of a standard loudspeaker.

The structural modification of the standard loudspeaker was informed by the non-dimensional structural-acoustic parameters established in chapter 2. The degree of structural-acoustic coupling is determined by the coupling factor given in equation (2.42). If all the acoustic characteristics and the structural loss factor in the coupling factor at a certain frequency are fixed, the coupling factor is proportional to the structural-acoustic stiffness ratio $\hat{K}$ and the inverse of the structural-acoustic natural frequency ratio $\hat{\omega}$. The coupling factor can be rewritten as

$$Y_S Z_{A0} \propto \frac{1}{\sqrt{K_s M_s}} \tag{3.20}$$

Hence a more *weakly coupled* case can be achieved by increasing the structural mass and stiffness.

Figure 3.14 shows the standard and modified loudspeakers for the *more strongly* and *more weakly coupled* cases respectively. The standard loudspeaker was composed of a paper cone with rubber suspension at its perimeter and is sealed by a metal cover on the back. The standard loudspeaker was modified by adding mass of 100g composed of lead shot and increasing stiffness with 3 aluminium beams mounted to the loudspeaker metal case instead of the rubber suspension. When it comes to the added mass on the loudspeaker, the mass needs to be determined in practical way because the standard loudspeaker has such a light moving mass. Even though more mass can produce a more *weakly coupled* condition, the added mass was limited so that the static displacement, due to weight, was small. The perimeter of the modified loudspeaker cone was sealed by using silicone to avoid air leakage between the aluminium beams and the wooden flange of the acoustic tube.

(a) Standard loudspeaker   *(b) Modified loudspeaker*
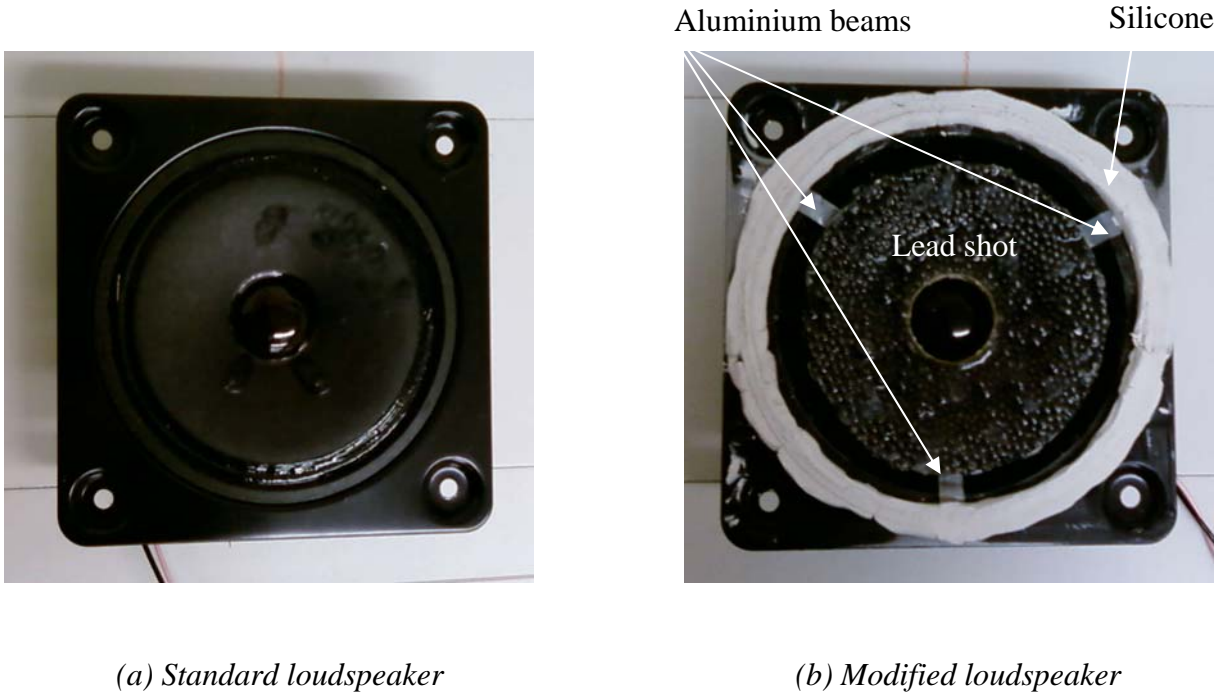
Figure 3.14 Loudspeakers used to excite the acoustic tube: (a) standard loudspeaker and (b) modified loudspeaker

The mechanical components of the standard and modified loudspeakers can be calculated from the measured frequency response functions with and without a known dummy mass. The natural frequency of the standard or the modified loudspeaker can be written based on the SDOF behaviour characteristics of a loudspeaker as

$$f_{s1} = \frac{1}{2\pi}\sqrt{\frac{K_s}{M_s}} \qquad\qquad f_{s2} = \frac{1}{2\pi}\sqrt{\frac{K_s}{M_s + m_s}} \qquad (3.21)$$

where f_{s1} and f_{s2} are the natural frequency of the standard or modified loudspeaker without and with a known dummy mass m_s respectively. The structural moving mass M_s and stiffness K_s of the loudspeaker can be calculated from equation (3.21), where the moving mass includes the mass of an accelerometer (B&K 4375) of $2.4g$. The structural loss factor η_s can be calculated from a quality factor and is given [Meirovitch (1986)] by

$$\eta_s = \frac{f_2 - f_1}{f_s} \tag{3.22}$$

where f_1 and f_2 are frequencies at the half-power points which are points with amplitude of $3\,\mathrm{dB}$ less than that at a natural frequency f_s.

Figures 3.15 and 3.16 show the measured transfer FRFs (frequency response functions) of the structural velocity with respect to the input voltage and the corresponding phase angle of the standard and the modified loudspeakers respectively. The FRFs were measured separately from the acoustic tube. The FRFs were measured by an accelerometer (B&K type 4375) on the diaphragm. Also, the measured acceleration was sent to a dynamic signal analyser (Data Physics) through a charge amplifier (B&K type 2635). The noisy results at around $50\,\mathrm{Hz}$ as shown in figure 3.15 were due to the power supply. The mechanical components of the standard and modified loudspeakers are presented in table 3.2.
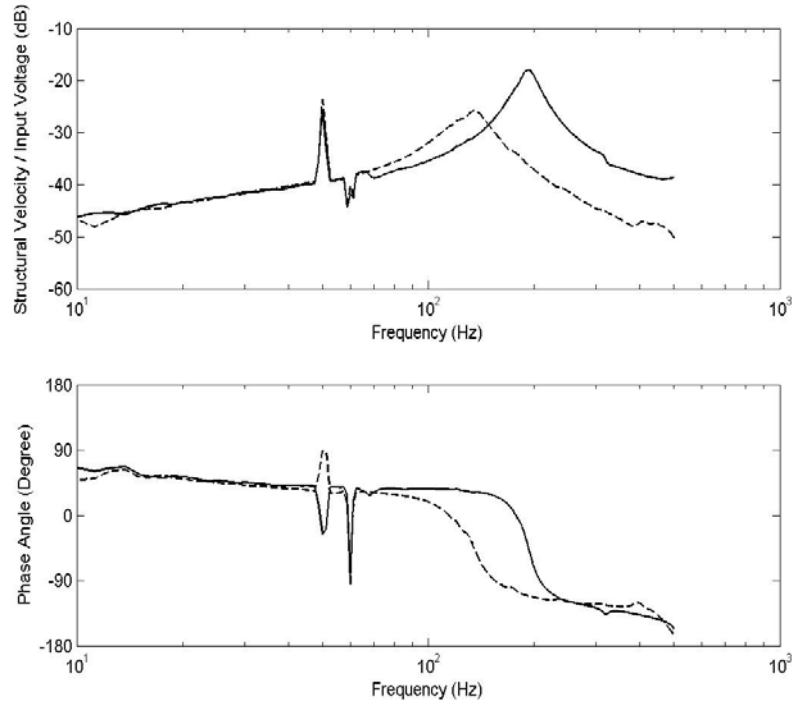
Figure 3.15 Structural velocity with respect to the input voltage to the loudspeaker and phage angle of the standard loudspeaker where the known dummy mass $m_s = 10g$, $f_{s1} = 190Hz$, $f_{s2} = 130Hz$ and the reference value for the amplitude of the FRF is $1V/V$ in dB scale (solid line: without the dummy mass and dotted line: with the dummy mass)
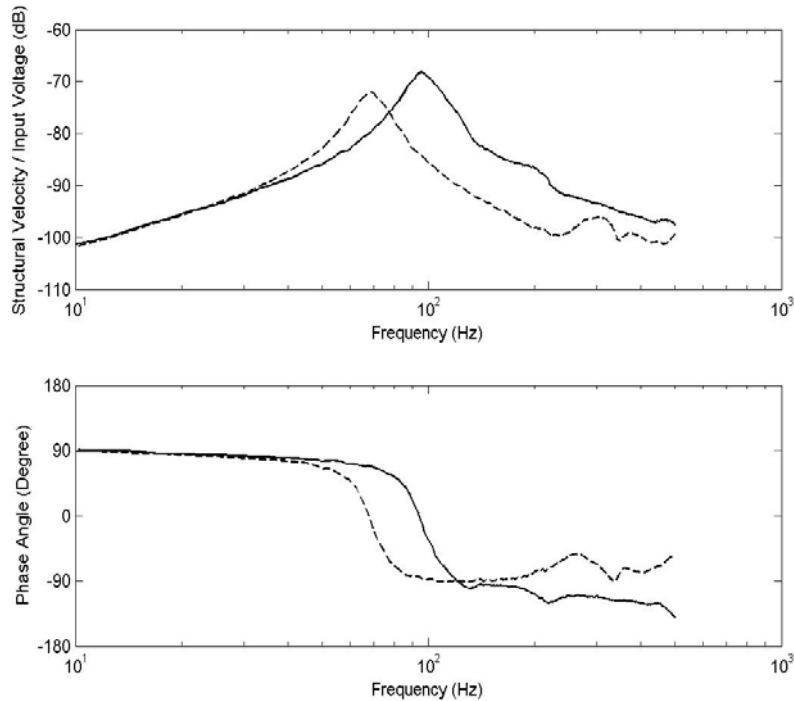
Figure 3.16 Structural velocity with respect to the input voltage to the loudspeaker and phage angle of the modified loudspeaker where the known dummy mass $m_s = 100g$, $f_{s1} = 96Hz$, $f_{s2} = 69Hz$ and the reference value for the amplitude of the FRF is $1V/V$ in dB scale (solid line: without the dummy mass and dotted line: with the dummy mass)

Table 3.2 Mechanical components of standard and modified loudspeakers

	Standard loudspeaker	Modified loudspeaker
Natural frequency f_s (Hz)	190	96
Moving mass M_s (g)	9	110
Stiffness K_s (N/m)	1.3×10^4	3.2×10^4
Loss factor η_s	0.16	0.2

3.4.3 Measuring acoustic potential energy

The acoustic pressure was measured at a discrete number of microphone locations in the acoustic tube since it was not possible to measure the acoustic pressure everywhere. Also, the acoustic potential energy per unit input in the vibro-acoustic system can be approximately calculated by summing up the squared magnitude of the measured FRFs of the sound pressure with respect to the input voltage at all the measuring positions. The acoustic potential energy defined in equation (2.46) can be approximated such that

$$E_{p\,FRF}(\omega) \approx \frac{1}{m} \frac{SL}{4\rho\,|c|^2} \sum_{i=1}^{m} | P_{FRF}(x_i, \omega) |^2 \qquad (3.23)$$

where $E_{p\,FRF}(\omega)$ and $P_{FRF}(x_i, \omega)$ are the acoustic potential energy and the transfer FRF of the sound pressure with respect to the input voltage respectively. Also, x_i is the ith measuring point and m is the number of measuring points. The approximated acoustic potential energy given in equation (3.23) can be rewritten in the vector form as

$$E_{p\,FRF}(\omega) \approx \frac{1}{m} \frac{SL}{4\rho\,|c|^2} \mathbf{p}_{FRF}{}^{H} \mathbf{p}_{FRF} \qquad (3.24)$$

where $\mathbf{p}_{FRF}$ is the measured FRF vector whose i^{th} component is $P_{FRF}(x_i, \omega)$ and $\mathbf{p}_{FRF}{}^{H}$ is the *Hermitian* transpose of the vector $\mathbf{p}_{FRF}$, which is the complex conjugate of the transpose.

3.4.4 Experimental results

Figures 3.17(a), (b) and 3.18(a), (b) show the acoustic potential energy, normalised by that at the static state ($\omega = 0$) for theory and that at 50Hz for experiment due to noisy results at low frequencies, in the *more strongly coupled* case and in the *more weakly coupled* case respectively. The main objective of this experiment was to investigate the acoustic potential energy under various structural-acoustic coupled conditions, which has only acoustic modes or both acoustic and structural modes. Hence, the normalised acoustic potential energy is available to give physical insight into the vibro-acoustic responses in the more *strongly* and *weakly coupled* cases.

In the *more strongly coupled* case as shown in figures 3.17(a) and (b), the theoretical and experimental results demonstrate that the acoustic potential energy has only acoustic modes. Also, the vibro-acoustic system behaves like a closed-closed tube, which has a fundamental acoustic mode at 170Hz and the second acoustic mode at 340Hz. The low amplitudes of the measured acoustic potential energy at low frequencies in figure 3.17(b) are due to the loudspeaker with poor performances at low frequencies.

In the *more weakly coupled* case as shown in figures 3.18(a) and (b), the theoretical and experimental acoustic potential energies have both acoustic and structural modes. The structural mode is at the structural natural frequency 96Hz due to the modified loudspeaker, which is not affected by the sound pressure in the tube. Also, the vibro-acoustic system has a fundamental acoustic mode at 170Hz and the second acoustic mode at 340Hz which are consistent with a closed-closed tube. The measured acoustic potential energy has low amplitudes at low frequencies as shown in figure 3.18(b) for the same reason as that in the *more strongly coupled* case.

A general observation is that the experimental results are generally predicted by the analytical model in the *more strongly coupled* case and in the *more weakly coupled* case. The acoustic potential energy in the vibro-acoustic system has only acoustic modes in the *more strongly coupled* case and both acoustic and structural modes in the *more weakly coupled* case.
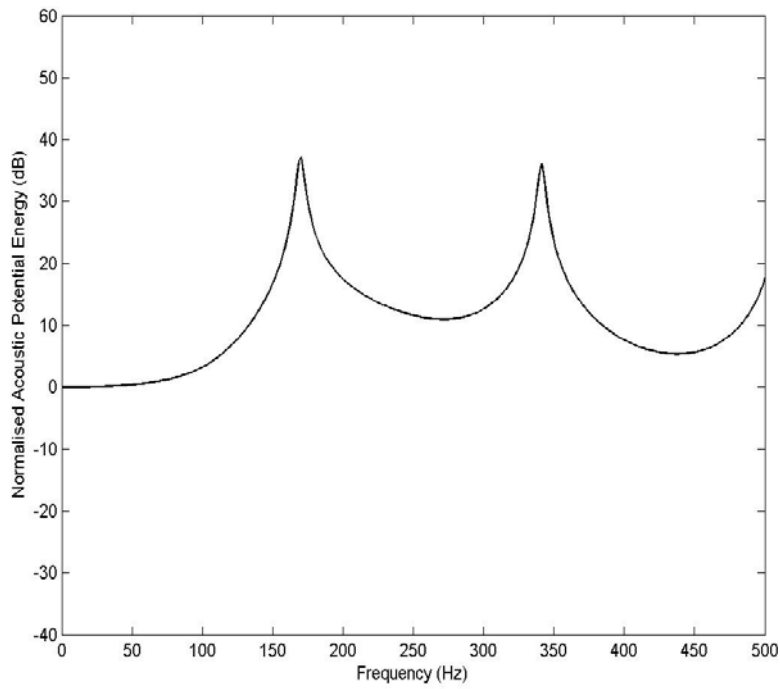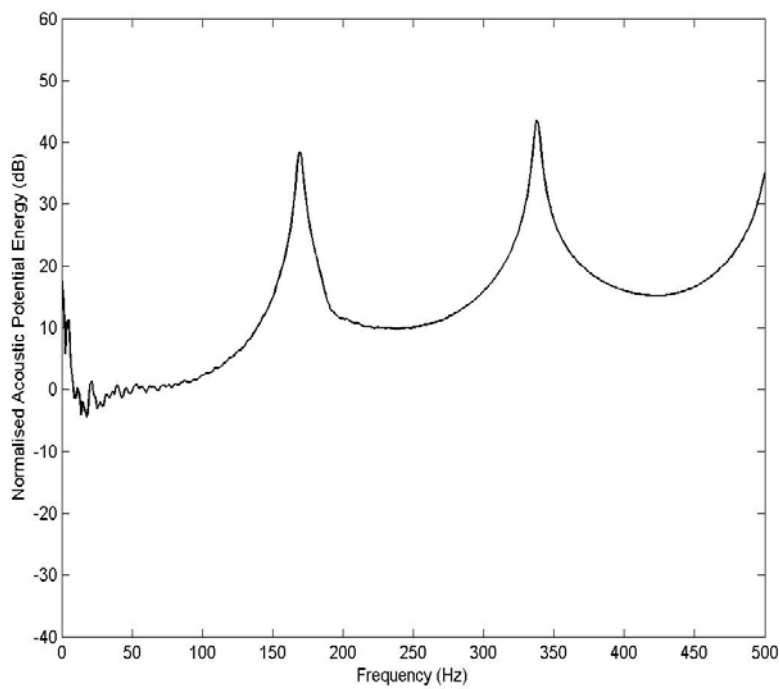
(a) Theory

(b)Experiment

Figure 3.17 Acoustic potential energy normalised by that at the static state ($L/\lambda = 0$) for theory and that at 50Hz for experiment in the more strongly coupled case where the stiffness ratio $K_a / K_s = 0.1$, the structural natural frequency is 190Hz ($\omega_a / \omega_s = 0.9$) and the loss factors $\eta_s = 0.16$, $\eta_a = 0.01$: (a) theory and (b) experiment
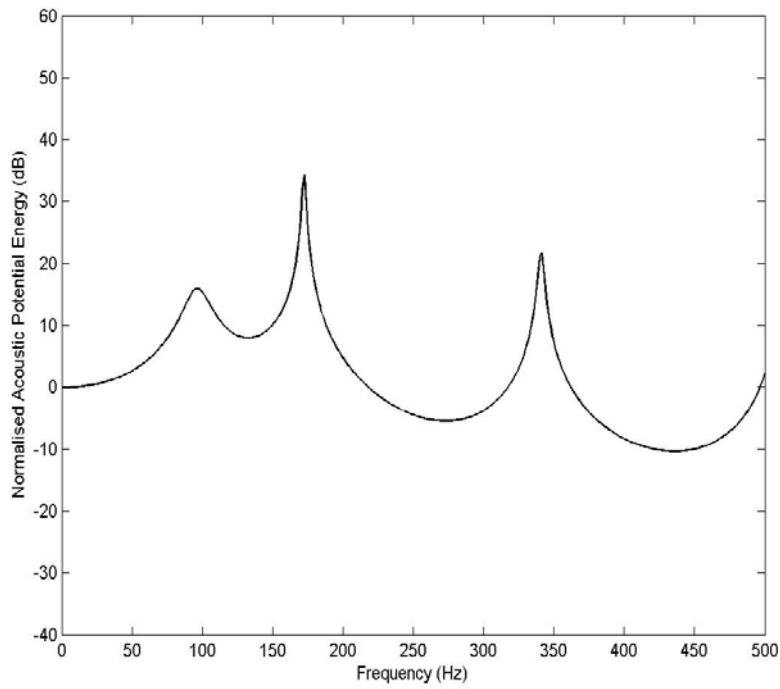
(a) Theory
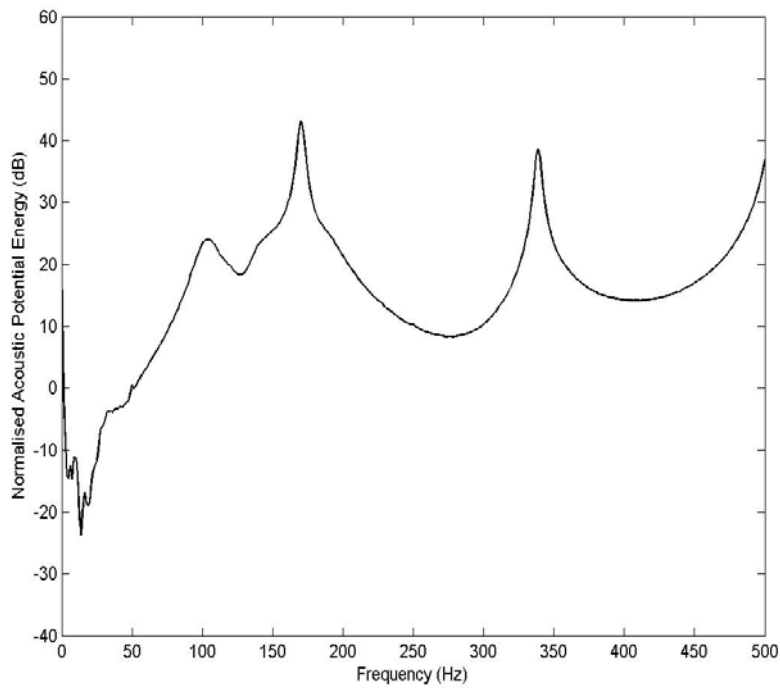
(b) Experiment

Figure 3.18 Acoustic potential energy normalised by that at the static state ($L/\lambda = 0$) for theory and by that at 50Hz for experiment in the more weakly coupled case where the stiffness ratio $K_a/K_s = 0.1$, the structural natural frequency is 96Hz ($\omega_a/\omega_s = 1.8$), and the loss factors $\eta_s = 0.2$, $\eta_a = 0.01$: (a) theory and (b) experiment

3.5 Conclusions

Passive control of the acoustic potential energy in a simple vibro-acoustic system has been investigated in various structural-acoustic coupling cases. The passive control measures were implemented by modifying stiffness, mass, structural damping, acoustic damping and adding an absorptive medium. The comparison of passive control performance on the acoustic potential energy in the various coupled cases demonstrates the following.

In the *strongly coupled* case, the acoustical modifications, involving the change of the acoustic loss factor or placing an absorptive medium in the cavity, are preferable for the reduction of the acoustic potential energy in both the cases of two values of the structural natural frequency.

In the *weakly coupled* case, the structural modifications, involving the change of the stiffness ratio, the natural frequency ratio or the structural loss factor, are preferable for the reduction of the acoustic potential energy. In the case when the structural natural frequency is below the fundamental acoustic mode, the change of the structural loss factor is more effective in the reduction of the acoustic potential energy. On the other hand, in the case when the structural natural frequency is above the fundamental acoustic mode, the change of the natural frequency ratio is a more effective passive treatment for the reduction of the acoustic potential energy.

In the *intermediate* case, the acoustical modifications, involving the change of the acoustic loss factor or placing an absorptive medium in the cavity, are more effective in the reduction of the acoustic potential energy compared to the structural modification. Also, in the case when the structural natural frequency is above the fundamental acoustic mode, the acoustic modifications had a more significant effect on the reduction of the acoustic potential energy.

In this chapter, the relative benefits of passive control treatments have been investigated in various structural-acoustic coupling cases through a parametric study of structural-acoustic non-dimensional parameters. In the following chapters, active control of the acoustic potential energy will be investigated under harmonic or broadband disturbance.

CHAPTER 4

ACTIVE FEEDFORWARD CONTROL OF ACOUSTIC POTENTIAL ENERGY IN A VIBRO-ACOUSTIC SYSTEM

4.1 Introduction

The aim of this chapter is to investigate the effectiveness of active feedforward control of the acoustic potential energy in the simple vibro-acoustic system described in chapter 2. The three coupled cases, discussed in chapter 2, are studied when the structural natural frequency is below and above the fundamental acoustic mode of a closed-closed tube respectively. The vibro-acoustic system is harmonically driven by a single-degree-of-freedom (SDOF) structure at one end of the acoustic tube and is controlled by a single acoustic piston at the other end using a feedforward control strategy. The feedforward control mechanism in the vibro-acoustic system is investigated based on the optimal controller and the optimal impedance. The optimal impedance is defined as the ratio of the control force to the velocity of the control piston with a sign reversal when the acoustic potential energy is minimised. Under the action of feedforward control, the control effect on the SDOF structure is discussed in terms of the structural kinetic energy.

In this chapter, the main concern is to investigate the performance of feedforward control of the acoustic potential energy in a combined SDOF structure – one dimensional acoustic tube system under various coupled conditions. In section 4.2, an analytical model of the vibro-

acoustic system, driven by a SDOF structure and controlled by an acoustic piston in a feedforward control scheme, is described. In section 4.3, the control performance on the acoustic potential energy is studied by investigating the optimal feedforward controller. In section 4.4, the physical characteristics of the optimal impedance are discussed to investigate the physical mechanism of the feedforward control on the acoustic potential energy. In section 4.5, the feedforward control effects on structural kinetic energy are discussed when the acoustic potential energy is minimised. In section 4.6, the quantitative feedforward control effect on the acoustic potential energy is investigated by presenting a cumulative sum of the acoustic potential energy over the frequency range of interest. In section 4.7, experimental validation on the control performance of the feedforward controller is carried out before the chapter is concluded in section 4.8.

4.2 Analytical model

Figure 4.1 depicts the combined SDOF structure – one dimensional acoustic tube system controlled by a single acoustic piston in a feedforward control scheme. The structure has the same mechanical components as those in the analytical model shown in figure 2.1. The one-dimensional acoustic tube is harmonically excited by a primary source (a SDOF structure) at $x = 0$ being subject to a primary force $f_P(t)\,(= F_P e^{j\omega t})$. Also, a feedforward controller, with a frequency response $G(j\omega)$, drives a secondary source (an acoustic piston) with a control force $f_S(t)\,(= F_S e^{j\omega t})$. The acoustic potential energy in the acoustic tube is controlled by the secondary source at each harmonic excitation frequency, thus there are no causality issues.

The secondary source is assumed to be a massless rigid piston supported by a spring with a complex stiffness $K_L(1 + j\eta_L)$ where η_L is a constant loss factor of the acoustic piston. A massless piston is considered since the main concern of this chapter is to investigate the control of the acoustic potential energy contributed by the structural mode and the acoustic cavity modes.
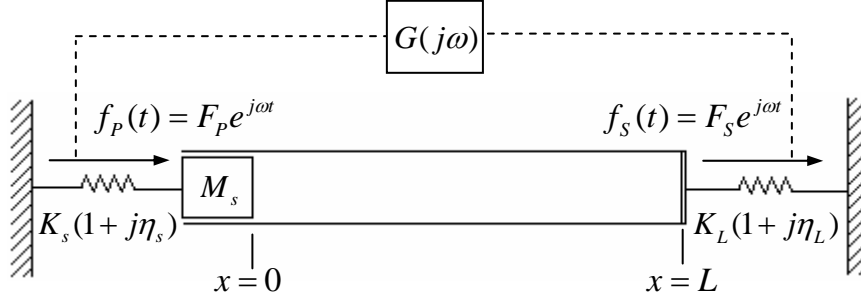
Figure 4.1 A combined SDOF structure – one dimensional acoustic tube system controlled by an acoustic piston in a feedforward control strategy

4.3 Acoustic potential energy under feedforward control

The primary source generates an acoustic pressure in the acoustic tube, and the acoustic potential energy is controlled by the secondary source using a feedforward control strategy. The acoustic potential energy in the acoustic tube can be calculated from the total sound pressure by linearly superimposing the sound pressure due to the primary source and the secondary source.

4.3.1 Primary source contribution

The primary source contribution to the total acoustic pressure in the acoustic tube can be obtained by calculating the acoustic pressure by setting the control force at the secondary source to zero.

The acoustic pressure and the particle velocity in the vibro-acoustic system, depicted in figure 2.1, are given in equations (2.32)~(2.33). The acoustic pressure and the particle velocity due to the primary force, in the vibro-acoustic system depicted in figure 4.1, can be written as

$$P_P(x,\omega) = \rho_0 c \frac{F_P}{Z_S + Z_{A0}} \frac{\dfrac{Z_L}{\rho_0 cS}\cos k(L-x) + j\sin k(L-x)}{\cos kL + j\dfrac{Z_L}{\rho_0 cS}\sin kL} \tag{4.1}$$

$$U_p(x,\omega) = \frac{F_p}{Z_S + Z_{A0}} \frac{\cos k(L-x) + j\dfrac{Z_L}{\rho_0 cS}\sin k(L-x)}{\cos kL + j\dfrac{Z_L}{\rho_0 cS}\sin kL} \tag{4.2}$$

which can be written in non-dimensional form as

$$\hat{P}_P(\hat{x},\hat{L}) = \frac{1}{\hat{Z}_S + \hat{Z}_{A0}} \frac{2}{2-j\eta_a} \frac{\hat{Z}_L \cos\left(\pi(2-j\eta_a)(1-\hat{x})\hat{L}\right) + j\dfrac{2}{2-j\eta_a}\sin\left(\pi(2-j\eta_a)(1-\hat{x})\hat{L}\right)}{\dfrac{2}{2-j\eta_a}\cos\left(\pi(2-j\eta_a)\hat{L}\right) + j\hat{Z}_L \sin\left(\pi(2-j\eta_a)\hat{L}\right)} \tag{4.3}$$

$$\hat{U}_p(\hat{x},\hat{L}) = \frac{1}{\hat{Z}_S + \hat{Z}_{A0}} \frac{\dfrac{2}{2-j\eta_a}\cos\left(\pi(2-j\eta_a)(1-\hat{x})\hat{L}\right) + j\hat{Z}_L \sin\left(\pi(2-j\eta_a)(1-\hat{x})\hat{L}\right)}{\dfrac{2}{2-j\eta_a}\cos\left(\pi(2-j\eta_a)\hat{L}\right) + j\hat{Z}_L \sin\left(\pi(2-j\eta_a)\hat{L}\right)} \tag{4.4}$$

where $\hat{P}_P(\hat{x},\hat{L}) = P_P(\hat{x},\hat{L})/P_s$ and $\hat{U}_p(\hat{x},\hat{L}) = U_p(\hat{x},\hat{L})/U$ with $P_s = F_P/S$ and $U = F_P/\rho_0 c_0 S$. The normalised structural impedance $\hat{Z}_S (= Z_S/\rho_0 c_0 S)$ and the normalised acoustic input impedance $\hat{Z}_{A0} (= Z_{A0}/\rho_0 c_0 S)$ are defined in equations (2.36) and (2.37) respectively.

Here the arbitrary impedance Z_L in equations (2.32)~(2.33) is the impedance of the secondary source. The secondary source is configured by a massless rigid piston supported by a spring as shown in figure 4.1 and the impedance of the secondary source is defined by

$$Z_L = -j\frac{K_L(1+j\eta_L)}{\omega} \tag{4.5}$$

Also, the normalised impedance $\hat{Z}_L (= Z_L/\rho_0 c_0 S)$ can be written in non-dimensional form as

$$\hat{Z}_L = -j\frac{1+j\eta_L}{2\pi\hat{K}_L\hat{L}} \tag{4.6}$$

where $\hat{K}_L (= K_a / K_L)$ is the ratio of the acoustic bulk stiffness to the stiffness of the secondary source and η_L is a constant loss factor of the secondary source.

4.3.2 Secondary source contribution

The secondary source contribution to the total acoustic pressure can be obtained by calculating the acoustic pressure in the acoustic tube excited by only the secondary control force.

The acoustic pressure $P_S(x,\omega)$ and the particle velocity $U_S(x,\omega)$, generated by the secondary control force, can be obtained using geometrical symmetry of the analytical model. The vibro-acoustic responses can be obtained by simply exchanging the primary force F_P and the primary source impedance Z_S with the secondary control force F_S and the secondary source impedance Z_L respectively in equations (4.1)~(4.2). Also, arbitrary positions in the acoustic tube are described by $L-x$ since the vibro-acoustic system is excited at $x=L$. The acoustic pressure and the particle velocity caused by the secondary control force are given by

$$P_S(x,\omega) = \rho_0 c \frac{F_S}{Z_L + Z_{AL}} \frac{\dfrac{Z_S}{\rho_0 cS} \cos kx + j \sin kx}{\cos kL + j \dfrac{Z_S}{\rho_0 cS} \sin kL} \tag{4.7}$$

$$U_S(x,\omega) = \frac{F_S}{Z_L + Z_{AL}} \frac{\cos kx + j \dfrac{Z_S}{\rho_0 cS} \sin kx}{\cos kL + j \dfrac{Z_S}{\rho_0 cS} \sin kL} \tag{4.8}$$

where Z_{AL} is the input impedance of the acoustic tube at the secondary source position and is defined in equation (2.24).

The acoustic pressure and the particle velocity given in equations (4.7)~(4.8) can be similarly written in non-dimensional form as

96

$$\hat{P}_{S}(\hat{x},\hat{L}) = \frac{G}{\hat{Z}_{L}+\hat{Z}_{AL}} \frac{2}{2-j\eta_{a}} \frac{\hat{Z}_{S}\cos\left(\pi(2-j\eta_{a})\hat{x}\hat{L}\right)+ j\dfrac{2}{2-j\eta_{a}}\sin\left(\pi(2-j\eta_{a})\hat{x}\hat{L}\right)}{\dfrac{2}{2-j\eta_{a}}\cos\left(\pi(2-j\eta_{a})\hat{L}\right)+ j\hat{Z}_{S}\sin\left(\pi(2-j\eta_{a})\hat{L}\right)} \tag{4.9}$$

$$\hat{U}_{S}(\hat{x},\hat{L}) = \frac{G}{\hat{Z}_{L}+\hat{Z}_{AL}} \frac{\dfrac{2}{2-j\eta_{a}}\cos\left(\pi(2-j\eta_{a})\hat{x}\hat{L}\right)+ j\hat{Z}_{S}\sin\left(\pi(2-j\eta_{a})\hat{x}\hat{L}\right)}{\dfrac{2}{2-j\eta_{a}}\cos\left(\pi(2-j\eta_{a})\hat{L}\right)+ j\hat{Z}_{S}\sin\left(\pi(2-j\eta_{a})\hat{L}\right)} \tag{4.10}$$

where $\hat{P}_{S}(\hat{x},\hat{L}) = P_{S}(\hat{x},\hat{L})/P_{s}$ and $\hat{U}_{S}(\hat{x},\hat{L}) = U_{S}(\hat{x},\hat{L})/U$. The secondary control force F_{S} is the product of the feedforward control gain $G(j\omega)$ and the primary force F_{P}. Also, the normalised input impedance $\hat{Z}_{AL}(= Z_{AL}/\rho_{0}c_{0}S)$ can be written in non-dimensional form using equation (2.24) as

$$\hat{Z}_{AL} = \frac{2}{2-j\eta_{a}} \frac{\hat{Z}_{S}\cos\left(\pi(2-j\eta_{a})\hat{L}\right)+ j\dfrac{2}{2-j\eta_{a}}\sin\left(\pi(2-j\eta_{a})\hat{L}\right)}{\dfrac{2}{2-j\eta_{a}}\cos\left(\pi(2-j\eta_{a})\hat{L}\right)+ j\hat{Z}_{S}\sin\left(\pi(2-j\eta_{a})\hat{L}\right)} \tag{4.11}$$

4.3.3 Minimisation of acoustic potential energy

In this section, an approximation of the acoustic potential energy E_{P}, defined in equation (2.46), is determined by summing the squares of the absolute values of the sound pressure at a number of positions in the tube. The approximation of the acoustic potential energy is given by

$$J_{P}(\hat{L}) = \frac{1}{m} \frac{SL|P_{s}|^{2}}{4\rho_{0}|c|^{2}} \mathbf{p}^{H}\mathbf{p} \tag{4.12}$$

where $\mathbf{p}$ is the m-length vector of the normalised total sound pressure. The approximation of the acoustic potential energy J_{P} tends to E_{P} in the limit of an infinite number of positions in the tube. The vector $\mathbf{p}$ comprises the vector $\mathbf{p}_{P}$ of the normalised sound pressure due to the

primary source given in equation (4.3) whose i^{th} component is $\hat{P}_P(\hat{x}_i, \hat{L})$ and the vector $\mathbf{p}_S$ of the normalised sound pressure due to the secondary source given in equation (4.9) whose i^{th} component is $\hat{P}_S(\hat{x}_i, \hat{L})$, so that

$$\mathbf{p} = \mathbf{p}_P + \mathbf{p}_S \tag{4.13}$$

The acoustic potential energy, given in equation (4.12), can be normalised by that at the static state ($\hat{L} = 0$) in the absence of control $J_P(0)$ and can be written in non-dimensional form as

$$\hat{J}_P(\hat{L}) = \frac{J_P(\hat{L})}{J_P(0)} = \frac{\mathbf{p}^H \mathbf{p}}{\mathbf{p}_{P0}^H \mathbf{p}_{P0}} \tag{4.14}$$

where

$$J_P(0) = \frac{1}{m} \frac{SL \, |P_s|^2}{4\rho_0 \, |c|^2} \mathbf{p}_{P0}^H \mathbf{p}_{P0} \tag{4.15}$$

where $\mathbf{p}_{P0}$ is the m-length vector of the normalised sound pressure due to the primary source whose i^{th} component is $\hat{P}_P(\hat{x}_i, 0)$.

Combining equations (4.13) and (4.14) gives the normalised acoustic potential energy in *Hermitian* quadratic form, which can be written as

$$\hat{J}_P(\hat{L}) = \frac{1}{\mathbf{p}_{P0}^H \mathbf{p}_{P0}} \left(G^* \mathbf{h}_S^H \mathbf{h}_S G + G^* \mathbf{h}_S^H \mathbf{p}_P + \mathbf{p}_P^H \mathbf{h}_S G + \mathbf{p}_P^H \mathbf{p}_P \right) \tag{4.16}$$

where $\mathbf{p}_S = G \mathbf{h}_S$ and G^* is the complex conjugate of the feedforward control gain G. Also, the vector $\mathbf{h}_S$ is the transfer function vector whose i^{th} component is $\hat{P}_S(\hat{x}_i, \hat{L})/G$.

When the acoustic potential energy has a unique global minimum, the optimal feedforward controller can be calculated and is given by [Nelson and Elliott (1992)]

$$G_{opt} = -\frac{\mathbf{h}_S^H \mathbf{p}_P}{\mathbf{h}_S^H \mathbf{h}_S} \tag{4.17}$$

Substituting the expression for the optimal feedforward controller, given in equation (4.17), into the normalised acoustic potential energy, given in (4.16), gives the normalised minimum level of the acoustic potential energy $\hat{J}_{P\min}(\hat{L})$, which is

$$\hat{J}_{P\min}(\hat{L}) = \frac{1}{\mathbf{p}_{P0}^H \mathbf{p}_{P0}} \left(G_{opt}^* \mathbf{h}_S^H \mathbf{h}_S G_{opt} + G_{opt}^* \mathbf{h}_S^H \mathbf{p}_P + \mathbf{p}_P^H \mathbf{h}_S G_{opt} + \mathbf{p}_P^H \mathbf{p}_P \right) \tag{4.18}$$

Figures 4.2(a), (b), (c) and figures 4.4(a), (b), (c) show the normalised acoustic potential energy, in the vibro-acoustic system under feedforward control, for a given stiffness ratio. The three different coupled cases are studied when the structural natural frequency is at $L/\lambda = 0.1$ and at $L/\lambda = 0.8$ respectively. Also, figures 4.3(a), (b) and 4.5(a), (b) show the modulus and the phase angle of the optimal feedforward controller, given in equation (4.17), in the respective cases. The optimal feedforward controller has a frequency response of the ratio of the secondary control force to the primary force when the acoustic potential energy in the cavity is minimised.

In the *strongly coupled* case with a structural-acoustic stiffness ratio $K_a/K_s = 10^3$ and the structural natural frequency at $L/\lambda = 0.1$, the acoustic potential energy has the acoustic modes of an open-closed tube at $L/\lambda = (2n-1)/4$ before control as shown in figure 4.2(a) where n is an integer. All the acoustic modes are controllable as shown in figure 4.2(a). The optimal feedforward controller produces an in-phase or $180°$ out-of-phase secondary control force with respect to the primary force as shown in figure 4.3(b). The phase angle of the control force is determined by the ODS (Operational Deflection Shapes) shown in figure 2.6(a). Under the control force, the acoustic piston releases and compresses the pressure at $x = L$ in the cavity when the real part of the acoustic pressure is positive and negative at the position respectively. At some frequencies between the resonances, the dips of the acoustic potential energy after control are the same as that before control as shown in figure 4.2(a), which is due to an insignificant control force at $L/\lambda = n/2$ as shown in figure 4.3(a) where n is an integer.

When the wavelength in the acoustic tube is large enough compared to the dimensions of the tube, the acoustic tube behaves like an acoustic spring as described in the low-frequency approximate model in Appendix. A. The potential energy of the acoustic spring can be set to zero by the optimal secondary control force, which provides zero pressure with an open condition at $x = L$. Therefore, at the static state ($L/\lambda = 0$), the controlled acoustic potential energy is zero as shown in figure 4.2(a). At low frequencies, the acoustic input impedance of an open-tube, defined in equation (2.22), behaves like a mass, which is the mass of the acoustic medium in the cavity. The controlled acoustic potential energy has a structural mode at about $L/\lambda = 0.005$ due to the acoustic mass in the cavity after control. At the structural mode, the modulus of the optimal feedforward controller has maximum value as shown in figure 4.3(a).

In the *weakly coupled* case with a structural-acoustic stiffness ratio $K_a / K_s = 10^{-3}$ and the structural natural frequency at $L/\lambda = 0.1$, the acoustic potential energy has a dominant structural mode at $L/\lambda = 0.1$ and acoustic modes of a closed-closed tube at $L/\lambda = n/2$ before control as shown in figure 4.2(b) where n is an integer. At the frequencies of the acoustic modes, the acoustic potential energy is effectively controlled. The optimal feedforward controller produces an in-phase or out-of-phase secondary control force with respect to the primary force as shown in figure 4.3(b) for the same reason as the *strongly coupled* case. The dips of the acoustic potential energy after control are the same as that before control as shown in figure 4.2(b), which is due to an insignificant control force at $L/\lambda = 0.3$, 0.8, 1.25 and 1.75 as shown in figure 4.3(a). At low frequencies below the fundamental acoustic mode at $L/\lambda = 0.5$, the control mechanism is the same as for the *strongly coupled* case. The boundary at $x = L$ is modified into an open-tube condition due to the optimal secondary control force. The amplitude of the structural mode is reduced after control due to the smaller acoustic loading caused by the acoustic stiffness. Also, the controlled acoustic potential energy is zero at the static state ($L/\lambda = 0$) as shown in figure 4.2(b). At the low frequencies, the optimal controller produces secondary control forces determined by the structural excitation to the acoustic spring in the low-frequency approximate model in Appendix. A. At the frequencies below the structural resonance, the structural excitation is determined by the structural spring, which is $180°$ out-of-phase to the primary force. At the frequencies above the structural resonance, the structural excitation is determined by the structural mass, which is in-phase to the primary force. The control force is

180° out-of-phase and in-phase to the primary force at these frequencies respectively as shown in figure 4.3(b) to set the pressure to zero at $x = L$.

In the *intermediate* case with a structural-acoustic stiffness ratio $K_a / K_s = 1$ and the structural natural frequency at $L/\lambda = 0.1$, the acoustic potential energy has a structural mode at $L/\lambda = 0.13$ and acoustic modes of a closed-closed tube at $L/\lambda = n/2$ before control as shown in figure 4.2(c) where n is an integer. All the acoustic modes are effectively controlled by the similar control mechanism to that in the *weakly coupled* case. Also, the amplitude of the structural mode at $L/\lambda = 0.13$ is reduced after control due to the smaller acoustic loading caused by the acoustic stiffness as in the *weakly coupled* case. The structural mode is shifted to the lower frequency (about $L/\lambda = 0.09$) after control for the same reason of the *strongly coupled* case. The optimal feedforward controller produces a maximum secondary control force at the shifted structural mode as shown in figure 4.3(a). At the frequencies around the structural mode, the secondary control force has similar phase information to that in the *weakly coupled* case.

In the *strongly coupled* case with a structural-acoustic stiffness ratio $K_a / K_s = 10^3$ and the structural natural frequency at $L/\lambda = 0.8$, the acoustic potential energy has similar behaviour to that in the case of the structural natural frequency at $L/\lambda = 0.1$ as shown in figure 4.4(a). The acoustic modes are controlled under the control force with the same control mechanism and the dips are same after control due to an insignificant control force at $L/\lambda = n/2$ as shown in figure 4.5(a) where n is an integer. The optimal controller provides an in-phase and out-of-phase secondary control force depending on the ODS for the same reason as for the *strongly coupled* case with the structural natural frequency at $L/\lambda = 0.1$. The controlled acoustic potential energy has a structural mode at about $L/\lambda = 0.005$ due to the mass of the acoustic medium in the open tube modified by the control force.

In the *weakly coupled* case with a structural-acoustic stiffness ratio $K_a / K_s = 10^{-3}$ and the structural natural frequency at $L/\lambda = 0.8$, the acoustic potential energy has a structural mode at $L/\lambda = 0.8$ and acoustic modes of a closed-closed tube at $L/\lambda = n/2$ before control as shown in figure 4.4(b) where n is an integer. Under feedforward control, all the acoustic modes are effectively controlled. Also, at some frequencies between resonances, the dips of the acoustic potential energy are the same as that before control due to an insignificant control

force at $L/\lambda = 0.3$, 0.8, 1.25 and 1.75 as shown in figure 4.5(a). The optimal feedforward controller produces effective secondary control forces at the frequencies of the acoustic modes with appropriate phase information as shown in figure 4.5(b), which is determined by the structural excitation as in the *weakly coupled* case with the structural natural frequency at $L/\lambda = 0.1$. The modulus of the optimal feedforward controller has a maximum value at the frequency of the structural mode at $L/\lambda = 0.8$. However, the structural mode is not controllable because the dynamic behaviour of the structure is insensitive to the change in acoustic loading in the cavity under *weakly coupled* condition.

In the *intermediate* case with a structural-acoustic stiffness ratio $K_a / K_s = 1$ and the structural natural frequency at $L/\lambda = 0.8$, the acoustic potential energy has only acoustic modes before control as shown in figure 4.4(c). Under feedforward control, the acoustic potential energy is effectively controlled at the frequencies of all the acoustic modes. The controlled acoustic potential energy has a structural mode at about $L/\lambda = 0.16$ due to the mass of the acoustic medium in the cavity for the same reason as in the *strongly coupled* case. The modulus of the optimal feedforward controller has a maximum value at the structural mode as shown in figure 4.5(a). Also, the optimal controller produces secondary control forces at the acoustic modes with the same control mechanism as that in the *strongly coupled* case as shown in figure 4.5(b).
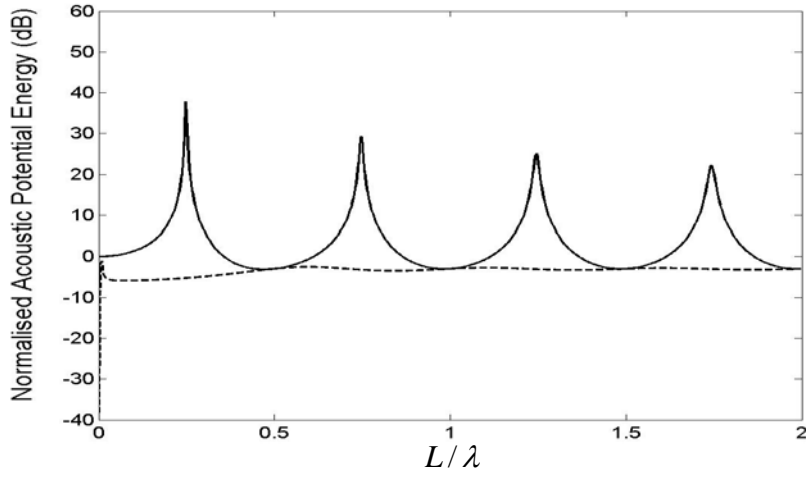
(a) Strongly coupled case ($K_a / K_s = 10^3$)
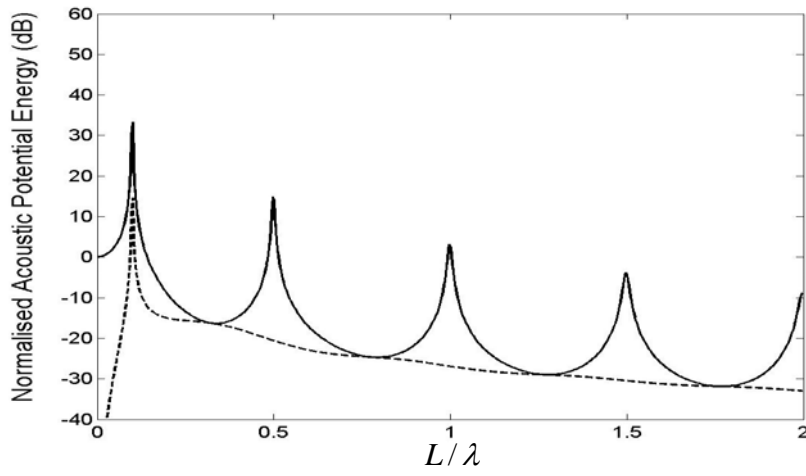
(b) Weakly coupled case ($K_a / K_s = 10^{-3}$)
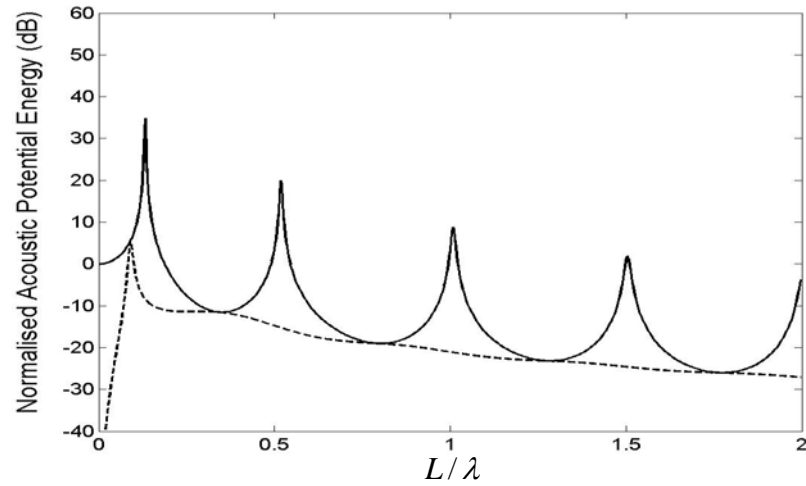
(c) Intermediate case ($K_a / K_s = 1$)

Figure 4.2 Acoustic potential energy normalised by that at the static state ($L/\lambda = 0$) in the absence of control for a given stiffness ratio when the structural natural frequency is at $L/\lambda = 0.1$ ($\omega_a / \omega_s = 5$) where the stiffness ratio $K_a / K_L = 10^{-3}$ and the loss factors $\eta_s = \eta_a = \eta_L = 10^{-2}$ (solid line: without control and dashed line: with feedforward control)
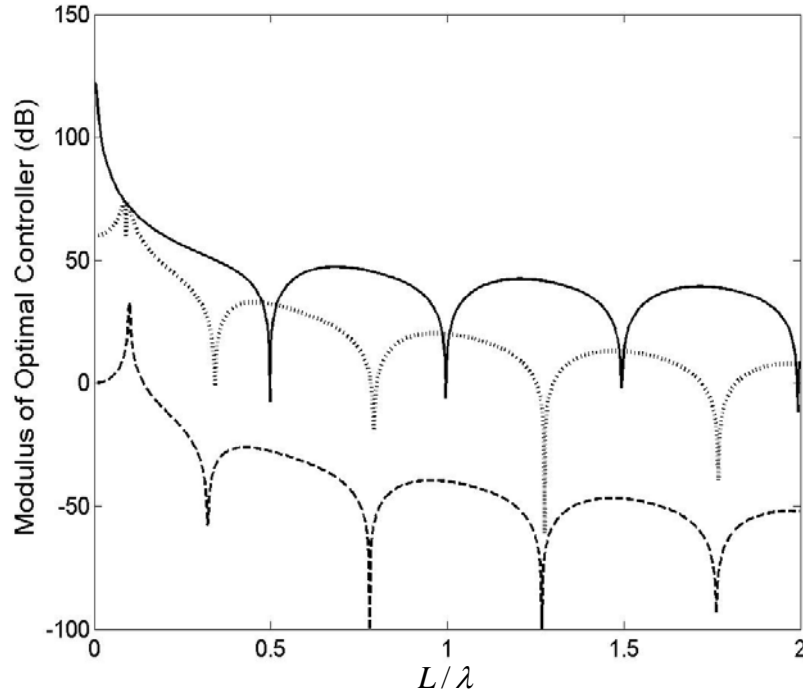
(a) Modulus of the optimal controller
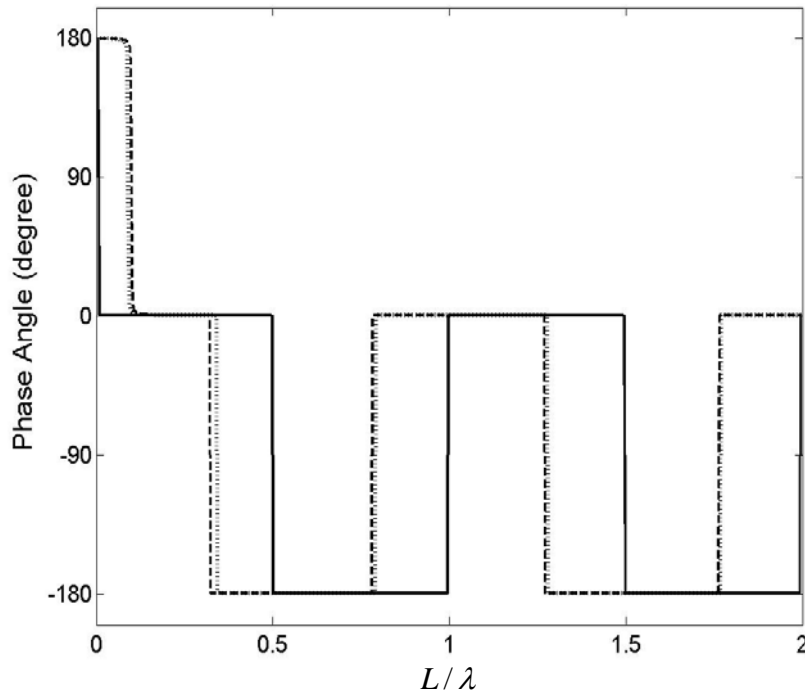
(b) Phase angle

Figure 4.3 Modulus and phase angle of the optimal feedforward controller given in equation (4.17) for a given stiffness ratio in the case when the structural natural frequency is at $L/\lambda = 0.1$ ($\omega_a/\omega_s = 5$) where the stiffness ratio $K_a/K_L = 10^{-3}$ and the loss factors $\eta_s = \eta_a = \eta_L = 10^{-2}$ (solid line: strongly coupled case with $K_a/K_s = 10^3$, dashed line: weakly coupled case with $K_a/K_s = 10^{-3}$ and dotted line: intermediate case with $K_a/K_s = 1$)
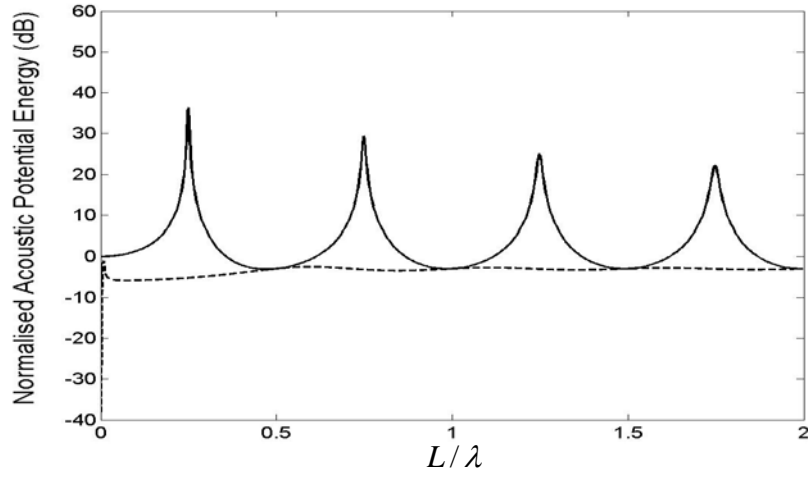
(a) Strongly coupled case ($K_a / K_s = 10^3$)
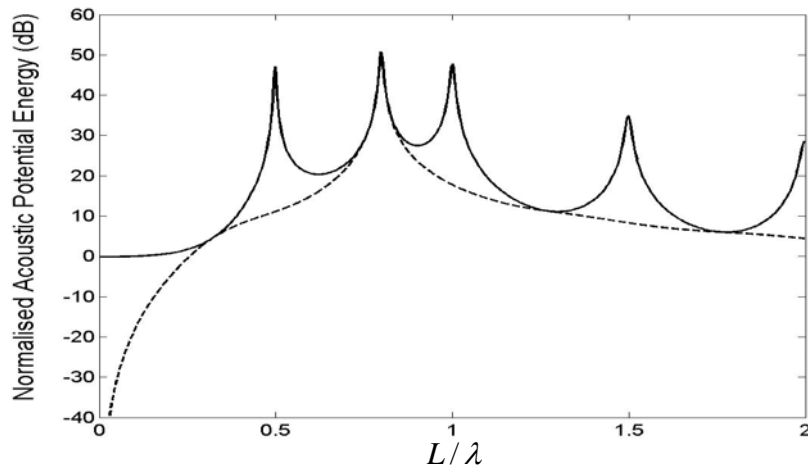
(b) Weakly coupled case ($K_a / K_s = 10^{-3}$)
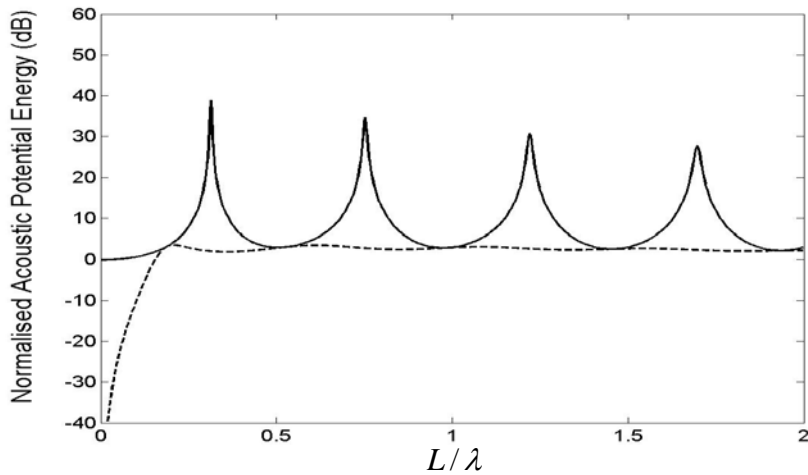
(c) Intermediate case ($K_a / K_s = 1$)

Figure 4.4 Acoustic potential energy normalised by that at the static state ($L/\lambda = 0$) in the absence of control for a given stiffness ratio when the structural natural frequency is at $L/\lambda = 0.8$ ($\omega_a / \omega_s = 0.6$) where the stiffness ratio $K_a / K_L = 10^{-3}$ and the loss factors $\eta_s = \eta_a = \eta_L = 10^{-2}$ (solid line: without control and dashed line: with feedforward control)
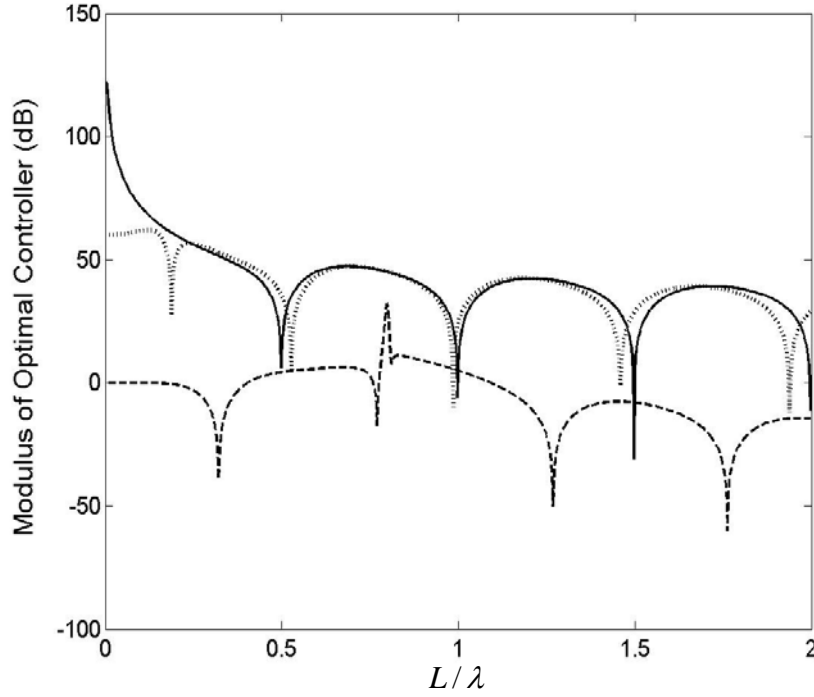
(a) Modulus of the optimal controller
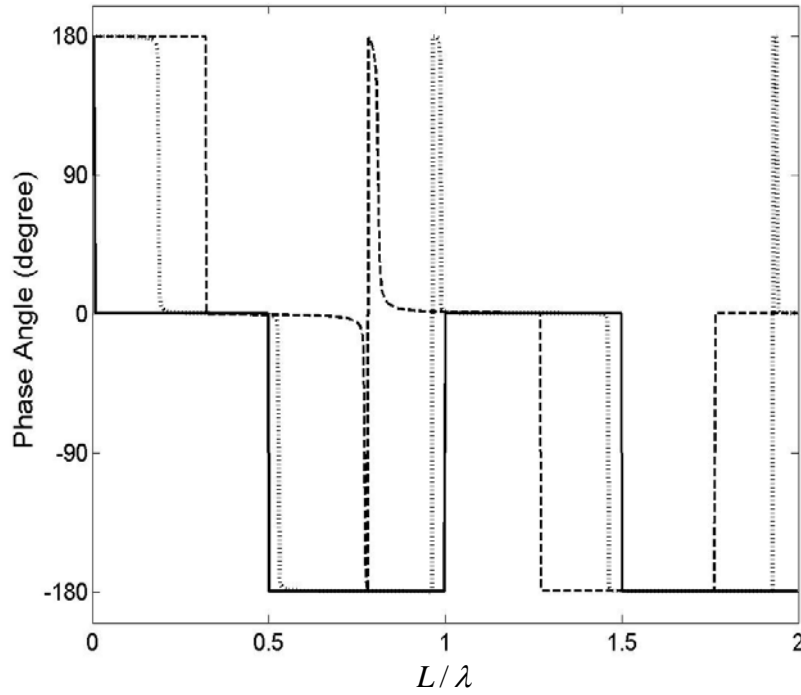
(b) Phase angle

Figure 4.5 Modulus and phase angle of the optimal feedforward controller given in equation (4.17) for a given stiffness ratio in the case when the structural natural frequency is at $L/\lambda = 0.8$ ($\omega_a/\omega_s = 0.6$) where the stiffness ratio $K_a/K_L = 10^{-3}$ and the loss factors $\eta_s = \eta_a = \eta_L = 10^{-2}$ (solid line: strongly coupled case with $K_a/K_s = 10^3$, dashed line: weakly coupled case with $K_a/K_s = 10^{-3}$ and dotted line: intermediate case with $K_a/K_s = 1$)

106

4.4 Optimal impedance of a feedforward control system

In this section, the optimal impedance is presented for the feedforward control system depicted in figure 4.1. The optimal impedance is defined as the ratio of the control force to the velocity of the control piston with a sign reversal when the acoustic potential energy is minimised. It is used to investigate the physical mechanism of the feedforward control of the acoustic potential energy. The three coupled cases, discussed in section 4.3, are studied when the structural natural frequency is at $L/\lambda = 0.1$ and is at $L/\lambda = 0.8$ respectively.

The optimal velocity at the secondary source position (at $x = L$) $U_{L\,opt}$ is the sum of the velocity due to both the primary force and the secondary control force, and is given by

$$U_{L\,opt} = U_{LP} + U_{LS\,opt} \tag{4.19}$$

where U_{LP} is the velocity due to the primary source and $U_{LS\,opt}$ is the velocity due to the secondary control force at the secondary source position. When the acoustic potential energy is minimised, the secondary control force $F_{S\,opt}$ can be represented by the product of the optimal control gain G_{opt} and the primary force F_P to give

$$F_{S\,opt} = G_{opt} F_P \tag{4.20}$$

The optimal impedance can be obtained by dividing the secondary control force, given in equation (4.20), by the velocity given in equation (4.19) with a sign reversal, so that

$$Z_{opt} = -\frac{F_{S\,opt}}{U_{L\,opt}} \tag{4.21}$$

Since the optimal impedance Z_{opt} shares the same velocity with the impedance of the secondary source Z_L, defined in equation (4.5), the optimal impedance can be illustrated as a parallel connection with the impedance of the secondary source as depicted in figure 4.6.
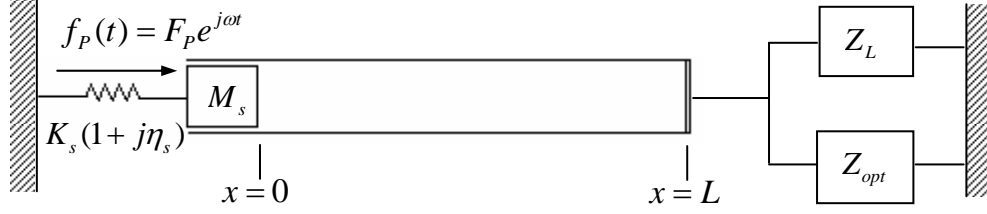
Figure 4.6 Conceptual representation of the vibro-acoustic system depicted in figure 4.1 in terms of the optimal impedance Z_{opt} and the impedance of the secondary source Z_L

The optimal impedance Z_{opt}, defined in equation (4.21), is determined by the secondary control force and the sum of the velocity due to both the primary force and the secondary control force. The resulting velocity, at the secondary source position, due to the primary force is significant at resonance frequencies in the cavity but is insignificant at off-resonance frequencies. In the case when the velocity due to the primary force is insignificant at the secondary source position, the optimal impedance Z_{opt} is determined largely by the secondary control force and the velocity due to only the secondary control force. In this case, setting the normalised arbitrary position $\hat{x}$ to 1 in equation (4.10) and combining equations (4.19)~(4.21) gives

$$Z_{opt} \approx -(Z_{AL} + Z_L) \qquad (4.22)$$

Note that the optimal impedance Z_{opt} is equal and opposite to the sum of the acoustic impedance at the secondary source position Z_{AL} and the impedance of the secondary source Z_L at off-resonance frequencies. The impedance Z_{AL}, defined in equation (2.24), is the input impedance of the acoustic tube at the secondary source position when the primary force is zero. The acoustic response is determined by the impedance ratio $Z_S / \rho_0 c_0 S$ in equation (2.24). If the impedance ratio is extremely small, the acoustic response has the acoustic modes of an open-closed tube. On the other hand, if the impedance ratio is infinitely large, the acoustic response has the acoustic modes of a closed-closed tube. In these two extreme cases, the structure has no contribution to the acoustic response. However, if the impedance ratio is

intermediate between two extreme values, the structural mode can be observed in the acoustic response.

Figures 4.7, 4.8 and 4.9 show (a) and (b) for the real part, (c) and (d) for the imaginary part, and (e) and (f) for the phase angle of the impedances Z_L (solid), Z_{AL} (dashed) and Z_{opt} (dotted). The same arbitrary normalisation is used for a given stiffness ratio when the structural natural frequency is at $L/\lambda = 0.1$ and at $L/\lambda = 0.8$ respectively.

In the *strongly coupled* case with an acoustic-structural stiffness ratio $K_a/K_s = 10^3$, the optimal impedance Z_{opt} has similar behaviour for the two natural frequency ratios ω_a/ω_s. At low frequencies below the first resonance at $L/\lambda = 1/4$, the optimal impedance is equal and opposite to the impedance Z_L as shown in figures 4.7(a), (b), (c) and (d). The optimal impedance has a negative real part which represents negative damping and a positive imaginary part which represents negative stiffness. The phase angle is $90°$ as shown in figures 4.7(e) and (f). At the low frequencies, the controlled vibro-acoustic system has an open-tube condition at the secondary source position (at $x = L$). The open-tube condition provides a free-end condition at one end of the acoustic spring depicted in the low-frequency approximate model in Appendix. A. At the resonance frequencies of an open-closed tube at $L/\lambda = (2n-1)/4$ where n is an integer, the optimal impedance has two control efforts. One of them is for the control of the sound pressure in the cavity due to the primary force and the other is for the modification of the boundary condition at the secondary source position. For the control of the sound pressure in the cavity, the optimal impedance has a negative real part, which represents negative damping, as shown in figures 4.7(a) and (b). The acoustic modes, which are apparent in the plots of the acoustic potential energy shown in figures 4.2(a) and 4.4(a), occur at the resonance frequencies. Also, the resonance frequencies of the acoustic potential energy correspond to those of the impedance Z_{AL}, which has a small impedance ratio $Z_S/\rho_0 c_0 S$ in equation (2.24). For the modification of the boundary condition, the optimal impedance is equal and opposite to the impedance Z_L as shown in figures 4.7(a), (b), (c) and (d). In the case when the impedance Z_L is zero, the phase angle of the optimal impedance, shown in figures 4.7(e) and (f), goes to $180°$. Physically, at the resonance frequencies of the impedance Z_{AL}, the secondary source radiates sound pressure with $180°$

phase shift into the cavity for the control of the sound pressure caused by the primary source. The larger modulus of the negative real part shown in figures 4.7(a) and (b), compared to that of the impedance Z_{AL}, is due to the real part of the impedance Z_L and the resulting velocity caused by the primary force. The velocity due to the primary force makes the sum of velocity at the secondary source position, in equation (4.19), smaller with $180°$ phase shift to that due to the secondary control force. Between resonances, the optimal impedance is equal and opposite to the sum of the acoustic impedance at the secondary source position Z_{AL} and the impedance of the secondary source Z_L as described in equation (4.22).

In the *weakly coupled* case with a structural-acoustic stiffness ratio $K_a / K_s = 10^{-3}$ and the structural natural frequency at $L/\lambda = 0.1$, at low frequencies below the first resonance at $L/\lambda = 1/2$ the optimal impedance Z_{opt} modifies the boundary condition into an open-tube at the secondary source position as shown in figures 4.8(a) and (c). At the low frequencies, the optimal impedance is equal and opposite to the impedance Z_L to provide an open-tube condition at the secondary source position as in the *strongly coupled* case. On the other hand, at the resonance frequencies of a closed-closed tube at $L/\lambda = n/2$ where n is an integer, the optimal impedance has a negative real part, which represents negative damping as shown in figure 4.8(a). The resonance frequencies correspond to those of the impedance Z_{AL}, which has a large impedance ratio $Z_S / \rho_0 c_0 S$ in equation (2.24). At the resonance frequencies, the secondary source generates sound pressure in the cavity with $180°$ phase shift for the control of the sound pressure due to the primary source as in the *strongly coupled* case. By virtue of the control effort of the optimal impedance at the resonance frequencies, the acoustic modes at $L/\lambda = n/2$, shown in figure 4.2(b), are effectively controlled where n is an integer. Also, the structural mode at $L/\lambda = 0.1$ is controlled to some degree by the modified open-tube condition at the secondary source position.

In the *weakly coupled* case, when the structural natural frequency is at $L/\lambda = 0.8$, the optimal impedance is generally similar to that in the case of the structural natural frequency at $L/\lambda = 0.1$. The optimal impedance is equal and opposite to the impedance Z_L at low frequencies below the first resonance at $L/\lambda = 1/2$ as shown in figures 4.8(b) and (d). Also, the optimal impedance has negative damping at resonance frequencies of the impedance Z_{AL}

corresponding to those of the acoustic modes in the acoustic potential energy shown in figure 4.4(b). In this case, the optimal impedance also has negative damping at $L/\lambda = 0.8$, which is the frequency of the structural mode. The negative damping at $L/\lambda = 0.8$ is due to the more strongly coupled structure into the cavity compared to the case of the structural natural frequency is at $L/\lambda = 0.1$. But the negative damping of the optimal impedance is not effective on the control of the structural mode due to the structure, which is insensitive to the change of the acoustic loading in the cavity under the *weakly coupled* condition.

In the *intermediate* case with a structural-acoustic stiffness ratio $K_a / K_s = 1$ and the structural natural frequency at $L/\lambda = 0.1$, the optimal impedance Z_{opt} has similar control efforts to those in the *weakly coupled* case at low frequencies and at resonances as shown in figures 4.9(a) and (c). In this case, the optimal impedance also has negative damping at $L/\lambda = 0.13$, which corresponds to the frequency of the structural mode shown in figure 4.2(c). The impedance Z_{AL} has an intermediate impedance ratio $Z_s / \rho_0 c_0 S$ in equation (2.24) and has a resonance at the frequency of the structural mode. Hence, in the *intermediate* case, both the structural and acoustic modes in the acoustic potential energy can be effectively controlled.

In the *intermediate* case, when the structural natural frequency is at $L/\lambda = 0.8$, the optimal impedance is generally similar to that in the *strongly coupled case* due to the more strongly coupled structure into the cavity. The optimal impedance provides an open-tube condition at the low frequencies below the first resonance at $L/\lambda = 1/4$. Also, the optimal impedance has negative damping at the resonance frequencies $L/\lambda = (2n-1)/4$ as shown in figures 4.9(b) and (d) where n is an integer. The resonance frequencies correspond to those of the acoustic modes in the acoustic potential energy shown in figure 4.4(c).

When the acoustic potential energy is minimised for a given stiffness ratio as shown figures 4.2(a), (b), (c) and 4.4(a), (b), (c) for the two natural frequency ratios ω_a / ω_s, the control mechanism can be summarised as follows.

At low frequencies below the fundamental acoustic mode in all the coupled cases, the acoustic potential energy can be reduced due to the open-tube condition at the secondary

source position ($x = L$). The optimal impedance is equal and opposite to the impedance of the secondary source Z_L.

At the frequency of the structural mode, in the *weakly coupled* case with structural natural frequency at $L/\lambda = 0.1$, the attenuation of the acoustic potential energy is due to the open-tube condition at the secondary source position ($x = L$) by virtue of the same control mechanism of the optimal impedance at low frequencies. However, in the *weakly coupled* case with structural natural frequency at $L/\lambda = 0.8$, the structural mode is not controlled due to the structure, which is insensitive to the change of the acoustic loading in the cavity under *weakly coupled* condition. In the *intermediate* case with structural natural frequency at $L/\lambda = 0.1$, the optimal impedance has negative damping at the structural mode ($L/\lambda = 0.13$). Hence, the acoustic potential energy can be effectively controlled at the structural mode ($L/\lambda = 0.13$).

At the natural frequencies of the acoustic modes in all the coupled cases, the acoustic potential energy can be effectively attenuated by the secondary source generating sound pressure with $180°$ phase shift with respect to the sound pressure due to the primary source. The controlled acoustic potential energy is not zero due to the residual modes.

Between resonances in all the coupled cases, the reduction on the acoustic potential energy is negligible due to the insignificant optimal impedance. At theses frequencies, the optimal impedance is equal and opposite to the sum of the acoustic impedance at the secondary source position Z_{AL} and the impedance of the secondary source Z_L.

(a) Real part

(b) Real part

(c) Imaginary part

(d) Imaginary part

(e) Phase angle

(f) Phase angle
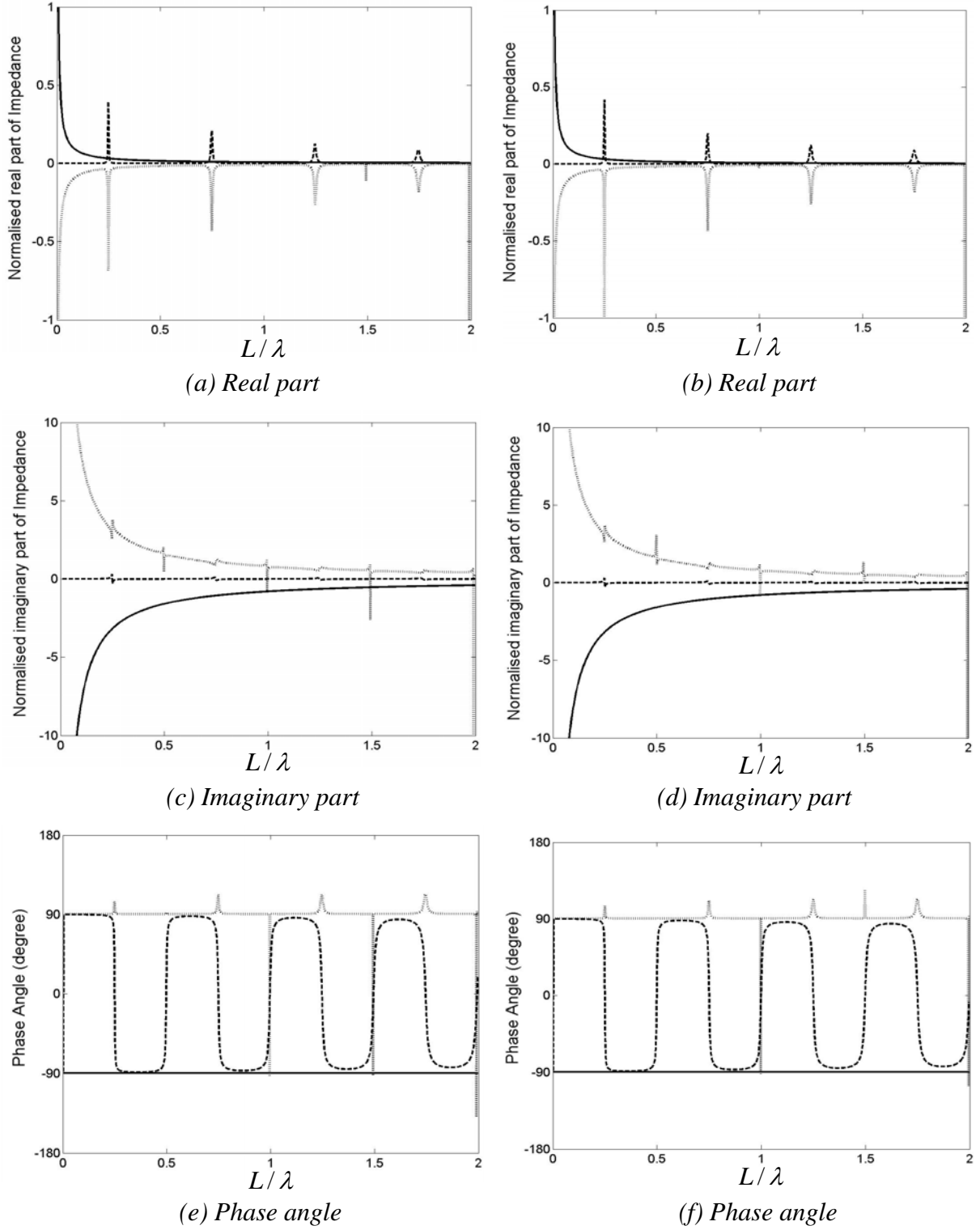
Figure 4.7 Strongly coupled case: impedances at the secondary source position (at $x = L$) as described in figure 4.5 with arbitrary normalisation where the structural natural frequency is at $L/\lambda = 0.1$ ($\omega_a/\omega_s = 5$) in figures (a), (c) and (e), and at $L/\lambda = 0.8$ ($\omega_a/\omega_s = 0.6$) in figures (b), (d) and (f) respectively, stiffness ratios $K_a/K_s = 10^3$ and $K_a/K_L = 10^{-3}$, loss factors $\eta_s = \eta_a = \eta_L = 10^{-2}$ (solid line: normalised impedance of the secondary source Z_L, dashed line: normalised acoustic input impedance at the secondary source position Z_{AL} and dotted line: normalised optimal impedance Z_{opt})

113

(a) Real part

(b) Real part

(c) Imaginary part

(d) Imaginary part

(e) Phase angle

(f) Phase angle

Figure 4.8 Weakly coupled case: impedances at the secondary source position (at $x = L$) as described in figure 4.5 with arbitrary normalisation where the structural natural frequency is at $L/\lambda = 0.1$ ($\omega_a / \omega_s = 5$) in figures (a), (c) and (e), and at $L/\lambda = 0.8$ ($\omega_a / \omega_s = 0.6$) in figures (b), (d) and (f) respectively, stiffness ratios $K_a / K_s = 10^{-3}$ and $K_a / K_L = 10^{-3}$, loss factors $\eta_s = \eta_a = \eta_L = 10^{-2}$ (solid line: normalised impedance of the secondary source Z_L, dashed line: normalised acoustic input impedance at the secondary source position Z_{AL} and dotted line: normalised optimal impedance Z_{opt})

(a) Real part

(b) Real part

(c) Imaginary part

(d) Imaginary part

(e) Phase angle

(f) Phase angle

Figure 4.9 Intermediate case: impedances at the secondary source position (at $x = L$) as described in figure 4.5 with arbitrary normalisation where the structural natural frequency is at $L/\lambda = 0.1$ ($\omega_a/\omega_s = 5$) in figures (a), (c) and (e), and at $L/\lambda = 0.8$ ($\omega_a/\omega_s = 0.6$) in figures (b), (d) and (f) respectively, stiffness ratios $K_a/K_s = 1$ and $K_a/K_L = 10^{-3}$, loss factors $\eta_s = \eta_a = \eta_L = 10^{-2}$ (solid line: normalised impedance of the secondary source Z_L, dashed line: normalised acoustic input impedance at the secondary source position Z_{AL} and dotted line: normalised optimal impedance Z_{opt})

115

4.5 Feedforward control effects on structural kinetic energy

When the acoustic potential energy is minimised in the various coupled cases, the secondary control force may affect the vibration of the SDOF structure at $x = 0$. The control effects are investigated on the kinetic energy of the structure defined in equation (2.54). In this section, the three coupled cases, discussed in section 4.3, are studied when the structural natural frequency is at $L/\lambda = 0.1$ and is at $L/\lambda = 0.8$ respectively.

When the acoustic potential energy, in the vibro-acoustic system under feedforward control as shown in figure 4.1, is minimised, the structural velocity U_s is the sum of the velocity due to the primary force and the velocity due to the secondary control force. This can be found by setting x equal to zero in equations (4.2) and (4.8) to give

$$U_s = U_P(0,\omega) + U_{S\,opt}(0,\omega) \tag{4.23}$$

where $U_P(0,\omega)$ is the velocity due to the primary force and $U_{S\,opt}(0,\omega)$ is the velocity due to the secondary control force at $x = 0$.

When the acoustic potential energy is minimised, the structural kinetic energy, given in equation (2.54), can be rewritten by combining equations (4.2), (4.8) and (4.23) to give

$$E_K(\omega) = \frac{1}{2} M_s \mid F_P \mid^2 \left| \frac{1}{Z_S + Z_{A0}} + \frac{G_{opt}}{Z_{AL} + Z_L} \frac{1}{\cos kL + j \dfrac{Z_S}{\rho_0 cS} \sin kL} \right|^2 \tag{4.24}$$

The structural kinetic energy, given in equation (4.24), can be written in non-dimensional form as

$$\hat{E}_K(\hat{L}) = \left| \frac{1}{\hat{Z}_S + \hat{Z}_{A0}} + \frac{G_{opt}}{\hat{Z}_{AL} + \hat{Z}_L} \frac{\dfrac{2}{2 - j\eta_a}}{\dfrac{2}{2 - j\eta_a} \cos\left(\pi(2 - j\eta_a)\hat{L}\right) + j\hat{Z}_S \sin\left(\pi(2 - j\eta_a)\hat{L}\right)} \right|^2 \tag{4.25}$$

where $\hat{E}_K(\hat{L}) = E_K(\hat{L}) / \frac{1}{2} M_s |F_P / \rho_0 c_0 S|^2$.

Figures 4.10(a), (b), (c) and figures 4.11(a), (b), (c) show the structural kinetic energy, in the vibro-acoustic system under feedforward control, for a given stiffness ratio when the structural natural frequency is at $L/\lambda = 0.1$ and at $L/\lambda = 0.8$ respectively. The structural kinetic energy is arbitrarily normalised by that at $L/\lambda = 2$ in the absence of control. The summed structural kinetic energy over the frequency range ($0 \le L/\lambda \le 2$) is presented in table 4.1.

In the *strongly coupled* case with an acoustic-structural stiffness ratio $K_a / K_s = 10^3$, the structural kinetic energy has similar behaviour for the two natural frequency ratios ω_a / ω_s as shown in figures 4.10(a) and 4.11(a). The structural kinetic energy has peaks at about $L/\lambda = 0.005$ and at $L/\lambda = (2n-1)/4$ where n is an integer after control. The peak at about $L/\lambda = 0.005$ is due to smaller acoustic loading and the acoustic mass in the cavity after control. The amplitudes of the peaks at $L/\lambda = (2n-1)/4$ increase due to smaller acoustic loading on the structure. The dips of the structural kinetic energy occur at the resonance frequencies of the acoustic input impedance under *strongly coupled* condition as described in chapter 2. The acoustic input impedance of an open tube at $x = L$, defined in equation (2.22), has resonances at $L/\lambda = (2n-1)/4$ where n is an integer. Also, the acoustic input impedance of a closed tube at $x = L$, defined in equation (2.23), has resonances at $L/\lambda = n/2$. Since the optimal impedance is equal and opposite to the sum of the impedance Z_{AL} and the impedance of the secondary source Z_L between resonances as described in section 4.4, the optimal impedance might move the dips to the resonance frequencies of an open tube at $x = L$. However, under the *strongly coupled* condition, the dips of the structural kinetic energy are the same as those before control due to the insignificant optimal impedance. In this case, the summed structural kinetic energy, over the frequency range of interest, increases by about 6dB as presented in table 4.1 due to smaller acoustic loading after control.

In the *weakly coupled* case with a structural-acoustic stiffness ratio $K_a / K_s = 10^{-3}$ and the structural natural frequency at $L/\lambda = 0.1$, the structural kinetic energy after control is the same as that before control as shown in figure 4.10(b). The structural kinetic energy has a

peak at $L/\lambda = 0.1$, which is not affected by the change in acoustic loading. Also, the structural kinetic energy is determined by only structural characteristics like an uncoupled structure.

In the *weakly coupled* case, when the structural natural frequency is at $L/\lambda = 0.8$, the structural kinetic energy has a peak at $L/\lambda = 0.8$, which is not subject to the acoustic loading change in the cavity after control as shown in figure 4.11(b). On the other hand, the structural kinetic energy has small increase at $L/\lambda = n/2$ where n is an integer due to the fact that the structure is more strongly coupled compared to the case of the structural natural frequency at $L/\lambda = 0.1$.

In the *intermediate* case with a structural-acoustic stiffness ratio $K_a/K_s = 1$ and the structural natural frequency at $L/\lambda = 0.1$, the amplitudes of the structural kinetic energy increase at the peaks as shown in figure 4.10(c) due to smaller acoustic loading on the structure. Also, the structural kinetic energy has a peak at about $L/\lambda = 0.09$ due to the acoustic mass in the cavity after control. The dips of the structural kinetic energy occur at lower frequencies due to the optimal impedance modifying the boundary condition at $x = L$. In this case, the summed structural kinetic energy, over the frequency range of interest, increases by about 6dB as presented in table 4.1 due to a peak at about $L/\lambda = 0.09$ and increased amplitudes of the other peaks.

In the *intermediate* case, when the structural natural frequency is at $L/\lambda = 0.8$, the amplitude of the structural kinetic energy increases at the peaks as shown in figure 4.11(c). Also, the structural kinetic energy has a peak at $L/\lambda = 0.16$ due to the acoustic mass in the cavity after control. The first dip occurs at $L/\lambda = 1/4$ due to the open-tube condition modified by the optimal impedance. The second dip moves to higher frequency due to the proximity to the first at $L/\lambda = 1/4$. Also, the rest of dips move to lower frequencies as in the case of the structural natural frequency at $L/\lambda = 0.1$. In this case, the summed structural kinetic energy, in the frequency range of interest, increases by about 6dB as presented in table 4.1 after control for the same reason as in the *strongly coupled* case.

To summarise the various cases considered, in the *strongly coupled* and *intermediate* cases, the amplitude of the structural kinetic energy increases at the resonance frequencies due to

smaller acoustic loading in the cavity. The smaller acoustic loading is due to the acoustic modes controlled by the negative damping of the optimal impedance, which generates 180° out-of-phase sound pressure to the sound pressure due to the primary source. Also, the structural kinetic energy has a peak at the low frequency due to the smaller acoustic loading and acoustic mass in the cavity after control. On the other hand, in the *weakly coupled* case, the structural kinetic energy generally has no change because the structure is insensitive to the acoustic loading change in the cavity.
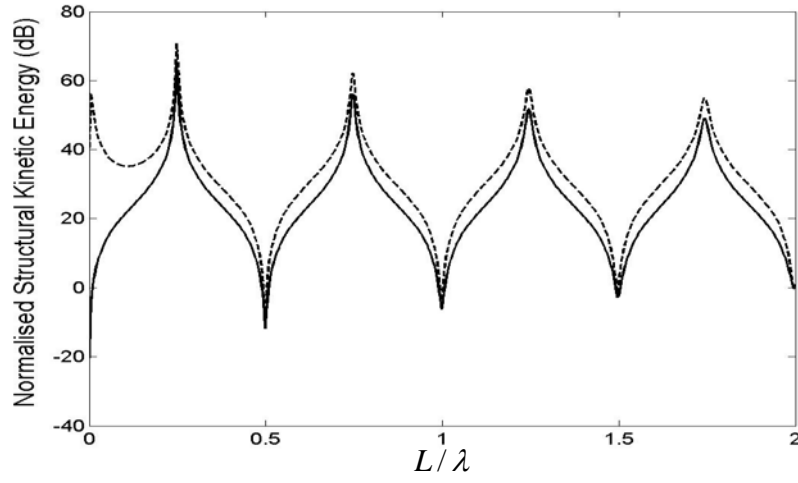
(a) Strongly coupled case ($K_a / K_s = 10^3$)
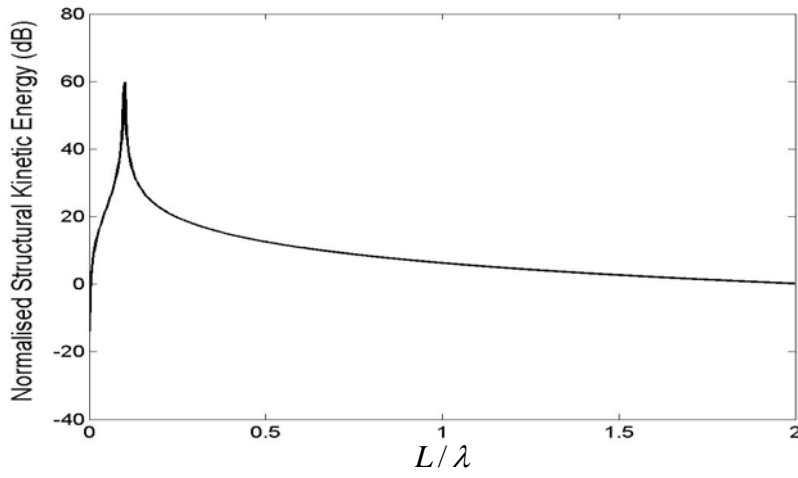
(b) Weakly coupled case ($K_a / K_s = 10^{-3}$)
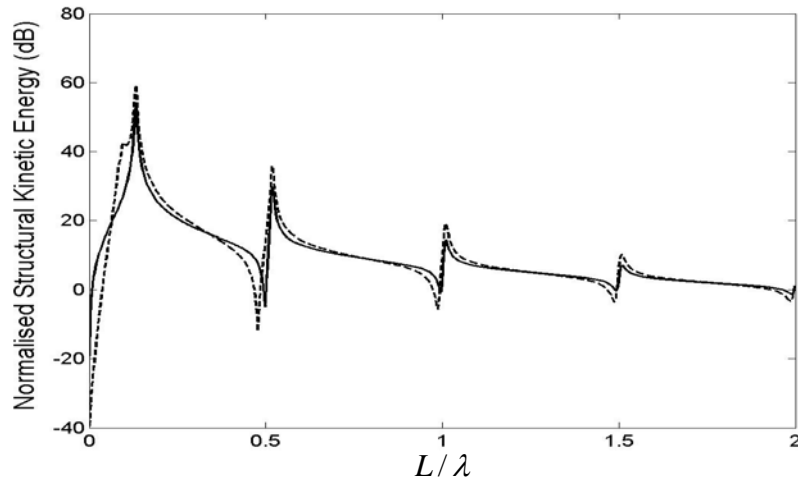
(c) Intermediate case ($K_a / K_s = 1$)

Figure 4.10 Structural kinetic energy arbitrarily normalised by that at $L/\lambda = 2$ in the absence of control for a given stiffness ratio where the structural natural frequency is at $L/\lambda = 0.1$ ($\omega_a / \omega_s = 5$), stiffness ratio $K_a / K_L = 10^{-3}$, loss factors $\eta_s = \eta_a = \eta_L = 10^{-2}$ (solid line: without control and dashed line: with feedforward control)
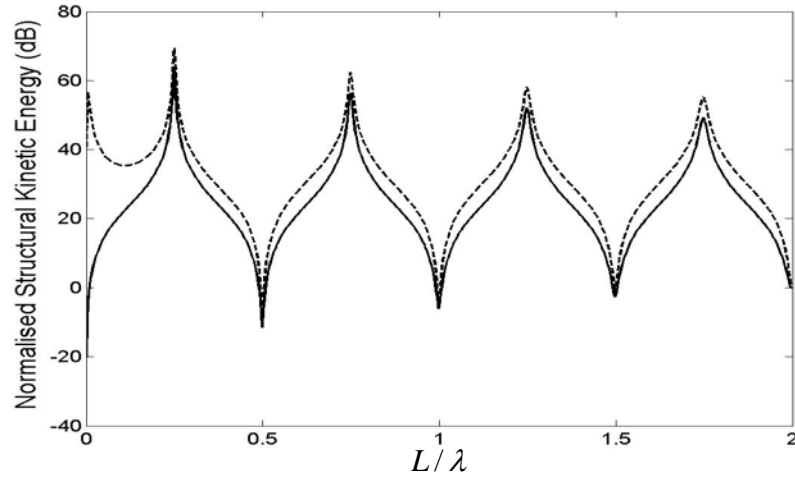
(a) Strongly coupled case ($K_a / K_s = 10^3$)
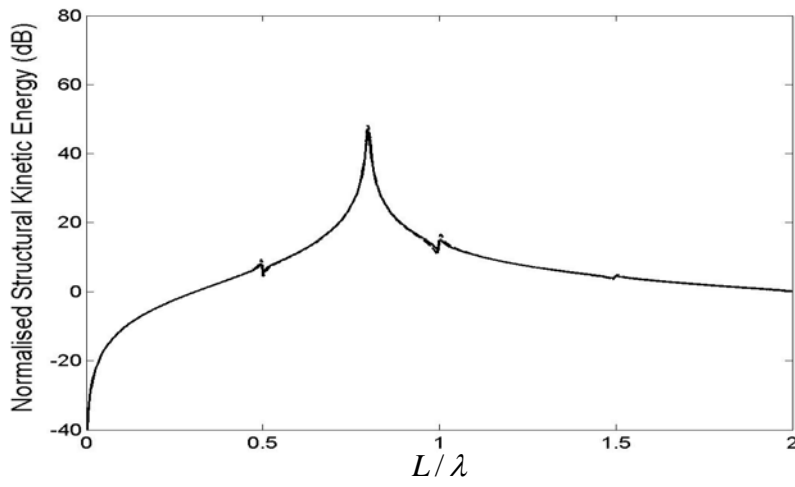
(b) Weakly coupled case ($K_a / K_s = 10^{-3}$)
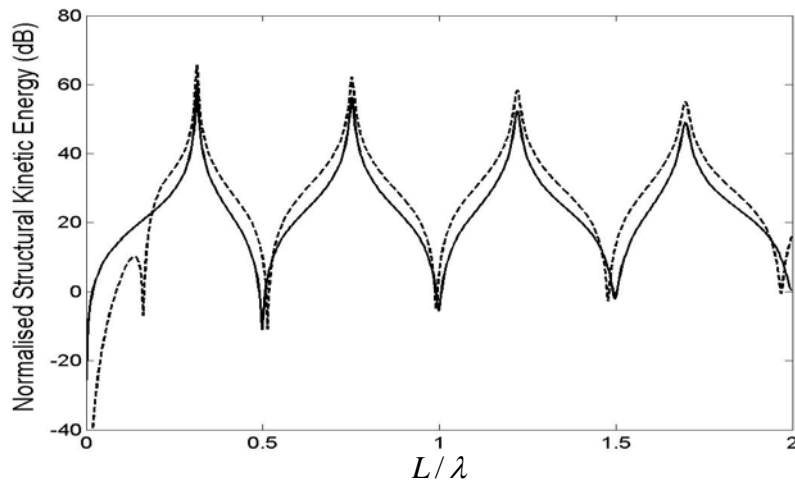
(c) Intermediate case ($K_a / K_s = 1$)

Figure 4.11 Structural kinetic energy arbitrarily normalised by that at $L/\lambda = 2$ in the absence of control for a given stiffness ratio where the structural natural frequency is at $L/\lambda = 0.8$ ($\omega_a / \omega_s = 0.6$), stiffness ratio $K_a / K_L = 10^{-3}$, loss factors $\eta_s = \eta_a = \eta_L = 10^{-2}$ (solid line: without control and dashed line: with feedforward control)

Table 4.1 Summed structural kinetic energy, over the frequency range ($0 \le L/\lambda \le 2$), normalised by that before control when the structural natural frequency is at $L/\lambda = 0.1$ ($\omega_a/\omega_s = 5$) and at $L/\lambda = 0.8$ ($\omega_a/\omega_s = 0.6$) respectively

Degree of coupling	Natural frequency ratio	
	$\omega_a/\omega_s = 5$	$\omega_a/\omega_s = 0.6$
Strong ($K_a/K_s = 10^3$)	6dB	6dB
Weak ($K_a/K_s = 10^{-3}$)	0dB	0dB
Intermediate ($K_a/K_s = 1$)	6dB	6dB

4.6 Cumulative sum of acoustic potential energy

The feedforward control effect on the acoustic potential energy is investigated in this section by presenting a cumulative sum of the acoustic potential energy over the frequency range ($0 \le L/\lambda \le 2$). Since the acoustic potential energy is controlled at each driving frequency, the cumulative sum is plotted to investigate the dominant mode with respect to the acoustic potential energy. The cumulative sum of the acoustic potential energy in the three coupled cases, discussed in section 4.3, is studied when the structural natural frequency is at $L/\lambda = 0.1$ and is at $L/\lambda = 0.8$ respectively. The control performance is evaluated by examining the summed acoustic potential energy over the frequency range of interest for the broadband control.

Figures 4.12(a), (b), (c) and figures 4.13(a), (b), (c) show the cumulative sum of the acoustic potential energy, over the frequency range ($0 \le L/\lambda \le 2$), for a given stiffness ratio when the structural natural frequency is at $L/\lambda = 0.1$ and at $L/\lambda = 0.8$ respectively. The cumulative sum of the acoustic potential energy is normalised by the summed acoustic potential energy over the frequency range in the absence of control. The values, at the upper limit of L/λ, demonstrate the achievable reductions on the summed acoustic potential energy over the frequency range of interest after control, which are presented in table 4.2.

In the *strongly coupled* case with a structural-acoustic stiffness ratio $K_a / K_s = 10^3$, the cumulative sum of the acoustic potential energy has similar behaviour for the two natural frequency ratios ω_a / ω_s. The acoustic potential energy before control is dominated by acoustic modes at $L / \lambda = (2n-1)/4$ where n is an integer as shown in figures 4.12(a) and 4.13(a). Also, the controlled acoustic potential energy increases gradually with frequency due to control of all the acoustic modes as shown in figures 4.2(a) and 4.4(a). In this case, the summed acoustic potential energy, over the frequency range of interest, can be reduced by about 18dB under feedforward control for the two natural frequency ratios ω_a / ω_s.

In the *weakly coupled* case with a structural-acoustic stiffness ratio $K_a / K_s = 10^{-3}$ and the structural natural frequency at $L / \lambda = 0.1$, the cumulative sum of the acoustic potential energy is dominated by the structural mode at $L / \lambda = 0.1$ before control as shown in figure 4.12(b). Under feedforward control, the cumulative sum of the acoustic potential energy is dominated by reduced structural mode shown in figure 4.2(b). In this case, the summed acoustic potential energy, over the frequency range of interest, can be reduced by about 19dB due to the controlled structural mode to some degree and control of all the acoustic modes.

In the *weakly coupled* case, when the structural natural frequency is at $L / \lambda = 0.8$, the structural mode at $L / \lambda = 0.8$ has more or less equivalent contribution to the cumulative sum of the acoustic potential energy to that of the acoustic modes at $L / \lambda = n/2$ as shown in figure 4.13(b) where n is an integer. Under feedforward control, the cumulative sum of the acoustic potential energy is dominated the structural mode due to the controlled acoustic modes shown in figure 4.4(b). Since the structural mode is uncontrollable, the reduction on the summed acoustic potential energy over the frequency range of interest is less than that in the case when the structural natural frequency is at $L / \lambda = 0.1$. In this case, the summed acoustic potential energy decreases by about 4dB.

In the *intermediate* case with a structural-acoustic stiffness ratio $K_a / K_s = 1$ and the structural natural frequency at $L / \lambda = 0.1$, the acoustic potential energy before control is mostly dominated by the structural mode at $L / \lambda = 0.13$ as shown in figure 4.12(c). On the other hand, the controlled acoustic potential energy is significantly featured by the structural mode at about $L / \lambda = 0.09$ shown in figure 4.2(c). In this case, the summed acoustic potential energy,

over the frequency range of interest, can be reduced by about 23dB due to the control of the structural and acoustic modes.

In the *intermediate* case, when the structural natural frequency is at $L/\lambda = 0.8$, the cumulative sum of the acoustic potential energy is similar to that in the *strongly coupled* case as shown in figure 4.13(c). In this case, the summed acoustic potential energy over the frequency range of interest decreases by about 16dB. The reduction on the summed acoustic potential energy is less than that in the case when the structural natural frequency is at $L/\lambda = 0.1$. The smaller reduction is due to the more strongly coupled structure, which causes only acoustic modes to feature significantly in the acoustic potential energy before control.

In summary, in the *strongly coupled* case, the cumulative sum of the acoustic potential energy gradually increases with frequency after control for the two natural frequency ratios. On the other hand, in the *weakly coupled* case, the controlled acoustic potential energy is dominated by the structural mode at $L/\lambda = 0.1$ and at $L/\lambda = 0.8$ respectively. In the *intermediate* case, the cumulative sum of the acoustic potential energy is similar to that of the *weakly coupled* case and of the *strongly coupled* when the structural natural frequency is at $L/\lambda = 0.1$ and $L/\lambda = 0.8$ respectively. The reduction on the summed acoustic potential energy over the frequency range of interest is more effective in the case when the structural natural frequency is below the fundamental acoustic mode as presented in table 4.2. Also, the reduction on the summed acoustic potential energy is most effective in the *intermediate* case with the structural natural frequency at $L/\lambda = 0.1$ due to control of both the structural and acoustic modes.
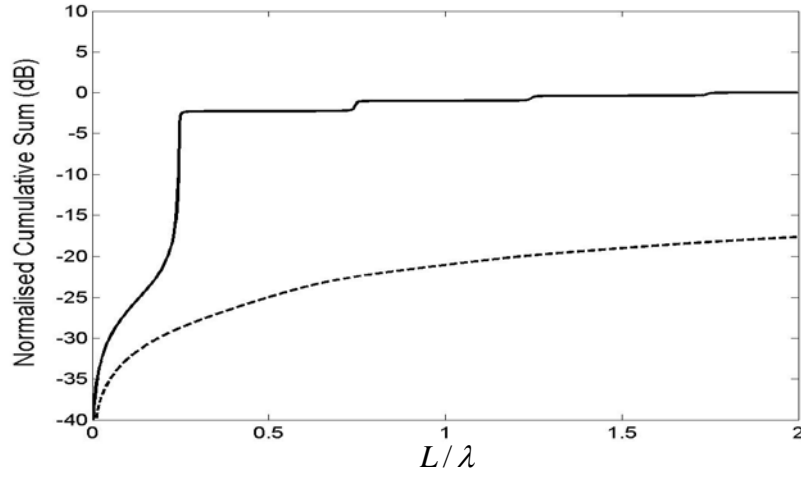
(a) Strongly coupled case ($K_a / K_s = 10^3$)
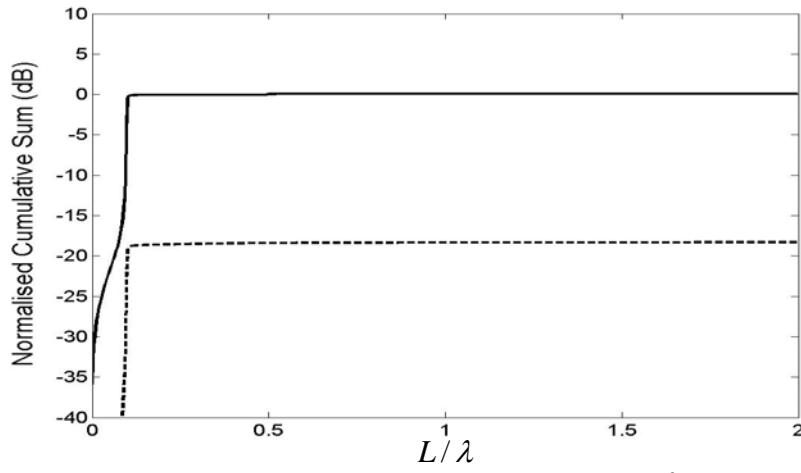
(b) Weakly coupled case ($K_a / K_s = 10^{-3}$)
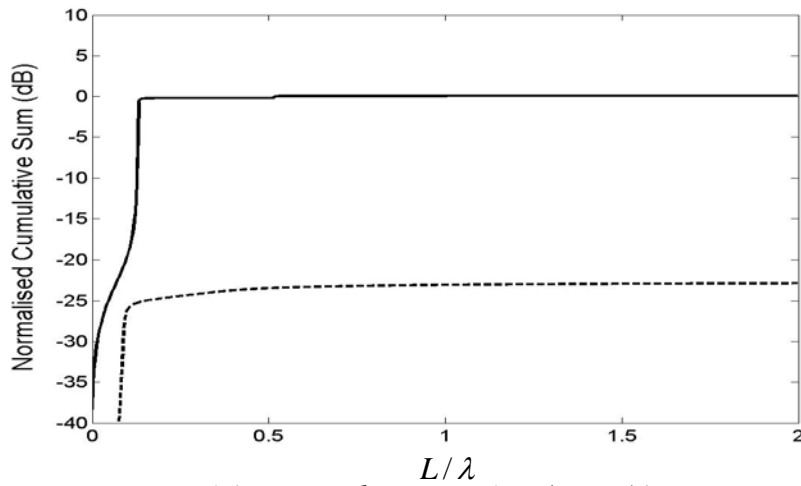
(c) Intermediate case ($K_a / K_s = 1$)

Figure 4.12 Cumulative sum of acoustic potential energy normalised by the summed acoustic potential energy in the absence of control for a given stiffness ratio where the structural natural frequency is at $L/\lambda = 0.1$ ($\omega_a / \omega_s = 5$), stiffness ratio $K_a / K_L = 10^{-3}$, loss factors $\eta_s = \eta_a = \eta_L = 10^{-2}$ (solid line: without control and dashed line: with feedforward control)
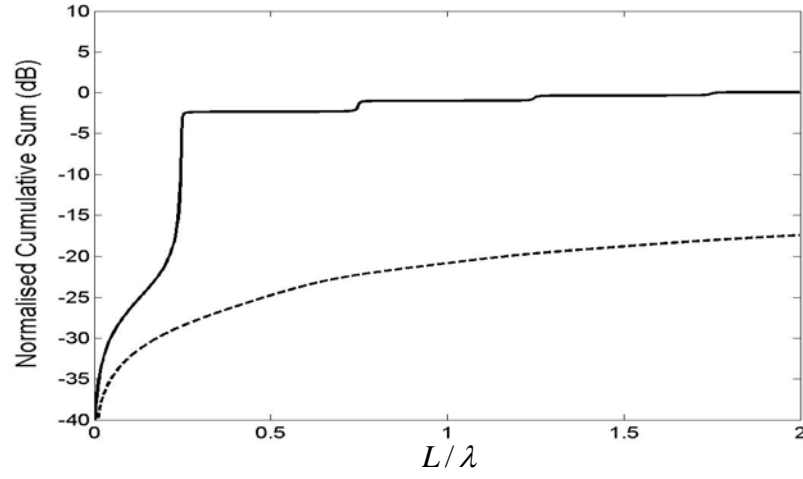
(a) Strongly coupled case ($K_a / K_s = 10^3$)
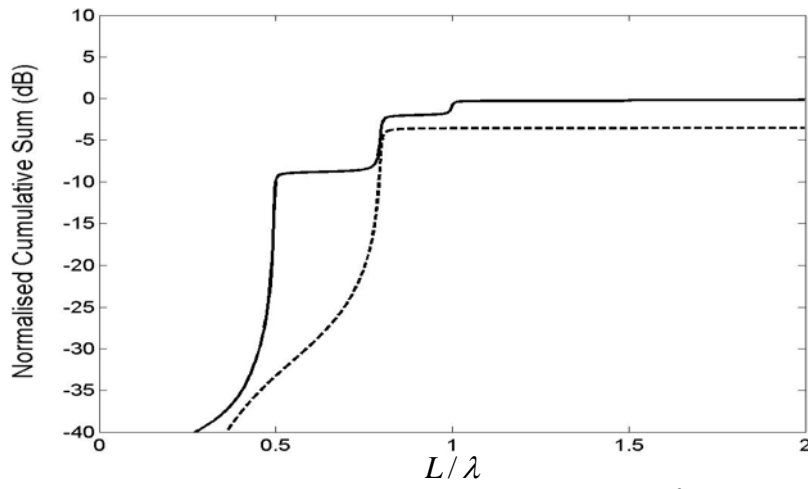
(b) Weakly coupled case ($K_a / K_s = 10^{-3}$)
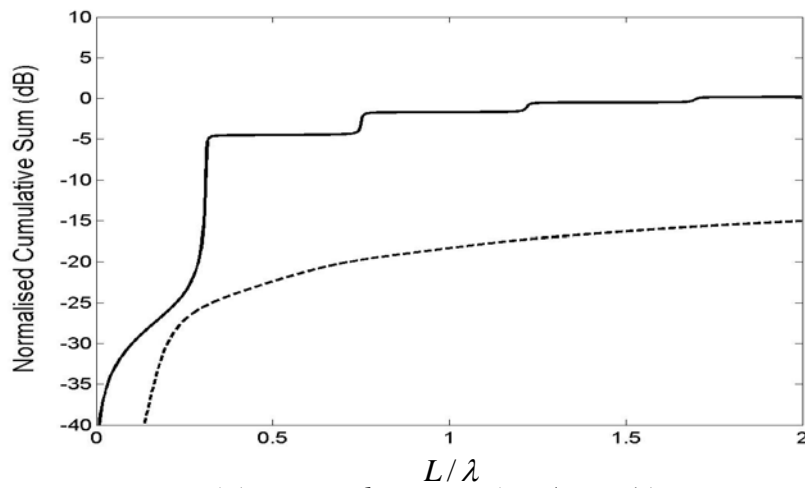
(c) Intermediate case ($K_a / K_s = 1$)

Figure 4.13 Cumulative sum of acoustic potential energy normalised by the summed acoustic potential energy in the absence of control for a given stiffness ratio where the structural natural frequency is at $L/\lambda = 0.8$ ($\omega_a / \omega_s = 0.6$), stiffness ratio $K_a / K_L = 10^{-3}$, loss factors $\eta_s = \eta_a = \eta_L = 10^{-2}$ (solid line: without control and dashed line: with feedforward control)

Table 4.2 Summed acoustic potential energy, over the frequency range ($0 \leq L/\lambda \leq 2$), normalised by that before control when the structural natural frequency is at $L/\lambda = 0.1$ ($\omega_a/\omega_s = 5$) and at $L/\lambda = 0.8$ ($\omega_a/\omega_s = 0.6$) respectively

	Natural frequency ratio	
Degree of coupling	$\omega_a/\omega_s = 5$	$\omega_a/\omega_s = 0.6$
Strong ($K_a/K_s = 10^3$)	-18dB	-18dB
Weak ($K_a/K_s = 10^{-3}$)	-19dB	-4dB
Intermediate ($K_a/K_s = 1$)	-23dB	-16dB

4.7 Experimental investigation on acoustic potential energy under feedforward control

To validate the theoretical predictions in this chapter, feedforward control was investigated experimentally for *more strongly and weakly coupled* cases. In the experiment, the main concern was to investigate the controllability of the acoustic potential energy under the different coupled conditions. The experimental results were calculated by using frequency-response functions measured at microphones along the acoustic tube with respect to the corresponding reference signal. The approximation of the acoustic potential energy, based on the measured frequency response functions, is defined in equation (3.24). In this experiment, the measured frequency response function vector is the sum of that due to the primary source and that due to the secondary source. For the feedforward control, the optimal control gain was calculated without real-time active control by measuring the frequency-response functions of the primary source and the secondary source independently. The physical interpretation of the control performance on the acoustic potential energy in a vibro-acoustic system could be achieved without considering control implementation issues.

4.7.1 Experimental setup

The experimental setup was generally similar to that for the investigation on the vibro-acoustic system, described in chapter 3, as shown in figure 4.14. The primary source was a standard and a modified loudspeaker as illustrated in figures 3.14(a) and (b) for the *more strongly and weakly coupled* cases. The reference signal to the primary speaker was provided by the dynamic signal analyser (Data Physics) through the acoustic amplifier (Cambridge Audio A1 V2.0). Another standard loudspeaker was used for the secondary source at the other end being subject to an excitation signal from the dynamic signal analyser through the acoustic amplifier. The frequency response functions, at omni-directional sub-miniature microphones along the centre line in the acoustic tube, were measured by driving the primary source and the secondary source independently. The measured acoustic pressures at seven microphones in the tube were fed back to the dynamic signal analyser through the 8-channel acoustic amplifier.
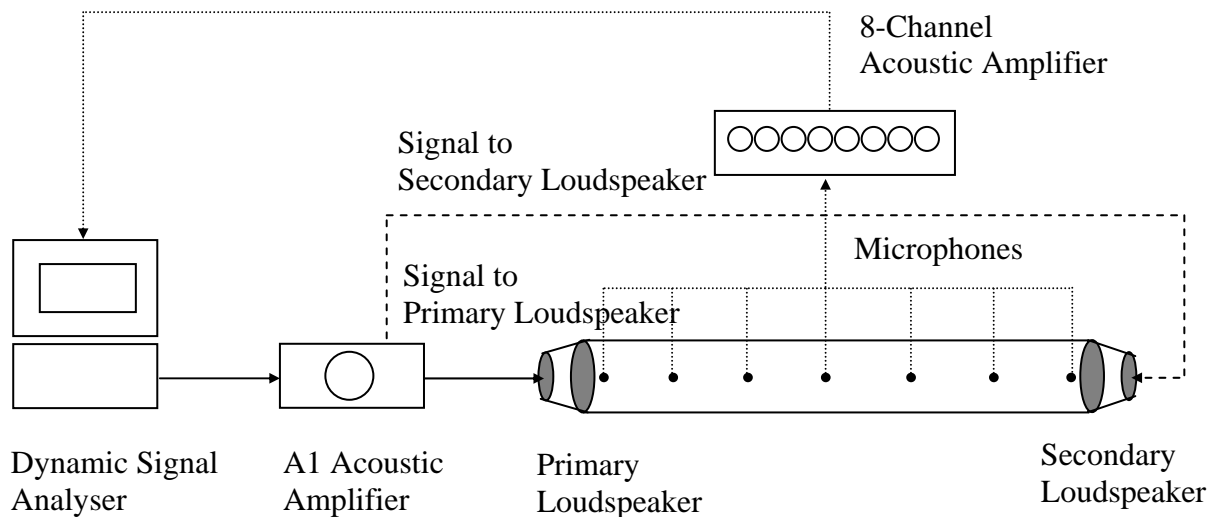
Figure 4.14 Schematic diagram of the experimental setup for the predicted acoustic potential energy in a structural-acoustic coupled system under feedforward control

4.7.2 Experimental results

The experimental work was carried out by measuring FRF (frequency response function) of primary and secondary paths under more *strongly or weakly coupled* conditions. The primary source was implemented by using the standard loudspeaker for the more *strongly coupled* condition and by using the modified loudspeaker for the more *weakly coupled* condition

respectively. The FRF of the primary path was identified by measuring the microphone array responses in the acoustic tube with respect to the reference signal to drive the primary source. Also, the secondary source was implemented by using a standard loudspeaker for both the more *strongly coupled* case and more *weakly coupled* case. In the same manner, the FRF of the secondary path was identified by measuring the microphone array responses with respect to the reference signal to drive the secondary source. The primary and secondary loudspeakers were excited individually up to 500Hz under broadband excitation. Since radial directional wave propagation starts at 1.7kHz, plane wave propagation in the acoustic tube can be achieved. The optimal control gain was calculated both from the theoretical model and experimental data following the solution procedure given in section 4.3. One structural mode and three acoustic modes were considered to contribute to the approximate acoustic potential energy in the acoustic tube.

Figures 4.15(a) and (b) show the theoretical and the experimental acoustic potential energy for the more *strongly coupled* case respectively, which are normalised by that at the static state ($f = 0$) for theory and that at 50Hz for experiment due to noisy results at low frequencies in the absence of control. Also, figures 4.16(a) and (b) show the theoretical and the experimental cumulative sum of the acoustic potential energy for the more *strongly coupled* case respectively, which are normalised by the summed acoustic potential energy over the frequency range ($0 \leq f \leq 500$ Hz) in the absence of control. The theoretical and experimental results, in figures 4.15(a) and (b), demonstrate that the acoustic modes at 170Hz, at 340Hz and at 510Hz in the acoustic potential energy are controllable. The noisy experimental results, below about 50Hz as shown in figure 4.15(b), were due to poor coherence between the reference signal and acoustic pressure in the acoustic tube. Also, the theoretical and experimental results, in figures 4.16(a) and (b), demonstrate that the cumulative sum of the acoustic potential energy is dominated by the acoustic modes before control and increases gradually after control due to the control of the acoustic modes. The difference at low frequencies between the theoretical and experimental results is due to the poor coherence in the experimental result.

Figures 4.17(a) and (b) show the theoretical and the experimental acoustic potential energy for the more *weakly coupled* case respectively. Also, figures 4.18(a) and (b) show the theoretical and the experimental cumulative sum of the acoustic potential energy for more

weakly coupled case respectively. The results are normalised in the same manner as in the more strongly coupled case. The theoretical and experimental results, in figures 4.17(a) and (b), demonstrate that the structural mode at 96Hz is not controllable and the acoustic modes at 170Hz, at 340Hz and at 510Hz are controllable. The smaller amplitudes, at off-resonances in the measured acoustic potential energy under control compared to the theory, are due to the modified loudspeaker which has an air cavity behind the modified loudspeaker cone. Also, the noisy results, at low frequencies after control, are due to poor performance of the loudspeakers. In this case, the cumulative sum of the acoustic potential energy is dominated by the structural mode at 96Hz after control as shown in figures 4.18(a) and (b). The difference at low frequencies between the theoretical and experimental results is due to the poor coherence in the experimental result as in the more *strongly coupled* case.
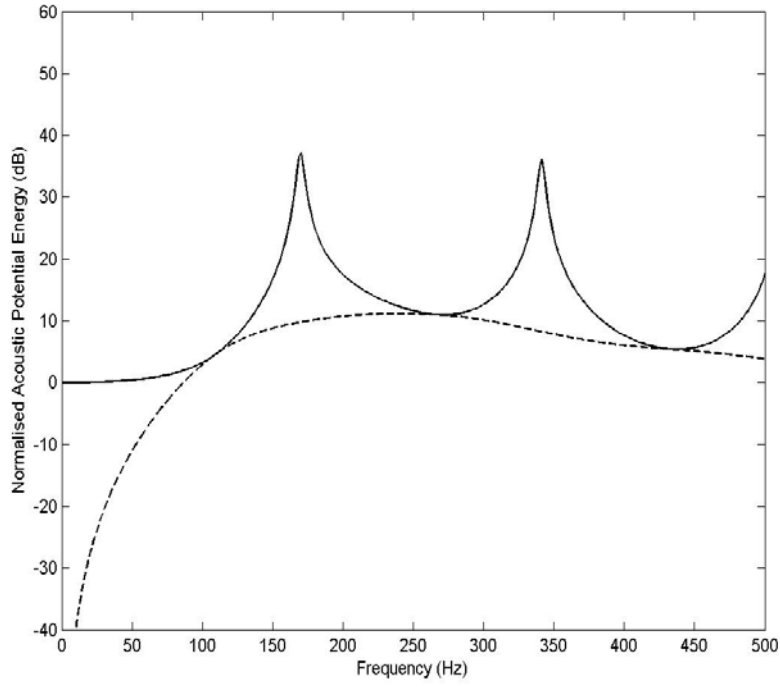
(a) Theory
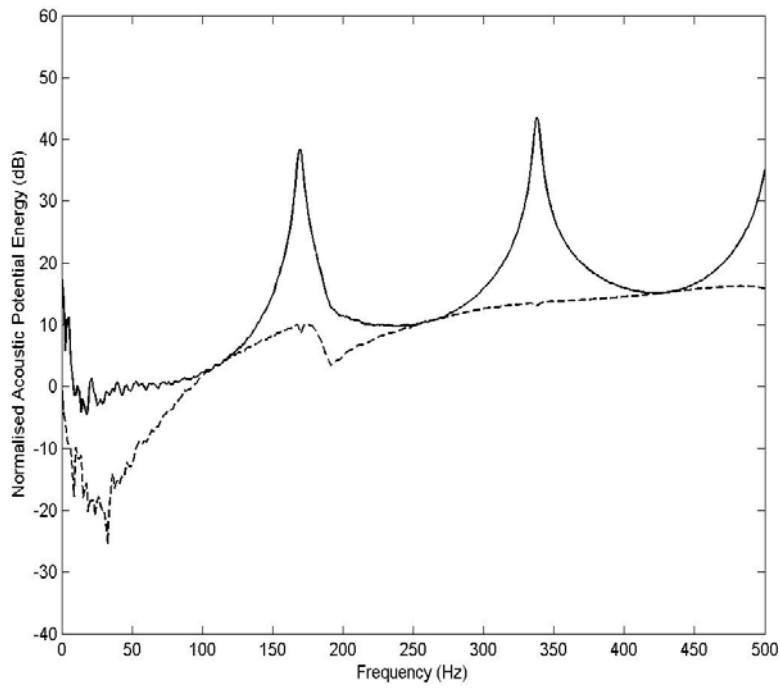
(b)Experiment

Figure 4.15 Strongly coupled case: acoustic potential energy normalised by that at the static state ($f = 0$) for theory and that at 50Hz for experiment where stiffness ratios $K_a / K_s = 0.1$, $K_a / K_L = 0.1$, uncoupled structural resonance is at 190Hz, and loss factors $\eta_s = \eta_L = 0.16$, $\eta_a = 0.01$ (solid line: before control and dashed line: after control)
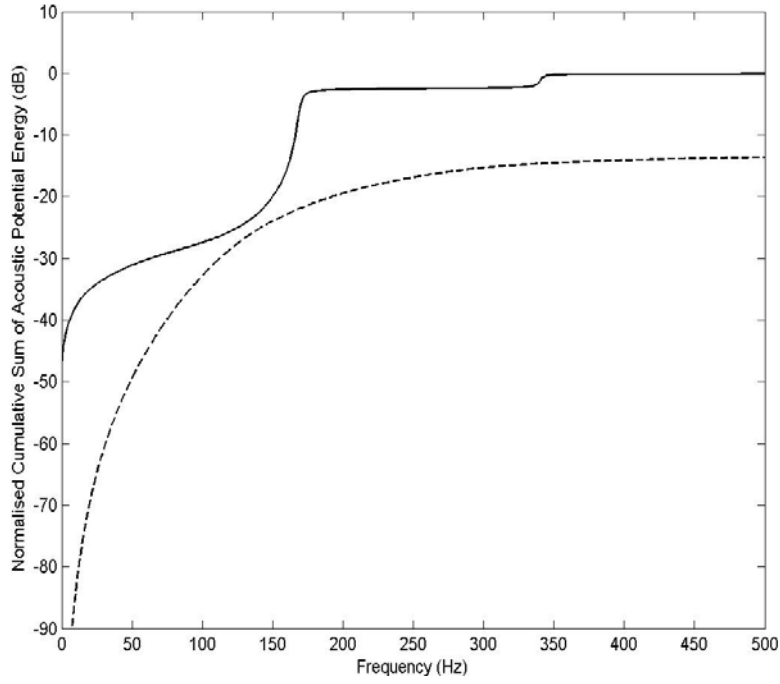
(a) Theory
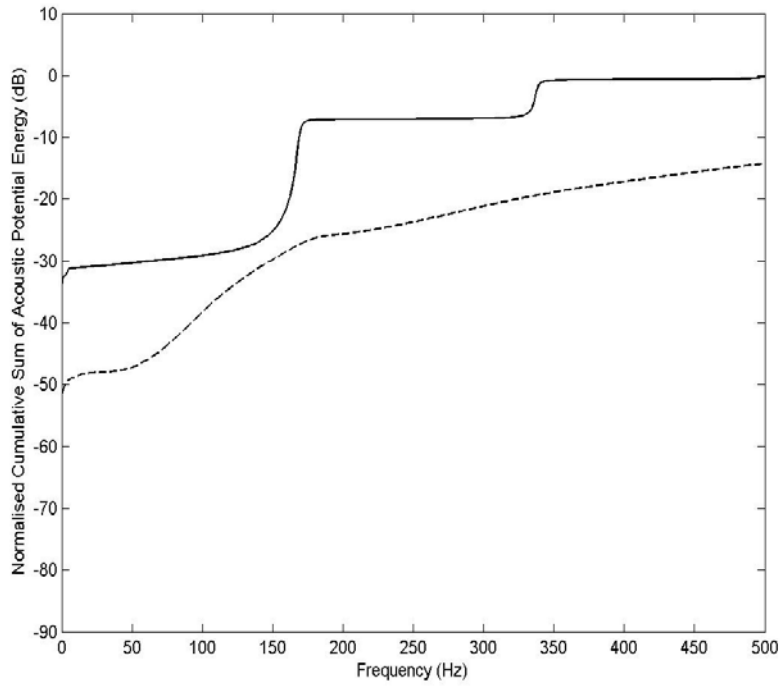
(a) Experiment

Figure 4.16 Strongly coupled case: cumulative sum of acoustic potential energy by the summed acoustic potential energy over the frequency range ($0 \leq f \leq 500\,Hz$) in the absence of control where stiffness ratios $K_a / K_s = 0.1$, $K_a / K_L = 0.1$, uncoupled structural resonance is at 190Hz, and loss factors $\eta_s = \eta_L = 0.16$, $\eta_a = 0.01$ (solid line: before control and dashed line: after control)
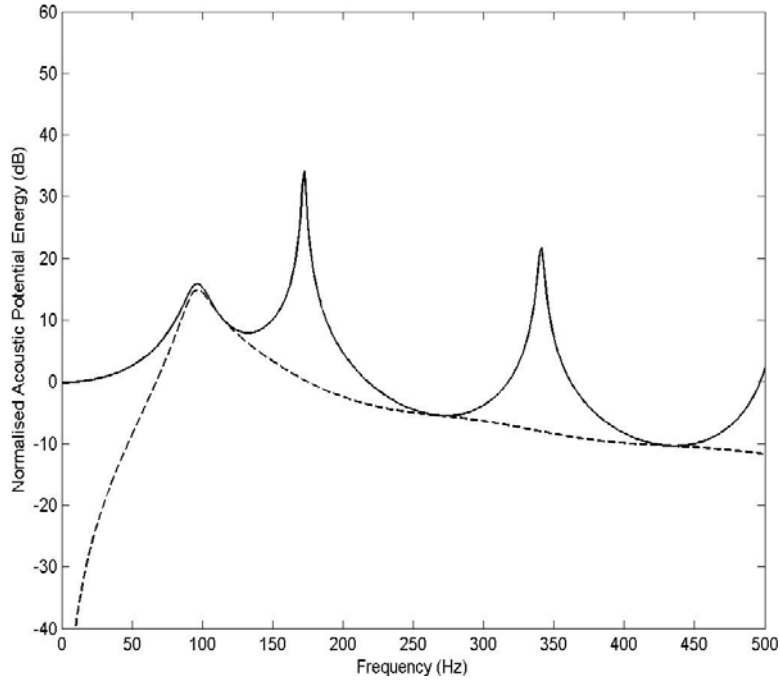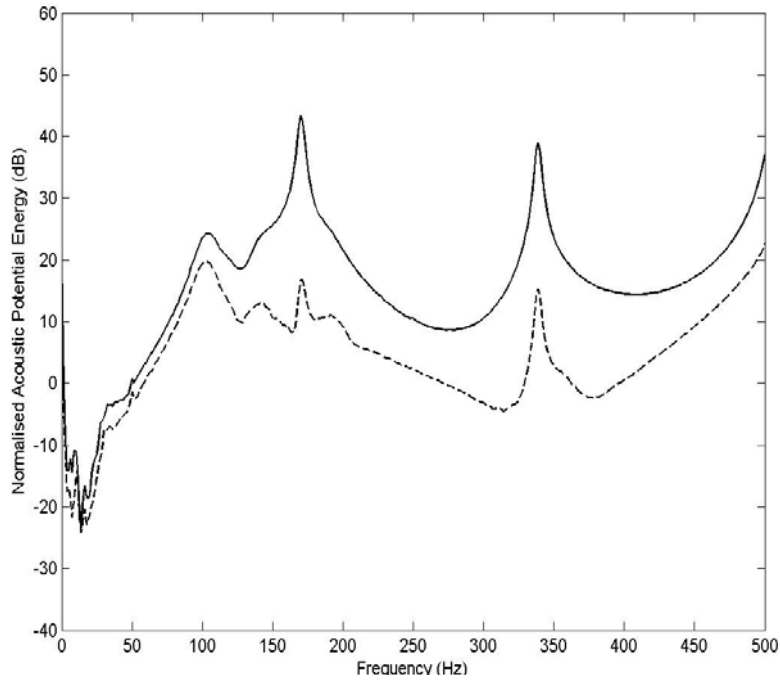
(a) Theory

(b) Experiment

Figure 4.17 Weakly coupled case: acoustic potential energy normalised by that at the static state ($f = 0$) for theory and that at 50Hz for experiment where stiffness ratios $K_a / K_s = 0.03$, $K_a / K_L = 0.1$, uncoupled structural resonance is at 96Hz, and loss factors $\eta_s = 0.2$, $\eta_L = 0.16$, $\eta_a = 0.01$ (solid line: before control and dashed line: after control)
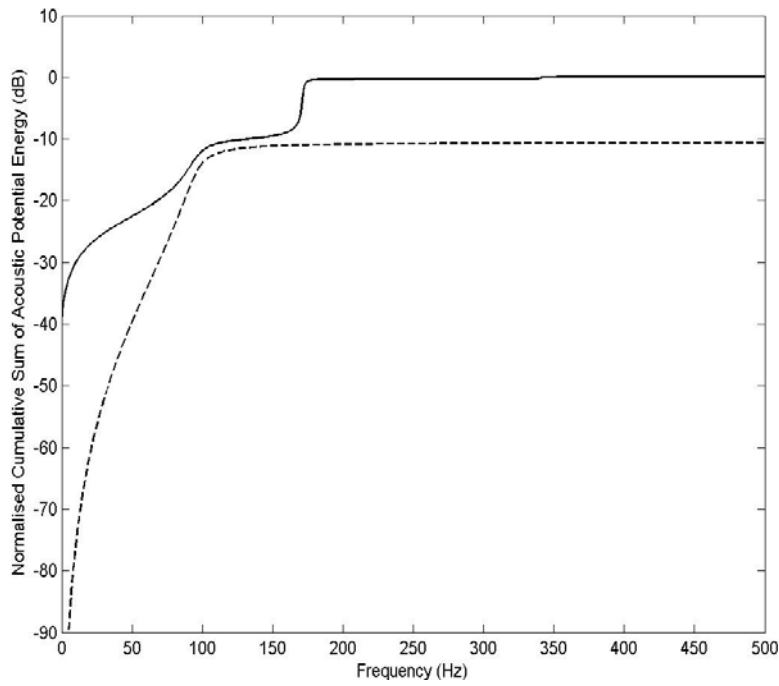
(a) Theory
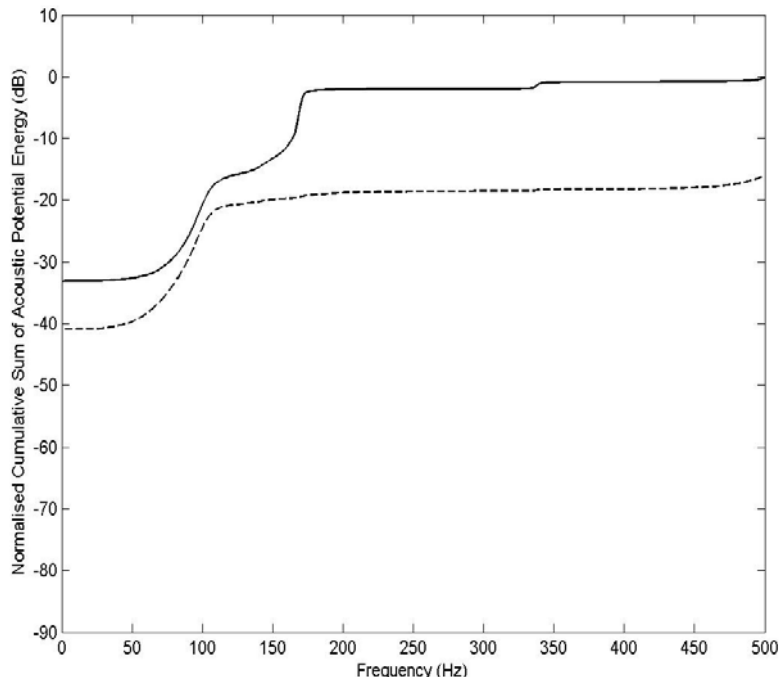
(a) Experiment

Figure 4.18 Weakly coupled case: cumulative sum of acoustic potential energy by the summed acoustic potential energy over the frequency range ($0 \leq f \leq 500\,Hz$) in the absence of control where stiffness ratios $K_a / K_s = 0.03$, $K_a / K_L = 0.1$, uncoupled structural resonance is at 96Hz, and loss factors $\eta_s = 0.2$, $\eta_L = 0.16$, $\eta_a = 0.01$ (solid line: before control and dashed line: after control)

4.8 Conclusions

Active control of the acoustic potential energy, in the simple vibro-acoustic system under feedforward control, has been investigated in this chapter for various structural-acoustic coupling cases when the structural natural frequency is below and above the fundamental acoustic mode of a closed-closed tube respectively. The optimal impedance of a feedforward control system was derived to investigate the physical mechanism of a feedforward controller for the control of the acoustic potential energy. Also, when the acoustic potential energy in the cavity was minimised, the control effect on the kinetic energy of the structure coupled to the cavity was investigated.

The control performance on the acoustic potential energy and the corresponding control effect on the structural kinetic energy can be summarised according to the degree of structural-acoustic coupling as follows.

In the *strongly coupled* case, the acoustic modes dominate the acoustic potential energy and can be effectively controlled when the structural natural frequency is below and above the fundamental acoustic mode. At the frequencies below the fundamental acoustic mode, the feedforward controller provides an open-tube condition at the secondary source position ($x = L$). At the natural frequencies of the acoustic modes, the feedforward controller generates the sound pressure with $180°$ phase shift with respect to the sound pressure due to the primary source. The controlled acoustic potential energy has a structural mode below the structural natural frequency due to the smaller acoustic loading and the acoustic mass in the cavity. When the acoustic potential energy is minimised, the structural kinetic energy increases due to smaller acoustic loading on the structure.

In the *weakly coupled* case with the structural natural frequency below the fundamental acoustic mode, the structural mode dominates the acoustic potential energy. The structural mode can be controlled to some degree below the fundamental acoustic mode for the same reason as in the *strongly coupled* case. The amplitude of the structural mode is reduced and the structural mode is predominant over the controlled acoustic potential energy. When the acoustic potential energy is minimised, the structural kinetic energy does not change after control due to the very small acoustic loading on the structure. On the other hand, in the

weakly coupled case with the structural natural frequency above the fundamental acoustic mode, the structural mode is not controllable because the structure is insensitive to the acoustic loading change. The structural kinetic energy generally has no change after control for the same reason as the case of the structural natural frequency below the fundamental acoustic mode. For both the natural frequency ratios, all the acoustic modes can be effectively controlled with the same control mechanism as in the *strongly coupled* case. Due to the uncontrollable structural mode and control of all the acoustic modes, the acoustic potential energy is dominated by the respective structural mode after control.

In the *intermediate* case with the structural natural frequency below the fundamental acoustic mode, both the structural and acoustic modes can be controlled. At the frequencies of the structural and acoustic modes, the control mechanism is the same as in the *strongly coupled* case. In this case, the reduction on the summed acoustic potential energy is most effective due to the control of both the structural and acoustic modes. The controlled acoustic potential energy has a structural mode below the structural natural frequency for the same reason in the *strongly coupled* case. Also, the structural mode is predominant in the controlled acoustic potential energy. At the frequency of the structural mode, the structural kinetic energy has a peak after control and increases due to smaller acoustic loading on the structure. In the *intermediate* case when the structural natural frequency is above the fundamental acoustic mode, all the acoustic modes can be controlled with the same control mechanism as in the *strongly coupled* case. The structural kinetic energy increases for the same reason as in the case of the structural natural frequency below the fundamental acoustic mode.

Active control of the acoustic potential energy was investigated in this chapter by using feedforward control, which is effective under periodic disturbance. When the disturbance is broadband, a feedback control strategy is preferable. In the next chapter, velocity feedback control will be investigated for the control of the acoustic potential energy in the three coupled cases discussed in this chapter.

CHAPTER 5

DECENTRALISED VELOCITY FEEDBACK CONTROL OF ACOUSTIC POTENTIAL ENERGY IN A VIBRO-ACOUSTIC SYSTEM

5.1 Introduction

Active control can be implemented by using either feedforward control, feedback control or both. Feedforward control has proved to be successful when the disturbance is periodic or can be measured well in advance of the required control input. However, when the disturbance is broadband, it might not be possible to measure the disturbance in sufficient time for the control signal to be applied. In this case, a feedback control strategy may be preferable. When damping is considered to be one of control treatments to minimise the response of the system of interest, the damping can be implemented passively or actively. *Active damping*, which is effective at resonance frequencies, can be achieved by using a velocity feedback control strategy [Fuller *et al* (1996)] and can be implemented by directly feeding back from the velocity sensors on vibrating systems to control actuators [Preumont (2002)].

The active velocity feedback control of the acoustic potential energy, in the simple vibro-acoustic model of interest in this thesis, is investigated under broadband disturbance in this chapter. The three coupled cases, discussed in chapter 2, are studied when the structural natural frequency is below and above the fundamental acoustic mode of a closed-closed tube respectively. The configuration of the active velocity feedback control involves a single-degree-of-freedom (SDOF) structure, under external broadband excitation, at the left end and an acoustic piston at the right end. The acoustic piston has the role of a secondary acoustic actuator when a velocity feedback control system is implemented. On the other hand, the SDOF structure at the left end shares both roles of a primary structure and a secondary structural actuator due to geometric simplicity when velocity feedback control is implemented. The active velocity feedback control system is configured in three ways: using (i) an acoustic actuator, (ii) a structural actuator and (iii) both the actuators. Relative control effectiveness of the acoustic actuator and the structural actuator, driven by velocity feedback controllers, is investigated. In section 5.2, the active velocity feedback control is implemented using an acoustic actuator located at the right end of the tube. The optimal gain of the velocity feedback controller is determined in each coupled case when the summed acoustic potential energy, over the frequency range of interest, is minimised in the vibro-acoustic system. In section 5.3, active velocity feedback control is implemented using a structural actuator located at the left end of the tube. The critical damping of the SDOF structure is used as the gain of the velocity feedback controller driving the secondary structural actuator since the velocity feedback unit works as a *skyhook damper* [Karnopp *et al* (1974)] and obviously stops the structure in the optimal condition. In the various coupled cases, the dynamic coupling between the structural actuator and the acoustic cavity is considered to investigate the control effectiveness of the acoustic potential energy. In section 5.4, decentralised velocity feedback control is implemented using both the acoustic actuator and the structural actuator. In section 5.5, the velocity feedback control effect is discussed in terms of the kinetic energy of the SDOF structure coupled into the acoustic cavity. In section 5.6, the relative control performance of the velocity feedback controllers is demonstrated in terms of the cumulative sum of the acoustic potential energy over the frequency range of interest. In the various coupled cases, the best control strategy is suggested. This chapter is completed in section 5.7 with some conclusions from the theoretical results. Since a velocity feedback control system can be generally implemented by using lightly damped actuators, experimental validation is not provided in this chapter due to the heavy damping in the loudspeakers as shown in chapter 3.

5.2 Velocity feedback control using an acoustic actuator

In this section, velocity feedback control is implemented in a simple vibro-acoustic system using an acoustic actuator driven by a velocity feedback controller. The acoustic actuator, located at the right end of the tube, induces active damping in the vibro-acoustic system. The optimal gain of the velocity feedback controller for the acoustic actuator is determined when the summed acoustic potential energy in the cavity over the frequency range of interest is minimised, for broadband control purposes, in the various structural-acoustic coupling cases. The control of the acoustic potential energy is investigated using the acoustic actuator under velocity feedback control in the three coupled cases when the structural natural frequency is at $L/\lambda = 0.1$ and at $L/\lambda = 0.8$ respectively.

5.2.1 Acoustic response due to an acoustic actuator

The acoustic actuator, driven by a velocity feedback controller, provides active damping in the vibro-acoustic system and changes the impedance at the secondary source position. The controlled impedance is defined by the ratio of the control force to the velocity at the secondary source position with a sign reversal. Acoustic pressure and particle velocity in the vibro-acoustic system can be derived using the controlled impedance at the secondary source position.

Figure 5.1 depicts the one-dimensional acoustic tube excited by a SDOF primary structure, under broadband disturbance, at $x = 0$ and controlled by a secondary acoustic actuator. The acoustic actuator is driven by the force F_{CA} from a velocity feedback controller with a feedback gain $-H_A$, at $x = L$. Apart from the controller, this system is the same as that discussed in chapter 4.
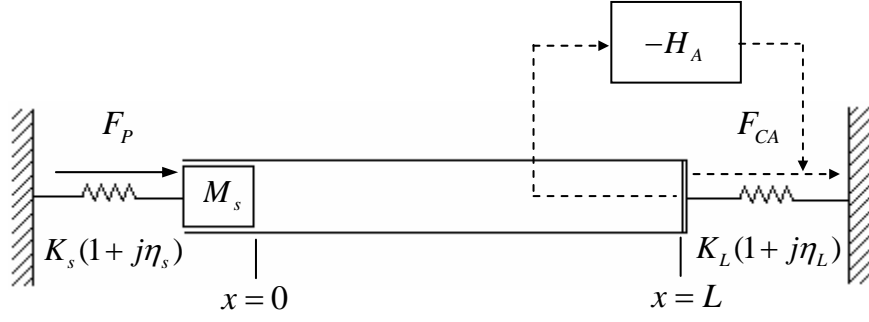
Figure 5.1 Model of a combined SDOF structure – one-dimensional acoustic tube system using an acoustic actuator driven by a velocity feedback controller at $x = L$

When direct velocity feedback control is applied, the control force is given by

$$F_{CA} = -H_A U_L \tag{5.1}$$

where H_A is restricted here to be a positive control gain for a stable control system and U_L is velocity at the secondary source position (at $x = L$). Equation (5.1) can be rewritten as

$$F_{CA} = -Z_{VA} U_L \tag{5.2}$$

where $Z_{VA}(= H_A)$ is the controlled impedance via a velocity feedback control using the acoustic actuator at the secondary source position and acts like a skyhook damper with damping constant H_A. Hence, the secondary source, in a velocity feedback control scheme, gives rise to active damping of H_A in the vibro-acoustic system.

The boundary at the secondary source position can be represented by the sum of the controlled impedance Z_{VA} and the impedance of the acoustic actuator Z_L, given in the equation (4.5), under the velocity feedback control since they share the same velocity at the position. When the velocity feedback control is applied using the acoustic actuator, acoustic pressure and particle velocity can be obtained by setting the impedance Z_L in equations (2.32)~(2.33) to the sum of the impedances Z_{VA} and Z_L to give

$$P(x,\omega) = \rho_0 c \frac{1}{Z_S + Z_{A0}} \frac{\dfrac{Z_L + Z_{VA}}{\rho_0 c S}\cos k(L-x) + j\sin k(L-x)}{\cos kL + j\dfrac{Z_L + Z_{VA}}{\rho_0 c S}\sin kL} \tag{5.3}$$

$$U(x,\omega) = \frac{F_P}{Z_S + Z_{A0}} \frac{\cos k(L-x) + j\dfrac{Z_L + Z_{VA}}{\rho_0 c S}\sin k(L-x)}{\cos kL + j\dfrac{Z_L + Z_{VA}}{\rho_0 c S}\sin kL} \tag{5.4}$$

Non-dimensionalised acoustic pressure and particle velocity are given by

$$\hat{P}(\hat{x},\hat{L}) = \frac{1}{\hat{Z}_S + \hat{Z}_{A0}} \frac{2}{2-j\eta_a} \frac{(\hat{Z}_L + \hat{Z}_{VA})\cos\left(\pi(2-j\eta_a)(1-\hat{x})\hat{L}\right) + j\dfrac{2}{2-j\eta_a}\sin\left(\pi(2-j\eta_a)(1-\hat{x})\hat{L}\right)}{\dfrac{2}{2-j\eta_a}\cos\left(\pi(2-j\eta_a)\hat{L}\right) + j(\hat{Z}_L + \hat{Z}_{VA})\sin\left(\pi(2-j\eta_a)\hat{L}\right)} \tag{5.5}$$

$$\hat{U}(\hat{x},\hat{L}) = \frac{1}{\hat{Z}_S + \hat{Z}_{A0}} \frac{\dfrac{2}{2-j\eta_a}\cos\left(\pi(2-j\eta_a)(1-\hat{x})\hat{L}\right) + j(\hat{Z}_L + \hat{Z}_{VA})\sin\left(\pi(2-j\eta_a)(1-\hat{x})\hat{L}\right)}{\dfrac{2}{2-j\eta_a}\cos\left(\pi(2-j\eta_a)\hat{L}\right) + j(\hat{Z}_L + \hat{Z}_{VA})\sin\left(\pi(2-j\eta_a)\hat{L}\right)} \tag{5.6}$$

where $\hat{P}(\hat{x},\hat{L}) = P(\hat{x},\hat{L})/P$, $\hat{U}(\hat{x},\hat{L}) = U(\hat{x},\hat{L})/U$ and $\hat{Z}_{VA} = Z_{VA}/\rho_0 c_0 S$. The other non-dimensional parameters are defined in equations (4.9) and (4.10). Also, the normalised acoustic impedance $\hat{Z}_{A0}(= Z_{A0}/\rho_0 c_0 S)$ can be obtained by setting $\hat{Z}_L$ into $\hat{Z}_L + \hat{Z}_{VA}$ in equation (2.37) to give

$$\hat{Z}_{A0} = \frac{2}{2-j\eta_a} \frac{(\hat{Z}_L + \hat{Z}_{VA})\cos\left(\pi(2-j\eta_a)\hat{L}\right) + j\dfrac{2}{2-j\eta_a}\sin\left(\pi(2-j\eta_a)\hat{L}\right)}{\dfrac{2}{2-j\eta_a}\cos\left(\pi(2-j\eta_a)\hat{L}\right) + j(\hat{Z}_L + \hat{Z}_{VA})\sin\left(\pi(2-j\eta_a)\hat{L}\right)} \tag{5.7}$$

5.2.2 Optimal feedback gains for various coupling conditions

When velocity feedback control is implemented using the acoustic actuator, the resulting active damping needs to be optimised to minimise the acoustic potential energy, defined in equation (2.46), in the cavity. The optimal feedback gain is obtained when the summed acoustic potential over the frequency range of interest is minimised in each coupled case.

Figures 5.2(a) and (b) show the summed acoustic potential energy over the frequency range $(0 \leq L/\lambda \leq 2)$ as a function of a feedback gain ratio $H_A / \rho_0 c_0 S$ for a given stiffness ratio when the structural natural frequency is at $L/\lambda = 0.1$ and at $L/\lambda = 0.8$ respectively. To compare each coupling case with a different stiffness ratio, the summed acoustic potential energy is normalised by that in the absence of control in each coupled case. The normalised summed acoustic potential energy at the upper limit of the ratio $H_A / \rho_0 c_0 S$ is generally the same as that in the vibro-acoustic system rigidly terminated at $x = L$. Also, the normalised summed acoustic potential energy at the lower limit of the ratio $H_A / \rho_0 c_0 S$ is the same as that in the vibro-acoustic system before control. It should be noted that the stiffness ratio K_a / K_L is 0.1 for a well-coupled acoustic actuator, so velocity feedback control is readily implemented by feeding back from the velocity sensor to the acoustic actuator. If the stiffness ratio K_a / K_L is smaller, the velocity at the secondary source position is less and hence the control force, driving the acoustic actuator, will be insignificant. The optimal feedback gain ratio $H_A / \rho_0 c_0 S$ in each coupled case can be determined when the corresponding normalised summed acoustic potential energy over the frequency range of interest is minimised. Table 5.1 presents the optimal feedback gain ratio $H_A / \rho_0 c_0 S$ and the summed acoustic potential energy normalised by that in the absence of control for a given stiffness ratio.

In the *strongly coupled* case with an structural-acoustic stiffness ratio $K_a / K_s = 10^3$, the optimal feedback gain ratio has similar behaviour for the two natural frequency ratios ω_a / ω_s as shown in figures 5.2(a) and (b). At the feedback gain ratio of 3.7, the summed acoustic potential energy, over the frequency range, can be reduced by about 9dB. Also, at around the optimal feedback gain ratio, the normalised summed acoustic potential energy has sharp changes.

In the *weakly coupled* case with a structural-acoustic stiffness ratio $K_a / K_s = 10^{-3}$ and the structural natural frequency at $L / \lambda = 0.1$, the optimal feedback gain ratio is 1 as shown in figure 5.2(a). In this case, the reduction on the summed acoustic potential energy, over the frequency range, is insignificant. The normalised summed acoustic potential is not very sensitive to a change in the feedback gain between 10^{-4} and 1. In the *weakly coupled* case, when the structural natural frequency is at $L / \lambda = 0.8$, the optimal feedback gain ratio is 3.9 as shown in figure 5.2(b). In this case, the summed acoustic potential energy can be reduced by about 5dB. The normalised summed acoustic potential energy is more sensitive to a change in the feedback gain. Also, the acoustic potential energy can be more effectively controlled compared to the case of the structural natural frequency at $L / \lambda = 0.1$.

In the *intermediate* case with a structural-acoustic stiffness ratio $K_a / K_s = 1$ and the structural natural frequency at $L / \lambda = 0.1$, the optimal feedback gain ratio is 11.5 as shown in figure 5.2(a). In this case, the normalised summed acoustic potential energy, over the frequency range, has sharp changes as in the *strongly coupled* case. Also, the summed acoustic potential energy can be reduced by about 4dB. In the *intermediate* case, when the structural natural frequency is at $L / \lambda = 0.8$, the optimal feedback gain is 2.5 with reduction on the summed acoustic potential energy by about 8dB as shown in figure 5.2(b). In this case, the normalised summed acoustic potential energy is more sensitive to a change in the feedback gain ratio compared to the case of the structural natural frequency at $L / \lambda = 0.8$. Also, the acoustic potential energy can be more effectively controllable under the velocity feedback control.

Physically, a larger feedback gain ratio means that the velocity feedback control, implemented by an acoustic actuator, applies more active damping in the cavity for the control of the acoustic potential energy. It is noticeable that in the *intermediate* case with the structural natural frequency at $L / \lambda = 0.1$, maximum active damping is applied for the control of the acoustic potential energy as presented in table 5.1. The reduction, on the summed acoustic potential energy over the frequency range of interest, generally increases when the vibro-acoustic system is more *strongly coupled* with the structural natural frequency above the fundamental acoustic mode for a given stiffness ratio.
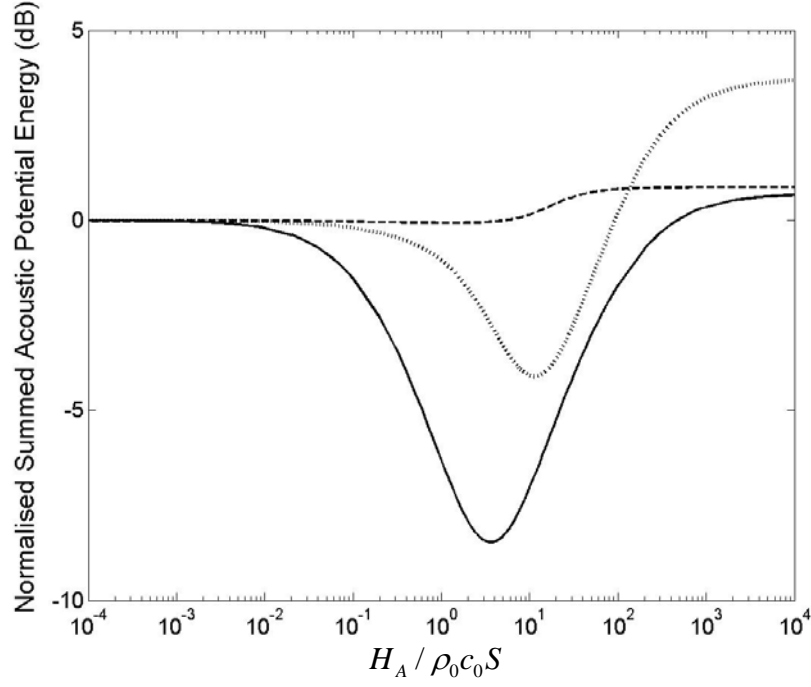
(a) Structural natural frequency at $L/\lambda = 0.1$
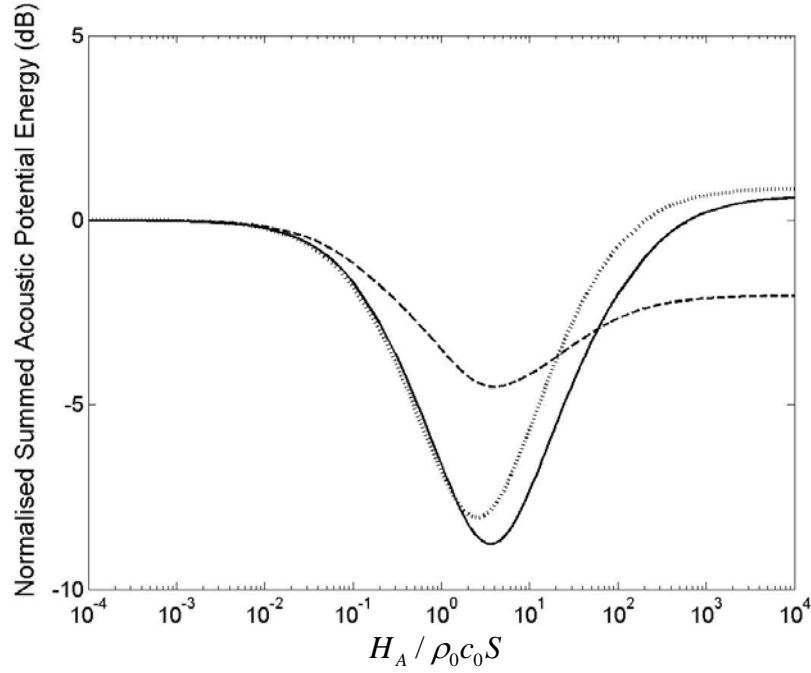
(b) Structural natural frequency at $L/\lambda = 0.8$

Figure 5.2 Summed acoustic potential energy as a function of a feedback gain ratio $H_A/\rho_0 c_0 S$ normalised by that in the absence of control for a given stiffness ratio when the structural natural frequency is at $L/\lambda = 0.1$ ($\omega_a/\omega_s = 5$) and at $L/\lambda = 0.8$ ($\omega_a/\omega_s = 0.6$) respectively where stiffness ratio $K_a/K_L = 0.1$ and loss factors $\eta_s = \eta_a = \eta_L = 10^{-2}$ (solid line: strongly coupled case with $K_a/K_s = 10^3$, dashed line: weakly coupled case with $K_a/K_s = 10^{-3}$ and dotted line: intermediate case with $K_a/K_s = 1$)

Table 5.1 Optimal feedback gain ratio ($H_A / \rho_0 c_0 S$) and summed acoustic potential energy over the frequency range ($0 \leq L / \lambda \leq 2$) normalised by that in the absence of control for a given stiffness ratio when the structural natural frequency is at $L / \lambda = 0.1$ ($\omega_a / \omega_s = 5$) and at $L / \lambda = 0.8$ ($\omega_a / \omega_s = 0.6$) respectively

Degree of coupling	Natural frequency ratio			
	$\omega_a / \omega_s = 5$		$\omega_a / \omega_s = 0.6$	
	Feedback gain ratio	Reduction	Feedback gain ratio	Reduction
Strong ($K_a / K_s = 10^3$)	3.7	-9dB	3.7	-9dB
Weak ($K_a / K_s = 10^{-3}$)	1	-0.1dB	3.9	-5dB
Intermediate ($K_a / K_s = 1$)	11.5	-4dB	2.5	-8dB

5.2.3 Control of acoustic potential energy using an acoustic actuator

In this section, controllability of the structural and acoustic modes is investigated under the active velocity feedback control implemented by the acoustic actuator in various coupled cases.

Figures 5.3(a), (b), (c) and figures 5.4(a), (b), (c) show the acoustic potential energy, under velocity feedback control using the acoustic actuator, for a given stiffness ratio when the structural natural frequency is at $L / \lambda = 0.1$ and at $L / \lambda = 0.8$ respectively. The acoustic potential energy is normalised by that at the static state ($L / \lambda = 0$) in the absence of control. The corresponding optimal feedback gain ratio, presented in table 5.1, is substituted for the normalised controlled impedance $\hat{Z}_{VA}$ in equations (5.5)~(5.6) for a given stiffness ratio.

In the *strongly coupled* case with a structural-acoustic stiffness ratio $K_a / K_s = 10^3$, the acoustic potential energy is governed by acoustic modes before control, which have the fundamental mode at $L / \lambda = 0.23$ for the two natural frequency ratios ω_a / ω_s as shown in figures 5.3(a) and 5.4(a). When the velocity feedback control system is active, the one-

dimensional tube is mostly open at $x = 0$ and has the boundary of the sum of the controlled impedance Z_{VA} and the impedance of the acoustic actuator Z_L at $x = L$. The resonance frequencies in the acoustic potential energy shift to higher frequencies after control due to the controlled impedance Z_{VA}, which increases the impedance of the boundary at $x = L$. The acoustic modes, in the controlled acoustic potential energy, move to those of an open-closed tube at $L/\lambda = (2n-1)/4$ where n is an integer. All the acoustic modes are effectively controlled at resonance frequencies. However, minor control spillover is observed at off-resonance frequencies due to the shifted acoustic modes under control. The control spillover increases with frequency due to the boundary condition at $x = L$. Before control, the boundary condition is determined by the impedance of the acoustic actuator Z_L reducing as $1/\omega$. This boundary condition moves the higher modes in the acoustic potential energy toward those of an open-open tube at $L/\lambda = n/2$ as shown in figures 5.3(a) and 5.4(a) where n is an integer. However, after control, the boundary condition is determined by the sum of the impedance Z_L and the controlled impedance Z_{VA}. The controlled impedance Z_{VA} applies constant acoustic damping with frequency in the cavity. Due to the constant acoustic damping, the controlled acoustic potential energy has the higher modes close to those of an open-closed tube at $L/\lambda = (2n-1)/4$ where n is an integer.

In the *weakly coupled* case with a structural-acoustic stiffness ratio $K_a/K_s = 10^{-3}$ and the structural natural frequency at $L/\lambda = 0.1$, the acoustic potential energy has a structural mode at $L/\lambda = 0.1$ and a fundamental acoustic mode at $L/\lambda = 0.45$ before control as shown in figure 5.3(b). When the velocity feedback control system is active, the one-dimensional tube is mostly closed at $x = 0$ and has the boundary of the sum of the controlled impedance Z_{VA} and the impedance of the acoustic actuator Z_L at $x = L$. The structural mode is not controllable, but all the acoustic modes are effectively suppressed at resonance frequencies. In this case, the acoustic modes have insignificant contribution to the overall acoustic potential energy in the cavity with negligible reduction on the summed acoustic potential energy as presented in table 5.1. Compared to the *strongly coupled* case, less control spillover is due to the smaller feedback gain ratio causing smaller controlled impedance Z_{VA}.

In the *weakly coupled* case, when the structural natural frequency is at $L/\lambda = 0.8$, the acoustic potential energy has a structural mode at $L/\lambda = 0.8$ and a fundamental acoustic

mode at $L/\lambda = 0.45$ before control as shown in figure 5.4(b). In this case, the vibro-acoustic system has boundary conditions, which are less structural impedance Z_S at $x = 0$, compared to the case of the structural natural frequency at $L/\lambda = 0.1$, and the sum of controlled impedance Z_{VA} and the impedance of the acoustic actuator Z_L at $x = L$. All the acoustic modes are effectively suppressed at resonance frequencies. Also, a minor reduction in the structural mode is observed. So, the more effective reduction on the summed acoustic potential energy can be achieved compared to the case of the structural natural frequency at $L/\lambda = 0.1$ as presented in table 5.1. However, the control spillover at off-resonance frequencies increases due to larger feedback gain ratio causing larger controlled impedance Z_{VA}.

In the *intermediate* case with a structural-acoustic stiffness ratio $K_a / K_s = 1$ and the structural natural frequency at $L/\lambda = 0.1$, the acoustic potential energy has a structural mode at $L/\lambda = 0.13$ and a fundamental acoustic mode at $L/\lambda = 0.48$ before control as shown in figure 5.3(c). In this case, the structural mode is controlled to some degree since the structure is more subjective to the acoustic loading change in the cavity compared to the *weakly coupled* case. Also, all the acoustic modes are effectively suppressed at resonance frequencies with some control spillover at off-resonance frequencies for the same reason as in the *strongly coupled* case. Compared to the previous two extreme cases, the larger feedback gain ratio is required for the control of the structural mode to some degree and all the acoustic modes as presented in table 5.1. The larger feedback gain ratio implements the velocity feedback control applying heavier active damping in the cavity via the acoustic actuator.

In the *intermediate* case, when the structural natural frequency is at $L/\lambda = 0.8$, the acoustic potential energy is governed by acoustic modes before control, which have a fundamental mode at $L/\lambda = 0.29$ as shown in figure 5.4(c). All the acoustic modes are effectively suppressed at resonance frequencies with some control spillover at off-resonance frequencies for the same reason as in the *strongly coupled* case. Compared to the case of the structural natural frequency ratio at $L/\lambda = 0.1$, more effective reduction on the summed acoustic potential energy can be achieved, as presented in table 5.1, due to the more strongly coupled structure into the cavity.

To summarise the various cases considered, the velocity feedback control, implemented by the acoustic actuator, is generally effective for the control of the acoustic potential energy in the more *strongly coupled* case. All the acoustic modes can be effectively suppressed at resonance frequencies in all the coupled cases. On the other hand, the structural mode is generally uncontrollable in the *weakly coupled* case. However, the structural mode is controllable to some degree in the *intermediate* case with the structural natural frequency at $L/\lambda = 0.1$. When the acoustic potential energy is controlled under the velocity feedback control, minor control spillover is observed at off-resonance frequencies due to the controlled impedance Z_{VA} causing more rigid boundary condition at $x = L$.
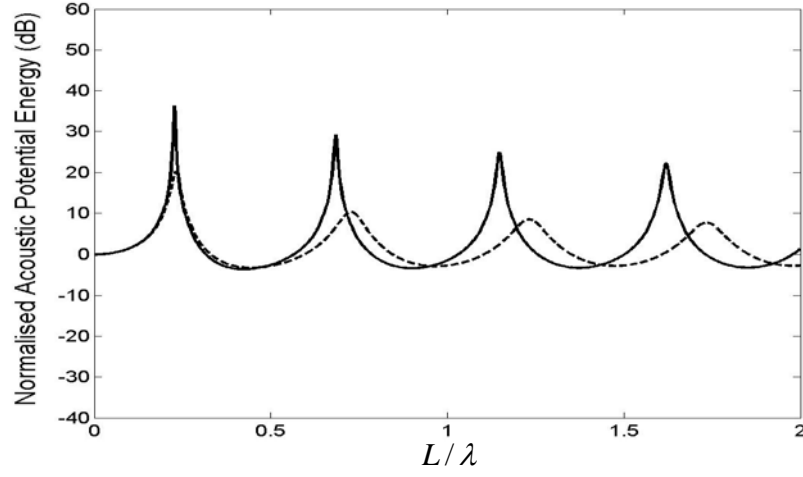
(a) Strongly coupled case ($K_a / K_s = 10^3$)
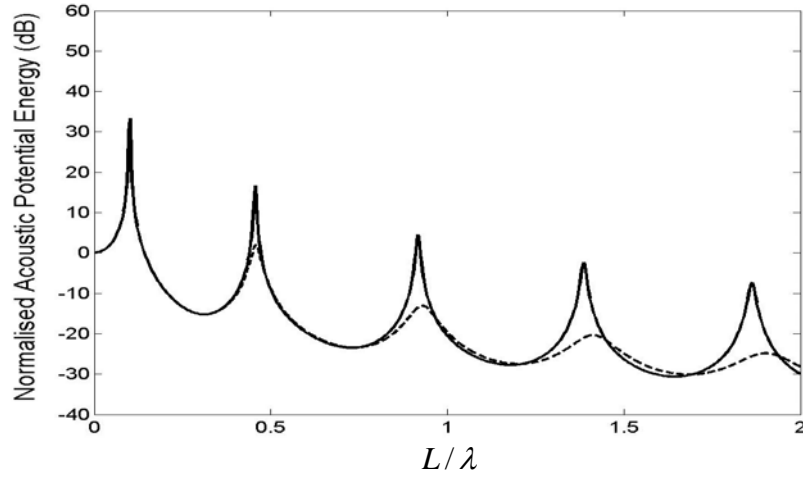
(b) Weakly coupled case ($K_a / K_s = 10^{-3}$)
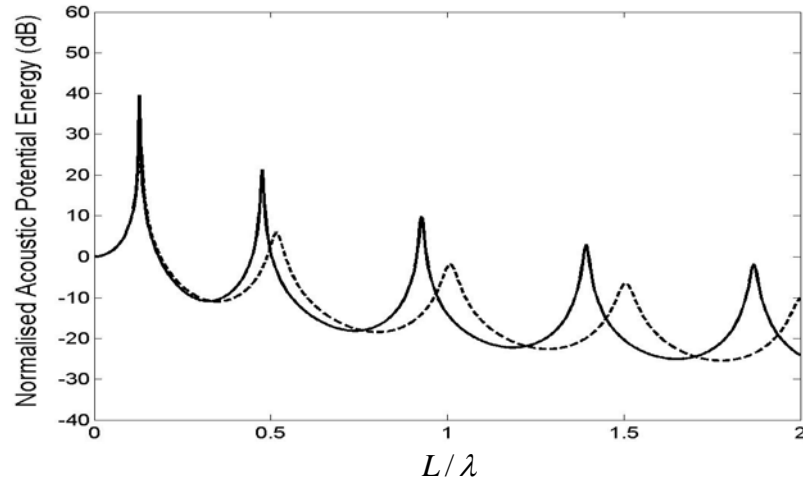
(c) Intermediate case ($K_a / K_s = 1$)

Figure 5.3 Acoustic potential energy normalised by that at the static state ($L/\lambda = 0$) in the absence of control for a given stiffness ratio where the structural natural frequency is at $L/\lambda = 0.1$ ($\omega_a / \omega_s = 5$), stiffness ratio $K_a / K_L = 0.1$, loss factors $\eta_s = \eta_a = \eta_L = 10^{-2}$ (solid line: without control and dashed line: with velocity feedback control using the acoustic actuator)
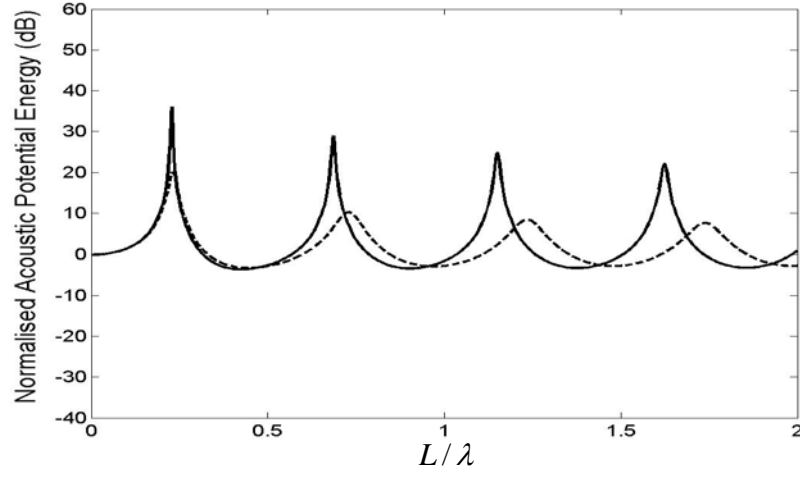
(a) Strongly coupled case ($K_a / K_s = 10^3$)
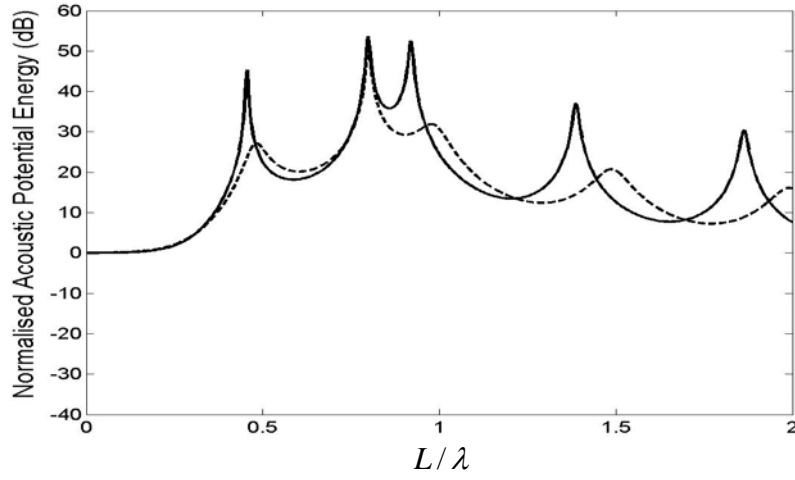
(b) Weakly coupled case ($K_a / K_s = 10^{-3}$)
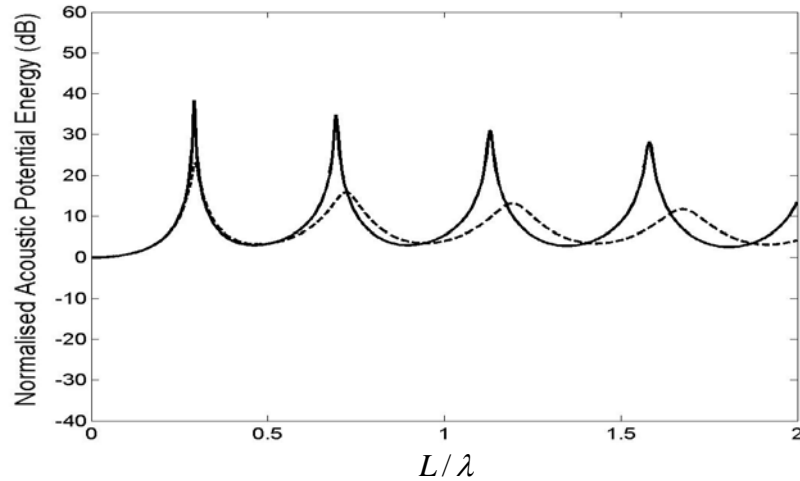
(c) Intermediate case ($K_a / K_s = 1$)

Figure 5.4 Acoustic potential energy normalised by that at the static state ($L/\lambda = 0$) in the absence of control for a given stiffness ratio where the structural natural frequency is at $L/\lambda = 0.8$ ($\omega_a / \omega_s = 0.6$), stiffness ratio $K_a / K_L = 0.1$, loss factors $\eta_s = \eta_a = \eta_L = 10^{-2}$ (solid line: without control and dashed line: with velocity feedback control using the acoustic actuator)

5.3 Velocity feedback control using a structural actuator

In this section, a velocity feedback control system is implemented at the primary structure. The velocity feedback control system, located at the left end of the tube, induces active damping in the primary structure. In this case, the primary structure has dual functions such as a primary structure and a secondary structural actuator due to geometric simplicity of the vibro-acoustic system. Critical damping of the primary structure is used as the criterion for the gain of the velocity feedback controller driving the secondary structural actuator. Since the velocity feedback unit works as a *skyhook damper* and the primary structure is totally stationary in the optimal condition. The control of the acoustic potential energy is investigated when using the structural actuator in the velocity feedback control scheme. The three coupled cases, discussed in section 5.2, are studied when the structural natural frequency is at $L/\lambda = 0.1$ and at $L/\lambda = 0.8$ respectively.

5.3.1 Acoustic response due to a structural actuator

When a velocity feedback control system is implemented on the structure, it provides active damping in the structure. The controlled impedance at the position ($x = 0$) can be obtained in the same manner as that caused by the acoustic actuator in section 5.2.1. Acoustic pressure and particle velocity in the vibro-acoustic system can be derived using the controlled impedance.

Figure 5.5 depicts a one-dimensional acoustic tube excited by a SDOF primary structure, under broadband disturbance and simultaneously controlled by a velocity feedback controller implemented on the structure with a feedback gain $-H_S$, at $x = 0$. This analytical model has the same system parameters of the primary structure and the acoustic actuator in the absence of control depicted in figure 5.1. When the primary structure, under the broadband excitation force F_P, induces vibro-acoustic disturbance in the cavity, the control force F_{CS}, provided by the velocity feedback controller implemented on the primary structure, controls the interior sound field in the cavity. The feedback controller directly feeds back from a velocity sensor to the structure with the feedback gain $-H_S$.
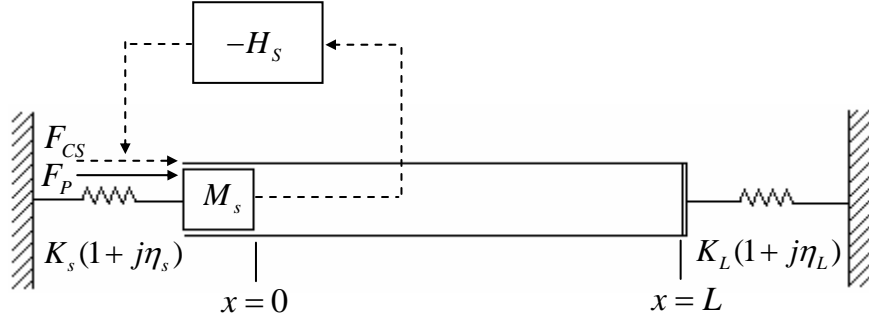
Figure 5.5 Model of a combined SDOF structure – one dimensional acoustic tube system using a structural actuator driven by a velocity feedback controller at $x = 0$

When direct velocity feedback control is applied, the control force F_{CS} is given by

$$F_{CS} = -H_S U_0 \qquad (5.8)$$

where $H_S (= 2\sqrt{K_s M_s})$ is the critical damping of the primary structure and U_0 is velocity at $x = 0$. Equation (5.8) can be rewritten as

$$F_{CS} = -Z_{VS} U_0 \qquad (5.9)$$

where $Z_{VS} (= H_S)$ is the controlled impedance via velocity feedback control using the structural actuator. The structural actuator in a velocity feedback control scheme gives rise to active damping of H_S in the vibro-acoustic system.

The impedance of the primary structure is modified into the sum of the controlled impedance Z_{VS} and the uncoupled structural impedance Z_S. When the velocity feedback control is applied using the structural actuator, acoustic pressure and particle velocity can be obtained by setting the impedance Z_S in equations (2.32)~(2.33) to the sum of the impedances Z_{VS} and Z_S.

$$P(x,\omega) = \rho_0 c \frac{1}{Z_S + Z_{VS} + Z_{A0}} \frac{\dfrac{Z_L}{\rho_0 cS} \cos k(L-x) + j \sin k(L-x)}{\cos kL + j \dfrac{Z_L}{\rho_0 cS} \sin kL} \qquad (5.10)$$

$$U(x,\omega) = \frac{F_P}{Z_S + Z_{VS} + Z_{A0}} \frac{\cos k(L-x) + j \dfrac{Z_L}{\rho_0 cS} \sin k(L-x)}{\cos kL + j \dfrac{Z_L}{\rho_0 cS} \sin kL} \qquad (5.11)$$

Non-dimensionalised acoustic pressure and particle velocity are given by

$$\hat{P}(\hat{x},\hat{L}) = \frac{1}{(\hat{Z}_S + \hat{Z}_{VS}) + \hat{Z}_{A0}} \frac{2}{2 - j\eta_a} \frac{\hat{Z}_L \cos\left(\pi(2 - j\eta_a)(1 - \hat{x})\hat{L}\right) + j\dfrac{2}{2 - j\eta_a} \sin\left(\pi(2 - j\eta_a)(1 - \hat{x})\hat{L}\right)}{\dfrac{2}{2 - j\eta_a} \cos\left(\pi(2 - j\eta_a)\hat{L}\right) + j\hat{Z}_L \sin\left(\pi(2 - j\eta_a)\hat{L}\right)} \quad (5.12)$$

$$\hat{U}(\hat{x},\hat{L}) = \frac{1}{(\hat{Z}_S + \hat{Z}_{VS}) + \hat{Z}_{A0}} \frac{\dfrac{2}{2 - j\eta_a} \cos\left(\pi(2 - j\eta_a)(1 - \hat{x})\hat{L}\right) + j\hat{Z}_L \sin\left(\pi(2 - j\eta_a)(1 - \hat{x})\hat{L}\right)}{\dfrac{2}{2 - j\eta_a} \cos\left(\pi(2 - j\eta_a)\hat{L}\right) + j\hat{Z}_L \sin\left(\pi(2 - j\eta_a)\hat{L}\right)} \quad (5.13)$$

where $\hat{Z}_{VS} = Z_{VS}/\rho_0 c_0 S$. The other non-dimensional parameters have the same arguments as those in equations (5.5)~(5.6). Also, the normalised acoustic impedance $\hat{Z}_{A0}(= Z_{A0}/\rho_0 c_0 S)$ is defined in equation (2.37).

5.3.2 Feedback gains for various coupling conditions

The feedback gain ratio $H_S/\rho_0 c_0 S$ can be written using non-dimensional structural-acoustic parameters as

$$\frac{H_S}{\rho_0 c_0 S} = \frac{2}{\pi} \frac{\hat{\omega}}{\hat{K}} \qquad (5.14)$$

The feedback gain ratio $H_S / \rho_0 c_0 S$ is proportional to the structural-acoustic natural frequency ratio $\hat{\omega}(= \omega_a / \omega_s)$ and is inversely proportional to the structural-acoustic stiffness ratio $\hat{K}(= K_a / K_s)$.

Table 5.2 presents the feedback gain ratio $H_S / \rho_0 c_0 S$ and the summed acoustic potential energy over the frequency range $(0 \leq L/\lambda \leq 2)$ normalised by that in the absence of control for a given stiffness ratio when the structural natural frequency is at $L/\lambda = 0.1$ and at $L/\lambda = 0.8$ respectively. The feedback gain ratio is a function of a natural frequency ratio and a stiffness ratio, as given in equation (5.14). The feedback gain ratio increases in the more *weakly coupled* case with the structural natural frequency below the fundamental acoustic mode as presented in table 5.2.

The reduction, on the summed acoustic potential energy over the frequency range of interest, generally increases when the vibro-acoustic system is more *weakly coupled* with the structural natural frequency below the fundamental acoustic mode. It is noticeable that in the *intermediate* case with the structural natural frequency at $L/\lambda = 0.1$, maximum reduction on the summed acoustic potential energy can be achieved.

Table 5.2 Feedback gain ratio ($H_S / \rho_0 c_0 S$) for critical damping and summed acoustic potential energy over the frequency range ($0 \leq L/\lambda \leq 2$) normalised by that in the absence of control for a given stiffness ratio when the structural natural frequency is at $L/\lambda = 0.1$ ($\omega_a / \omega_s = 5$) and at $L/\lambda = 0.8$ ($\omega_a / \omega_s = 0.6$) respectively

Degree of coupling	Natural frequency ratio			
	$\omega_a / \omega_s = 5$		$\omega_a / \omega_s = 0.6$	
	Feedback gain ratio	Reduction	Feedback gain ratio	Reduction
Strong ($K_a / K_s = 10^3$)	3.2×10^{-3}	-1dB	4×10^{-4}	-0.1dB
Weak ($K_a / K_s = 10^{-3}$)	3.2×10^3	-14dB	4×10^2	-16dB
Intermediate ($K_a / K_s = 1$)	3.2	-19dB	4×10^{-1}	-11dB

5.3.3 Control of acoustic potential energy using a structural actuator

Active control of the acoustic potential energy is investigated using the structural actuator driven by a velocity feedback controller. The three coupled cases, discussed in section 5.2, are studied when the structural natural frequency is at $L/\lambda = 0.1$ and is at $L/\lambda = 0.8$ respectively. In the three structural-acoustic coupled cases, the dynamic coupling between the structural actuator and the acoustic cavity varies. Under the *strongly* or *weakly coupled* conditions, the structural actuator is weakly coupled with the acoustic cavity. On the other hand, in the *intermediate* case, the structural actuator is strongly coupled with the acoustic cavity. When the velocity feedback control is implemented using the structural actuator, the degree of the actuator coupling into the cavity is investigated for the control effectiveness on the acoustic potential energy.

Figures 5.6(a), (b), (c) and figures 5.7(a), (b), (c) show the acoustic potential energy, under velocity feedback control using the structural actuator for a given stiffness ratio, when the structural natural frequency is at $L/\lambda = 0.1$ and at $L/\lambda = 0.8$ respectively. The acoustic potential energy is normalised by that at the static state ($L/\lambda = 0$) in the absence of control. The corresponding feedback gain ratio, presented in table 5.2, is substituted for the normalised controlled impedance $\hat{Z}_{VS}$ in equations (5.12)~(5.13) for a given stiffness ratio.

In the *strongly coupled* case with a structural-acoustic stiffness ratio $K_a/K_s = 10^3$, the acoustic potential energy, governed by the acoustic modes with a fundamental mode at $L/\lambda = 0.23$, is not effectively controlled for the two natural frequency ratios ω_a/ω_s as shown in figures 5.6(a) and 5.7(a). The acoustic potential energies before and after control are mostly overlapped and the summed acoustic potential energy, over the frequency range of interest, can be reduced by up to about 1dB as presented in table 5.2. In this case, the structure has insignificant impedance compared to the acoustic input impedance. Due to the insignificant structural impedance, the induced active damping on the structure is not influential on the acoustic potential energy. The structural actuator, driven by a velocity feedback controller, has generally negligible effects on the control of the acoustic potential energy dominated by the acoustic modes.

In the *weakly coupled* case with a structural-acoustic stiffness ratio $K_a / K_s = 10^{-3}$ and the structural natural frequency at $L / \lambda = 0.1$, the structural mode at $L / \lambda = 0.1$ can be effectively controlled as shown in figure 5.6(b). The acoustic modes, whose fundamental mode is at $L / \lambda = 0.45$, are not controllable. The active damping, induced by the structural actuator under the velocity feedback control, is only effective on the structural mode. In this case, the summed acoustic potential, over the frequency range of interest, can be reduced by about 14dB as presented in table 5.2 due to the control of the dominating structural mode.

In the *weakly coupled* case, when the structural natural frequency is at $L / \lambda = 0.8$, the structural mode at $L / \lambda = 0.8$ is effectively controlled as shown in figure 5.7(b). Also, all the acoustic modes, with a fundamental mode at $L / \lambda = 0.45$, can be suppressed down to some degree. Compared to the *weakly coupled* case with the structural natural frequency at $L / \lambda = 0.1$, the more effective control of the acoustic potential energy is due to more broad damping control region and more strongly coupled structural actuator. The more broad damping control region is caused by the less structural mass with the same structural stiffness for a given stiffness ratio. Due to the effectively controlled structural mode and the suppressed acoustic modes to some degree, the summed acoustic potential energy, over the frequency range of interest, can be reduced by about 16dB as presented in table 5.2.

In the *intermediate* case with a structural-acoustic stiffness ratio $K_a / K_s = 1$ and the structural natural frequency at $L / \lambda = 0.1$, the structural mode at $L / \lambda = 0.13$ can be effectively controlled as shown in figure 5.6(c). Also, the fundamental and second acoustic modes, at $L / \lambda = 0.48$ and at $L / \lambda = 0.9$ respectively, can be suppressed at the resonance frequencies to some degree due to strongly coupled structural actuator compared to the two extreme cases. The control effect on the acoustic modes diminishes with frequency since the active damping effect, induced by the structural actuator, is significant at the structural mode and decreases with frequency. In this case, the summed acoustic potential energy, over the frequency range of interest, can be reduced by about 19dB as presented in table 5.2 due to the control of both the structural mode and the acoustic modes to some degree.

In the *intermediate* case, when the structural natural frequency is at $L / \lambda = 0.8$, all the acoustic modes, with a fundamental mode at $L / \lambda = 0.29$, can be suppressed at resonance frequencies as shown in figure 5.7(c). Compared to the *intermediate* case with the structural

natural frequency at $L/\lambda = 0.1$, the more effective control of the acoustic potential energy is due to the more broad damping control region and more strongly coupled structural actuator for the same reason as in the *weakly coupled* case.

In summary, the velocity feedback control, implemented by the structural actuator, is generally effective for the control of the acoustic potential energy in the more *weakly coupled* case with the structural actuator strongly coupled into the cavity. In the *weakly coupled* and *intermediate* case with structural natural frequency at $L/\lambda = 0.1$, the control effect is mainly significant at the structural mode. On the other hand, when the structural natural frequency at $L/\lambda = 0.8$ under the same coupled condition, the active damping, induced the structural actuator, is effective on the acoustic modes as well due to increased damping control region and more strongly coupled structural actuator into the cavity. Under this velocity feedback control implemented by the structural actuator, control spillover is not observed in the controlled acoustic potential energy on the contrary to the velocity feedback control implemented by the acoustic actuator, discussed in section 5.2.
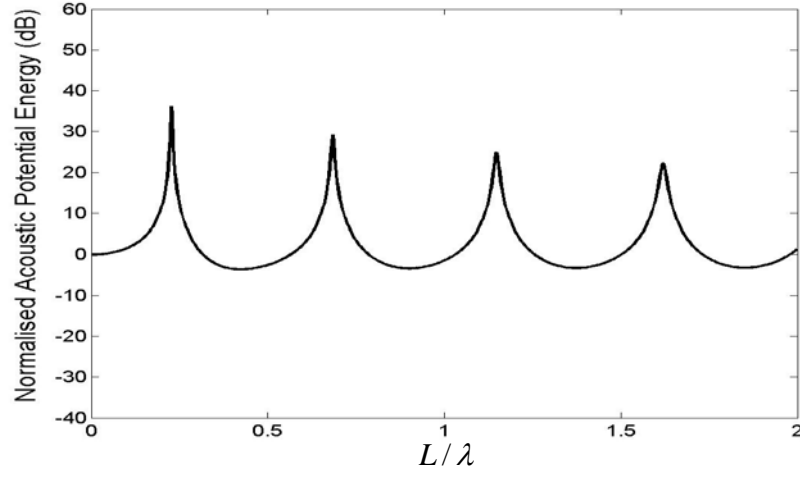
(a) Strongly coupled case ($K_a / K_s = 10^3$)
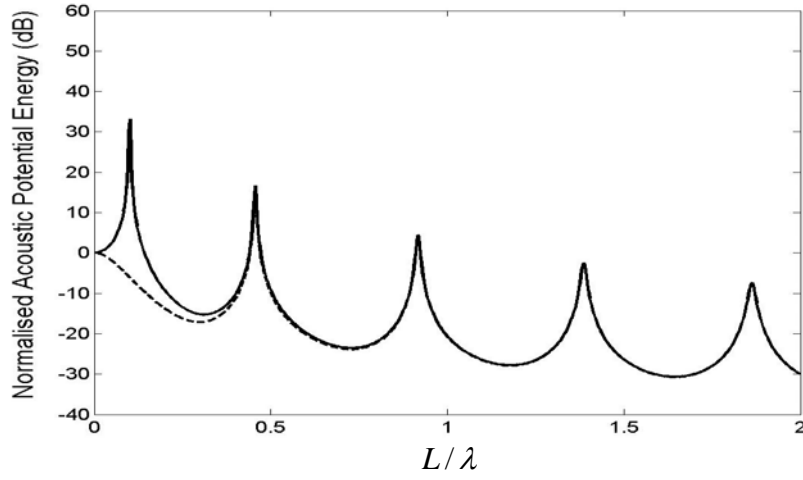
(b) Weakly coupled case ($K_a / K_s = 10^{-3}$)
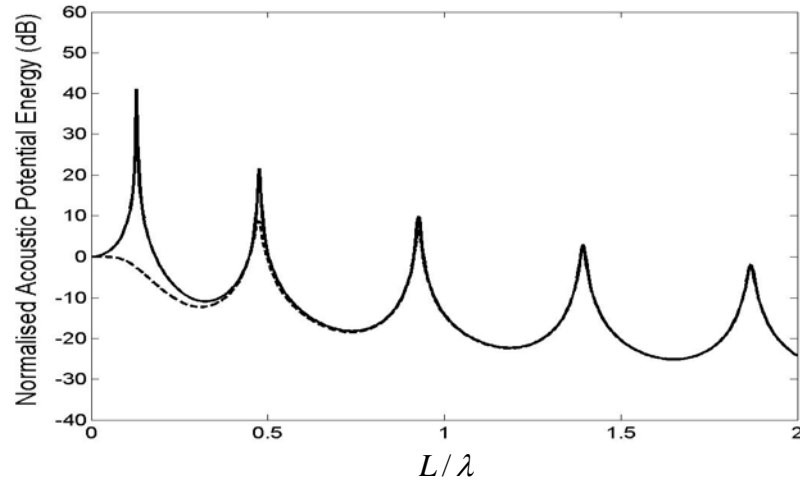
(c) Intermediate case ($K_a / K_s = 1$)

Figure 5.6 Acoustic potential energy normalised by that at the static state ($L/\lambda = 0$) in the absence of control for a given stiffness ratio where the structural natural frequency is at $L/\lambda = 0.1$ ($\omega_a / \omega_s = 5$), stiffness ratio $K_a / K_L = 0.1$, loss factors $\eta_s = \eta_a = \eta_L = 10^{-2}$ (solid line: without control and dashed line: with velocity feedback control using the structural actuator)

159
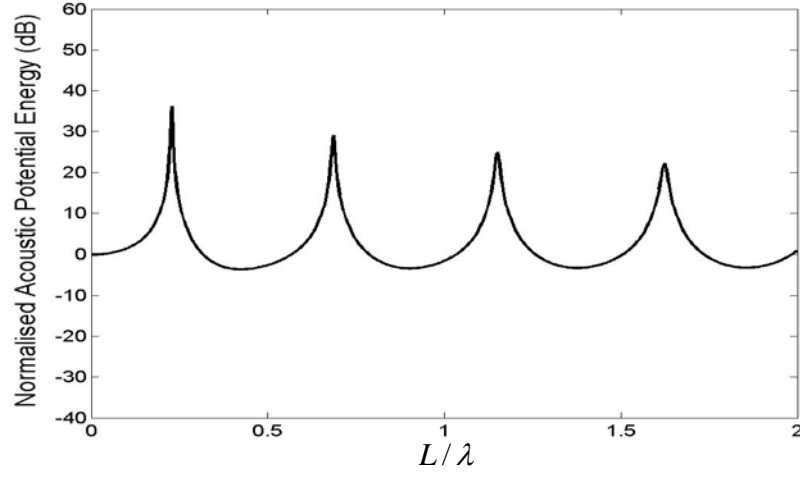
(a) Strongly coupled case ($K_a / K_s = 10^3$)
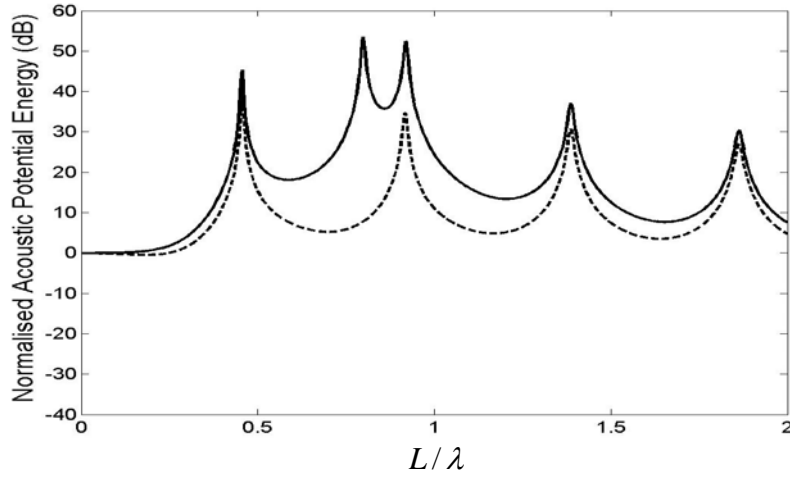
(b) Weakly coupled case ($K_a / K_s = 10^{-3}$)
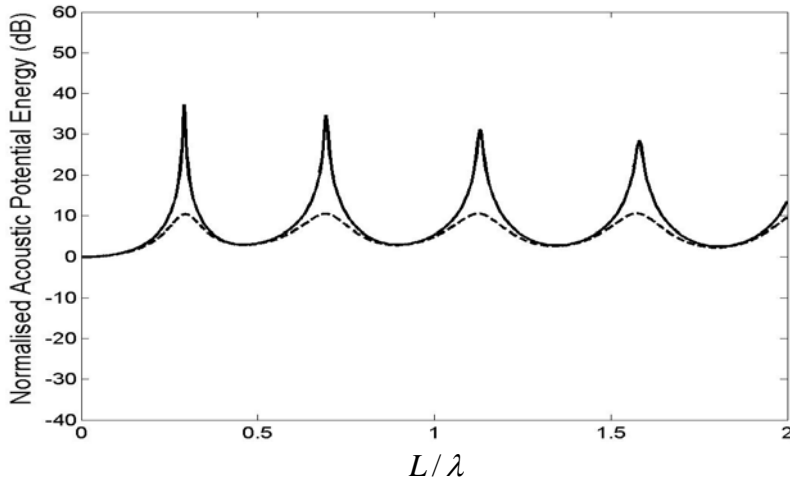
(c) Intermediate case ($K_a / K_s = 1$)

Figure 5.7 Acoustic potential energy normalised by that at the static state ($L/\lambda = 0$) in the absence of control for a given stiffness ratio where the structural natural frequency is at $L/\lambda = 0.8$ ($\omega_a / \omega_s = 0.6$), stiffness ratio $K_a / K_L = 0.1$, loss factors $\eta_s = \eta_a = \eta_L = 10^{-2}$ (solid line: without control and dashed line: with velocity feedback control using the structural actuator)

160

5.4 Decentralised velocity feedback control using both actuators

Decentralised velocity feedback control can be implemented in the simple vibro-acoustic system by using both the acoustic actuator at the right end and the structural actuator at the left end, discussed in section 5.2 and 5.3 respectively. The independent localised control units provide controlled impedances, which are Z_{VA}, given in equation (5.2), for the acoustic actuator and Z_{VS}, given in equation (5.9), for the structural actuator. Acoustic response in the vibro-acoustic system can be derived using the controlled impedances at the both ends. The control of the acoustic potential energy is investigated when the decentralised velocity feedback control is implemented using both the actuators. The three coupled cases, discussed in section 5.2 and 5.3, are studied when the structural natural frequency is at $L/\lambda = 0.1$ and at $L/\lambda = 0.8$ respectively.

5.4.1 Acoustic response due to a decentralised controller

Acoustic pressure and particle velocity in a one-dimensional tube, under the decentralised velocity feedback control, can be derived using controlled impedances at both ends of the tube via the acoustic and structural actuators.

Figure 5.8 depicts a one-dimensional acoustic tube excited by a primary SDOF structure, under broadband disturbance, and simultaneously controlled by a secondary structural actuator at $x = 0$ and a secondary acoustic actuator at $x = L$. The structural and acoustic actuators are driven by velocity feedback controllers with a feedback gain $-H_S$ and with a feedback gain $-H_A$ respectively. This analytical model has the same system parameters of the primary structure and the acoustic actuator as depicted in figures 5.1 and 5.5. When the primary structure, under the broadband excitation force F_P, induces vibro-acoustic disturbance in the cavity, the control forces F_{CS} and F_{CA}, via the structural and acoustic actuators, control the interior sound field in the cavity.
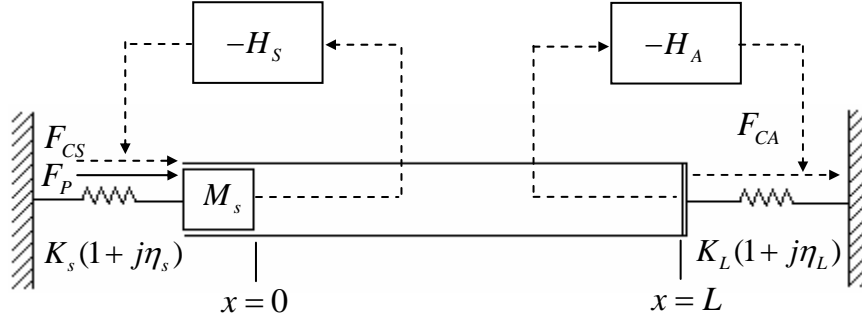
Figure 5.8 Model of a combined SDOF structure – one dimensional acoustic tube system using structural and acoustic actuators driven by velocity feedback controllers at $x = 0$ and at $x = L$ respectively

When the decentralised velocity feedback control is active, the boundary at $x = L$ can be represented by the sum of the controlled impedance via the acoustic actuator Z_{VA} and the impedance of the acoustic actuator in the absence of control. Also, the boundary at $x = 0$ can be represented by the sum of the controlled impedance via the structural actuator Z_{VS} and that of the primary structure Z_S. When the decentralised velocity feedback control is active, acoustic pressure and particle velocity can be obtained by setting the impedance Z_L and the impedance Z_S in equations (2.32)~(2.33) to the sum of the impedances Z_{VA} and Z_L, and the sum of the impedances Z_{VS} and Z_S respectively to give

$$P(x,\omega) = \rho_0 c \frac{1}{Z_S + Z_{VS} + Z_{A0}} \frac{\dfrac{Z_L + Z_{VA}}{\rho_0 cS} \cos k(L-x) + j\sin k(L-x)}{\cos kL + j\dfrac{Z_L + Z_{VA}}{\rho_0 cS} \sin kL} \tag{5.15}$$

$$U(x,\omega) = \frac{F_P}{Z_S + Z_{VS} + Z_{A0}} \frac{\cos k(L-x) + j\dfrac{Z_L + Z_{VA}}{\rho_0 cS} \sin k(L-x)}{\cos kL + j\dfrac{Z_L + Z_{VA}}{\rho_0 cS} \sin kL} \tag{5.16}$$

Non-dimensionalised acoustic pressure and particle velocity are given by

$$\hat{P}(\hat{x}, \hat{L}) = \frac{1}{(\hat{Z}_S + \hat{Z}_{VS}) + \hat{Z}_{A0}} \frac{2}{2 - j\eta_a} \frac{(\hat{Z}_L + \hat{Z}_{VA})\cos\left(\pi(2 - j\eta_a)(1 - \hat{x})\hat{L}\right) + j\frac{2}{2 - j\eta_a}\sin\left(\pi(2 - j\eta_a)(1 - \hat{x})\hat{L}\right)}{\frac{2}{2 - j\eta_a}\cos\left(\pi(2 - j\eta_a)\hat{L}\right) + j(\hat{Z}_L + \hat{Z}_{VA})\sin\left(\pi(2 - j\eta_a)\hat{L}\right)} \quad (5.17)$$

$$\hat{U}(\hat{x}, \hat{L}) = \frac{1}{(\hat{Z}_S + \hat{Z}_{VS}) + \hat{Z}_{A0}} \frac{\frac{2}{2 - j\eta_a}\cos\left(\pi(2 - j\eta_a)(1 - \hat{x})\hat{L}\right) + j(\hat{Z}_L + \hat{Z}_{VA})\sin\left(\pi(2 - j\eta_a)(1 - \hat{x})\hat{L}\right)}{\frac{2}{2 - j\eta_a}\cos\left(\pi(2 - j\eta_a)\hat{L}\right) + j(\hat{Z}_L + \hat{Z}_{VA})\sin\left(\pi(2 - j\eta_a)\hat{L}\right)} \quad (5.18)$$

where non-dimensional parameters are defined in equations (5.5)~(5.6) and equations (5.12) ~(5.13). Also, the normalised acoustic input impedance $\hat{Z}_{A0}$ is that when using the acoustic actuator in a velocity feedback control scheme and is given in equation (5.7).

5.4.2 Feedback gains for various coupling conditions

When the decentralised velocity feedback control is implemented using both the actuators, the active damping of the acoustic actuator needs to be optimised under the velocity feedback control implemented by the structural actuator. The optimal feedback gain of the acoustic actuator is obtained when the summed acoustic potential energy over the frequency range of interest is minimised in each coupled case.

Figures 5.9(a) and (b) show the summed acoustic potential energy over the frequency range ($0 \le L/\lambda \le 2$) as a function of a feedback gain ratio $H_A / \rho_0 c_0 S$ for a given stiffness ratio when the velocity feedback control is implemented in the primary structure. The summed acoustic potential energy is normalised by that under the velocity feedback control using only the structural actuator in each coupled case when the structural natural frequency is at $L/\lambda = 0.1$ and at $L/\lambda = 0.8$ respectively. The normalised summed acoustic potential energy at the upper limit of the ratio $H_A / \rho_0 c_0 S$ is generally the same as that in the vibro-acoustic system rigidly terminated at $x = L$ under the velocity feedback control using only the structural actuator. Also, the normalised summed acoustic potential energy at the lower limit of the ratio $H_A / \rho_0 c_0 S$ is the same as that in the vibro-acoustic system under the velocity

feedback control using only the structural actuator. The level at the value of the ratio $H_A / \rho_0 c_0 S$, minimising the summed acoustic potential energy, represents achievable extra reduction using the acoustic actuator after the velocity feedback control is implemented by the structural actuator. Table 5.3 presents the optimal feedback gain ratio $H_A / \rho_0 c_0 S$ under the decentralised velocity feedback control and the extra reduction on the summed acoustic potential energy using the acoustic actuator for a given stiffness ratio.

In the *strongly coupled* case with an structural-acoustic stiffness ratio $K_a / K_s = 10^3$, the optimal feedback gain ratio is 3.5 and 3.7 when the structural natural frequency is at $L / \lambda = 0.1$ and at $L / \lambda = 0.8$ respectively as shown figures 5.9(a) and (b). At around the optimal feedback gain ratio, the normalised summed acoustic potential energy has sharp changes for the two natural frequency ratios ω_a / ω_s. Under the decentralised velocity feedback control, the summed acoustic potential energy can be more reduced by about 8dB and about 9dB for the respective natural frequency ratio compared to that in the case of using only the structural actuator as presented in table 5.3. In this case, the control performance of the decentralised velocity feedback control is more or less equivalent to that in the case of using only the acoustic actuator. This is due to the fact that the induced active damping on the structure is not influential on the acoustic potential energy as discussed when using only the structural actuator in section 5.3.

In the *weakly coupled* case with a structural-acoustic stiffness ratio $K_a / K_s = 10^{-3}$, the optimal feedback gain ratio is 2.7 and 2.3 when the structural natural frequency is at $L / \lambda = 0.1$ and at $L / \lambda = 0.8$ respectively as shown figures 5.9(a) and (b). The normalised summed acoustic potential energy has sharp changes at around the optimal feedback gain ratio since the dominating structural mode is controlled by the active damping induced by the structural actuator. In this case, the summed acoustic potential energy can be more reduced by about 4dB and about 9dB for the respective natural frequency ratio compared to that in the case of using only the structural actuator as presented in table 5.3. When the structural natural frequency is at $L / \lambda = 0.8$, the relative lager reduction is due to the more strongly coupled structure, which causes a structural mode with less contribution to the acoustic potential energy.

In the *intermediate* case with a structural-acoustic stiffness ratio $K_a / K_s = 1$, the optimal feedback gain ratio is 3 and 1.8 when the structural natural frequency is at $L/\lambda = 0.1$ and at $L/\lambda = 0.8$ respectively as shown figures 5.9(a) and (b). When the structural natural frequency is at $L/\lambda = 0.1$, the normalised summed acoustic potential energy has sharp changes at around the optimal feedback gain ratio for the same reason as in the *weakly coupled* case. On the other hand, when the structural natural frequency is at $L/\lambda = 0.8$, the normalised summed acoustic potential energy is less sensitive to the change of the feedback gain ratio. Because all the acoustic modes can be suppressed at resonance frequencies by the structural actuator in a velocity feedback control scheme as discussed in section 5.3. Under the decentralised velocity feedback control, the summed acoustic potential energy can be more reduced by about 6dB and 2dB for the respective natural frequency ratio.
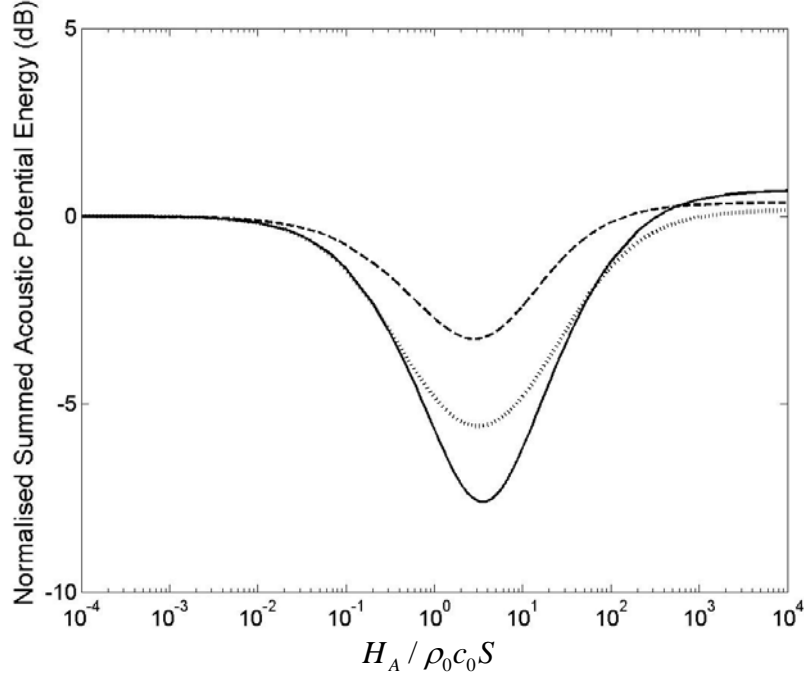
(a) Structural natural frequency at $L/\lambda = 0.1$
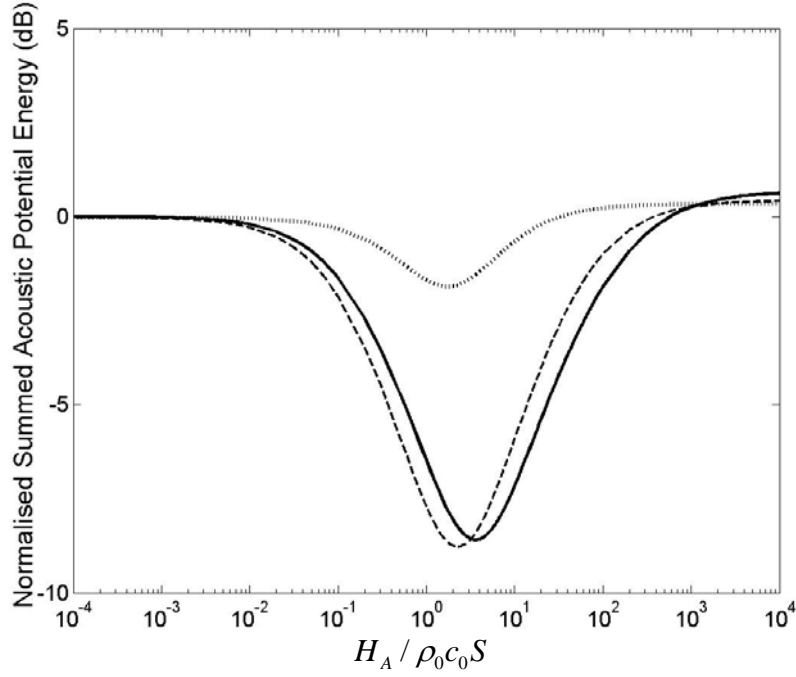
(b) Structural natural frequency at $L/\lambda = 0.8$

Figure 5.9 Summed acoustic potential energy as a function of a feedback gain ratio $H_A / \rho_0 c_0 S$ normalised by that under control using only the structural actuator for a given stiffness ratio when the structural natural frequency is at $L/\lambda = 0.1$ ($\omega_a / \omega_s = 5$) and at $L/\lambda = 0.8$ ($\omega_a / \omega_s = 0.6$) respectively where stiffness ratio $K_a / K_L = 0.1$ and loss factors $\eta_s = \eta_a = \eta_L = 10^{-2}$ (solid line: strongly coupled case with $K_a / K_s = 10^3$, dashed line: weakly coupled case with $K_a / K_s = 10^{-3}$ and dotted line: intermediate case with $K_a / K_s = 1$)

Table 5.3 Feedback gain ratio for the acoustic actuator ($H_A / \rho_0 c_0 S$) and summed acoustic potential energy over the frequency range ($0 \leq L/\lambda \leq 2$) normalised by that under the velocity feedback control implemented by the structural actuator for a given stiffness when the structural natural frequency is at $L/\lambda = 0.1$ ($\omega_a/\omega_s = 5$) and at $L/\lambda = 0.8$ ($\omega_a/\omega_s = 0.6$) respectively

Degree of coupling	Natural frequency ratio			
	$\omega_a/\omega_s = 5$		$\omega_a/\omega_s = 0.6$	
	Feedback gain ratio	Reduction	Feedback gain ratio	Reduction
Strong ($K_a/K_s = 10^3$)	3.5	-8dB	3.7	-9dB
Weak ($K_a/K_s = 10^{-3}$)	2.7	-4dB	2.3	-9dB
Intermediate ($K_a/K_s = 1$)	3	-6dB	1.8	-2dB

5.4.3 Control of acoustic potential energy using a decentralised controller

Decentralised velocity feedback control of the acoustic potential energy is investigated in this section. The three coupled cases, discussed in section 5.2 and 5.3, are studied when the structural natural frequency is at $L/\lambda = 0.1$ and is at $L/\lambda = 0.8$ respectively.

Figures 5.10(a), (b), (c) and figures 5.11(a), (b), (c) show the acoustic potential energy, under the decentralised velocity feedback control using both the actuators, for a given stiffness ratio when the structural natural frequency is at $L/\lambda = 0.1$ and at $L/\lambda = 0.8$ respectively. The acoustic potential energy is normalised by that at the static state ($L/\lambda = 0$) in the absence of control. The feedback gain ratios, presented in tables 5.2 and 5.3, are substituted for the normalised controlled impedances $\hat{Z}_{VS}$ and $\hat{Z}_{VA}$ respectively in equations (5.17)~(5.18) for a given stiffness ratio. Table 5.4 presents the summed acoustic potential energy, over the frequency range ($0 \leq L/\lambda \leq 2$), normalised by that in the absence of control for a given stiffness ratio.

In the *strongly coupled* case with a structural-acoustic stiffness ratio $K_a / K_s = 10^3$, all the acoustic modes can be effectively suppressed at resonance frequencies for the two natural frequency ratios ω_a / ω_s as shown in figures 5.10(a) and 5.11(a). In this case, the acoustic actuator mainly contributes to the control of the acoustic potential energy as shown in figures 5.3(a) and 5.4(a). The controlled acoustic potential energy has control spillover at off-resonance frequencies for the same reason as the case of using only the acoustic actuator. The reduction on the summed acoustic potential energy, over the frequency range of interest, is equivalent to that using only the acoustic actuator as presented in tables 5.1 and 5.4.

In the *weakly coupled* case with a structural-acoustic stiffness ratio $K_a / K_s = 10^{-3}$ and the structural natural frequency at $L / \lambda = 0.1$, both the structural mode at $L / \lambda = 0.1$ and acoustic modes, whose fundamental mode is at $L / \lambda = 0.45$, can be controlled as shown in figure 5.10(b). In this case, the decentralised velocity feedback control has both the control benefits of the acoustic and structural actuators. They are effective on the control of the acoustic and structural modes respectively as shown in figures 5.3(b) and 5.6(b). Due to the controllability of both the structural and acoustic modes, the summed acoustic potential energy, over the frequency range of interest, can be reduced by about 20dB as presented in table 5.4.

In the *weakly coupled* case, when the structural natural frequency is at $L / \lambda = 0.8$, both the structural mode at $L / \lambda = 0.8$, and acoustic modes, whose fundamental mode is at $L / \lambda = 0.45$, can be controlled as shown in figure 5.11(b). It is noticeable that the control spillover caused by the acoustic actuator, as shown in figure 5.4(b), reduces due to effectively suppressed acoustic modes by the structural actuator, as shown in figure 5.7(b). In this case, the reduction on the summed acoustic potential energy, over the frequency range of interest, can be achieved by about 25dB as presented in table 5.4. Compared to the *weakly coupled* case with the structural natural frequency at $L / \lambda = 0.1$, more effective reduction on the summed acoustic potential energy is due to the increased damping control region of the structure as discussed in section 5.3.

In the *intermediate* case with a structural-acoustic stiffness ratio $K_a / K_s = 1$ and the structural natural frequency at $L / \lambda = 0.1$, both the structural mode at $L / \lambda = 0.13$ and acoustic modes, whose fundamental mode is at $L / \lambda = 0.48$, can be effectively suppressed at resonance frequencies as shown in the figure 5.10 (c). However, the controlled acoustic potential energy

has minor control spillover at off-resonance frequencies due to the controlled impedance by the acoustic actuator as shown in figure 5.3(c). In this case, the summed acoustic potential energy, over the frequency range of interest, can be reduced by about 22dB as presented in table 5.4 due to both the control of the structural and acoustic modes.

In the *intermediate* case, when the structural natural frequency is at $L/\lambda = 0.8$, all the acoustic modes are effectively suppressed at resonance frequencies as shown in figure 5.11(c). The control of the acoustic potential energy is mainly contributed by the structural actuator as shown in figure 5.7(c). Also, the control effect increases due to the acoustic actuator as shown in figure 5.4(c). In this case, the summed acoustic potential energy, over the frequency range of interest, can be reduced by about 13dB as presented in table 5.4. Compared to the *intermediate* case with the structural natural frequency at $L/\lambda = 0.1$, the smaller reduction in the summed acoustic potential energy is due to the more strongly coupled structure causing only acoustic modes.

In summary, the control mechanism of the decentralised velocity feedback control is to reduce sound radiation from the vibrating primary structure and to absorb the acoustic energy in the cavity via respective induced active damping by structural and acoustic actuators. The decentralised velocity feedback control, implemented by both the structural and acoustic actuators, is effective on the control of the acoustic potential energy in all the coupled cases. In the *strongly coupled* case, the controlled acoustic potential energy is mainly contributed by the acoustic actuator, which is effective on the control of the acoustic modes. In the *weakly coupled* and *intermediate* case, both the structural and acoustic modes can be effectively suppressed at resonance frequencies due to the control benefits of both the actuators.
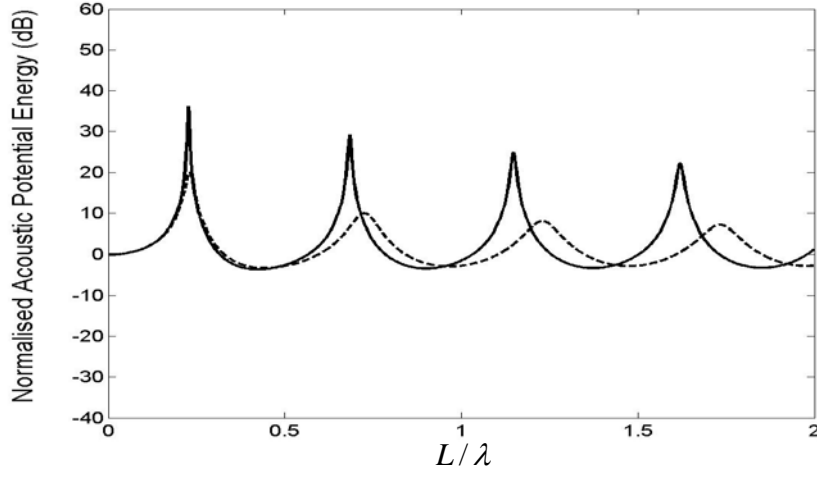
(a) Strongly coupled case ($K_a / K_s = 10^3$)
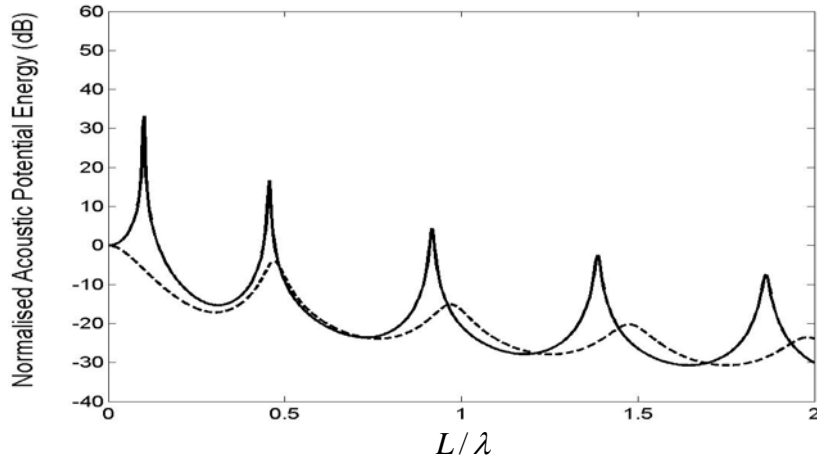
(b) Weakly coupled case ($K_a / K_s = 10^{-3}$)
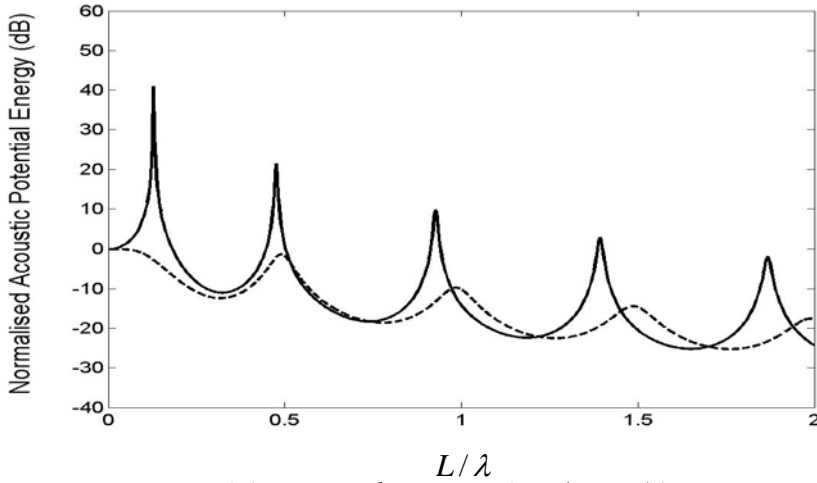
(c) Intermediate case ($K_a / K_s = 1$)

Figure 5.10 Acoustic potential energy normalised by that at the static state ($L/\lambda = 0$) in the absence of control for a given stiffness ratio where the structural natural frequency is at $L/\lambda = 0.1$ ($\omega_a / \omega_s = 5$), stiffness ratio $K_a / K_L = 0.1$, loss factors $\eta_s = \eta_a = \eta_L = 10^{-2}$ (solid line: without control and dashed line: with decentralised velocity feedback control using both the actuators)
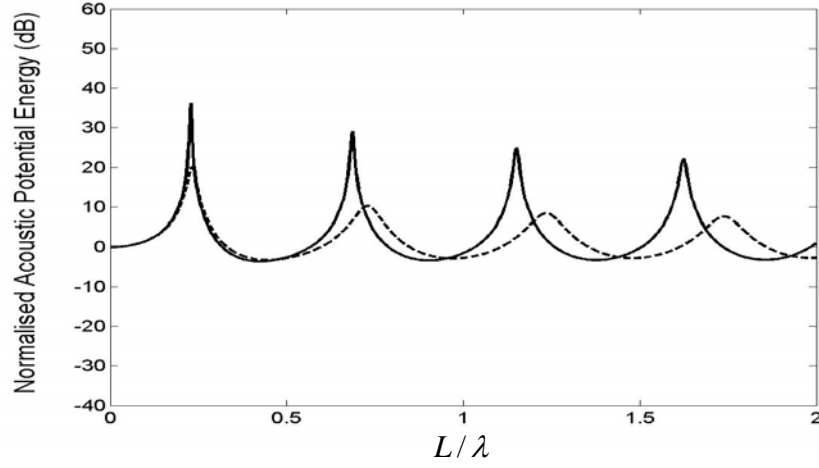
(a) Strongly coupled case ($K_a / K_s = 10^3$)
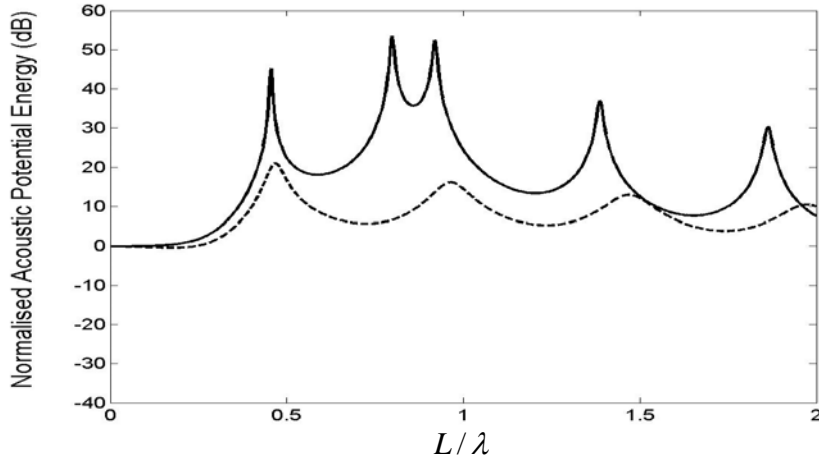
(b) Weakly coupled case ($K_a / K_s = 10^{-3}$)
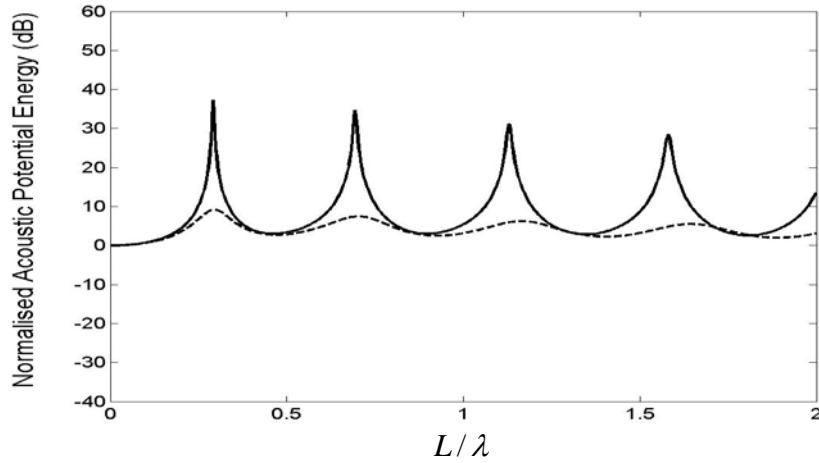
(c) Intermediate case ($K_a / K_s = 1$)

Figure 5.11 Acoustic potential energy normalised by that at the static state ($L/\lambda = 0$) in the absence of control for a given stiffness ratio where the structural natural frequency is at $L/\lambda = 0.8$ ($\omega_a / \omega_s = 0.6$), stiffness ratio $K_a / K_L = 0.1$, loss factors $\eta_s = \eta_a = \eta_L = 10^{-2}$ (solid line: without control and dashed line: with decentralised velocity feedback control using both the actuators)

171

Table 5.4 Summed acoustic potential energy, over the frequency range ($0 \leq L/\lambda \leq 2$), normalised by that before control when the structural natural frequency is at $L/\lambda = 0.1$ ($\omega_a / \omega_s = 5$) and at $L/\lambda = 0.8$ ($\omega_a / \omega_s = 0.6$) respectively

Degree of coupling	Natural frequency ratio	
	$\omega_a / \omega_s = 5$	$\omega_a / \omega_s = 0.6$
Strong ($K_a / K_s = 10^3$)	-9dB	-9dB
Weak ($K_a / K_s = 10^{-3}$)	-20dB	-25dB
Intermediate ($K_a / K_s = 1$)	-22dB	-13dB

5.5 Velocity feedback control effects on structural kinetic energy

When velocity feedback control is implemented in a vibro-acoustic system, the dynamic response of a primary structure can be affected by the change of the acoustic potential energy in the cavity. In this section, the control effect on the dynamic response of the primary structure is investigated in terms of the structural kinetic energy, defined in equation (2.54). The three coupled cases, discussed in section 5.2, 5.3 and 5.4, are studied when the velocity feedback control is implemented using the acoustic actuator, the structural actuator or both the actuators.

When the decentralised velocity feedback control is active, the structural velocity at the input position ($x = 0$) can be obtained by setting the normalised arbitrary position x to zero in equation (5.16). Substituting the structural velocity into equation (2.54) gives the structural kinetic energy. Also, the structural kinetic energy can be written in non-dimensional form as

$$\hat{E}_K(\hat{L}) = \left| \frac{1}{(\hat{Z}_S + \hat{Z}_{VS}) + \hat{Z}_{A0}} \right|^2 \tag{5.19}$$

The acoustic input impedance ratio $\hat{Z}_{A0}$ is given in equation (5.7), which is that under the velocity feedback control implemented by using only the acoustic actuator. On the other hand, when the velocity feedback control is implemented by using an individual actuator, the structural kinetic energy can be obtained by adjusting the impedances in equation (5.19). In the case of using only the acoustic actuator, the structural kinetic energy can be obtained by setting the controlled impedance ratio $\hat{Z}_{VS}$ to zero. Also, in the case of using only the structural actuator, the acoustic input impedance ratio $\hat{Z}_{A0}$ is that in the absence of control given in equation (2.37).

The structural kinetic energy is a function of the structural impedance ratio $\hat{Z}_S$, the controlled impedance ratio $\hat{Z}_{VS}$ and the acoustic input impedance ratio $\hat{Z}_{A0}$ as given in equation (5.19). The controlled impedance ratio $\hat{Z}_{VS}$, induced by the structural actuator, causes active damping on the primary structure to reduce sound radiation into the cavity. Also, the dynamic response of the structure can be affected by the acoustic input impedance ratio $\hat{Z}_{A0}$. In this case, the acoustic input impedance ratio $\hat{Z}_{A0}$ has resonances at around $L/\lambda = n/2$ for small acoustic loss factor η_a where n is an integer. When the velocity feedback control is implemented by the acoustic actuator, the resonances shift toward those in a closed tube with smaller amplitudes due to the controlled impedance ratio $\hat{Z}_{VA}$. Also, the acoustic input impedance ratio $\hat{Z}_{A0}$ has larger damping ratio at off-resonance frequencies since the controlled impedance ratio $\hat{Z}_{VA}$ provides active damping in the cavity, which is constant with frequency. So, under the decentralised velocity feedback control, the structural kinetic energy is affected by the active damping in the structure, induced by the structural actuator, and the increased damping of the acoustic input impedance at off-resonance frequencies caused by the acoustic actuator.

Figures 5.12(a), (b), (c) and figures 5.13(a), (b), (c) show the structural kinetic energy, under the velocity feedback control, for a given stiffness ratio when the structural natural frequency is at $L/\lambda = 0.1$ and at $L/\lambda = 0.8$ respectively. The structural kinetic energy is arbitrarily normalised by that at $L/\lambda = 2$ in the absence of control for a given stiffness ratio. Also, the summed structural kinetic energy over the frequency range ($0 \leq L/\lambda \leq 2$), normalised by that

in the absence of control, is presented in table 5.5 for a given stiffness ratio according to the actuator type.

In the *strongly coupled* case with a structural-acoustic stiffness ratio $K_a/K_s = 10^3$, the structural kinetic energy in the absence of control is generally subject to the acoustic resonances with the fundamental mode at $L/\lambda = 0.23$ for the two natural frequency ratios ω_a/ω_s as shown in figures 5.12(a) and 5.13(a). When the velocity feedback control is implemented by the acoustic actuator, the peaks of the structural kinetic energy reduce due to the increased damping of the acoustic input impedance. After control, the structural kinetic energy shifts to higher frequencies due to the shifted acoustic resonances as discussed in section 5.2. When the velocity feedback control is implemented by the structural actuator, the control effect on the structural kinetic energy is insignificant due to the dominating acoustic resonances. In this case, the structural kinetic energy mostly overlaps with that in the absence of control. When the decentralised velocity feedback control is implemented by both the actuators, the structural kinetic energy is generally the same as that in the case of using only the acoustic actuator being overlapped. The summed structural kinetic energy can be reduced by about 9dB as presented in table 5.5 and is mainly contributed by the acoustic actuator.

In the *weakly coupled* case with a structural-acoustic stiffness ratio $K_a/K_s = 10^{-3}$ and the structural natural frequency at $L/\lambda = 0.1$, the structural kinetic energy is determined by only structural characteristics before control as shown in figure 5.12(b). So, under the velocity feedback control implemented by the acoustic actuator, the control effect is insignificant on the structural kinetic energy being overlapped with that before control. On the other hand, when using the structural actuator or both the actuators, the induced active damping gives rise to effective reduction on the structural kinetic energy. The structural kinetic energy, under the decentralised velocity feedback control, overlaps with that in the case of using only the structural actuator. In this case, the summed structural kinetic energy, over the frequency range of interest, reduces by about 22dB in both the control schemes as presented in table 5.5. Under the decentralised velocity feedback control, the reduction on the summed structural kinetic energy is mainly contributed by the structural actuator.

In the *weakly coupled* case, when the structural natural frequency is at $L/\lambda = 0.8$, the structural kinetic energy has a dominating peak at $L/\lambda = 0.8$ determined by the structural

characteristics as shown in figure 5.13(b). Also, the structural kinetic energy has small peaks at $L/\lambda = n/2$ being subject to the acoustic resonances in the cavity where n is an integer. Under the velocity feedback control implemented by the acoustic actuator, the amplitude of the small peaks reduces due to the active damping in the cavity. However, the reduction on the summed structural kinetic energy, over the frequency range of interest, is negligible because the control effect is insignificant on the dominating peak at $L/\lambda = 0.8$. When using the structural actuator or both the actuators, broad reduction on the structural kinetic energy is observed in both the control schemes. Compared to the *weakly coupled* case with structural natural frequency at $L/\lambda = 0.1$, relative larger reduction is due to the increased damping control region of the structure as discussed in section 5.3. In this case, the summed structural kinetic energy reduces by about 26dB in both the control schemes as presented in table 5.5. The main contribution on the reduction of the summed structural kinetic energy is achieved by the induced active damping via the structural actuator.

In the *intermediate* case with a structural-acoustic stiffness ratio $K_a/K_s = 1$ and the structural natural frequency at $L/\lambda = 0.1$, the structural kinetic energy is dominated by the peak at $L/\lambda = 0.13$ before control as shown in figure 5.12(c). Also, the structural kinetic energy has peaks being subject to the acoustic resonances, whose fundamental resonance is at $L/\lambda = 0.48$. When using only the acoustic actuator, the peak at $L/\lambda = 0.13$ has no change. On the other hand, the amplitude of the other peaks reduces due to the active damping in the cavity. After control, the peaks shift to higher frequencies for the same reason as in the *strongly coupled* case. In this case, the summed structural kinetic energy, over the frequency range of interest, reduces by about 8dB as presented in table 5.5. When using the structural actuator, the amplitude of the peak at $L/\lambda = 0.13$ reduces significantly due to the induced active damping on the structure. Also, the second and third peaks can be reduced to some degree. The control effect dies out with frequency because the active damping is effect at around structural resonance frequency. In this case, the summed structural kinetic energy reduces by about 24dB due to the reduced dominating peak at $L/\lambda = 0.13$. When using both the actuators, the peak at $L/\lambda = 0.13$ and the other peaks are reduced by the active damping induced via the structural and acoustic actuators respectively. Under the decentralised velocity feedback control, the reduction on the summed structural kinetic energy is equivalent to that in the case of using only the structural actuator as presented in table 5.5.

In the *intermediate* case, when the structural natural frequency is at $L/\lambda = 0.8$, the structure has similar kinetic energy to that in the *strongly coupled* case as shown in figures 5.13(a) and (c) before control. When using the acoustic actuator, all the peaks are reduced and shift to higher frequencies for the same reason as in the *strongly coupled* case. In this case, the summed structural kinetic energy, over the frequency range of interest, reduces by about 9dB as presented in table 5.5. The reduction level is equivalent to that in the *strongly coupled* case. On the other hand, when using the structural actuator, the induced active damping is more effective on the reduction of the structural kinetic energy due to more strongly coupled structural actuator into the cavity compared to that in the *strongly coupled* case. In this case, the summed structural kinetic energy reduces by about 13dB. When using both the actuators, the structural kinetic energy is reduced by the induced active damping via both the actuators with about 15dB reduction on the summed structural kinetic energy as presented in table 5.5.

In summary, when the velocity feedback control is active, the kinetic energy of the structure coupled into the cavity can be reduced in all the coupled cases depending on the actuator type. The reduction on the structural kinetic energy is mainly contributed by the acoustic actuator and by the structural actuator in the *strongly coupled* case and in the *weakly coupled* case respectively. In the *intermediate* case, both the actuators contribute on the reduction of the structural kinetic energy.

176

(a) Strongly coupled case ($K_a / K_s = 10^3$)

(b) Weakly coupled case ($K_a / K_s = 10^{-3}$)

(c) Intermediate case ($K_a / K_s = 1$)
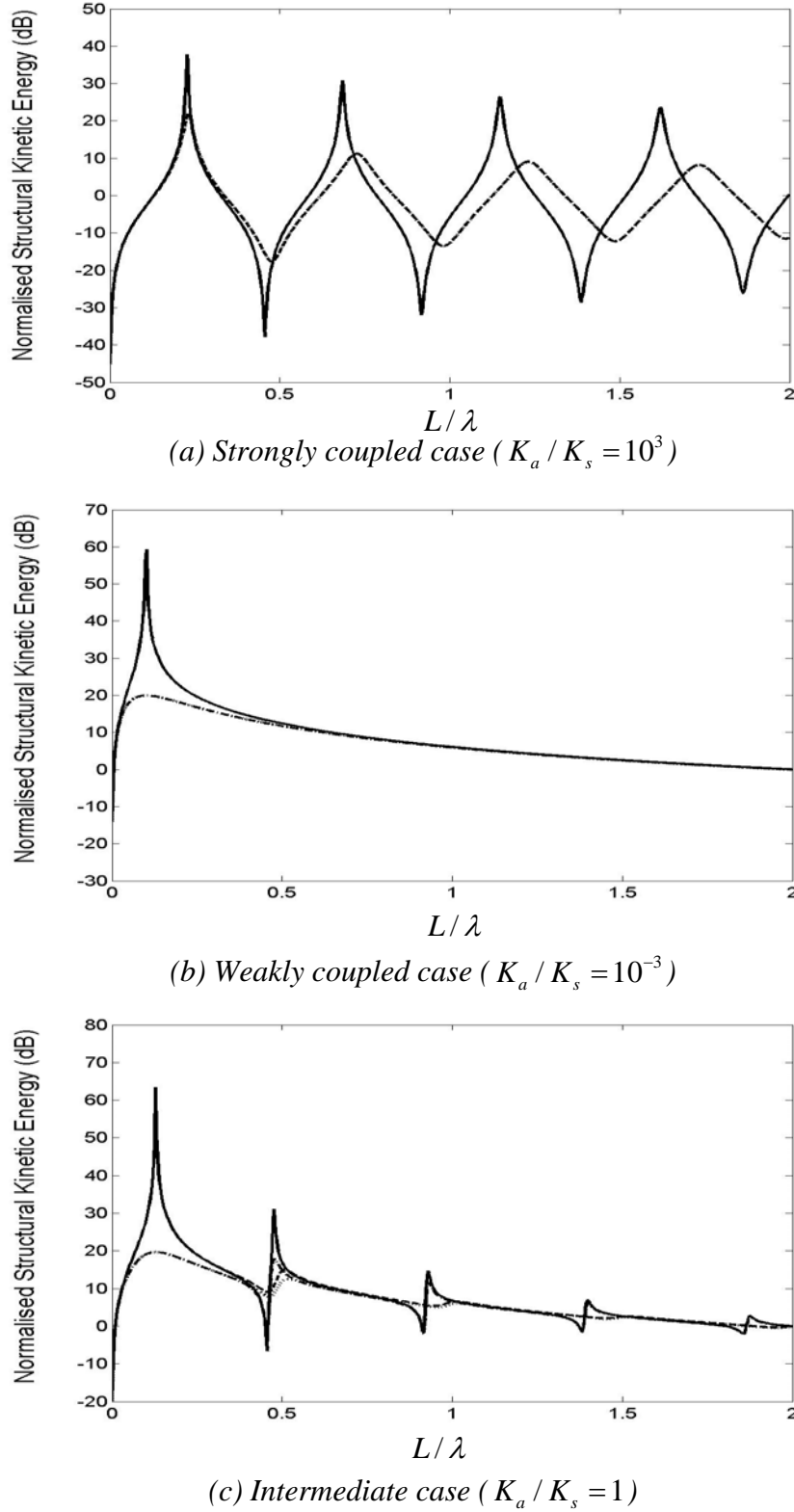
Figure 5.12 Structural kinetic energy arbitrarily normalised by that at $L/\lambda = 2$ in the absence of control for a given stiffness ratio where the structural natural frequency is at $L/\lambda = 0.1$ ($\omega_a / \omega_s = 5$), stiffness ratio $K_a / K_L = 0.1$, loss factors $\eta_s = \eta_a = \eta_L = 10^{-2}$ (solid line: without control, dashed line: with velocity control using the acoustic actuator, dashed-dotted line: with velocity control using the structural actuator and dotted line: with decentralised velocity feedback control using both the actuators)

177

(a) Strongly coupled case ($K_a / K_s = 10^3$)

(b) Weakly coupled case ($K_a / K_s = 10^{-3}$)

(c) Intermediate case ($K_a / K_s = 1$)
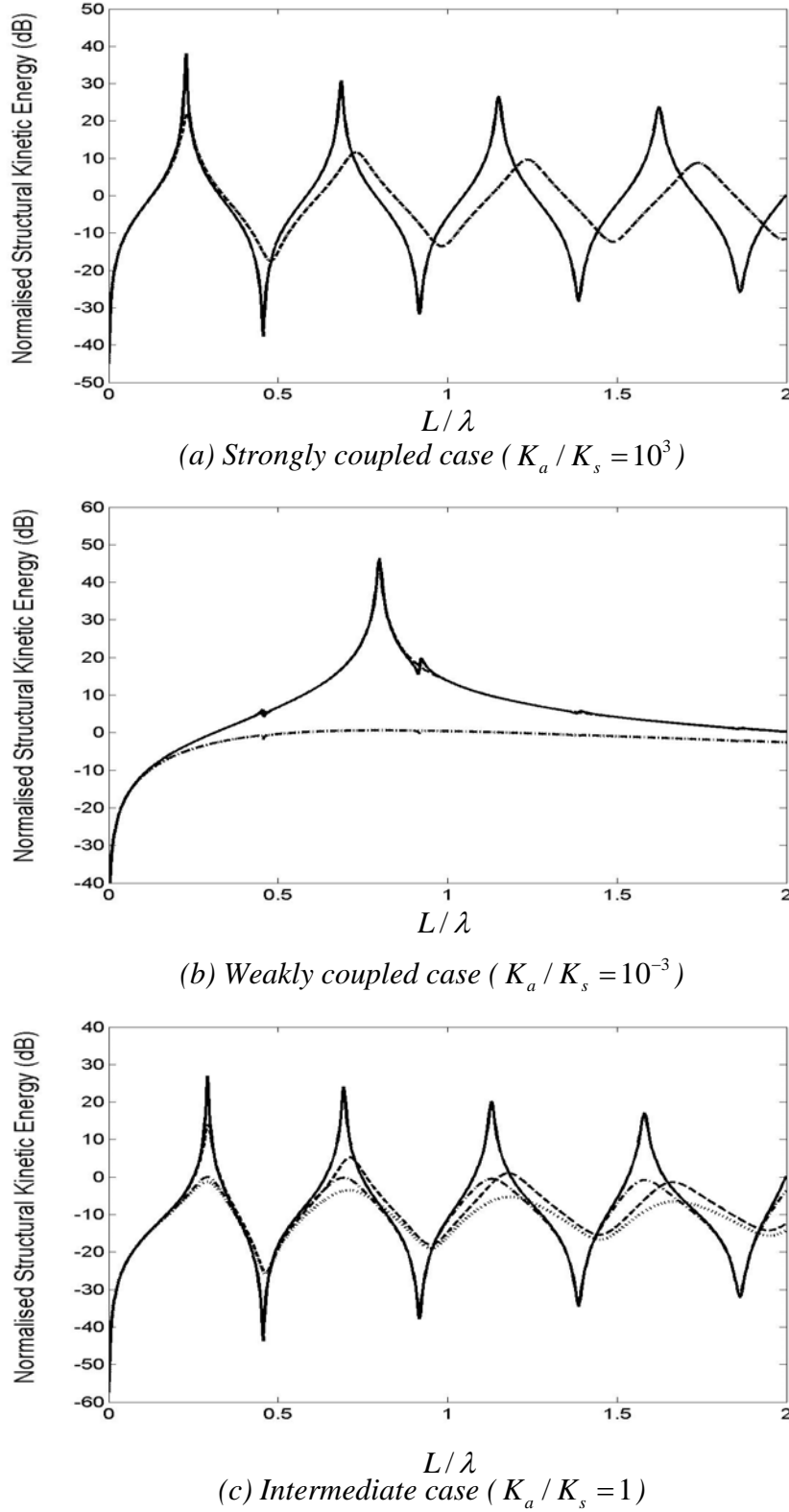
Figure 5.13 Structural kinetic energy arbitrarily normalised by that at $L/\lambda = 2$ in the absence of control for a given stiffness ratio where the structural natural frequency is at $L/\lambda = 0.8$ ($\omega_a / \omega_s = 0.6$), stiffness ratio $K_a / K_L = 0.1$, loss factors $\eta_s = \eta_a = \eta_L = 10^{-2}$ (solid line: without control, dashed line: with velocity control using the acoustic actuator, dashed-dotted line: with velocity control using the structural actuator and dotted line: with decentralised velocity feedback control using both the actuators)

Table 5.5 Summed structural kinetic energy over the frequency range ($0 \leq L/\lambda \leq 2$) according to the actuator type, normalised by that in the absence of control, for a given stiffness ratio when the structural natural frequency is at $L/\lambda = 0.1$ ($\omega_a/\omega_s = 5$) and at $L/\lambda = 0.8$ ($\omega_a/\omega_s = 0.6$) respectively

	Natural frequency ratio					
Degree of coupling	$\omega_a/\omega_s = 5$			$\omega_a/\omega_s = 0.6$		
	Acoustic	Structural	Both	Acoustic	Structural	Both
Strong ($K_a/K_s = 10^3$)	-9dB	0dB	-9dB	-9dB	0dB	-9dB
Weak ($K_a/K_s = 10^{-3}$)	0dB	-22dB	-22dB	0dB	-26dB	-26dB
Intermediate ($K_a/K_s = 1$)	-8dB	-24dB	-24dB	-9dB	-13dB	-15dB

5.6 Cumulative sum of acoustic potential energy

Velocity feedback control effects on the acoustic potential energy have been investigated using the acoustic actuator, the structural actuator or both the actuators. In this section, the relative control performance of the velocity feedback controllers is demonstrated in terms of cumulative sum of acoustic potential energy over the frequency range of interest. Best control strategies are suggested in the three coupled cases, discussed in the previous sections, when the structural natural frequency is at $L/\lambda = 0.1$ and at $L/\lambda = 0.8$ respectively.

Figures 5.14(a),(b),(c) and 5.15(a),(b),(c) show the cumulative sum of acoustic potential energy over the frequency range ($0 \leq L/\lambda \leq 2$), normalised by the summed acoustic potential energy in the absence of control, for a given stiffness ratio when the structural natural frequency is at $L/\lambda = 0.1$ and at $L/\lambda = 0.8$ respectively. The values at the upper frequency limit demonstrate achievable reductions on the summed acoustic potential energy, over the frequency range of interest, according to the actuator type in the velocity feedback control scheme, which are presented in tables 5.1, 5.2 and 5.4.

In the *strongly coupled* case with a structural-acoustic stiffness ratio $K_a / K_s = 10^3$, the acoustic potential energy is governed by acoustic modes before control, whose fundamental mode is at $L/\lambda = 0.23$, for the two natural frequency ratios ω_a / ω_s as shown in figures 5.14(a) and 5.15(a). The cumulative sum of the acoustic potential energy increases in tiers at their resonance frequencies. When using the acoustic actuator, the controlled acoustic potential energy gradually increases with frequency. The increase of the controlled acoustic potential energy is due to effective reduction at resonance frequencies and minor control spillover at off-resonance frequencies as shown in figures 5.3(a) and 5.4(a). On the other hand, when using the structural actuator, the reduction on the acoustic potential energy is insignificant. When the structural natural frequency is at $L/\lambda = 0.8$, the relative smaller reduction is due to smaller structural critical damping caused by smaller structural mass. When using both the actuators, the control performance on the acoustic potential energy is equivalent to that in the case of using only the acoustic actuator. The acoustic potential energies in these two control strategies are generally overlapped with frequency.

In the *weakly coupled* case with a structural-acoustic stiffness ratio $K_a / K_s = 10^{-3}$ and the structural natural frequency at $L/\lambda = 0.1$, the acoustic potential energy is governed by the predominating structural mode at $L/\lambda = 0.1$ and has the acoustic modes, whose fundamental mode is at $L/\lambda = 0.45$ as shown in figure 5.14(b). When using the acoustic actuator, the acoustic modes can be suppressed at resonance frequencies but the dominating structural mode is not controllable as shown in figure 5.3(b). In this case, the acoustic potential energy is dominated by the structural mode with minor reduction after control as shown in figure 5.14(b). On the other hand, when using the structural actuator, the structural mode can be effectively suppressed at the resonance frequency but the acoustic modes are not controllable as shown in figure 5.6(b). In this case, the acoustic potential energy is dominated by the acoustic modes after control as shown in figure 5.14(b). When using both the actuators, both the control benefits cause best control performance on the acoustic potential energy by controlling both the structural and acoustic modes as shown in figure 5.14(b).

In the *weakly coupled* case, when the structural natural frequency is at $L/\lambda = 0.8$, the acoustic potential energy is contributed by the structural mode at $L/\lambda = 0.8$ and the acoustic modes, whose fundamental mode at $L/\lambda = 0.45$ before control as shown in figure 5.15(b). When using the acoustic actuator, all the acoustic modes are effectively suppressed at

resonance frequencies and the structural mode is controllable to some degree as shown in figure 5.4(b). In this case, the acoustic potential energy is dominated by the residual structural mode after control as shown in figure 5.15(b). On the other hand, when using the structural actuator, the structural mode is effectively suppressed at the resonance frequency and the acoustic modes are controllable to some degree as shown in figure 5.7(b). In this case, the acoustic potential energy is dominated by the residual acoustic modes after control as shown in figure 5.15(b). When using both the actuators, the control performance on the acoustic potential energy is most effective, as shown in figure 5.15(b), as in the *weakly coupled* case with the structural natural frequency at $L/\lambda = 0.1$.

In the *intermediate* case with a structural-acoustic stiffness ratio $K_a/K_s = 1$ and the structural natural frequency at $L/\lambda = 0.1$, the acoustic potential energy is contributed by the structural mode at $L/\lambda = 0.13$ and acoustic modes, whose fundamental mode is at $L/\lambda = 0.48$ as shown in figure 5.14(c). The relative control performance of the actuators is similar to that in the weakly coupled case with the structural natural frequency at $L/\lambda = 0.8$. When using the acoustic actuator, all the acoustic modes are effectively suppressed at resonance frequencies and the structural mode is controllable to some degree as shown in figure 5.4(c). In this case, the acoustic potential energy is dominated by the residual structural mode after control as shown in figure 5.14(c). On the other hand, when using the structural actuator, the structural mode is effectively suppressed at the resonance frequency and the acoustic modes are controllable to some degree as shown figure 5.6(c). In this case, the acoustic potential energy is dominated by the residual acoustic modes after control as shown in figure 5.14(c). When using both the actuators, best control performance can be achieved as shown in figure 5.14(c) due to the both the control benefits.

In the *intermediate* case, when the structural natural frequency is at $L/\lambda = 0.8$, the acoustic potential energy is governed by the acoustic modes, whose fundamental mode at $L/\lambda = 0.29$ before control as shown in figure 5.15(c). When using the acoustic actuator, all the acoustic modes are suppressed at resonance frequencies as shown in figure 5.4(c). In this case, the cumulative sum of the acoustic potential energy increases gradually with frequency as shown in figure 5.15(c) due to the effective reduction at resonance frequencies and minor control spillover at off-resonance frequencies. When using the structural actuator, all the acoustic modes are more effectively suppressed at resonance frequencies as shown in figure 5.7(c).

Compared to the case using the acoustic actuator, the more effective control of the acoustic potential energy is due to the more strongly coupled structural actuator into the cavity as discussed in section 5.3. In this case, the cumulative sum of the acoustic potential energy gradually increases with relative larger reduction as shown in figure 5.15(c). When using both the actuators, best control performance on the acoustic potential energy can be achieved as shown in figure 5.15(c) as in the *intermediate* case with the structural natural frequency at $L/\lambda = 0.1$.
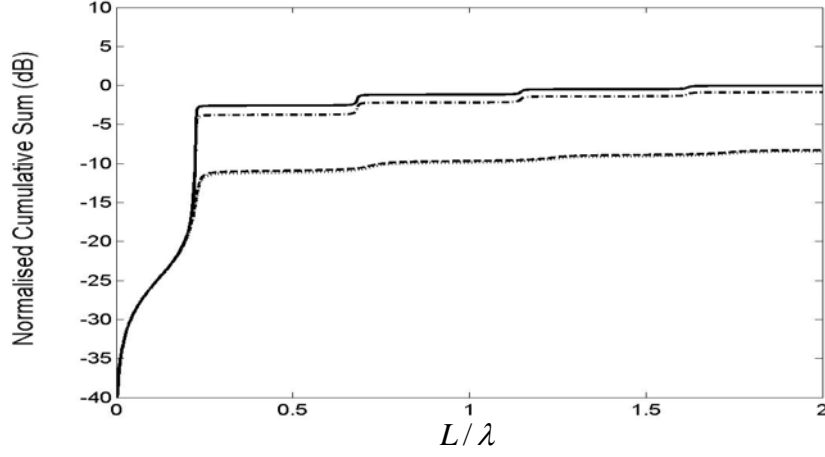
(a) Strongly coupled case ($K_a / K_s = 10^3$)
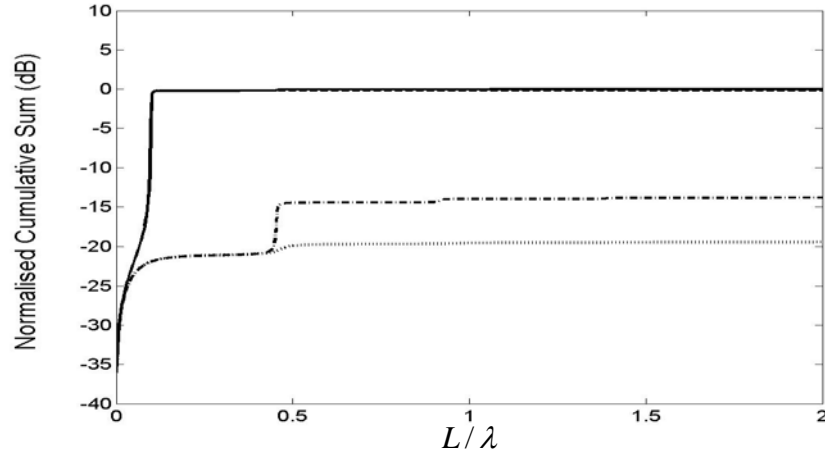
(b) Weakly coupled case ($K_a / K_s = 10^{-3}$)
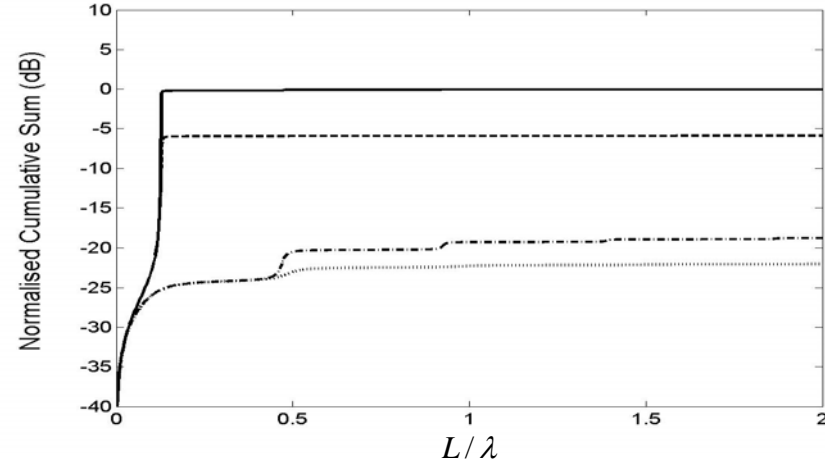
(c) Intermediate case ($K_a / K_s = 1$)

Figure 5.14 Cumulative sum of acoustic potential energy normalised by the summed acoustic potential energy in the absence of control for a given stiffness ratio where the structural natural frequency is at $L/\lambda = 0.1$ ($\omega_a / \omega_s = 5$), stiffness ratio $K_a / K_L = 10^{-3}$, loss factors $\eta_s = \eta_a = \eta_L = 10^{-2}$ (solid line: without control, dashed line: with control using the acoustic actuator, dashed-dotted line: with control using the structural actuator, dotted line: with control using both the actuators)

(a) Strongly coupled case ($K_a / K_s = 10^3$)
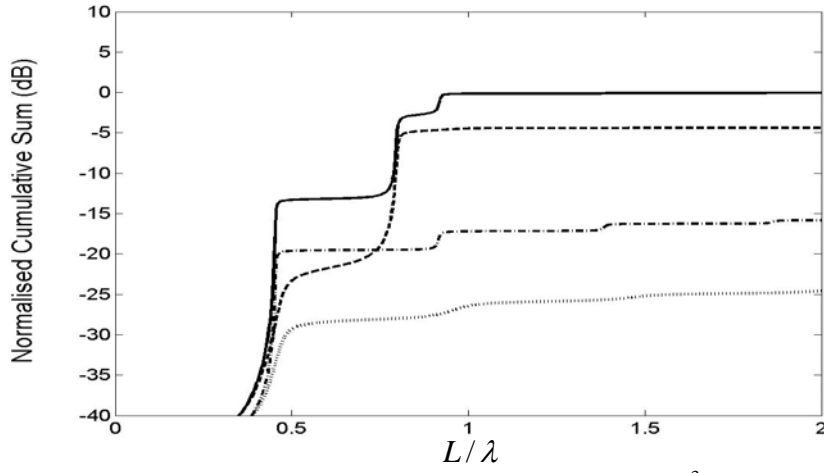
(b) Weakly coupled case ($K_a / K_s = 10^{-3}$)
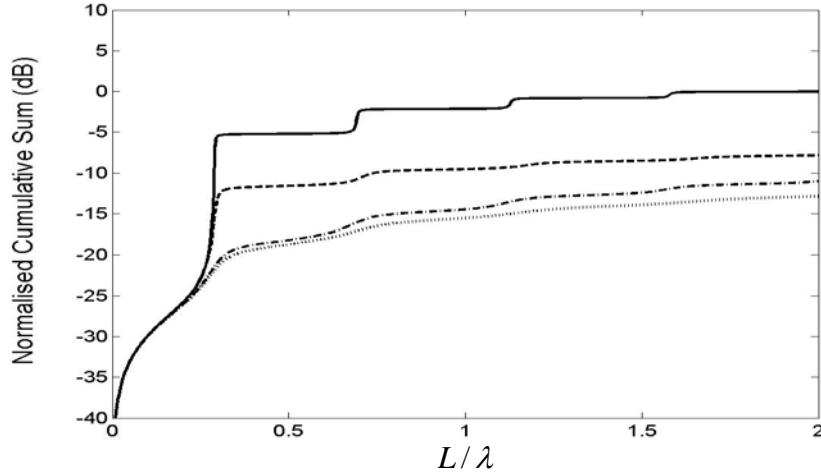
(c) Intermediate case ($K_a / K_s = 1$)

Figure 5.15 Cumulative sum of acoustic potential energy normalised by the summed acoustic potential energy in the absence of control for a given stiffness ratio where the structural natural frequency is at $L/\lambda = 0.8$ ($\omega_a / \omega_s = 0.6$), stiffness ratio $K_a / K_L = 10^{-3}$, loss factors $\eta_s = \eta_a = \eta_L = 10^{-2}$ (solid line: without control, dashed line: with control using the acoustic actuator, dashed-dotted line: with control using the structural actuator, dotted line: with control using both the actuators)

5.7 Conclusions

Active velocity feedback control of the acoustic potential energy in a vibro-acoustic system, has been investigated using the acoustic actuator, the structural actuator and both the actuators for a given stiffness ratio when the structural natural frequency is below and above the fundamental acoustic mode of a closed-closed tube. The control mechanisms of the acoustic actuator and the structural actuator in a velocity feedback control scheme are to absorb the acoustic energy in the cavity and to reduce sound radiation from the vibrating primary structure via induced active damping respectively. The decentralised control strategy has either or both the control benefits of the acoustic actuator and the structural actuator, which are effective on the acoustic modes and the structural mode in the acoustic potential energy respectively according to the degree of structural-acoustic coupling. Under the velocity feedback control, the control effects on the dynamic behaviour of the primary structure were quantified by the structural kinetic energy. The best control strategy for the control of the acoustic potential energy and the control effect on the structural kinetic energy can be summarised in the various coupling cases as follows.

In the *strongly coupled* case, for the control of the acoustic potential energy, the control strategy of using the acoustic actuator, in a velocity feedback control scheme, is preferable. However, minor control spillover is observed at off-resonance frequencies due to the shifted acoustic modes caused by the controlled impedance via the acoustic actuator. Under this velocity feedback control, significant reduction on the kinetic energy of the primary structure can be obtained at the peaks due to increased damping of the acoustic input impedance. The structural kinetic energy shifts to higher frequencies due to the shifted acoustic resonances.

In the *weakly coupled* case, the decentralised velocity feedback control strategy using both the actuators is preferable for the control of the acoustic potential energy. In this case, both the control benefits of the acoustic and structural actuators cause best control performance on the acoustic potential energy. Under this decentralised velocity feedback control, the structural kinetic energy decreases due to the induced active damping on the structure via only the structural actuator. In the case of the structural natural frequency above the fundamental acoustic mode of a closed-closed tube, more reduction on the acoustic potential energy and the structural kinetic energy can be achieved due to the increased damping control region. The

increased damping control region is caused by the less structural mass for a given stiffness ratio.

In the *intermediate* case, the decentralised velocity feedback control strategy using both the actuators is preferable as in the *weakly coupled* case. When using the acoustic actuator or the structural actuator, the acoustic potential energy is dominated by the residual structural or acoustic modes respectively after control. On the other hand, when using both the actuators, best control performance on the acoustic potential energy can be achieved by virtue of both the control benefits of the acoustic and structural actuators. Under this decentralised velocity feedback control, the structural kinetic energy decreases at the peaks due to the active damping via the structural actuator and the increased damping of the acoustic input impedance.

CHAPTER 6

CONCLUSIONS AND RECOMMENDATIONS FOR FUTURE WORK

6.1 Conclusions

In this chapter, general conclusions of this thesis are given since detail conclusions have been included in each chapter. The influence of structural-acoustic coupling effects on the dynamic behaviour of a one-dimensional vibro-acoustic system has been investigated under passive/active control. The coupling mechanism was investigated based on the mobility-impedance approach to provide the threshold of the degree of coupling, which determined the acoustic potential energy (chapter 2). The main objectives were tackled by three following control strategies such as a passive control strategy (chapter 3), an active feedforward control strategy (chapter 4) and a decentralised velocity feedback control strategy (chapter 5) in various coupled cases.

In chapter 2, the dynamic behaviour of a simple vibro-acoustic system has been investigated in the *strongly coupled, weakly coupled or intermediate* cases when a structural natural frequency was below and above the fundamental acoustic mode of a closed-closed tube

respectively. The simple vibro-acoustic system consisted of a finite one-dimensional (1D) acoustic tube excited by a single-degree-of-freedom (SDOF) structure at one end and terminated by an arbitrary impedance at the other end. In order to investigate the mutual structural-acoustic interaction, a coupling factor was derived using the mobility-impedance approach. The dynamic behaviour of the vibro-acoustic system was discussed by investigating the acoustic potential energy in the cavity and the kinetic energy of the structure.

The investigation in this chapter demonstrated that the vibro-acoustic response can be characterised by the degree of the structural-acoustic coupling in the simple vibro-acoustic system. In the *strongly coupled* case, the acoustic potential energy was contributed by only acoustic modes and the structural kinetic energy was subject to the acoustic loading in the cavity. On the other hand, in the *weakly coupled* case, the acoustic potential energy was dominated by the structural mode and the structural kinetic energy was generally determined by only the structural characteristics as though it is *in-vacuo*. In the *intermediate* case, the vibro-acoustic responses showed compound behaviour of the previous two extreme cases.

Based on the analysis of the coupling mechanism, chapter 3 considered the effects of passive control treatments on the reduction of the acoustic potential energy in a combined SDOF structure - 1D finite closed tube system. The three coupled cases, discussed in chapter 2, were studied when the structural natural frequency was below and above the fundamental acoustic mode of a closed-closed tube respectively. The passive control treatments involved structural and acoustical modifications. The structural modifications were implemented by changing structural stiffness, structural mass and structural damping. Also, the acoustical modifications were implemented by changing acoustic damping and placing absorptive medium in the cavity.

The comparison of passive control performance demonstrated that in the *strongly coupled* case, the acoustical modifications were preferable for the reduction of the acoustic potential energy in both the cases of two values of the structural natural frequency. In the *weakly coupled* case, the structural modifications were preferable for the reduction of the acoustic potential energy. In the case when the structural natural frequency was below the fundamental acoustic mode, the structural loss factor was more effective on the reduction of the acoustic potential energy. On the other hand, in the case when the structural natural frequency was above the fundamental acoustic mode, the change of the natural frequency ratio was more

effective on the reduction. In the *intermediate* case, the acoustical modifications were more effective on the reduction of the acoustic potential energy. The acoustical modification had more significant effects on the reduction when the structural natural frequency was above the fundamental acoustic mode.

Chapter 4 considered the effectiveness of active feedforward control of the acoustic potential energy in the simple vibro-acoustic system depicted in chapter 2. The three coupled cases, discussed in chapter 2, were studied when the structural natural frequency was below and above the fundamental acoustic mode of a closed-closed tube respectively. The simple vibro-acoustic system was harmonically driven by the SDOF structure at one end of the acoustic tube and was controlled by the single acoustic piston at the other end using a feedforward control strategy. The feedforward control mechanism was investigated based on the optimal controller and the optimal impedance. The optimal impedance was defined as the ratio of the control force to the velocity of the control piston with a sign reversal when the acoustic potential energy was minimised. Under the feedforward control, the control effect on the structure was discussed in terms of the structural kinetic energy.

The results in this chapter demonstrated that in the *strongly coupled* case, the acoustic modes were effectively controlled in both the cases of two values of the structural natural frequency. In the *weakly coupled* case, all the acoustic modes were effectively controlled with the same control mechanism as in the *strongly coupled* case. On the other hand, the structural mode was controlled to some degree and was uncontrollable when the structural natural frequency was below and above the fundamental acoustic mode respectively. In the *intermediate* case, both the structural and acoustic modes were generally controllable. Under the feedforward control, the structural kinetic energy did not change in the *weakly coupled* case but increased in the *strongly coupled* and *intermediate* case due to smaller acoustic loading on the structure.

Chapter 5 considered active velocity feedback control of the acoustic potential energy, in the simple vibro-acoustic system under broadband excitation, using the acoustic actuator, the structural actuator or both the actuators. The three coupled cases, discussed in chapter 2, were studied when the structural natural frequency was below and above the fundamental acoustic mode of a closed-closed tube respectively. The control mechanisms of the acoustic actuator and the structural actuator in the velocity feedback control schemes were to absorb the acoustic energy in the cavity and to reduce sound radiation from the vibrating primary

structure using induced active damping respectively. Under the velocity feedback control, the control effects on the dynamic behaviour of the primary structure were quantified by the structural kinetic energy. The best control configuration for the control of the acoustic potential energy was suggested in the various coupled cases.

The results in this chapter demonstrated that in the *strongly coupled* case, the control configuration of using the acoustic actuator, in a velocity feedback control scheme, was preferable. However, minor control spillover was observed at off-resonance frequencies due to the shifted acoustic modes caused by the controlled impedance via the acoustic actuator. In the *weakly coupled* case, the decentralised velocity feedback control strategy using both the actuators was preferable. In this case, both the control benefits of the acoustic and structural actuators caused best control performance on the acoustic potential energy. In the *intermediate* case, the decentralised velocity feedback control strategy using both the actuators was preferable as in the *weakly coupled* case. Under the velocity feedback control, the structural kinetic energy was reduced at the peaks due to the active damping via the structural actuator and the increased damping of the acoustic input impedance.

Overall, this thesis has shown that the acoustical treatments are preferable in the *strongly coupled* case for the reduction of the acoustic potential energy under passive/active control. On the other hand, in the *weakly coupled* and *intermediate* case, both the structural and acoustical treatments are generally required for the best control performance on the acoustic potential energy.

6.2 Recommendations for future work

This thesis studied the influence of structural-acoustic coupling on the dynamic behaviour of the simple vibro-acoustic system under passive/active control. The cost function was the global acoustic potential energy in the one-dimensional acoustic tube under SDOF structural excitation. The work could be extended to study the local control of the acoustic potential energy in a three-dimensional acoustic enclosure excited by flexible structure under an external force. The analysis of the general vibro-acoustic problem might require the geometric coupling relationship between the uncoupled structural and acoustic mode shape functions on the surface of the vibrating structure. The best control configuration may be of concern for the local control of the acoustic potential energy in the enclosure. The local control of the acoustic potential energy would be useful for some practical applications.

Investigation into the control effectiveness of the decentralised velocity feedback control, using both the structural and acoustic actuators, could be recommended. A low-impedance acoustic actuator might need to be developed for experimental validation.

A logical extension of the research in this thesis is investigation into the control performance of the structural and acoustic actuators, in the velocity feedback scheme, for the local control of the acoustic potential energy in various coupled conditions.

APPENDIX A

ANALYSIS OF A LOW-FREQUENCY APPROXIMATE ONE-DIMENSIONAL VIBRO-ACOUSTIC SYSTEM

The simple vibro-acoustic system, depicted in figure 2.1, is approximated at low frequencies below the first acoustic resonance based on the impedance-mobility approach. It helps to understand the physical characteristics of the vibro-acoustic responses at low frequencies. The approximate model is described by a single-degree-of-freedom (SDOF) structure coupled with an acoustic spring, which has static acoustic stiffness of the acoustic tube. When a feedforward control system is engaged, the control effects on the acoustic potential energy and the structural kinetic energy are discussed. Also, closed-form solutions are derived to demonstrate the effects of non-dimensional structural-acoustic parameters on the vibro-acoustic responses.

A.1 Dynamic behaviour of a low-frequency approximate simple vibro-acoustic system

For the acoustic tube in the one-dimensional vibro-acoustic system, the impedance matrix of the tube is given in equation (2.18) and repeated here for convenience

$$\begin{bmatrix} P_1 \\ P_2 \end{bmatrix} = \begin{bmatrix} \rho_0 c \dfrac{\cos kL}{j \sin kL} & -\rho_0 c \dfrac{1}{j \sin kL} \\ -\rho_0 c \dfrac{1}{j \sin kL} & \rho_0 c \dfrac{\cos kL}{j \sin kL} \end{bmatrix} \begin{bmatrix} U_1 \\ U_2 \end{bmatrix} \tag{A.1}$$

where ρ_0 is ambient density, $c(= c_0 /(1 - j\frac{1}{2}\eta_a))$ is a complex sound speed in lossy acoustic medium with a constant acoustic loss factor η_a, c_0 is a sound speed in lossless acoustic medium, $k(= \omega/c)$ is a complex acoustic wave number and L is acoustic tube length. P_1 and U_1 are the acoustic pressure and the particle velocity at $x = 0$ respectively, and P_2 and U_2 are the resultant acoustic pressure and the resultant particle velocity at $x = L$ respectively. When the wavelength in the acoustic tube is large enough compared to the dimensions of the acoustic tube, the impedance matrix, given in equation (A.1), can be approximated, which is

$$\begin{bmatrix} P_1 \\ P_2 \end{bmatrix} = \begin{bmatrix} \rho_0 c \dfrac{1}{jkL} & -\rho_0 c \dfrac{1}{jkL} \\ -\rho_0 c \dfrac{1}{jkL} & \rho_0 c \dfrac{1}{jkL} \end{bmatrix} \begin{bmatrix} U_1 \\ U_2 \end{bmatrix} \tag{A.2}$$

where $\sin kL \approx kL$ and $\cos kL \approx 1$. The point impedance of the acoustic tube at $x = 0$ is defined as

$$Z_A = \frac{SP_1}{U_1}\bigg|_{U_2=0} \tag{A.3}$$

where Z_A is the point impedance at $x = 0$ and S is cross-sectional area of the acoustic tube. Also, the impedance Z_A can be approximately written for a small acoustic loss factor by combining equations (A.2) and (A.3), which is

$$Z_A \approx \frac{1}{j\omega} K_a (1 + j\eta_a) \tag{A.4}$$

where $K_a = \rho_0 c_0^2 S / L$.

Physically, the acoustic tube behaves like an acoustic spring with complex stiffness $K_a(1 + j\eta_a)$ at low frequencies below the first acoustic resonance of the tube. Figure A.1 describes the low-frequency approximation of the one-dimensional vibro-acoustic system depicted in figure 2.1.
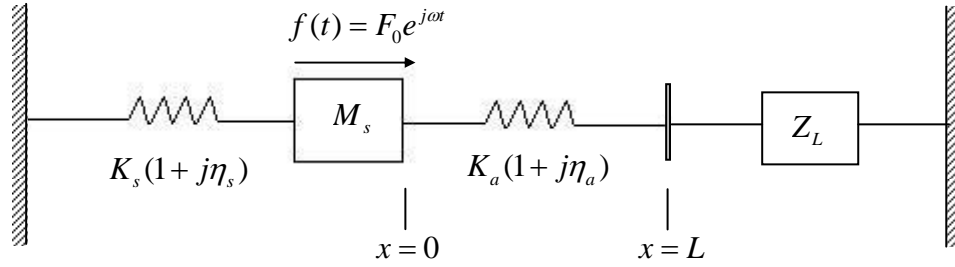
Figure A.1 Low-frequency approximation of the one-dimensional vibro-acoustic system depicted in figure 2.1 which is under the external time harmonic force on the structure, $f(t) = F_0 e^{j\omega t}$ at $x = 0$ and is terminated by arbitrary impedance Z_L at $x = L$. M_s and K_s are the structural mass and the stiffness of a spring with a constant structural loss factor η_s respectively. Also, $j = \sqrt{-1}$ and ω is a driving frequency.

The strain energy stored in the acoustic spring, in the approximated model depicted in figure A.1, can be written as [Meirovitch (1986)]

$$E_A(\omega) = \frac{1}{2} K_a \left| X_0 - X_L \right|^2 \tag{A.5}$$

where $E_A(\omega)$ is the strain energy of the acoustic spring, X_0 and X_L are displacements at $x = 0$ and at $x = L$ respectively.

The velocity at $x = 0$ is the ratio of the excitation force F_0 to the sum of impedances at the position. Hence, the displacement at $x = 0$ can be written as

$$X_0 = \frac{F_0}{j\omega}\left(\frac{Z_A + Z_L}{Z_S(Z_A + Z_L) + Z_A Z_L}\right) \tag{A.6}$$

where F_0 is the excitation force, Z_S is the uncoupled structural impedance and Z_A is the impedance of the acoustic spring defined in equation (A.4). Also, the displacement at $x = L$ can be obtained from the definition of the impedance, which is the ratio of the reaction force to the velocity at the position. The reaction force at the position is equal to that of the acoustic spring at $x = 0$, which is difference between the excitation force F_0 and that applied on the structure. Hence, the displacement at $x = L$, X_L can be written as

$$X_L = \frac{1}{j\omega}\frac{F_0 - j\omega X_0 Z_S}{Z_L} \tag{A.7}$$

The strain energy of the acoustic spring, in the approximate low-frequency model depicted in figure A.1, can be written by combining equations (A.5)~(A.7) as

$$E_A(\omega) = \frac{1}{2}\frac{K_a |F_0|^2}{\omega^2}\left|\frac{Z_L}{Z_S(Z_A + Z_L) + Z_A Z_L}\right|^2 \tag{A.8}$$

In the case when the impedance Z_L is large enough compared to the impedance of the acoustic spring Z_A in figure A.1, the strain energy, given in equation (A.8), can be rewritten as

$$E_A(\omega) = \frac{K_a |F_0|^2}{2}\left|\frac{1}{-\omega^2 M_s + K_s\left((1 + j\eta_s) + \dfrac{K_a}{K_s}(1 + j\eta_a)\right)}\right|^2 \tag{A.9}$$

The strain energy, at low frequencies below the first acoustic resonance, is generally determined by the structural-acoustic stiffness ratio K_a/K_s. In the case when the stiffness ratio K_a/K_s is much larger than 1, the amplitude of the strain energy is subject to the acoustic loss factor η_a at the resonance frequency. On the other hand, in the case when the stiffness ratio K_a/K_s is much smaller than 1, the amplitude of the strain energy is subject to

the structural loss factor η_s at the resonance frequency. Also, in the intermediate case when the stiffness ratio K_a / K_s is equal to 1, the amplitude of the strain energy is affected by both the structural and acoustic loss factors.

A.2 Feedforward control effects on low-frequency vibro-acoustic responses

When the vibro-acoustic system, depicted in figure A.1, is under feedforward control, the vibro-acoustic system can be represented by the optimal impedance. The optimal impedance is defined by the ratio of the secondary control force to the velocity at the secondary source position with a sine reversal when the acoustic potential energy in the cavity is minimised. Figure A.2 depicts the low-frequency approximation of the vibro-acoustic system under feedforward control. The optimal impedance Z_{opt} shares the same velocity with the impedance of the secondary source Z_L defined in equation (4.2).
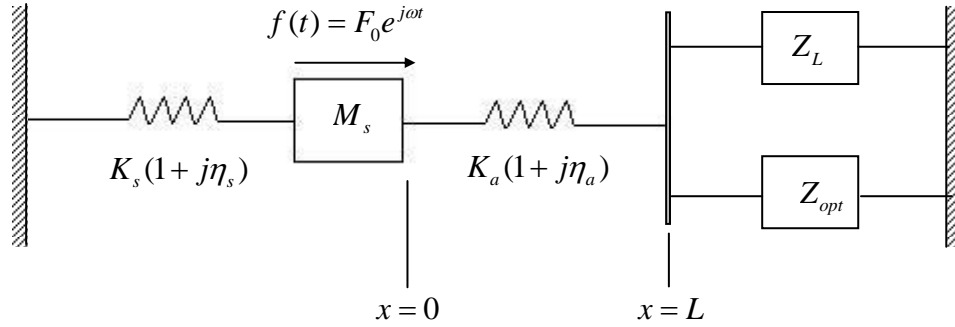
Figure A.2 Low frequency approximation of the vibro-acoustic system, depicted in figure A.1, under feedforward control depicted where Z_L is the impedance of the secondary source and Z_{opt} is the optimal impedance

The optimal impedance, in the approximate low-frequency model, can be obtained when the strain energy of the acoustic spring is zero. In other words, the acoustic spring has a free-end condition at the secondary source position. The optimal impedance Z_{opt} cancels the

impedance Z_L to obtain free-end condition of the acoustic spring at the secondary source position, which can be written using equation (4.2) as

$$Z_{opt} = j \frac{K_L (1 + j\eta_L)}{\omega} \qquad (A.10)$$

where K_L and η_L are the stiffness and the constant loss factor of the secondary source respectively.

A.2.1 Closed-form solution of strain energy

Closed-form solutions are derived in order to demonstrate the effects of non-dimensional structural-acoustic parameters on the strain energy of the acoustic spring, in the approximate low-frequency model depicted in figure A.2, for a given stiffness ratio. Under feedforward control, the displacements at both the ends of the acoustic spring can be obtained by simply setting the impedance Z_L in equations (A.6) and (A.7) to the sum of impedances Z_L and Z_{opt} . The displacement at $x = 0$, given in equation (A.6), can be rewritten as

$$X_0 = \frac{F_0}{j\omega} \left(\frac{Z_A + Z_L + Z_{opt}}{Z_S (Z_A + Z_L + Z_{opt}) + Z_A (Z_L + Z_{opt})} \right) \qquad (A.11)$$

Also, the displacement at the secondary source position ($x = L$), given in equation (A.7), can be rewritten as

$$X_L = \frac{1}{j\omega} \frac{F_0 - j\omega X_0 Z_S}{Z_L + Z_{opt}} \qquad (A.12)$$

Under feedforward control, the strain energy of the acoustic spring, defined in equation (A.5), can be rewritten by combining equations (A.5), (A.11) and (A.12) to give

$$E_{A\,opt}(\omega) = \frac{1}{2} \frac{K_a \,|\, F_0 \,|^2}{\omega^2} \left| \frac{Z_L + Z_{opt}}{Z_S (Z_A + Z_L + Z_{opt}) + Z_A (Z_L + Z_{opt})} \right|^2 \qquad \text{(A.13)}$$

The strain energy of the acoustic spring, under feedforward control, is zero since the acoustic spring has a free-end condition at the secondary source position. Hence, passive application is considered to make a quasi-optimal condition by applying only the imaginary part of the optimal impedance. In the passive application, the strain energy can be derived by using only the imaginary part of the optimal impedance Z_{opt} in equation (A.10) to give

$$E_{A\,psv}(\omega) = \frac{K_a \,|\, F_0 \,|^2}{2} \left| \frac{jK_L\eta_L}{\left(-\omega^2 M_s + K_s(1+j\eta_s)\right)\left(K_a(1+j\eta_a) + jK_L\eta_L\right) + jK_L\eta_L K_a(1+j\eta_a)} \right|^2 \quad \text{(A.14)}$$

where $E_{A\,psv}(\omega)$ is the strain energy in the passive application.

For broadband control effect, the strain energy is summed up to the nth arbitrary frequency using the integral of the of square frequency response functions given in Appendix C. The summed strain energy in the absence of control can be obtained by integrating the strain energy, given in equation (A.9), using equations (C.2a) and (C.2b) in Appendix C, which is

$$\sum_{i=1}^{n} E_A(\omega_i) \approx \pi \frac{K_a \,|\, F_0 \,|^2}{2} \frac{\omega_s}{(K_s + K_a)(K_s\eta_s + K_a\eta_a)} \qquad \text{(A.15)}$$

where $E_A(\omega_i)$ is the strain energy at the ith frequency and $\omega_s (= \sqrt{(K_s + K_a)/M_s})$ is the structural resonance in the absence of control. In the same manner, the summed strain energy in the passive application can be obtained by integrating the strain energy, given in equation (A.14), using equations (C.3a) and (C.3b) in Appendix B, which is

$$\sum_{i=1}^{n} E_{A\,psv}(\omega_i) \approx \pi \frac{K_a \,|\, F_0 \,|^2}{2} \frac{\omega_{s\,psv}(K_L\eta_L)^2}{\left(K_s\eta_s K_a + K_L\eta_L(K_s + K_a)\right)\left(K_s K_a + K_L\eta_L(K_s\eta_s + K_a\eta_a)\right) - K_a K_s^2 K_L\eta_L} \quad \text{(A.16)}$$

where $E_{A\,psv}(\omega_i)$ is the strain energy at the ith frequency and $\omega_{s\,psv}(=\sqrt{K_s/M_s})$ is the structural resonance in the passive application. Also, the summed strain energy in the passive application, normalised by that in the absence of control, can be written by combining equations (A.15) and (A.16) to give

$$\frac{\sum_{i=1}^{n} E_{A\,psv}(\omega_i)}{\sum_{i=1}^{n} E_{A}(\omega_i)} \approx \frac{1}{\sqrt{1+\hat{K}}} \tag{A.17}$$

where $\hat{K}(= K_a/K_s)$ is the acoustic-structural stiffness ratio. The summed strain energy of the acoustic spring in the passive application, normalised by that in the absence of control, is inversely proportional to $\sqrt{1+\hat{K}}$.

In the more *strongly coupled* case with a large acoustic-structural stiffness ratio $\hat{K}$, the normalised strain energy of the acoustic spring has more reduction. In this case, the structural mass, depicted in figure A.2, behaves like mostly disconnected with the structural spring and causes more relative displacement between the both ends of the acoustic spring.

In the more *weakly coupled* case with a small acoustic-structural stiffness ratio $\hat{K}$, the strain energy of the acoustic spring, in the passive application, has less change compared to that in the absence of control. In this case, the movement of the structural mass is restricted by the structural spring and causes less relative displacement between the both ends of the acoustic spring.

A.2.2 Closed-form solution of structural kinetic energy

Structural kinetic energy is another issue when a vibro-acoustic system is controlled. Closed-form solutions are derived in order to demonstrate the effects of non-dimensional structural-acoustic parameters on the structural kinetic energy, in the approximate low-frequency model depicted in figure A.2, for a given stiffness ratio. The structural kinetic energy is defined in equation (2.54).

In the special case, when the impedance Z_L is large enough compared to the impedance of the acoustic spring Z_A in figure A.1, the structural velocity, in the absence of control, can be written as

$$U_s = F_0 \frac{j\omega}{-\omega^2 M_s + j\omega \left(\dfrac{K_s \eta_s + K_a \eta_a}{\omega_s} \right) + K_s + K_a} \tag{A.18}$$

where U_s is the structural velocity and $\omega_s (= \sqrt{(K_s + K_a)/M_s})$ is the structural resonance frequency in the absence of control respectively.

The passive application is considered to make a quasi-optimal condition by applying only the imaginary part of the optimal impedance. In the passive application the relative displacement between the both ends of the acoustic spring is approximately zero. Thus, the structural velocity in the passive application is decided by only the structure, which is

$$U_{s\,psv} = F_0 \frac{j\omega}{-\omega^2 M_s + j\omega \left(\dfrac{K_s \eta_s}{\omega_{s\,psv}} \right) + K_s} \tag{A.19}$$

where $U_{s\,psv}$ is the structural velocity and $\omega_{s\,psv}(= \sqrt{K_s/M_s})$ is the structural resonance frequency in the passive application respectively.

For broadband control effect, the structural kinetic energy is summed up to the nth arbitrary frequency using the integral of the of square frequency response functions given in Appendix C. The structural kinetic energy in the absence of control can be obtained by combining equations (2.54) and (A.18). Also, the summed structural kinetic energy in the absence of control can be calculated by using equations (C.2a)~(C.2b) in Appendix C to give

$$\sum_{i=1}^{n} E_K(\omega_i) \approx \pi \frac{|F_0|^2}{2} \frac{\omega_s}{K_s \eta_s + K_a \eta_a} \tag{A.20}$$

where $E_K(\omega_i)$ is the structural kinetic energy at the ith frequency in the absence of control.

The structural kinetic energy in the passive application can be obtained by combining equations (2.54) and (A.19). Also, the summed structural kinetic energy in the passive application can be calculated by using equations (C.2a)~(C.2b) in Appendix C to give

$$\sum_{i=1}^{n} E_{K\,psv}(\omega_i) \approx \pi \frac{|F_0|^2}{2} \frac{\omega_{r\,psv}}{K_s \eta_s} \tag{A.21}$$

where $E_{K\,psv}(\omega_i)$ is the structural kinetic energy at the ith frequency in the passive application.

The summed structural kinetic energy in the passive application, normalised by that in the absence of control, can be obtained by combining equations (A.20)~(A.21) to give

$$\frac{\sum_{i=1}^{n} E_{K\,psv}(\omega_i)}{\sum_{i=1}^{n} E_K(\omega_i)} \approx \frac{\eta_s + \eta_a \hat{K}}{\eta_s} \frac{1}{\sqrt{1 + \hat{K}}} \tag{A.22}$$

where $\hat{K}(= K_a / K_s)$ is the acoustic-structural stiffness ratio, η_s is the constant structural loss factor and η_a the constant acoustic loss factor.

Table A.1 presents closed-form solutions of the normalised summed structural kinetic energy in terms of non-dimensional structural-acoustic parameters for a given stiffness ratio. The normalised summed structural kinetic energy, under feedforward control, is generally similar to that in the passive application.

In the *strongly coupled* case with an acoustic-structural stiffness ratio $\hat{K} = 10^3$, the normalised summed structural kinetic energy in the passive application increases by about 15dB as shown in table A.1. In this case, the normalised summed structural kinetic energy is proportional to the loss factor ratio η_a / η_s and the square root of the stiffness ratio $\sqrt{\hat{K}}$. If the acoustic spring has relatively larger loss factor or stiffness compared to that of the structural spring, the

structural mass is subject to less reaction force of the acoustic spring and the structural kinetic energy increases more after control.

In the *weakly coupled* case with an acoustic-structural stiffness ratio $\hat{K} = 10^{-3}$, the summed structural kinetic energy, in the passive application, has no change compared to that in the absence of control as shown in table A.1. In this case, the reaction force of the acoustic spring on the structural mass is insignificant before control and the structural kinetic energy is mainly determined by only the structural characteristics.

In the *intermediate* case with an acoustic-structural stiffness ratio $\hat{K} = 1$, the normalised summed structural kinetic energy increases by about 1.5dB as shown in table A.1. In this case, the normalised summed structural kinetic energy is determined by both the characteristics of the structural spring and the acoustic spring.

Table A.1 Summed structural kinetic energy normalised by that before control

$$(\sum_{i=1}^{n} E_{k\,psv}(\omega_i) / \sum_{i=1}^{n} E_k(\omega_i))\ where\ loss\ factors\ \eta_s = \eta_a = \eta_L = 10^{-2}\ and\ \hat{K}_L = 10^3$$

Degree of coupling	Normalised summed structural kinetic energy		Closed-form solutions
	Feedforward control	Passive application	in the passive application
Strong ($\hat{K} = 10^3$)	15dB	15dB	$\dfrac{\eta_a}{\eta_s}\sqrt{\hat{K}}$
Weak ($\hat{K} = 10^{-3}$)	0dB	0dB	1
Intermediate ($\hat{K} = 1$)	1.5dB	1.5dB	$\dfrac{\eta_s + \eta_a \hat{K}}{\eta_s}\dfrac{1}{\sqrt{1+\hat{K}}}$

APPENDIX B

SOUND PRESSURE AT ARBITRARY POSITION IN A TUBE WITH TWO DIFFERENT MEDIA USING THE TRANSFER MATRIX METHOD

The transfer matrix method is reviewed in order to derive acoustic pressure and particle velocity at arbitrary positions in a tube with two different acoustic media. The acoustic characteristics in the tube can be represented by two state variables of sound pressure, particle velocity and transfer matrix relating two sides of an acoustic element. Figure B.1 describes an acoustic tube with two acoustic elements, which has a medium 1 in the region of $0 \leq x \leq L_1$ and a medium 2 in the region of $L_1 \leq x \leq L$. The acoustic pressure and particle velocity on each side of the acoustic element are described P_1 and U_1 at $x = 0$, P_2 and U_2 at $x = L_1$, and P_3 and U_3 at $x = L$ respectively.
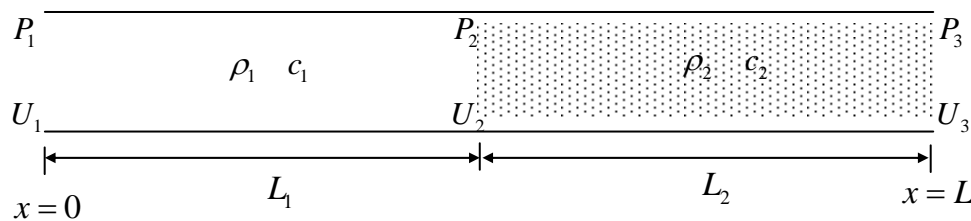
Figure B.1 Acoustic tube with two different media such as: (a) a medium 1 in the region of $0 \leq x \leq L_1$ and (b) a medium 2 in the region of $L_1 \leq x \leq L$ where ρ_1, c_1, ρ_2 and c_2 are ambient density and sound speed of corresponding acoustic medium respectively

The transfer matrix relating the sound pressure and particle velocity on each side of the acoustic element 1 shown in figure B.1 is given by

$$\begin{bmatrix} P_1 \\ U_1 \end{bmatrix} = \begin{bmatrix} T_{11} & T_{12} \\ T_{21} & T_{22} \end{bmatrix} \begin{bmatrix} P_2 \\ U_2 \end{bmatrix}$$
(B.1)

The four-pole parameters of the transfer matrix can be calculated such as

When $U_2 = 0$,
$$T_{11} = \frac{P_1}{P_2}$$
(B.2)

$$T_{21} = \frac{U_1}{P_2}$$
(B.3)

When $P_2 = 0$,
$$T_{12} = \frac{P_1}{U_2}$$
(B.4)

$$T_{22} = \frac{U_1}{U_2}$$
(B.5)

These relations for the four-pole parameters T_{11}, T_{12}, T_{21} and T_{22} have individual physical meaning. The parameter T_{11} is the ratio of the downstream pressure to upstream pressure and T_{21} is the ratio of the velocity at the down stream to the upstream pressure when the acoustic element 1 is rigidly terminated at $x = L_1$. Also, T_{12} is the ratio of the downstream pressure to the velocity at the upstream and T_{22} is the ratio of the velocity at the downstream and the velocity at the upstream when the acoustic element 1 is open at $x = L_1$.

The acoustic pressure and particle velocity in the acoustic element 1 take the form of two travelling waves in opposite directions [Kinsler *et al* (1982)], which are given by

$$P(x, \omega) = A e^{-jkx} + B e^{jkx}$$
(B.6)

$$U(x,\omega) = \frac{1}{\rho c}(Ae^{-jkx} - Be^{jkx}) \tag{B.7}$$

where A and B are complex wave amplitudes. Also, ρ, c and $k(=\omega/c)$ are ambient density, sound speed and acoustic wavenumber respectively.

The sound pressures and particle velocities on both sides of the acoustic element 1 can be related by the transfer matrix given in equation (B.1). The sound pressure and particle velocity at $x=0$ are given using equations (B.6)~(B.7) by

$$P_1 = A + B \tag{B.8}$$

$$U_1 = \frac{1}{\rho_1 c_1}(A - B) \tag{B.9}$$

Similarly, the sound pressure and particle velocity at $x = L_1$ are given by

$$P_2 = (A + B)\cos k_1 L_1 - j(A - B)\sin k_1 L_1 \tag{B.10}$$

$$U_2 = \frac{1}{\rho_1 c_1}\big((A - B)\cos k_1 L_1 - j(A + B)\sin k_1 L_1\big) \tag{B.11}$$

where $k_1(=\omega/c_1)$ is the acoustic wavenumber in the medium 1. The complex amplitudes A and B can be calculated combining equations (B.10)~(B.11), and which are

$$A = \frac{1}{2}(\cos k_1 L_1 + j\sin k_1 L_1)(P_2 + \rho_1 c_1 U_2) \tag{B.12}$$

$$B = \frac{1}{2}(\cos k_1 L_1 - j\sin k_1 L_1)(P_2 - \rho_1 c_1 U_2) \tag{B.13}$$

Substituting the complex amplitudes A and B given in equations (B.12)~(B.13) into equations (B.8)~(B.9) gives

$$P_1 = \left(\cos k_1 L_1\right) P_2 + \left(j \rho_1 c_1 \sin k_1 L_1\right) U_2 \tag{B.14}$$

$$U_1 = \left(\sin k_1 L_1 / \rho_1 c_1\right) P_2 + \left(\cos k_1 L_1\right) U_2 \tag{B.15}$$

The transfer matrix relating the acoustic pressures and particle velocities on both sides of the acoustic element 1 can be derived by rewriting equations (B.14)~(B.15) in the matrix form given in equation (B.1) as

$$\begin{bmatrix} P_1 \\ U_1 \end{bmatrix} = \begin{bmatrix} \cos k_1 L_1 & j \rho_1 c_1 \sin k_1 L_1 \\ j \sin k_1 L_1 / \rho_1 c_1 & \cos k_1 L_1 \end{bmatrix} \begin{bmatrix} P_2 \\ U_2 \end{bmatrix} \tag{B.16}$$

Similarly, the transfer matrix relation of the acoustic element 2 can be obtained using same arguments and is given by

$$\begin{bmatrix} P_2 \\ U_2 \end{bmatrix} = \begin{bmatrix} \cos k_2 L_2 & j \rho_2 c_2 \sin k_2 L_2 \\ j \sin k_2 L_2 / \rho_2 c_2 & \cos k_2 L_2 \end{bmatrix} \begin{bmatrix} P_3 \\ U_3 \end{bmatrix} \tag{B.17}$$

where $k_2 (= \omega / c_2)$ is the acoustic wavenumber in the medium 2. The transfer relations of whole acoustic tube with two different media can be written combining equations (B.16) ~(B.17) to give

$$\begin{bmatrix} P_1 \\ U_1 \end{bmatrix} = \begin{bmatrix} \cos k_1 L_1 & j \rho_1 c_1 \sin k_1 L_1 \\ j \sin k_1 L_1 / \rho_1 c_1 & \cos k_1 L_1 \end{bmatrix} \begin{bmatrix} \cos k_2 L_2 & j \rho_2 c_2 \sin k_2 L_2 \\ j \sin k_2 L_2 / \rho_2 c_2 & \cos k_2 L_2 \end{bmatrix} \begin{bmatrix} P_3 \\ U_3 \end{bmatrix} \tag{B.18}$$

The sound pressure and particle velocity at arbitrary positions in the tube needs to be derived for the analysis of the wave propagation through the two different media. Figure B.2 shows the sound pressure P and particle velocity U at arbitrary position in the acoustic element 1 shown in figure B.1.

Figure B.2 Acoustic pressure P and particle velocity U at arbitrary position in the acoustic medium 1 ($0 \leq x_1 \leq L_1$)

The inverse of the transfer matrix relation given in equation (B.16) is given by

$$\begin{bmatrix} P_2 \\ U_2 \end{bmatrix} = \begin{bmatrix} \cos k_1 L_1 & -j\rho_1 c_1 \sin k_1 L_1 \\ -j \sin k_1 L_1 / \rho_1 c_1 & \cos k_1 L_1 \end{bmatrix} \begin{bmatrix} P_1 \\ U_1 \end{bmatrix} \tag{B.19}$$

The transfer matrix relation for the sound pressure and particle velocity at arbitrary position in the acoustic element 1 can be derived by simply replacing P_2, U_2 and L_1 with P, U and x_1 given in equation (B.19), which is

$$\begin{bmatrix} P \\ U \end{bmatrix} = \begin{bmatrix} \cos k_1 x_1 & -j\rho_1 c_1 \sin k_1 x_1 \\ -j \sin k_1 x_1 / \rho_1 c_1 & \cos k_1 x_1 \end{bmatrix} \begin{bmatrix} P_1 \\ U_1 \end{bmatrix} \tag{B.20}$$

Figure B.3 shows the sound pressure P and particle velocity U at arbitrary position in the acoustic element 2 shown in figure B.1.
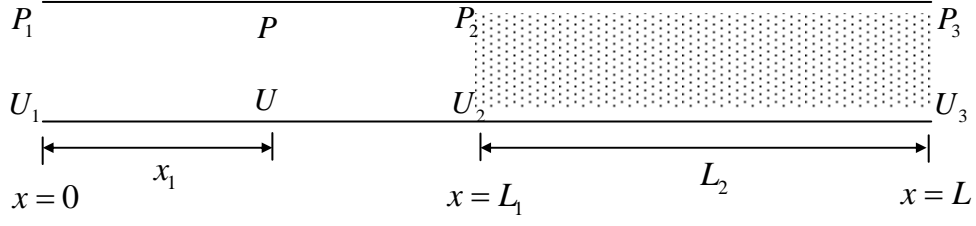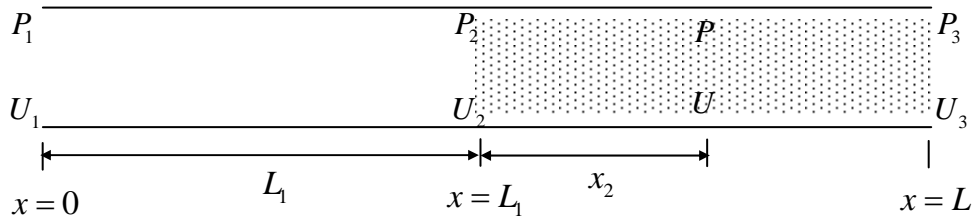

Figure B.3 Acoustic pressure P and particle velocity U at arbitrary position in the acoustic medium 2 ($L_1 \leq x_2 \leq L$)

The acoustic pressure and particle velocity at arbitrary position in the acoustic element 2 can be derived in the same way as that of the acoustic medium 1 given in equation (B.20), which is

$$
\begin{bmatrix} P \\ U \end{bmatrix} = \begin{bmatrix} \cos k_2 x_2 & -j\rho_2 c_2 \sin k_2 x_2 \\ -j\sin k_2 x_2 / \rho_2 c_2 & \cos k_2 x_2 \end{bmatrix} \begin{bmatrix} P_2 \\ U_2 \end{bmatrix}
\tag{B.21}
$$

The equation (B.21) can be rewritten substituting equation (B.19) for the analysis of whole acoustic tube with two different media as

$$
\begin{bmatrix} P \\ U \end{bmatrix} = \begin{bmatrix} \cos k_2 x_2 & -j\rho_2 c_2 \sin k_2 x_2 \\ -j\sin k_2 x_2 / \rho_2 c_2 & \cos k_2 x_2 \end{bmatrix} \begin{bmatrix} \cos k_1 L_1 & -j\rho_1 c_1 \sin k_1 L_1 \\ -j\sin k_1 L_1 / \rho_1 c_1 & \cos k_1 L_1 \end{bmatrix} \begin{bmatrix} P_1 \\ U_1 \end{bmatrix}
\tag{B.22}
$$

APPENDIX C

INTEGRAL OF THE MODULUS SQUARED FREQUENCY RESPONSE FUNCTIONS

[S.H CRANDALL (1963)]

The integral of certain forms of a square frequency response function is tabulated in order to investigate broadband control effects on vibro-acoustic responses in an approximate low-frequency vibro-acoustic system. The strain energy of a spring is proportional to the square magnitude of relative displacements at the both ends. Also, when the strain energy is controlled, the kinetic energy of the structure coupled with the spring can be changed. The structural kinetic energy is proportional to the square magnitude of structural velocity. The broadband control effects on the vibro-acoustic responses can be investigated by calculating summed vibro-acoustic responses over interesting frequency range. The summed vibro-acoustic responses can be easily obtained using the following integral formulae of square frequency response functions.

(1)
$$H(\omega) = \frac{B_0}{j\omega A_1 + A_0}$$
(C.1a)

$$\int_{-\infty}^{\infty} |H(\omega)|^2 \, d\omega = \pi \frac{B_0^2}{A_0 A_1}$$
(C.1b)

(2)
$$H(\omega) = \frac{j\omega B_1 + B_0}{-\omega^2 A_2 + j\omega A_1 + A_0} \qquad \text{(C.2a)}$$

$$\int_{-\infty}^{\infty} |H(\omega)|^2 \, d\omega = \pi \frac{(B_0^2 / A_0) A_2 + B_1^2}{A_1 A_2} \qquad \text{(C.2b)}$$

(3)
$$H(\omega) = \frac{-\omega^2 B_2 + j\omega B_1 + B_0}{-j\omega^3 A_3 - \omega^2 A_2 + j\omega A_1 + A_0} \qquad \text{(C.3a)}$$

$$\int_{-\infty}^{\infty} |H(\omega)|^2 \, d\omega = \pi \frac{(B_0^2 / A_0) A_2 A_3 + A_3 (B_1^2 - 2B_0 B_2) + A_1 B_2^2}{A_1 A_2 A_3 - A_0 A_3^2} \qquad \text{(C.3b)}$$

(4)
$$H(\omega) = \frac{-j\omega^3 B_3 - \omega^2 B_2 + j\omega B_1 + B_0}{\omega^4 A_4 - j\omega^3 A_3 - \omega^2 A_2 + j\omega A_1 + A_0} \qquad \text{(C.4a)}$$

$$\int_{-\infty}^{\infty} |H(\omega)|^2 \, d\omega = \pi \frac{(B_0^2 / A_0)(A_2 A_3 - A_1 A_4) + A_3 (B_1^2 - 2B_0 B_2)}{A_1 (A_2 A_3 - A_1 A_4) - A_0 A_3^2}$$

$$+ \pi \frac{A_1 (B_2^2 - 2B_1 B_3) + (B_3^2 / A_4)(A_1 A_2 - A_0 A_3)}{A_1 (A_2 A_3 - A_1 A_4) - A_0 A_3^2} \qquad \text{(C.4b)}$$

REFERENCES

M. AL-BASSYIOUNI and B. BALACHANDRAN 2005, *Journal of Sound and Vibration*, **284**, 467-486, Sound transmission through a flexible panel into an enclosure: structural-acoustics model

B. BALACHANDRAN, A. SAMPATH and J. PARK 1996, Smart Mater. Struct. **5**, Active control of interior noise in a three-dimensional enclosure

A.J. BULLMORE, P.A. NELSON, A.R.D. CURTIS and S.J. ELLIOTT 1987, *Journal of Sound and Vibration*, **117** (1), 15-33. The active minimization of harmonic enclosed sound fields, part II: A computer simulation

A.J. BULLMORE, P.A. NELSON and S.J. ELLIOTT 1990, *Journal of Sound and Vibration*, **140** 191-217, Theoretical studies of the active control of propeller-induced cabin noise

A. CRAGGS and E.O. AYORINDE 1990, *Journal of Sound and Vibration*, **142**(2), 360-363, Isochronous oscillators: their importance in low-frequency sound transmission in passengers vehicles

C.E. CREDE 1965, *Shock and Vibration Concepts in Engineering Design*, Englewood Cliffs, NJ: Prentice Hall

L. CREMER, M. HECKL and E. UNGAR 1973, *Structure-Borne Sound*, Springer-Verlag, New York

F. CURA, G. CURTI and M. MANTOVANI 1996, *Journal of Sound and Vibration*, **190**(4), 661-675, Study of the forced response of a clamped circular plate coupled to a uni-dimensional acoustic cavity

E.H. DOWELL, G.F. GORMAN, III and D.A. SMITH 1977, *Journal of Sound Vibration*, **52** (4), 519-542. Acoustoelasticity: General Theory, Acoustic Natural Modes and Forced Response to Sinusoidal Excitation, Including Comparisons with Experiments

E.H. DOWELL and H.M. VOSS 1963, *American Institute of Aeronautics and Astronautics Journal,* **1**, 476-477. The Effect of a Cavity on Panel Vibration

S.J. ELLIOTT, A.R.D CURTIS, A.J. BULLMORE and P.A. NELSON 1987, *Journal of Sound and Vibration*, **117**(1), 35-58, The active minimization of harmonic enclosed sound fields part III: Experimental verification

S.J. ELLIOTT, I.M. STOTHERS, P.A. NELSON and C.C. BOUCHER 1990, *Journal of Sound and Vibration*, **140** 219-238, In-flight experiments on the active control of propeller-induced cabin noise

S.J. ELLIOTT, P. GARDONIO, T.J. SORS and M.J. BRENNAN 2002, *Journal of the Acoustical Society of America*, **111** (2) 908-915, Active vibroacoustic control with multiple local feedback loops

S.J. ESTEVE and M.E. JOHNSON 2005, *Journal of Sound and Vibration*, **288**, 1105-1130, Adaptive Helmholtz resonators and passive vibration absorbers for cylinder interior noise control

C.R. FULLER 1990, *Journal of Sound and Vibration*, **136**(1), 1-15, Active control of sound transmission/radiation from elastic plates by vibration inputs: I. Analysis

C.R. FULLER and J.D. JONES 1987, *Journal of Sound and Vibration*, **112**, 389-395, Experiments on reduction of propeller induced interior noise by active control of cylinder vibration

C.R. FULLER, S.J. ELLIOTT and P.A. NELSON 1996, *Active Control of Vibration*, Academic Press Limited

F.J. FAHY 1985, *Sound and Structural Vibration: Radiation, Transmission and Response.* London: Academic Press Limited

F.J. FAHY 2001, *Foundations of Engineering Acoustics*, Academic Press.

P. GARDONIO, E. BIANCHI and S.J. ELLIOTT 2004, *Journal of Sound and Vibration*, **274**, 163-192, Smart panel with multiple decentralised units for the control of sound transmission. Part I: theoretical predictions

P. GARDONIO, E. BIANCHI and S.J. ELLIOTT 2004, *Journal of Sound and Vibration*, **274**, 193-213, Smart panel with multiple decentralised units for the control of sound transmission. Part II: design of the decentralised control units

S. GRIFFIN, C. HANSEN and B. CAZZOLATO 1999, *Journal of the Acoustical Society of America*, **106** (5), Feedback control of structurally radiated sound into enclosed spaces using structural sensing

C. GUIGOU and C.R. FULLER 1999, *Journal of Sound and Vibration*, **220** (3) 541-557, Control of aircraft interior broadband noise with foam-PVDF smart skin

R.W. GUY and A.J. PRETLOVE 1973, *Journal of Sound and Vibration*, **27**, 128-129, Cavity-backed panel resonance

D.J. HENDY 1986, *PhD. Thesis, University of Southampton*. The influence of added damping on sound generated by vibrating sandwich plates

H. HIMMELBLAU Jr and S. RUBIN 1988, *Vibration of resiliently supported rigid body*. Chapter 3 in Shock and Vibration Handbook 3rd edition, New York: McGraw-Hill

K.L. HONG and J. KIM 1995, *Journal of Sound and Vibration*, **188**, 561-575, Analysis of free vibration of structure-acoustic coupled system, part I: development and verification of the procedure

K.L. HONG and J. KIM 1996, *Journal of Sound and Vibration*, **192**(2), 465-480, New analysis method for general acoustic-structural coupled systems

X. HUANG, S.J. ELLIOTT and M.J. BRENNAN 2003, *Journal of Sound and Vibration*, **263**, 357-376, Active isolation of a flexible structure from base vibration

M.E. JOHNSON and S.J. ELLIOTT 1995, *Journal of the Acoustical Society of America*, **98** (4), Active control of sound radiation using volume velocity cancellation

D. KARNOPP, M.J. CROSBY and R.A. HARWOOD 1974, *J. Eng. Ind.*, 619-626, Vibration control using the semiactive force generators

LAWRENCE E. KINSLER, AUSTINE R. FREY, ALAN B. COPPENS and JAMES V. SANDERS 1982, *Fundamentals of Acoustics*, John Wiley & Sons, Inc.

S.M. KIM and M.J. BRENNAN 1999, *Journal of Sound and Vibration*, **223**(1) 97-113, A compact matrix formulation using the impedance and mobility approach for the analysis of structural-acoustic systems

S.M. KIM and M.J. BRENNAN 1999, *Journal of Sound and Vibration*, **226**(3), 549-571, A comparative study of feedforward control of harmonic and random sound transmission into an acoustic enclosure

O. LACOUR, M.A. GALLAND and D. THENAIL 2000, *Journal of Sound and Vibration*, **230**(1), 69-99, Preliminary experiments on noise reduction in cavities using active impedance changes

B.J. LAZAN 1959, *Energy dissipation mechanisms in structures, with particular reference to material damping*, Section 1 in *Structural Damping*, New York: American Society of Mechanical Engineers

Z.S. LIU, H.P. LEE and C. LU 2006, *Applied acoustics*, **67**, 112-134, Passive and active interior noise control of box structures using the structural intensity method

P. LUEG 1936, *US Patent No. 2043416*, Process of silencing sound oscillations

R.H. LYON 1963, *Journal of the Acoustical Society of America*, **35**(11), Noise reduction of rectangular enclosures with one flexible wall

J.A. MACINANTE 1984, *Seismic Mountings for Vibration Isolation*, New York: McGraw-Hill

T. MASAHIRO, T. MIKITO and T. DAIJI 2007, *Applied acoustics*, **68**, 71-85, Reduction of acoustic radiation by perforated board and honeycomb layer systems

G.P. MATHUR, B.N. TRAN and M.A. SIMPSON 1997, *AIAA-97-1636-CP*, Broadband active structural acoustic control of aircraft cabin noise-laboratory tests

A.J. MCMILLAN and A.J. KEANE 1996, *Journal of sound Vibration*, **192**, *549-562*. Shifting resonances from a frequency band by applying concentrated masses to a thin rectangular plate

A.J. MCMILLAN and A.J. KEANE 1997, *Journal of sound Vibration*, **202**, *549-562*. Vibration isolation in a thin rectangular plate using a large number of optimally positioned point massed

D.J. MEAD 1999, *Passive Vibration Control,* London: John Wiley & Sons Ltd.

D.J. MEAD 1960, *Aircraft Engineering*, **32**, 64-72. The effect of a damping compound on jet-efflux excited vibration

L. MEIROVITCH and S. THANGJITHAM 1990, *Journal of Vibration and Acoustics*, 112, 237-244, Active control of sound radiation pressure

J.I. MOHAMMAD and S.J. ELLIOTT 2005, *Internoise*, Active control of fully-coupled structural-acoustic systems

J.B. MORELAND 1984, *Noise Control Engineering Journal*, **23**(3), Low frequency noise reduction of acoustic enclosures

S. NARAYANAN and R.L. SHANBHAG 1981, *Journal of Sound and Vibration*, **77**, 251-270, Sound transmission through elastically supported sandwich panels into a rectangular enclosure

A.D. NASHIF, D.I.G. JONES and J.P. HENDERSON 1985, *Vibration Damping,* New York: John Wiley

J.D. NEFSKE, J.A. WOLF and L.J. HOWELL 1982, *Journal of Sound and Vibration*, **80** 247-266, Structural-acoustic finite element analysis of the automobile passenger compartment: A review of current practice

P.A. NELSON and S.J. ELLIOTT, 1992, *Active Control of Sound*, Academic Press Limited

P.A. NELSON, A.R.D. CURTIS, S.J. ELLIOTT and A.J. BULLMORE 1987, *Journal of Sound and Vibration*, **117**(1), 1-13, The active minimization of harmonic enclosed sound fields part I: Theory

J.E. OH and S.H. KIM 1999, *JSME*, 42(1), 24-32, Interior and exterior noise reduction of a rectangular enclosure according to the determination of suitable thickness of the foamed aluminium sheet absorber

N. OLHOFF 1974, *International Journal of Solids and Structures*, **10**, *91-109.* Optimal design of vibrating rectangular plates

J. PAN 1992, *Journal of the Acoustical Society of America*, **91** (2), The forced response of an acoustic-structural coupled system

J. PAN, C.H. HANSEN and D.A. BIES 1989, *Journal of the Acoustical Society of America*, **87** (5), Active control of noise transmission through a panel into a cavity: I. Analytical study

C. PARK, C.R. FULLER and M. KINDNER 2002, *Proceedings of Active 2002, Southampton UK*, 275-284, Evaluation and demonstration of advanced active noise control in a passenger automobile

B. PETITJEAN, I. LEGRAIN, F. SIMON and S. PAUZIN 2002, *Journal of Sound and Vibration*, **252** (1) 19-36, Active control experiments for acoustic radiation reduction of a sandwich panel: feedback and feedforward investigations

A.J. PRETLOVE 1965, *Journal of Sound and Vibration*, **2** (3), 197-209. Free vibrations of a Rectangular Panel Backed by a Closed Rectangular Cavity

A.J. PRETLOVE 1966, *Journal of Sound and Vibration*, **3** (3), 252-261. Forced vibrations of a Rectangular Panel Backed by a Closed Rectangular Cavity

A. PREUMONT 2002, *Vibration Control of Active Structures*, 2nd Edition, Kluwer Academic Publishers, Dordrecht

E.J. RICHARDS and D.J. MEAD 1968, *Noise and Acoustic Fatigue in Aeronautics*, London: John Wiley

B.W. ROSS and R.A. BURDISSO 1999, *Journal of the Acoustical Society of America*, **106** (1), Low frequency passive noise control of a piston structure with a weak radiating cell

F. SCARPA 2000, *Journal of Vibration and Acoustics*, **122**, 109-115, Parametric sensitivity analysis of coupled acoustic-structural systems

S.D. SNYDER and N. TANAKA 1993, *Journal of the Acoustical Society of America*, **94** (4), On feedforward active control of sound and vibration using vibration error signals

T.J. SUTTON, S.J. ELLIOTT and A.M. MCDONALD 1994, *Noise Control Engineering Journal*, **42** 137-147, Active control of road noise inside vehicles

B. P. WANG, L. KITIS, W.D. PILKEY and A. PALAZZOLO 1982, *Journal of Aircraft,* **19**, *499-504.* Structural modification to achieve antiresonance in helicopters

B.T. WANG, C.R. FULLER and E.K. DIMITRIADIS 1991, *Journal of the Acoustical Society of America*, **90** (5), Active control of noise transmission through rectangular plates using multiple piezoelectric or point force actuators